APPLICATION OF ELECTRONIC SPECKLE PATTERN INTERFEROMETRY TO THE STUDY OF THREE-DIMENSIONAL MECHANICAL VIBRATIONS

by

Michael C. Shellabear
B.Tech., A.M.I.Mech.E.

A Doctoral Thesis submitted in partial
fulfilment of the requirements for the
award of Doctor of Philosophy of the
Loughborough University of Technology

March 1991

To my parents

"To the elementary parts of a solid body any arbitrary displacements may be given, subject to conditions of continuity. It is only by a process of abstraction of the kind so constantly practised in Natural Philosophy, that solids are treated as rigid, fluids as incompressible, and other simplifications introduced so that the position of a system comes to depend on a finite number of co-ordinates. It is not, however, our intention to exclude the consideration of systems possessing infinitely various freedom; on the contrary, some of the most interesting applications.. ..will lie in that direction. But such systems are most conveniently conceived as limits of others, whose freedom is of a more restricted kind. We shall accordingly commence with a system, whose position is specified by a finite number of independent co-ordinates...."

Lord Rayleigh

The Theory of Sound

1877

ABSTRACT

Electronic speckle pattern interferometry (ESPI) has become an established technique for mechanical vibration analysis, but in the past has been restricted to uniaxial measurements and has suffered from producing results which require skilled interpretation. The work reported here has extended the range of application of the technique to include three-dimensional vibration studies, and has made progress in automating the acquisition and processing of data. After establishing the importance of empirical vibration analysis and the practical advantages of ESPI, the theoretical requirements for measuring three-dimensional motion are considered. An experimental rig has been constructed using a continuous wave laser which has demonstrated that ESPI is capable of measuring time-averaged in-plane vibrations, an ability which was previously in some doubt. The rig has been used to study the three-dimensional resonant behaviour of simple structures and real engineering components in laboratory conditions. Some limitations were encountered and, in order to overcome these, a pulsed laser was introduced to the system. This has enabled the method to be extended to unstable objects, large amplitudes and non-resonant behaviour. Image processing and phase-stepping techniques have also been applied, enabling quantitative in-plane and out-of-plane displacement plots to be computed from the ESPI data. Experimental results are presented showing modal analyses of flat plates, an ultrasonic forming die, a turbocharger blade and an ultrasonic cutting system. The application of pulsed ESPI to the study of travelling waves, unstable objects and factory environment measurements is also demonstrated. The performance of three-dimensional ESPI is compared with alternative techniques, and the potential for further improving the technique is discussed. It is concluded that the method offers particular advantages for some types of study, and that it compliments the existing range of empirical techniques.

ACKNOWLEDGEMENTS

This work has been carried out in the Department of Mechanical Engineering at Loughborough University of Technology between April 1987 and March 1991. The work was supervised by Dr. John Tyrer, whose encouragement and advice have been much appreciated, and directed by Professor Jim Hewit. Most of the work was undertaken as part of a research project funded by the Science and Engineering Research Council and Metal Box plc, and financial support whilst writing up was provided by Rolls-Royce Motor Cars Ltd.

The author would like to thank colleagues in the Optics Group (including David Kerr, Paul King, Fernando Mendoza Santoyo, Andy Moore and Terry West) and Dynamics Group (Graham Chapman and Margaret Lucas) for advice and assistance on many occasions, and all the other postgraduate researchers in the department for providing inspiration and friendship throughout the duration of the research. Thanks are also due to the technical staff in the department for their contributions, especially Vic Roulstone for manufacturing and maintaining equipment, and Ken Topley and Vin Scouthern for preparing the photographs.

Results from studies of the ultrasonic forming die (sections 5.1 and 6.3) and ultrasonic cutting system (section 5.2) are reproduced by kind permission of Mr. Paul Porucznik at CMB Packaging Technology (formerly Metal Box) plc, and Dr. Frank Rawson at FFR Ultrasonics respectively. Finite element plots have been reproduced courtesy of Chris Cheers (Figure 27 to Figure 31), Margaret Lucas (Figure 43) and Xu Wang (Figure 46 and Figure 47). Accelerometer results in Figure 34, Figure 37 and Figure 38 are also courtesy of Margaret Lucas. The work in Chapter 6 was performed jointly with Fernando Mendoza Santoyo.

Finally, the author would like to express sincere gratitude to Dr. Angela Moreland for her love and support during the long process of writing up.

CONTENTS

1. INTRODUCTION

This thesis documents a programme of research into the application of electronic speckle pattern interferometry (ESPI) to the study of three-dimensional mechanical vibrations in an engineering context. The background which led to this work is briefly outlined in section 1.1, together with the stated aims of the programme. Section 1.2 gives an overview of the field of vibration engineering, explaining the types of information which engineers need to know and the importance of empirical techniques in obtaining it. The parameters and requirements of experimental systems in general are discussed in section 1.3, and the specific technique of ESPI is described in section 1.4. Chapter 2 contains a review of previous relevant work from the literature, covering the range of theoretical and experimental methods applicable to this type of study, and ESPI in particular. Chapter 3 explains the theory and practice of making three-dimensional measurements with ESPI. Section 3.1 explains two particular interferometer configurations which can be used to satisfy the theoretical requirements for three-dimensional measurements. The experimental apparatus used for this study are described in section 3.2 with a discussion of the practical considerations, and section 3.3 explains how image processing technology and the technique of phase-stepping have been applied to improve the quality of results and information obtained. Chapters 4, 5 and 6 contain the results of the experimental work. In chapter 4 the experimental methods are demonstrated on simple structures which display one-, two- and three-dimensional vibrations, and for which analytical solutions are known, in order to verify the theory. Having proved the viability of the method, it is extended in Chapter 5 to more complex structures and systems. These are more representative of typical engineering problems, and are presented as problem-solving case studies. Finally chapter 6 deals with non-ideal environments, demonstrating the application of pulsed ESPI to solve some of the problems previously encountered. The results are discussed in Chapter 7 with regard to the aims and requirements as stated in Chapter 1, including a critical assessment of the technique and suggestions for potential applications. Suggestions for further work and conclusions are given in Chapters 8 and 9 respectively. Aspects of ESPI and vibration theory which are required for the results and discussion are given in the Appendices.

1.1 BACKGROUND AND AIMS OF RESEARCH

This research arose from the fusion of two different research programmes: (i) the ongoing research into optical methods in engineering metrology in the Department of Mechanical Engineering at Loughborough University; and (ii) a project by the Research and Development division of Metal Box plc to investigate the application of ultrasonic vibrations to the forming of containers, in particular the die necking of metal cans. The two were brought together as a collaborative research project[1] in order to apply the existing expertise and research facilities at Loughborough to help solve the problems of the Metal Box programme. It was known from previous studies that the forming dies were likely to exhibit three-dimensional vibration behaviour, but it had not been possible to measure these vibrations accurately using the existing facilities. The technique of electronic speckle pattern interferometry (ESPI), which had been invented and developed as part of the Loughborough research, appeared to have the potential to enable such measurements to be made effectively.

The principles of ESPI are explained in section 1.4. Previous work had demonstrated that it could measure orthogonal out-of-plane and in-plane components of static displacement, thus enabling the three-dimensional displacement to be completely characterised. The method of measuring out-of-plane displacements had also been successfully applied to measuring vibrations, however there appeared to be some dispute as to whether or not the in-plane method could be applied to vibration measurement (see section 2.2.1). There did not appear to be any logical reason why it could not, therefore the initial aim of this research was to determine whether or not it is possible to measure in-plane vibrations with ESPI and, if so, to demonstrate that it could be implemented in practice. If successful, the next aim was to derive the theory for making three-dimensional vibration measurements, and to verify this theory experimentally. Further aims were to investigate areas of engineering vibration analysis where the technique could usefully be applied, and to refine both the experimental hardware and the processing of results to make it more versatile, quicker and easier to use.

The overall aim of the research is to produce a new tool to add to those available to vibration engineers. This should either offer advantages over the existing techniques for some applications, or enable information to be obtained which was not previously possible. In order to achieve this it is necessary to consider what information is required in engineering vibration studies, which measurements need to be made to determine that information, and the requirements for obtaining those measurements. These points are considered in the following two sections. Alternative methods which have been used in the past will be considered in section 2.1.

1.2 VIBRATION MEASUREMENT IN ENGINEERING

There are many situations in engineering where it is necessary to understand the vibration behaviour of a structure or system. Some understanding can be obtained by considering vibration theory (see Appendix B) and applying analytical or computational methods to predict behaviour, but it is often necessary and always desirable to verify the results with empirical measurements. In other circumstances it may simply be necessary to test whether the vibration of an object is within acceptable limits under certain conditions, and again empirical measurements are required. Hence the ability to measure mechanical vibrations is of great importance in engineering both for testing and design, as explained in the following paragraphs.

1.2.1 Vibration testing

The process of measuring the dynamic response of a component or system under particular specified conditions is known as 'vibration testing'. This may be performed as part of a design process to discover how the system is likely to behave under certain conditions, or for quality control to test whether the performance of the system is acceptable within specified limits. An example of the former would be determining the locations and amplitudes of significant vibration under the expected operating conditions of a new component. In the latter case it may be required to limit the maximum vibration amplitude in response to a specified excitation, or to ensure that a particular natural mode of vibration does not occur within a specified frequency range.

1.2.2 Modal analysis

The process of completely defining the vibration behaviour of a system is known as 'modal analysis'. The vibration behaviour can be described in terms of the modal parameters (frequency, damping and mode shape) for each of the natural modes of the system (see Appendix B for theory), and therefore by measuring certain critical parameters it is possible to predict the response to conditions other than those actually tested. Two approaches to modal analysis are commonly used. The 'normal mode method' uses the fact that the vibration behaviour can be fully defined by a set of independent differential equations expressed in terms of the normal modes of the system. Hence the response to any given excitation can be calculated as a linear combination of those equations. To use this method it is necessary to obtain the modal parameters for each of the normal modes in turn, and substitute the appropriate values into the equations. For a continuous system there will theoretically be an infinite number of normal modes, but in practice only a limited number need to be considered to obtain reasonable accuracy within a limited frequency range. A practical problem as an experimental technique is that it is often not easy to excite each normal mode independently of all the others. The 'frequency response method' uses a different approach. Rather than measuring the modal parameters at discrete frequencies, it measures the excitation (i.e. input force) and response of the system at discrete spatial points over a range of frequencies, and then transforms this data into the frequency domain (typically using a fast Fourier transform) in order to extract the modal parameters. A practical consideration here is that the spatial resolution is limited by the number of measurement points used.

1.3 REQUIREMENTS OF EXPERIMENTAL SYSTEMS

Mechanical vibrations can be characterised by a wide range of observable parameters including displacement, velocity, acceleration, stress, strain, etc. Experimental methods are available for measuring any of these, and the choice of most appropriate method for a particular application depends on both the information required and the constraints imposed by the system being measured. When choosing or developing a new experimental technique it is important to consider the attributes of the measuring system and the parameters which will affect the data obtained. These parameters include:

(i) Ease of use. It is desirable that measurements can be made without complicated or lengthy setting up, and without requiring high levels of training for the operator.

(ii) Ease of interpretation of results. The form in which the data is presented may not be easy to interpret for obtaining the information that is required.

(iii) Accuracy and resolution of measurement. These may vary with the magnitude of the quantity being measured, and impose limits on the range of application of the technique.

(iv) Spatial and temporal continuity. Most techniques produce results which are discontinuous in space or time; these may require curve fitting or interpolation in order to be useful. Data which has been averaged over a time or an area may mask significant features, and techniques with directional sensitivity may not detect important effects in other directions.

(v) Speed of data acquisition. The duration of the sampling period limits the temporal resolution, and some techniques may also require a significant time to convert the measured quantity into a useful form.

(vi) Format and compatibility of results. It may be useful or necessary to compare the results with other data presented in a particular format, or to interface the measurement system with a computer or other device.

(vii) Tolerance to environmental conditions. Sensitivity to temperature, electric fields, external vibrations, etc. may render a technique inaccurate or unsuitable for certain applications.

1.4 ELECTRONIC SPECKLE PATTERN INTERFEROMETRY

ESPI is one of a family of coherent light techniques which also includes holographic and speckle interferometry. The operating principle of these techniques is based on the phenomenon of interference between coherent wavefronts. When two mutually coherent wavefronts are combined, they interfere constructively or destructively to form an interference pattern which is characteristic of the phase relationship between them. Hence if the phase relationship is caused to change by the displacement of a reflecting (or scattering) surface, then the resulting interference pattern will contain information about that displacement. If that information can be extracted then interferometry can be used as a technique for measuring surface displacement.

ESPI works by generating interference patterns (called 'interferograms') from the interaction of the two coherent wavefronts and the surface being studied, imaging them with a video camera to capture the optical information they contain, and performing an electronic image-correlation to reveal the displacement data for the test surface. The results of this correlation are in the form of a 'fringe pattern' of dark and bright interference bands, superimposed on the image of the test surface, which correspond to loci of constant optical path difference between the interfering wavefronts. This optical path difference is directly related to the motion of the test surface during the measurement period, and hence information about the vibration can be obtained from the fringe pattern. Measurement sensitivity is in the order of one wavelength of the illuminating light, and for visible wavelengths the fringe spacing is typically ~0.3µm surface displacement. Depending on the methods used it can be possible to measure either the time-averaged amplitude or the displacement at discrete points in time. A single interferometer can only measure displacements in one direction, which is determined by the optical configuration. Different experimental arrangements and how they can be used are explained in section 3.1. Typically the interferometer is arranged to measure either out-of-plane or in-plane motion with respect to the test surface; by combining these it is possible to measure motion in three dimensions. (see ref. The intensity distribution of the fringe pattern is a function of the surface motion, and also depends on the type of illumination used; the theory for this is given in Appendix A.

2. LITERATURE REVIEW

The purpose of this chapter is to identify and review previous work which is relevant to the present study. This can be divided into two classes. First, experimental studies of mechanical vibrations using techniques other than ESPI, which can be used for comparison with the results of this work and to judge its success. Second, the historical development of empirical methods which led to the invention of ESPI, and the subsequent research and development which has refined the technique to its present status. There is considerable overlap between these classes because many studies of mechanical vibrations have been performed using the relevant empirical techniques. Consequently the studies of mechanical vibrations are incorporated within the methods for vibration analysis, which are reviewed in section 2.1. The development of ESPI is covered separately in section 2.2.

2.1 METHODS FOR VIBRATION ANALYSIS

Very many different techniques have been used for vibration analysis, so it is necessary to restrict the scope of this review to those which are most relevant to this study. This includes techniques which share ESPI's ability to make whole-field measurements without requiring surface preparation or contact, and studies of objects which have particular relevance to the results reported here. These will be considered in depth. Techniques which do not fall into this category are nevertheless very important in engineering vibration analysis and some have also been used in this study for comparison with ESPI results. These will be reviewed briefly in general terms: theoretical methods in section 2.1.1, and empirical point measurement techniques in section 2.1.2. The whole-field techniques are divided into four classifications presented in chronological order of their invention. These start with the Chladni method (section 2.1.3) and then follow the development of optical techniques from classical interferometry (section 2.1.4) through holographic interferometry (section 2.1.5) to speckle techniques (section 2.1.6).

2.1.1 Analytical and numerical methods

The purpose of analytical study is to obtain mathematical expressions which accurately describe the phenomena observed in practice, and which can be used to predict unknown information. The scientific study of mechanical vibrations started in the 18th century, and by the end of the 19th century equations had been derived for the main classes of vibration of simple beams, plates and shells which provided reasonably accurate results. This early work has been comprehensively reviewed by Love[2]. Research since then has improved methods of analysis, and has gradually removed constraints to obtain solutions to a much wider variety of geometries, material properties and boundary conditions. Many different analysis methods have been developed, some of which are still in common use today (for example the 'Rayleigh-Ritz' method[3]). The difficulty with the analytical approach is that the derivations tend to become extremely complicated for anything other than very simple cases and, even then, it is often not possible to obtain exact solutions. One answer is to use approximate numerical methods, of which a number have been developed. Numerous texts now exist which document the present extent of knowledge in analytical and numerical vibration analysis, a good example being by Timoshenko et al[4]. Even using approximate numerical methods the calculations become very involved and time-consuming as the geometry or other factors become more complex, and it was only with the advent of the digital computer that it became feasible to consider theoretical analysis of complicated structures. In particular the development of the finite element (FE) method[5] and powerful computers has enabled complex dynamic analyses to be undertaken, and these are now commonplace. Although computer modelling is a powerful and useful technique, the method is by definition an approximation, and the accuracy of the results is dependent on the authenticity of the model. For this reason it can never completely replace empirical testing, but must be considered a complimentary technique.

2.1.2 Point measurement techniques

Modal analysis can be performed using the frequency response method by measuring vibration response at discrete points (see section 1.2.2). In practice measurements are inevitably averaged over a finite area, but if the size of measuring area is small compared to the wavelength of the vibration then it must be considered a point measurement (as opposed to a whole-field measurement). The method requires measurements of excitation and response, and as stated in section 1.3 these can be detected in a variety of ways. The excitation (which is typically a sine sweep, white noise or impulse function) is usually measured by a force transducer, and response can be measured as displacement (for example using an eddy current induction probe or a linear variable differential transformer); velocity (laser velocimeter or velocity seismometer); acceleration (piezoelectric accelerometer); strain (electrical resistance strain gauge); etc. Each of these instruments uses point measurement, and the different results can be related as being derivatives of displacement with respect to either time or distance. Most measure a single component of motion and therefore require multiple measurements for three-dimensional quantification. Strain gauge rosettes can measure total in-plane strain, and triaxial accelerometers can measure acceleration vectors in three dimensions, although the latter can be subject to significant errors[6]. Accelerometers in particular have become widely used for modal analysis, with the result that hardware and software for processing and analysing results have become well developed[7,8]. By connecting the measuring transducers via appropriate instrumentation to a spectrum analyser it is possible to obtain: frequency response plots (amplitude and phase) from any given pair of measuring points; waterfall plots of sets of data; curve fitting of data sets to yield spatial mode shapes; etc. This data can also be interfaced with a personal computer to construct a 'modal model' of the test system (similar to a finite element model) which can be used to predict the effects of structural modification.

Apart from the limitations imposed by the particular instrumentation used, the main drawback of the point measurement techniques is that in order to obtain whole-field data, for example mode shapes, it is necessary to take measurements at a set of different points. Generally a matrix of measurement points is used, where the grid spacing determines the spatial resolution obtainable. Where the spacing between nodal lines is small (and generally this decreases with increasing frequency) a large number of points may be necessary. For contact measurement techniques this requires either a large number of transducers for rapid measurement (with consequent increased mass loading effects), or slow data acquisition measuring point by point. These problems are largely overcome by the technique of scanning laser Doppler velocimetry[9,10]. This measures surface velocity at a grid of points and produces results in a similar form to accelerometers, enabling modal analysis to be performed from non-contact measurements.

2.1.3 Chladni method

The first practicable method for visualizing mode shapes on plates, and therefore for performing experimental vibration analysis, was invented by Chladni in the 1780s. The method involves sprinkling a fine powder, for example sand, onto the surface of the plate, and therefore is not a non-contact technique. If the plate is then excited to vibrate in one of its resonant modes, the surface motion causes the powder to move from vibrating to stationary regions, thereby indicating the nodal pattern for that mode (N.B. some methods use very fine powders which settle at regions of maximum motion after vibration has ceased, thereby indicating antinodal patterns). This method has been studied in detail by Waller; her book[11] catalogues studies of circular, elliptical, rectangular and other polygonal shaped plates, as well as giving practical and historical notes. The results include extensive graphical tables of observed mode shapes, a method of mode shape classification, and discussion of how these shapes arise. Of particular interest to the present study (section 4.2) are her study of free circular plate vibrations[12] and discussion of combined and degenerate modes[13]. Grinsted[14] extended the application of the method to study impeller, turbine and propeller blades, starting from the similarity to cantilevered plates, and attempting to classify the results into normal and 'compounded' modes in the manner of Waller. This work raised a number of interesting questions, which are discussed in the same reference. The method has been further extended by McMahon[15], who used it to study the vibrations of solid cylinders. This three-dimensional study used sand on horizontal surfaces and electrostatically charged lucite particles on vertical surfaces. Although more sophisticated techniques have mostly replaced the Chladni method in research, it has still been used in some recent studies. Ravenhall and Som[16] effectively repeated some of Waller's work and proposed new equations relating the modal frequencies to the numbers of nodal circles and diameters. Caldersmith and Rossing[17] have studied the modal coupling in isotropic and orthotropic rectangular plates, with particular reference to modes which are important in musical instrument design.

An optical method which is more akin to Chladni than to the interferometric methods described below has been used by Theocaris[18] to study plate vibrations. This uses reflected light to obtain nodal patterns, with the advantage that compound modes can be observed in different phase combinations. No contact is required, but the surface has to be polished to give specular reflection. Bergmann[19] also used reflected light to study membrane vibrations by observing soap films, in this case obtaining very clear antinodal patterns.

2.1.4 Optical interferometry

Optical interferometry has long been regarded as a useful technique for observing small amplitude vibrations due to its high sensitivity (measuring amplitudes in the order of visible wavelengths), the advantage of being non-contacting, and the ability to make whole-field measurements. Early studies mostly concentrated on the vibrations of quartz crystals and other electrical oscillators, and included both continuous and stroboscopic illumination. These were the precursors of the methods used for the work in this thesis. Osterberg[20] was the first to develop the fringe function theory for time-averaged observation of simple harmonic motion under continuous illumination. He used this method to observe resonant vibrations in quartz crystals of different cuts, illuminating with a single spectral line from a mercury lamp. Only out-of-plane motion was observed, but this enabled the flexural modes to be identified and also longitudinal modes with some uncertainty. Some modal coupling was noted, and also persistence of modes during variation of frequency. Shaw[21] used stroboscopic illumination from a helium lamp to observe multiple beam Fizeau fringes simultaneously on both sides of a vibrating barium titanate disk. Again only out-of-plane motion was observed, but the observed modes were able to be classified as radial dilatational or thickness dilatational using measurements of amplitude distribution, frequency and electromechanical coupling coefficient.

Moiré interferometry is an alternative to classical interferometry in which fringe patterns are formed by the interaction of structured light patterns rather than by interference between coherent wavefronts. The light patterns can be formed either by projecting or physically applying gratings. Advantages are that white light can be used, and the fringe sensitivity can be varied from fractions of a micron up to several millimetres by adjusting the spatial frequency of the gratings and using different techniques. A great many variations of the moiré method have been investigated, as reviewed by Sciammarella[22]. Depending on the optical configuration used, the method can be made sensitive either to displacement or to surface tilt (usually partial slope), and can therefore detect either nodal or antinodal regions. Hazell and Niven[23] have combined two techniques to visualize both nodes and antinodes of vibrating plates. Some of the slope-sensitive techniques which are applicable to measuring static and dynamic flexure of plates have been summarised by Kao and Chiang[24]. Vest and Sweeney[25] have used projected fringes from a laser interferometer to measure time-averaged amplitudes, producing results in a similar form to ESPI.

Another technique which produces whole-field visualisation of vibration modes is stress pattern analysis by thermal emission (SPATE)[9]. This is a non-contact technique, measuring changes in thermal emission which are proportional to the sum of the principal stresses at each point.

2.1.5 Holographic interferometry

Holography is an optical technique whereby the interfering wavefronts of two mutually coherent laser beams are recorded photographically and can be reconstructed to produce a three-dimensional image of an object. In holographic interferometry (HI), holograms of an object in different states are combined to form an interferogram with fringe patterns indicating differences between the states[26]. HI was first reported in 1965 by Powell and Stetson[27], who recorded time-average holograms of vibrating objects. They also derived the theory of the fringe formation in terms of the illumination geometry and the surface motion. The method showed great potential for engineering vibration analysis and much research followed. Molin and Stetson[28] showed that the technique could be used to study vibrations which were combinations of classical modes, and Wilson extended this work by studying combinations of vibration modes at rationally and irrationally related frequencies[29,30]. Stetson subsequently developed theory for using HI to perform vibration analysis by the normal mode method[31] (see section 1.2.2) and structural design by a perturbation method[32].

All the above studies used a single holographic view and hence could only resolve a single component of the surface motion. In order to obtain three-dimensional measurements it is necessary to use at least three views, either by recording separate holograms with different illumination directions or by viewing a single hologram from different directions (see reference 26, chapter 2). Tonin and Bies[33,34] used the former method to study single and coupled vibrations of cylinders, determining component amplitudes and phases using the method of least squares. In a conventional holographic configuration it is not possible to obtain orthogonal components directly, so it is usually necessary to solve simultaneous equations to separate the component motions. Katzir and Glaser[35] have demonstrated a method of separating the in-plane and out-of-plane components optically by using a dual illumination beam method borrowed from speckle metrology (see section 2.1.6). Pirodda and Griffiths[36] have also measured in-plane displacements directly, using a method called 'conjugate-wave HI'. However, neither of these methods has been applied to vibration studies.

The process of time-averaging, as used in all the above studies, removes the optical phase information of a hologram, and hence it is necessary to use other techniques to determine the phase of a vibrating object. Phase determination in HI was first demonstrated by Neumann et al[37] by vibrating a mirror in either the object or reference beam of the interferometer at the same frequency as the vibrating object; this is called phase modulation. An alternative method is to derive the reference beam from a point on the vibrating object itself, thus creating a phase reference within the image. This configuration forms a common-path interferometer and therefore also has improved stability. Rowley[38] has used this method to design a compact holocamera which can be operated from an unisolated platform. Levitt and Stetson[39] used phase modulation to generate vibration-phase contour maps which show how the phase of vibration varies across an object. However these techniques required lengthy analysis with graphical constructions to obtain a phase map, and it is highly desirable to automate the procedure for computer processing. This can be achieved with time-average HI[40], but the non-periodic nature of the Bessel function fringes (see Appendix A.3) means that the analysis is fairly complex. This problem can be overcome by using stroboscopic or pulsed illumination to produce fringe patterns with a periodic sinusoidal intensity profile, which is much more amenable to automatic processing. Hariharan et al[41] used stroboscopic illumination with digital phase-shifting and multiple illumination directions to determine the magnitude, phase and two-dimensional direction of vibrations of a compressor blade. An additional advantage of pulsed holography is that the very short duration of the illumination enables transient events to be studied. Aprahamian et al[42] used a single pulse ruby laser in 1971 to study propagating waves, and the method was later improved by Fällström et al[43] using a double pulse ruby laser. The abilities of double pulsed HI as a tool for industrial vibration analysis were demonstrated by Felske and Happe[44], who studied self-excited internal combustion engines and other automotive components. Hyodo and Konomi[45] applied both time-average and pulsed HI to modal analysis of a car engine, using computerised fringe analysis to determine the normal mode contributions in observed resonances. Other applications of pulsed holography for industrial vibration analysis have been reviewed by Tozer[46], including the use of fibre optic delivery systems. Double pulsed holograms of acceptable quality were obtained using a 200µm diameter fibre for the reference beam and a 6mm diameter fibre bundle for the object beam. The state of the art in 1990 was demonstrated by Crawforth et al[47], combining a twin-cavity injection-seeded Nd:YAG pulsed laser with phase-stepping to study the impact response of a magnetic disk drive system.

HI has been used for a number of previous studies of components similar to those considered in chapters 4, 5 and 6. Aprahamian and Evensen[48] observed flexural vibrations of a cantilevered beam at frequencies up to 99 kHz, comparing the results with Timoshenko beam theory. In a companion paper[49] the same authors studied flexural vibrations of a rectangular plate. Pryputniewicz[50] studied flexural and torsional modes of a cantilevered plate, comparing the HI results with FE calculations and discussing unification of the two techniques to control the errors inherent in the numerical method. Engelstad et al[51] made a similar study of a cantilevered plate, and Hazell and Mitchell[52] have studied flexural vibrations of square and rectangular clamped plates, in both cases comparing the results with theoretical predictions. Little experimental work seems to have been applied to in-plane vibrations, although Gottenberg[53] has obtained pulsed interferograms of an extensional shock wave propagating along an aluminium bar. Two other studies are particularly relevant to the ultrasonic forming die and the ultrasonic cutting system which will be considered in chapter 5. Tuschak and Allaire[54] studied a longitudinal mode of a cylindrical ultrasonic resonator driven by piezoelectric elements, determining the radial and longitudinal components of the axisymmetric motion. Manderscheid[55] demonstrated how HI can be used for adjustment and testing of ultrasonic machining tools, by measuring the frequency and mode shape at resonance. The use of HI for turbomachinery blade investigations has been reviewed by Erf[56], and studies using HI have been made by MacBain[57] and Anderson[58].

2.1.6 Speckle techniques

The phenomenon of 'speckle' occurs whenever coherent light is scattered diffusely, and is caused by mutual interference of the many individual scattered wavefronts. Although it is an undesirable feature in holography, Groh[59] proposed in 1968 that speckle could be used as the basis for a range of measurement techniques by correlating two laser-produced speckle patterns and observing the resultant intensity distribution. Ek and Molin[60] later demonstrated that speckle interferometry can be used to detect nodal lines and vibration amplitudes in a similar way to HI. Leendertz[61] showed how different configurations of speckle interferometer could be used to measure either normal (out-of-plane) or in-plane components of displacement (see section 3.1) over an entire surface at one time, and Hung and Hovanesian[62] extended the same method to three-dimensional measurements. Both of these studies were confined to static or quasi-static displacements, but they opened the way for the same methods to be applied to vibration studies. Tiziani[63] and Archbold and Ennos[64] developed alternative speckle techniques for analysing in-plane vibrations, applicable to whole-field measurements. Chiang and Juang[65] used Fourier filtering of time-averaged speckle interferograms to observe flexural (out-of-plane) vibrations of plates and shells. Other speckle techniques have also been investigated, including white light speckle methods[66,67] which enable whole-field observation of in-plane and out-of-plane vibrations. However this is cumbersome to perform, requiring different techniques to obtain all the required information. Speckle metrology techniques in general have been reviewed by Erf[68].

2.2 DEVELOPMENT OF ESPI

ESPI has been developed over the last twenty years from the holographic and speckle techniques described in the previous sections. For the first fifteen years the majority of the research and development was undertaken by two research groups, led by Butters and later Tyrer at Loughborough University, and by Løkberg at the Norwegian Institute of Technology in Trondheim. In the last five years or so many other research groups have become interested and made contributions to ESPI technology. During this period ESPI has become much more widely used in research and industry, and a number of companies have successfully marketed ESPI systems. This section reviews first the state of ESPI research at the commencement of this research project in April 1987, followed by developments elsewhere during the course of this research, and finally reviews recent work in the research programme at Loughborough (of which this thesis is a part).

2.2.1 State of the art in 1987

The theory and applications of ESPI as of 1983 have been documented by Jones and Wykes[69]. The range of applications included: out-of-plane and in-plane sensitive interferometers for displacement and strain measurement; surface contouring techniques; arrangements for viewing very small areas; time-averaged, stroboscopic, phase modulated and pulsed vibration measurement. Double pulsed ESPI had been demonstrated with a ruby laser by Cookson et al[70], with applications for vibration and transient analysis.

The applicability of the in-plane sensitive interferometer to vibration measurement was uncertain at this time, and no reports on its application had been published. In a 1982 paper[71] Wykes had stated: "It should be noted that only out-of-plane vibration can be observed using ESPI". Subsequently a more specific statement was made by Jones and Wykes (reference 69, p.196) that "only out-of-plane sensitive time-averaged fringes can be observed". No direct justification was given for these assertions, although the same authors had also stated (reference 69, p.195) with regard to pulsed ESPI that "In-plane measurements use two speckled beams and therefore require the use of the subtraction process". In 1985 Løkberg published a study of in-plane vibrations of metal plates and piezoelectric crystals[72], using an out-of-plane sensitive interferometer viewing the object at an oblique angle to give some sensitivity to the in-plane components. In his introduction the author implied that in-plane vibrations could be observed with an in-plane sensitive configuration, but only by using image subtraction to obtain sufficient fringe quality. Tyrer[73] reviewed recent developments in 1986 and stated that phase modulation could be applied to in-plane ESPI by vibrating a mirror in one of the illuminating beams, although no demonstration of this had been published.

Studies of particular relevance to this thesis include observations by Løkberg of flexural vibrations of square[74] and circular[75] plates, and his study of in-plane vibrations[72]. Davies et al[76] discussed the application of ESPI to modal analysis, demonstrating speckle averaging, strobing and phase modulation for observing vibrations of a car engine. The principle of phase modulation was extended by Moran et al[77] to produce a sophisticated optically phase-locked ESPI system. Phase-shifting of time-averaged ESPI fringes was demonstrated by Nakadate[78], and the application of pulsed holography and double pulsed ESPI to vibrating structures was discussed by Tyrer[79]. The analysis of fringe patterns produced by interferometric techniques such as ESPI had also received much research, and was reviewed by Reid[80] in 1986.

2.2.2 Developments since 1987

Very little work had been done prior to 1988 concerning in-plane vibrations or three-dimensional measurements in general. In 1988 Winther[81] measured three-dimensional static strains using ESPI in the conventional holographic configuration of three illumination vectors with a single reference beam, and also incorporated contouring of the object surface. A variation on this method has since been reported by Button et al[82], using three dual object beam interferometers (similar to an in-plane interferometer) to measure three-dimensional static deformations. Also in 1988, Gülker et al[83] demonstrated the measurement of two-dimensional deformations of stone surfaces using one out-of-plane and one in-plane ESPI configuration. By 1990[84] the same team were able to measure three-dimensional displacements over long periods, with automatic fringe analysis displaying in-plane and out-of-plane displacement plots. Joenathan et al[85] have shown how the in-plane configuration can also be used for surface contouring.

Much of the recent progress in ESPI vibration analysis has been through improvements in fringe analysis, and linking the interferometer directly to an image processing computer. In particular there has been widespread research and rapid progress in the field of automatic phase measurement (as reviewed by Creath[86]), including phase unwrapping techniques (reviewed by Osten and Höfling[87]). A recent development which enables phase unwrapping of complicated or noisy fringe patterns is the use of cellular automata[88]. A number of researchers including Breuckmann[89] and Ellingsrud[90] have reported methods which use phase-shifting to produce direct graphical output of vibrating mode shapes. Stetson has combined a TV speckle interferometer (equivalent to ESPI) with a sophisticated image processor to create a system which has been named 'electro-optic holography' or 'electronic holography'[91]. This incorporates speckle averaging and phase modulation and produces fringe patterns of near holographic quality, but requires up to eight video frame memories. Oh and Pryputniewicz[92] have used this system to study the vibrations of a cantilever plate with concentrated mass loading, comparing the results with finite element predictions. Their predictions included one in-plane rotational mode, but they were unable to verify this experimentally as only an out-of-plane sensitive system was used. Buckberry and Davies[93] have developed a versatile system incorporating fibre optic illumination with stroboscopic and phase modulation facilities, and have successfully applied a cellular automaton method to the phase unwrapping of complex fringe patterns. Valera et al[94] have developed an ESPI system which incorporates a fibre optic laser Doppler velocimeter (LDV) and enables mutual phase locking for automatic phase modulation. Pechersky and Bergen[95] have demonstrated the benefits of using LDV in conjunction with ESPI to enable measurement of drive point mobilities at the same time as mode shapes.

There has been relatively little recent activity in pulsed ESPI except at Loughborough (see section 2.2.3). Preater[96] has for several years been using a pulsed ruby laser to study in-plane strains on rotating components, and has proposed the use of a modulated diode laser in conjunction with fibre optics. Spooren[97] has investigated the performance of a single oscillator double pulsed Nd:YAG laser in an ESPI system for studying out-of-plane plate vibrations, obtaining double pulse addition fringes but concluding that double pulse performance is significantly worse than single pulse.

Several manufacturers currently market off-the-shelf ESPI systems which are suitable for performing vibration analysis. Two of these have developed out of the Loughborough research. The 'Vidispec', marketed by Ealing[98], has been available for several years and uses a continuous wave helium-neon (HeNe) laser for time-averaged observation of vibrations. The HC4000 speckle camera from Newport[99] uses a solid state diode laser which emits continuous wave illumination at a near infra-red wavelength. The equivalent commercial spin-off from the Trondheim research is the 'Retra' TV-holography system marketed by Conspectum[100]. This also uses a 5mW HeNe laser but is more specifically intended for vibration studies and includes a phase modulation mirror; electro-optic crystal modulation and speckle averaging are available as options. Eos[101] markets PSC phase-shift speckle cameras using HeNe, diode or argon lasers with optional stroboscopic modulator, fibre optic illuminator and in-plane optics. These are linked to a dedicated fringe analysis computer developed by Breückmann[89]. Stetson's electro-optic holography system is marketed by Recognition Technology[102]. In the closing stages of this research Spectradata[103] launched the SD800-ESPI system, using a 40mW semiconductor laser with piezoelectric phase-shifter and dedicated fringe processing software. This is a modular system based on the techniques of Gülker et al[84], and claims to measure simultaneously the deformations of out-of-plane and both in-plane components. At the time of writing it was not available in the UK and its abilities for three-dimensional vibration analysis are not known.

2.2.3 Recent research at Loughborough

Since the early work reported by Jones and Wykes[69] the Optics Group at Loughborough University has continued to pursue research into ESPI and other related fields, resulting in three recent doctoral theses. Montgomery[104] considered practical ways of improving the existing ESPI technology, in particular investigating optical design, noise reduction techniques and electronic speckle contouring. Mendoza Santoyo[105] undertook a study of the underlying optical mechanisms of ESPI, investigating spatial frequency response, system resolution and reference beam considerations. Tyrer[106] has shown how HI and ESPI have become commercially realistic technologies through improvements in lasers, optical components, electronic systems and computer-based fringe pattern analysis. In addition, Kerr et al have developed a methodology for automating the analysis of ESPI fringe patterns[107], including Fourier filtering[108] to remove speckle noise and a novel single-phase-step method[109] for phase determination. These techniques have been applied to vibration analysis[110], using a pulsed Nd:YAG laser specially designed and developed for an ESPI system[111,112]. The pulsed laser greatly increased the versatility of ESPI measurement, and was used in the later stages of this research project. Moore is currently applying three-dimensional ESPI to fracture mechanics problems, and has developed an interferometer which can simultaneously measure both in-plane components of displacement[113]. ESPI has also been used alongside finite element modelling and accelerometer-based modal analysis to study the vibrations of turbocharger blades[114] and assemblies[115].

3. ESPI THEORY AND PRACTICE

The purpose of this chapter is to derive the theory for measuring three-dimensional vibration data using ESPI, and to describe the experimental apparatus and methods which have been used. Section 3.1 describes how ESPI can be used to make three-dimensional measurements, and derives the theory for extracting those measurements from the observed fringe patterns. The types of experimental system which have been used to obtain the fringe patterns are explained in section 3.2, together with practical details of the equipment. Section 3.3 describes the image processing and fringe analysis methods which have been used to help extract the required information from the fringe patterns.

3.1 THEORY FOR THREE DIMENSIONAL MEASUREMENTS

In order to measure mechanical vibrations with ESPI it is necessary to know the relationship between the fringe pattern and the surface motion. This relationship, called the 'fringe function', depends on both the type of illumination (continuous, stroboscopic or pulsed) and the optical configuration of the interferometer. The general fringe function for any interferometer configuration is derived in Appendix A, which explains how quantitative vibration or displacement data can be obtained from time-averaged or pulsed interferograms. This section describes how measurements from different interferometer configurations can be combined to enable three-dimensional measurements, and derives the theory for doing so.

It was stated in section 1.4 that any two-beam interferometer (including holographic interferometry and ESPI) is only sensitive to displacements in a single direction, and therefore is only capable of measuring one resolved component at a time. The direction of the resolved component is determined by the 'sensitivity vector', which is a function of the optical geometry of the interferometer. If the direction of the vibration which is to be measured is known *a priori* then it can be aligned with the sensitivity vector for direct measurement. However in general it is necessary to record a minimum of three sets of data, each with a different sensitivity vector, and solve them simultaneously to determine the resultant displacement in three-dimensional space. The computational errors introduced in solving the data sets depend on the spatial separation of the sensitivity vectors (see reference 26, chapter 2) and will be minimum if the vectors are mutually orthogonal.

Using ESPI it is possible to construct interferometer configurations which have sensitivity either parallel to or perpendicular to the observation vector, and these can be combined to satisfy the ideal requirement of three mutually orthogonal sensitivity vectors (as discussed above). If the observation vector is made perpendicular to the observed surface then the three measurements correspond directly to in-plane and out-of-plane components, which are commonly required in many engineering problems. This is a distinct advantage over holographic interferometry, in which it is not possible to obtain in-plane components directly. Moreover, the three measurements can be recorded sequentially on one camera, thereby eliminating any problems of matching object points from different perspective views. Alternatively, two or more cameras can be used in a single imaging system[113] to enable simultaneous measurement.

The fringe function for ESPI is derived in Appendix A in terms of a phase change term $\Delta\psi$, which can be expressed as:

$$\Delta\psi = k\Gamma d_n \tag{3.1}$$

where $k = 2\pi/\lambda$ is the wave number (and λ is the wavelength of the illuminating light); Γ is a fringe sensitivity factor (which determines how many fringes correspond to a given surface displacement); and d_n is the component of object displacement resolved along the sensitivity vector $\mathbf{n}$. Γ and $\mathbf{n}$ are determined by the optical geometry of the interferometer, and are derived for out-of-plane and in-plane sensitive interferometers in sections 3.1.1 and 3.1.2. With continuous wave illumination the fringe intensity follows a Bessel function of the time-averaged surface displacement, whereas with pulsed illumination it is a cosinusoidal function of the absolute displacement between pulses (see Appendix A).

3.1.1 Out-of-plane sensitivity

The conditions for out-of-plane sensitivity in a speckle interferometer are that the object should be illuminated and viewed along its surface normal, and that the light scattered from the object should be combined with a reference wavefront. Figure 1 shows a practical optical configuration which can closely approximate this, using a beam-combining cube to introduce the reference beam. A Cartesian coordinate system is defined such that the object is viewed along the z-axis, and any point Q(x,y,z) in the object space is focused to a corresponding point P(x′,y′) in the image plane (see Appendix A.2). The object beam lies in the xz plane and is

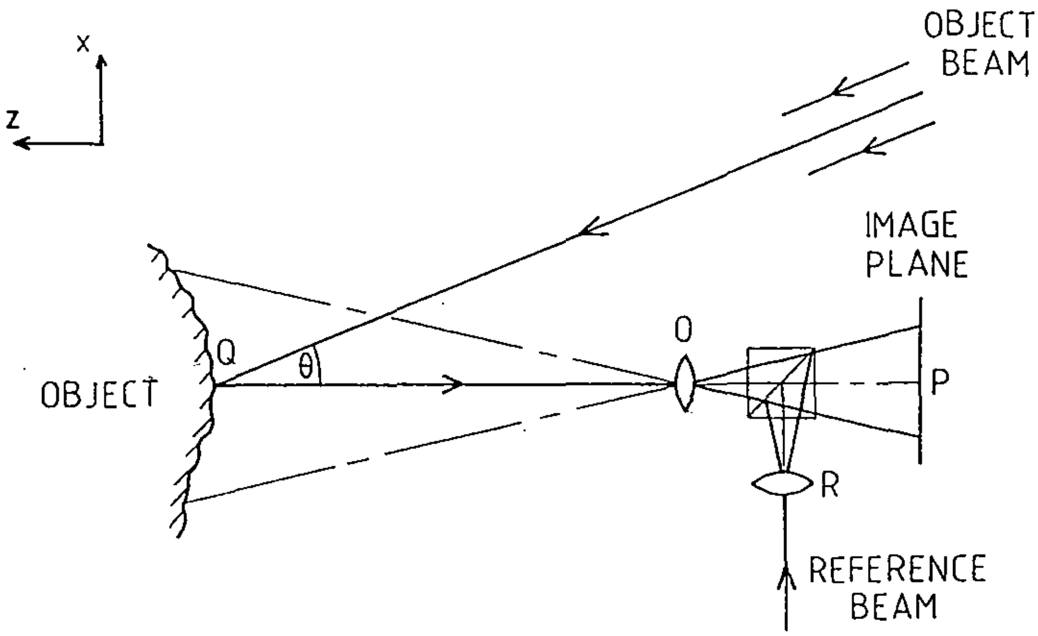

Figure 1: Out-of-plane sensitive interferometer

offset from the viewing axis by a small angle θ. When the object undergoes a small general displacement **d** having components d_x, d_y, d_z, such that a point Q(x,y,z) moves to Q′($x+d_x,y+d_y,z+d_z$), the change in optical path length Δl of the reflected object beam is as shown in Figure 2:

$$\Delta l = d_z(1 + \cos\theta) + d_x\sin\theta \tag{3.2}$$

where d_z and d_x can take positive or negative values. For static object and reference beam illumination, the total phase change at the image plane (see Appendix A, equation A.8) is:

$$\Delta\psi = \frac{2\pi}{\lambda}\{d_z(1 + \cos\theta) + d_x\sin\theta\} \tag{3.3}$$

If θ is small (approximately <5°) then the d_x term becomes negligible relative to

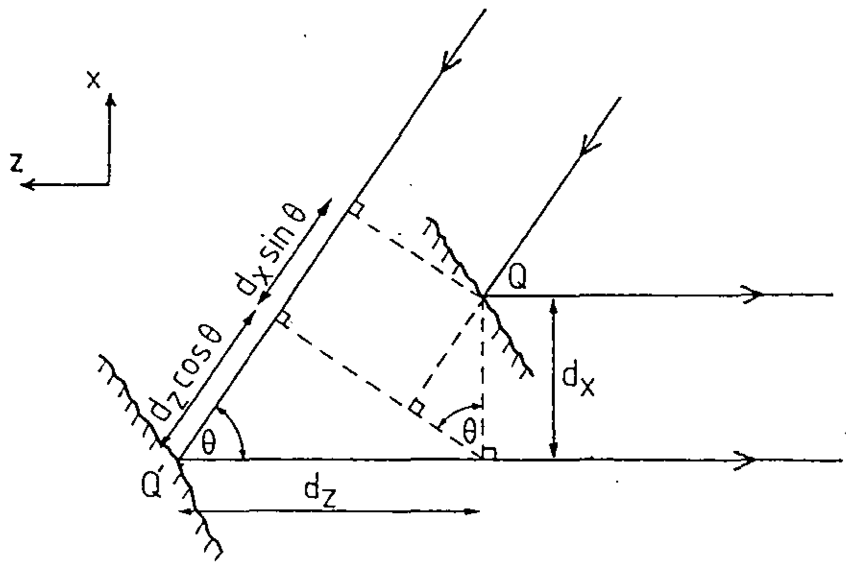

Figure 2: Path length change due to object displacement

the d_z term, and the system can be considered sensitive to d_z motion only:

$$\Delta\psi = \frac{2\pi}{\lambda} d_z(1 + \cos\theta) \tag{3.4}$$

For pure out-of-plane sensitivity the illumination and viewing directions should be coaxial and normal to the object surface. Equation (3.3) then simplifies to:

$$\Delta\psi = \frac{4\pi}{\lambda} d_z \tag{3.5}$$

Substituting into equation (3.1) gives the fringe sensitivity factor for this configuration as $\Gamma = 2$, and the sensitivity vector is a unit vector in the observation direction, $\mathbf{n} = \hat{\mathbf{z}}$.

3.1.2 In-plane sensitivity

The optical arrangement for an in-plane sensitive interferometer requires two collimated illuminating beams at equal angles to the surface normal. A practical arrangement for achieving this is shown in Figure 3. Referring again to Figure 2, a small general object displacement **d** will cause path length changes of:

$$\begin{aligned} \Delta l_A &= d_z(1 + \cos\theta) + d_x \sin\theta \\ \Delta l_B &= d_z(1 + \cos\theta) - d_x \sin\theta \end{aligned} \tag{3.6}$$

This produces a total phase change at the image plane of:

$$\begin{aligned} \Delta\psi &= \frac{2\pi}{\lambda} \{\Delta l_A - \Delta l_B\} \\ &= \frac{4\pi}{\lambda} d_x \sin\theta \end{aligned} \tag{3.7}$$

Hence the fringe sensitivity factor $\Gamma = 2\sin\theta$, and the sensitivity vector $\mathbf{n} = \hat{\mathbf{x}}$. If the two illuminating beams are rotated to lie in the yz plane then the same

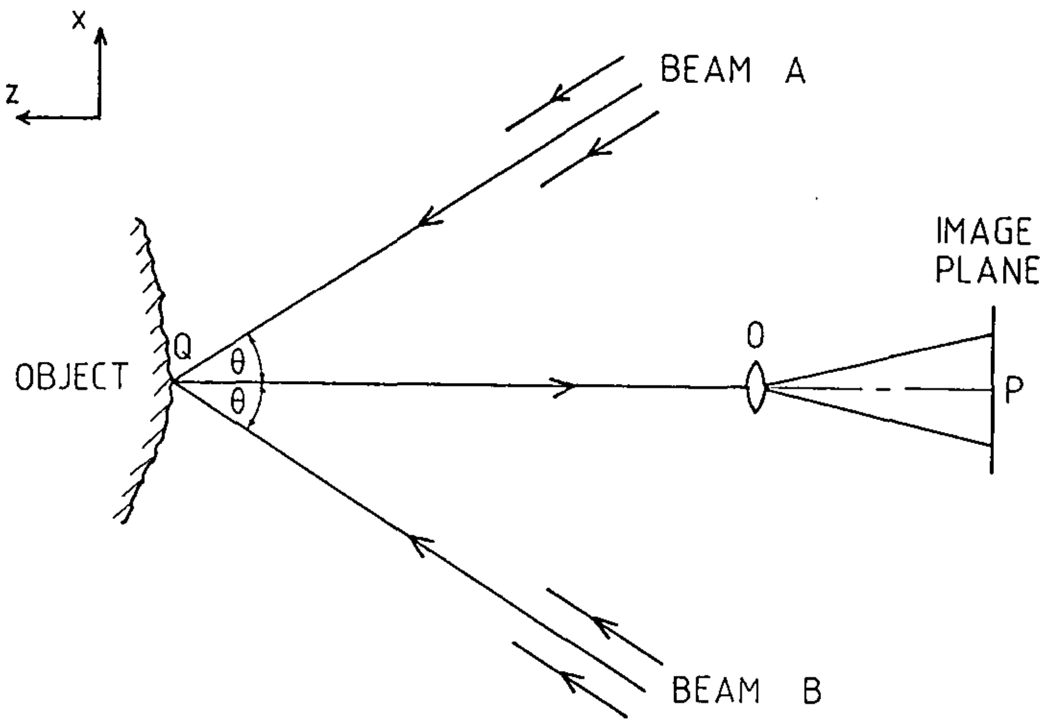

Figure 3: In-plane sensitive interferometer

analysis can be used to show that $\Gamma = 2\sin\theta$ and $\mathbf{n} = \hat{\mathbf{y}}$. An alternative arrangement uses beam A at $+\theta$ in the xz plane and beam B at $+\theta$ (or $-\theta$) in the yz plane, which gives the same fringe sensitivity factor but a sensitivity vector $\mathbf{n} = \hat{\mathbf{x}} - \hat{\mathbf{y}}$ (or $\mathbf{n} = \hat{\mathbf{x}} + \hat{\mathbf{y}}$), i.e. at +45° or -45° to the x-axis in the xy plane respectively. This is known as the 'orthogonal arrangement' (see reference 69, p.161).

The sensitivity vector **n** for all the in-plane configurations described above lies in the plane of the illuminating wavefront propagation vectors and is perpendicular to their bisector (the z axis in Figure 3). If the object surface lies in the xy plane then this gives pure in-plane sensitivity; however if the surface is not planar then this configuration will inevitably give some out-of-plane sensitivity at points where the surface normal is not parallel to the z axis. The values of Γ and **n** are only constant across the object for the case of plane wavefronts, requiring collimated illuminating beams. With spherical wavefronts the sensitivity factor will decrease in magnitude as the radial distance increases from the intersection of the propagation vectors, and the sensitivity vector will rotate to give some z-sensitivity. These variations can be minimised by diverging the beams from a remote point so that the angle subtended at the object is small. It should be noted that $\Delta\psi$ is independent of the viewing direction in equation (3.7), so that the only effect of viewing obliquely is to change the perspective of the image.

3.1.3 Three-dimensional measurements

Three-dimensional measurements can be made by combining one out-of-plane and two in-plane sensitive interferometer configurations. This is shown schematically in Figure 4, where the three different illumination geometries are shown relative to the same object and imaging system. The three interferometers can be used to determine the x-, y- and z-components of the vibration, which can be summed to give the total three-dimensional vibration vector at any point in the image plane:

$$\boldsymbol{a} = a_x + a_y + a_z \tag{3.8}$$

This vector addition requires knowledge of the relative phases of the orthogonal vibration components (i.e. the sign of each component of **a**). This phase information is lost in the time-averaging process (see Appendix A, equation A.14), but can be determined by other means as discussed in section 3.3.2. However, even without the phase information it is still possible to determine the total amplitude from the measured component amplitudes:

$$|\boldsymbol{a}| = \sqrt{|a_x|^2 + |a_y|^2 + |a_z|^2} \tag{3.9}$$

In producing a focused image, the viewing lens transforms the three-dimensional object space onto a two-dimensional image, hence the three-dimensional displacement **d**(x,y,z) is represented as **d**(x′,y′). The inverse transformation from **d**(x′,y′) to **d**(x,y,z) requires knowledge of the object shape, which can be measured with the same apparatus using ESPI contouring techniques[81,85]. It should also be noted that the global x-, y- and z-components measured by the ESPI system only

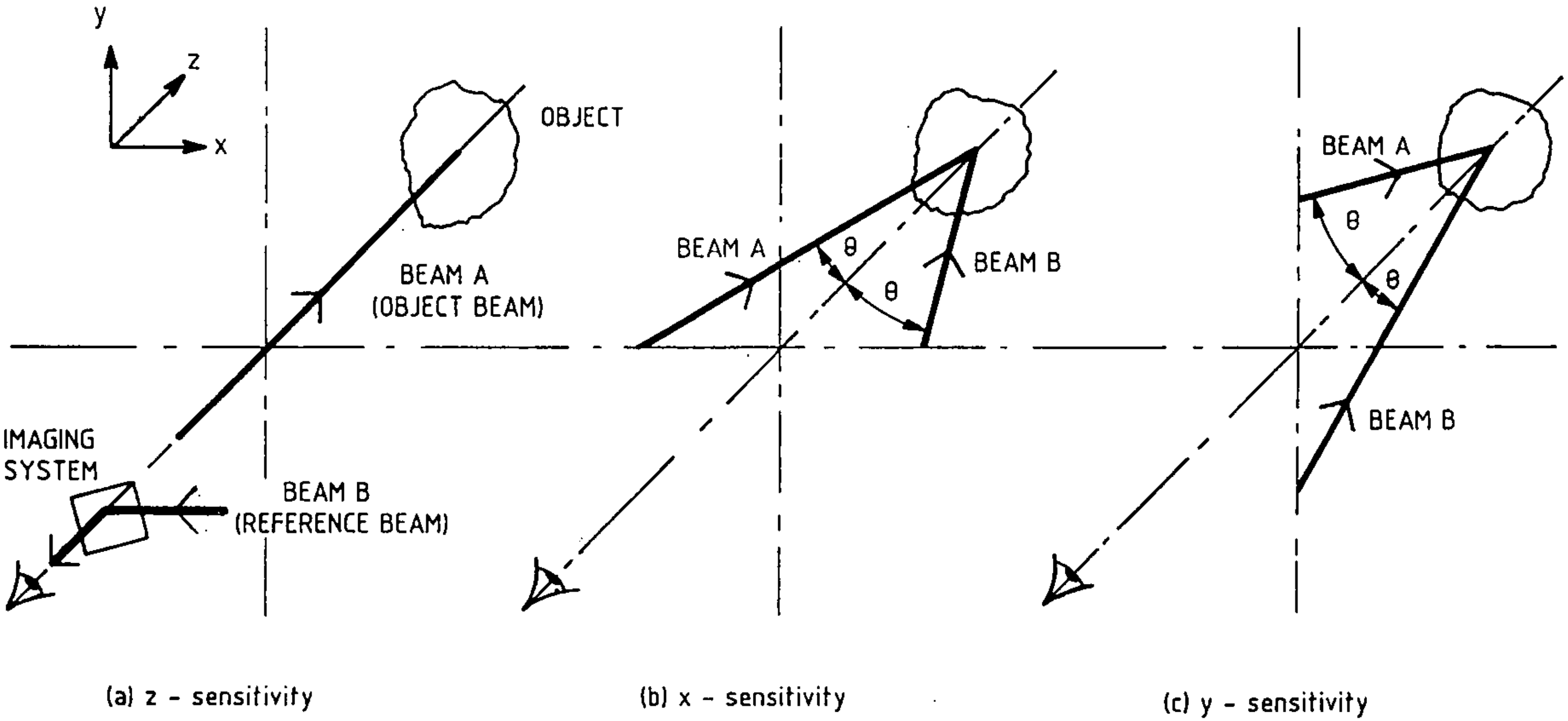

Figure 4: Illumination geometries for three-dimensional ESPI

correspond directly to in-plane and out-of-plane components at the object when the local surface normal is parallel to the z-axis. In general, calculation of the local in-plane and out-of-plane components requires a mathematical transformation involving the orientation of the surface normal to the global coordinate axes at all points in the image. These transformations can be performed either by using *a priori* knowledge of the object shape[33,41], or by measuring it as mentioned above.

3.2 EXPERIMENTAL APPARATUS

During the course of this research several different experimental rigs have been used, with many variations according to the object being studied, the type of information that was required, the availability of equipment, and the current state of knowledge and technology. The following section describes the basic system used for studying three-dimensional time-averaged vibrations and the various features that have been added to it, whilst section 3.2.2 describes the differences of the pulsed ESPI system.

3.2.1 Time-average ESPI

The basic system used for three-dimensional time-averaged ESPI is shown schematically in Figure 5. Time-average ESPI is used to observe steady-state vibrations, and under steady-state conditions it is possible to record sequentially the three images required for three-dimensional measurements. This is done by arranging the optics so as to enable any of the illumination geometries shown in Figure 4 to be used with the same imaging system shown in the dashed box in Figure 5, and switching between them for the different recordings. This method is economical of both laser power and optical components, as the laser beam only ever needs to be split two ways. If the object can be conveniently rotated about the z-axis without disturbing the conditions of vibration then only two illumination geometries are required, as observing with an x-sensitive system after a 90° rotation is equivalent to observing with a y-sensitive system. This reduces the number of components required and enables all the illumination to be kept in a horizontal plane.

The laser used for most of the time-average studies was a continuous wave argon ion laser, operating with an intra-cavity etalon to give single frequency output at a wavelength $\lambda = 0.514$ µm and a maximum power of approximately 1 Watt. The power can be varied according to the experimental requirements either by the laser controls or by using a variable attenuator. The x- and y-sensitive interferometers require equal beam intensities, whereas the z-sensitive interferometer requires variable object:reference beam intensity ratio in order to balance the wavefronts at the image plane; hence a means is required for variable beam splitting. This has been achieved very simply by using a removable mirror on a kinematic mount to direct the incident beam to one of two beam-splitters for the two interferometers. A 50:50 ratio intensity splitting cube is used for the x-sensitive interferometer, whilst the z-sensitive interferometer uses a cube or wedge of approximately 90:10 object:reference beam intensity ratio, with a further variable attenuator in the reference beam for intensity balancing at the image plane.

Two methods have been used for producing the required illumination geometries. The first is to use steering mirrors to guide the unexpanded laser beams, and microscope objective lenses to expand them through pinhole spatial filters to produce diverging spherical wavefronts. The second method is to couple the laser beams into single-mode optical fibres, which both guide the light to where it is required and produce a smooth, spatially-filtered diverging output. In the latter case the divergence angle is determined by the numerical aperture of the fibre, but can be varied by using converging or diverging lenses. The principal advantage of using optical fibres is that they minimise the need for time-consuming re-alignment, and create a flexible system in which the illumination geometry can be altered quickly and simply. However they do require very precise alignment to

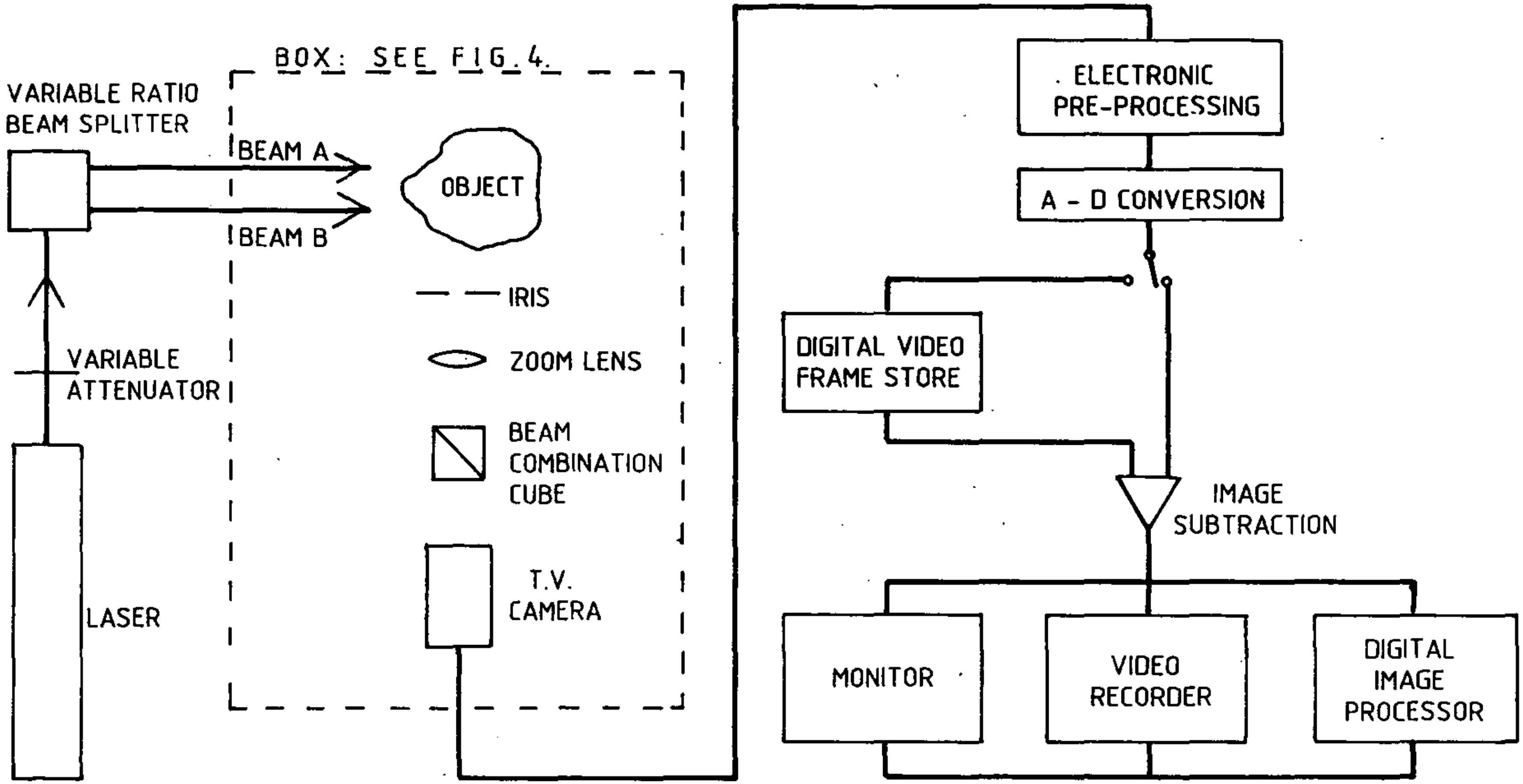

Figure 5: Schematic arrangement for three-dimensional ESPI

couple the laser beam into the core (typically 4 μm diameter), and even then it is difficult to achieve a coupling efficiency of more than 50% in practice.

The beam combination cube is used to introduce the reference beam in the z-sensitive interferometer so that it is conjugate with the imaged object beam. The reference beam can be either smooth or speckled at the image plane, but a smooth wavefront gives better quality results and was used whenever possible.[105] The object beam is diverged from a point adjacent to the imaging lens so that the error due to angular misalignment from the observation axis is minimised. The cube does not affect the operation of the x-sensitive interferometer. For objects up to 150 mm diameter the illuminating beams could be collimated by reflecting the diverging beams from concave mirrors, but for larger objects the beams were diverged from a suitable distance to subtend a small angle at the object (<10° in every case).

The imaging system uses a variable aperture zoom lens. The zoom facility enables different sizes and portions of object to be viewed easily, whilst the aperture controls the object beam intensity and speckle size in the image plane. The image is focused onto the sensor of a chalnicon or CCD type video camera, which records 25 image frames per second (each frame comprising two scanned fields). The electronic analogue video signal from the camera is first band-pass filtered to remove the d.c. and high frequency components, then rectified, then converted to a digital signal (typically 512x512x6 bit resolution). In most cases the subtraction process as described in Appendix A.3 is used to improve the fringe visibility. This is done by grabbing a reference frame into a solid-state memory and digitally subtracting all subsequent frames from it. The reference frame can be grabbed or replaced at any time, and the image subtraction occurs in real time (i.e. at video rate). For all the time-average studies, the electronic pre-processing and image subtraction were performed by a FM-60 frame memory unit, manufactured by FOR-A and modified by West* at Loughborough to include an additional filter.

The output signal from the subtraction unit is displayed on a standard video monitor, and can also be recorded on magnetic tape for storage or subsequent

* West, T.C., Loughborough University of Technology, UK, private communication.

analysis. Hard copy output can be obtained from a video printer, or by photographing images from a monitor screen. If it is required to post-process the results then the video images can be input to a digital image processor. This enables certain processes to be performed such as contrast stretching, thresholding, smoothing etc. to alter the appearance of the fringe pattern. Image processing will be considered in more detail in section 3.3.

One method which is particularly useful for enhancing the appearance of time-average vibration fringes is speckle averaging, and this has been applied for some of the studies undertaken. In a single time-averaged ESPI fringe pattern the fringes are loci of constant speckle contrast,[69] so that the bright fringes contain individual speckles having a range of intensities from bright through to dark. As the phase of the incident illumination is varied, the intensity of each speckle cycles between dark and a maximum value determined by the fringe function. Averaging over a number of images having different illumination phase converts the variations in contrast to variations in intensity, and has the effect of smoothing out the high frequency speckle noise. The averaging process also decreases the maximum intensity, but this can be compensated by contrast stretching or normalizing the grey levels of the speckle-averaged image. Different methods of varying the illumination phase have been studied by Montgomery[104]. In the apparatus described above it has been achieved by either rotating a ground glass diffuser plate in one of the object beams or, in the case of fibre optic illumination, slowly translating the output end of the fibre by means of a motorised translation stage.

One example of a time-averaging rig used during this study is shown in Figure 6. This system has x- and z-sensitive interferometer configurations and uses an Ealing Vidispec unit for the imaging system, but with an external argon ion laser source. Illumination for the x-sensitive (in-plane) interferometer is labelled on the transparent overlay, and is via two single mode optical fibres at illumination angle $\theta=30°$. Positioning the removable mirror converts the system to z-sensitivity (out-of-plane), which utilises the reference beam path length compensator and beam

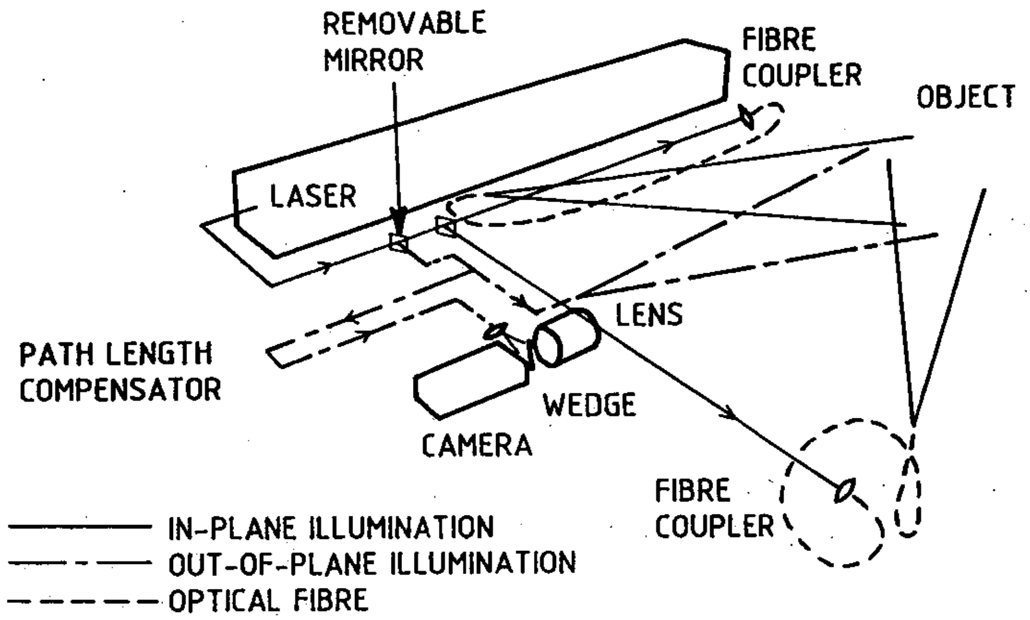
REMOVABLE MIRROR
FIBRE COUPLER
OBJECT
LASER
LENS
PATH LENGTH COMPENSATOR
WEDGE
CAMERA
FIBRE COUPLER
IN-PLANE ILLUMINATION
OUT-OF-PLANE ILLUMINATION
OPTICAL FIBRE

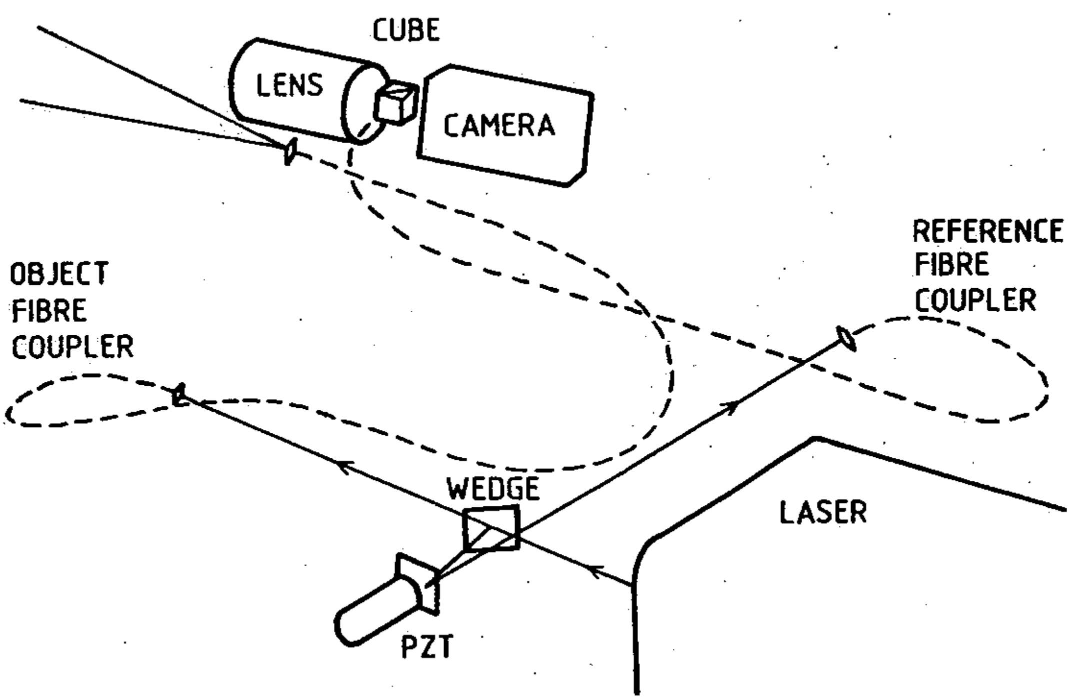
CUBE
LENS
CAMERA
REFERENCE FIBRE COUPLER
OBJECT FIBRE COUPLER
WEDGE
LASER
PZT

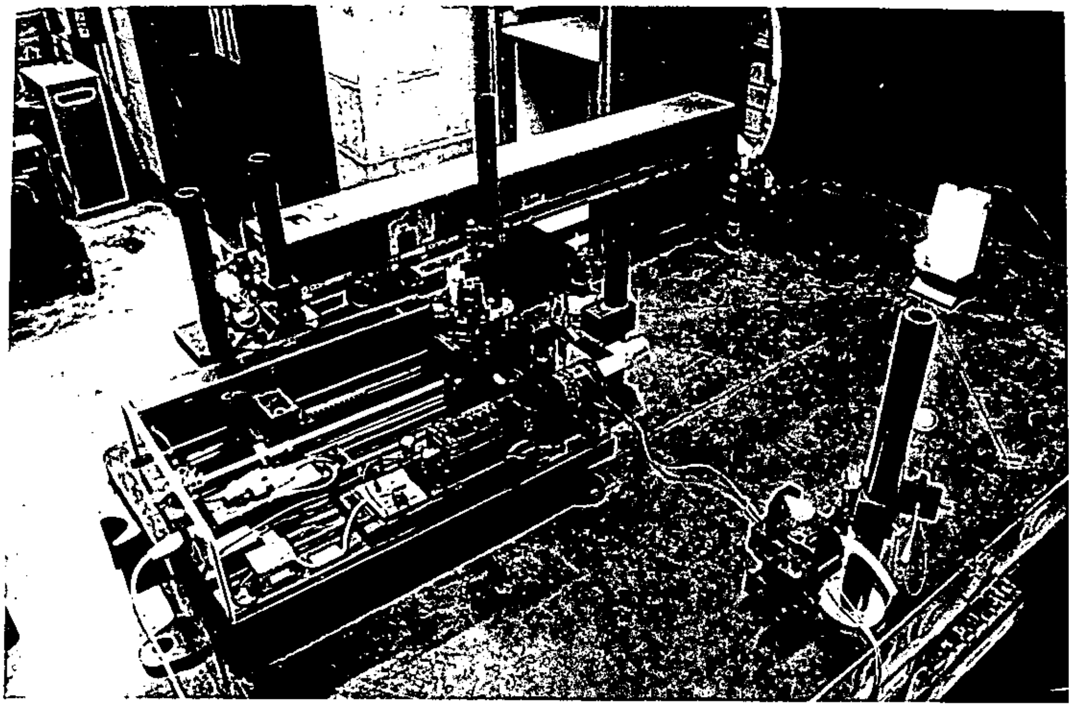

Figure 6: Experimental rig for time-average ESPI

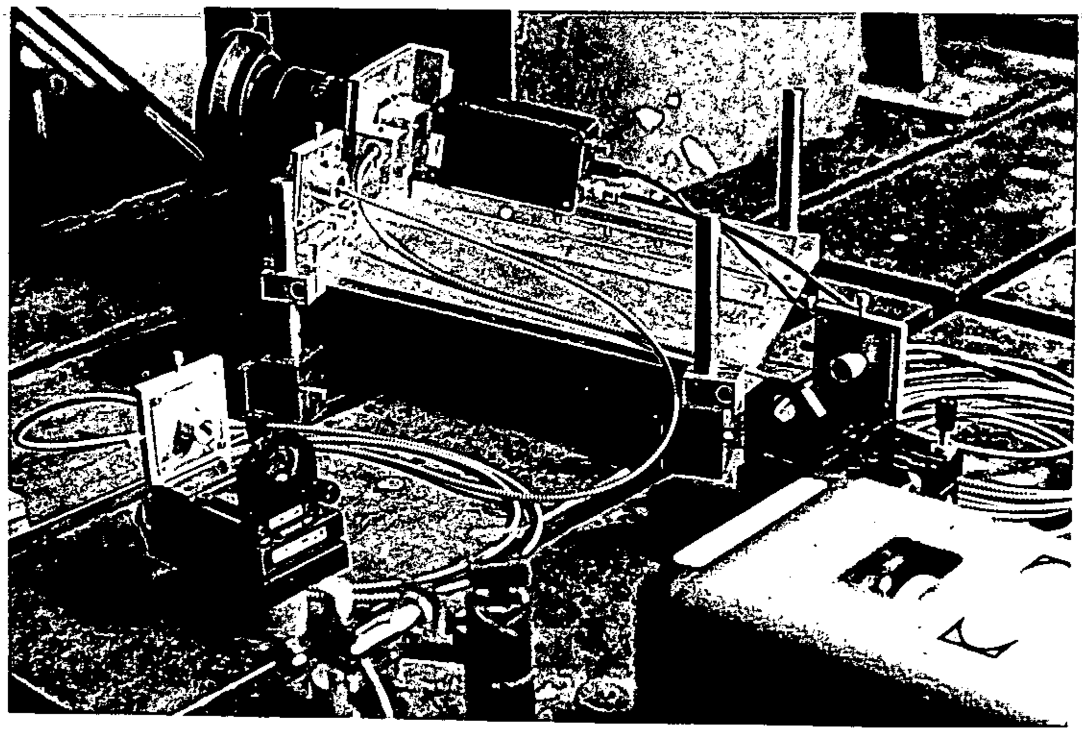

Figure 7: Fibre-optic ESPI head

diffuser plate which can be used for speckle averaging. The object shown in the figure is the cantilever beam which is studied in section 4.1.1.

Subsequently a more versatile fibre-optic ESPI head has been developed, primarily for out-of-plane measurements, as shown in Figure 7 . This uses two 'LDS' armoured single mode polarisation-preserving fibres* (manufactured by York VSOP) with built-in coupling lenses at the input and diverging lenses at the output. The input ends are positioned adjacent to the laser, and the beam is coupled into them via a fixed beam-splitter, so that the output ends can be moved around without having to alter any alignment. A self-contained ESPI head has been manufactured containing a zoom lens, beam combination cube and CCD video camera, with fittings enabling the fibre output ends to be rapidly attached as object and reference beams. The reference fibre is approximately four metres longer than the object fibre to match the path lengths to within the laser coherence length when viewing objects at up to three metres distance (allowing for refractive index ~1.5 in the fibre). However with equal length fibres the same system could be used as an in-plane interferometer. Reference beam attenuation (for intensity matching) is easily achieved by slight rotation of the fibre input to reduce the coupling efficiency. This system greatly reduces the set-up time when changing viewing directions, as the head can be repositioned and requires no adjustment except for reference beam intensity, lens aperture and focus.

3.2.2 Pulsed ESPI

The introduction of pulsed ESPI into this project arose from the successful development of a twin cavity frequency-doubled Nd:YAG laser specifically designed for pulsed ESPI, in another Loughborough research project. Practical details of the laser and its control circuitry are described in detail elsewhere[106], so only a brief description will be given here.

* N.B. Non polarization-preserving fibres are also satisfactory for this application.

The essential practical difference between pulsed and time-average measurement is that the results of pulsed ESPI are a function of the timing of the laser pulses. Hence in order to produce useful results it is necessary to control the timing of the pulses with respect to the motion of the object being studied. So, in contrast to the 'stand alone' time-average system, the pulsed ESPI system must be linked to the target object by a control circuit. This is shown schematically in Figure 8. In the system shown the object is a plate excited from a frequency generator via an amplifier and a piezoelectric crystal. In this case the same generator output can synchronise the pulse timing. When it is not possible to obtain a synchronised signal directly from source, for example when the object is excited by internal forces, then a suitable signal can usually be obtained from a transducer such as

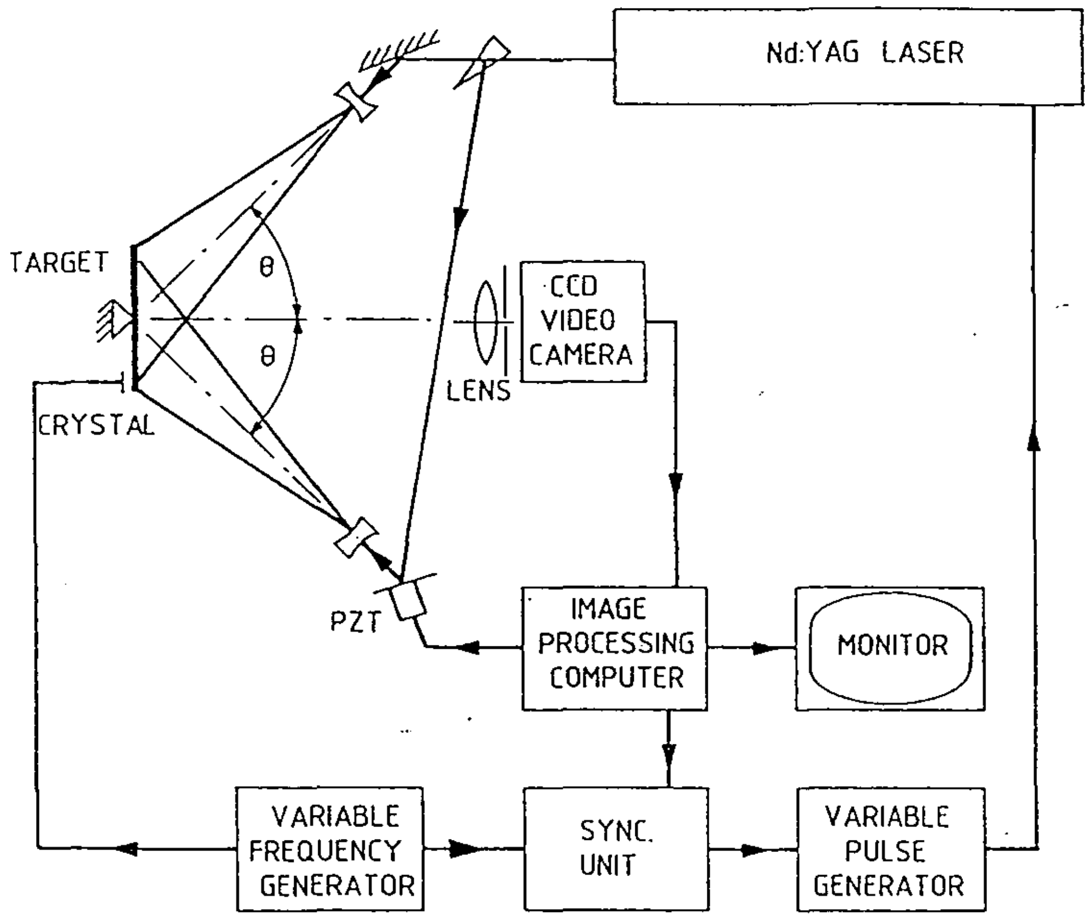

Figure 8: Schematic arrangement for pulsed ESPI

an accelerometer or strain gauge attached to the object. The synchronisation unit is set to detect a particular phase epoch (for example the rising zero-crossing) of the object vibration cycle and triggers a pair of pulse generators, each with variable delay, which in turn trigger the Q-switching of the laser. In this way the laser pulses can be fired at any desired point on the vibration cycle, and this can be monitored using an oscilloscope. Only one pulse generator is required for single-pulse subtraction ESPI, but both are used for double-pulse addition (see Appendix A.4).

The laser itself contains two oscillator cavities, both injection seeded by a common diode laser but with independent Q-switching. This enables it to produce double-pulses from the two cavities which are mutually coherent and have variable timing, the pulse separation being controllable effectively down to zero. The temporal resolution of the system is therefore limited only by the pulse duration, which is in the range 10-20 ns. The laser operates at a repetition rate of 50 pulses or double-pulses per second (European TV field rate), the timing of the pulses within each video frame being controlled by the pulse generators. The output beam paths from the two cavities are aligned to be collinear, and pass through a frequency doubling crystal to produce a visible wavelength of 0.532 μm.

The optical configuration shown in Figure 8 is for in-plane sensitivity, but any or all of the geometries shown in Figure 4 can be used in the same way as for time-averaging. It is not possible to expand the beams using converging lenses because the pulse energy density at the focus would be sufficiently high to ionise the air and degrade the wavefront, so instead the beams are expanded using diverging lenses or diffuser plates. One of the interferometer beams is also reflected from a mirror mounted on a piezoelectric translator (labelled PZT), which enables the optical path length to be varied very precisely for phase determination (see section 3.3.2).

The target is viewed with a CCD camera, and the video signal is output to a personal computer (PC) containing an image processing board which can perform all the necessary filtering, storage, subtraction etc. The camera also sends a synchronising signal via the computer to the synchronisation unit, to ensure that the laser pulses are not fired during the blanking periods of the camera (approximately 1 ms in every 20 ms). In the system used for the reported experiments the PC was linked to a minicomputer having more powerful image processing facilities, which also controlled the PZT via a custom built digital to analogue convertor called a universal asynchronous receiver transmitter (UART). The results from the image processor are output to a video monitor.

A typical experimental system that was used for some of the pulsed studies is shown in Figure 9. (a) shows the laser and ESPI head set up for out-of-plane interferometry. (b) shows the entire apparatus with the laser power supply, control electronics and computer in the background, and an alternative in-plane interferometer set up to the left of the laser. The ESPI head (i.e. camera, lens and combining wedge) is mounted on a plate which can be rotated for either the out-of-plane or in-plane configurations. The target shown in Figure 9(a) is the plate from section 4.2.3, and the video monitor in (b) is showing a result from section 6.1.

In the late stages of the project a fibre-optic delivery system was developed for the Nd:YAG laser as well as the argon laser. Single mode fibres cannot be used for the same reason as converging lenses, because the energy density produced by focusing the pulses into a core of only a few microns diameter would destroy the fibre. This problem was overcome by coupling the laser output directly (i.e. without focusing lenses) into 1000μm diameter single core fibres*, which have sufficiently large cross-sectional area. The large diameter also transmits multiple modes, and therefore gives a speckled rather than a smooth output. This was found to be quite acceptable for object beams (which are diffusely scattered from the object anyway), but for a reference beam it was necessary to pass the output through a fine diffuser plate to reduce the speckle size. This system was successfully demonstrated for both in-plane and out-of-plane vibration measurements, although in the out-of-plane interferometer the support of the reference fibre output was found to be critical to the stability of the fringe pattern.

* N.B. The beam diameter was larger than the fibre diameter.

a

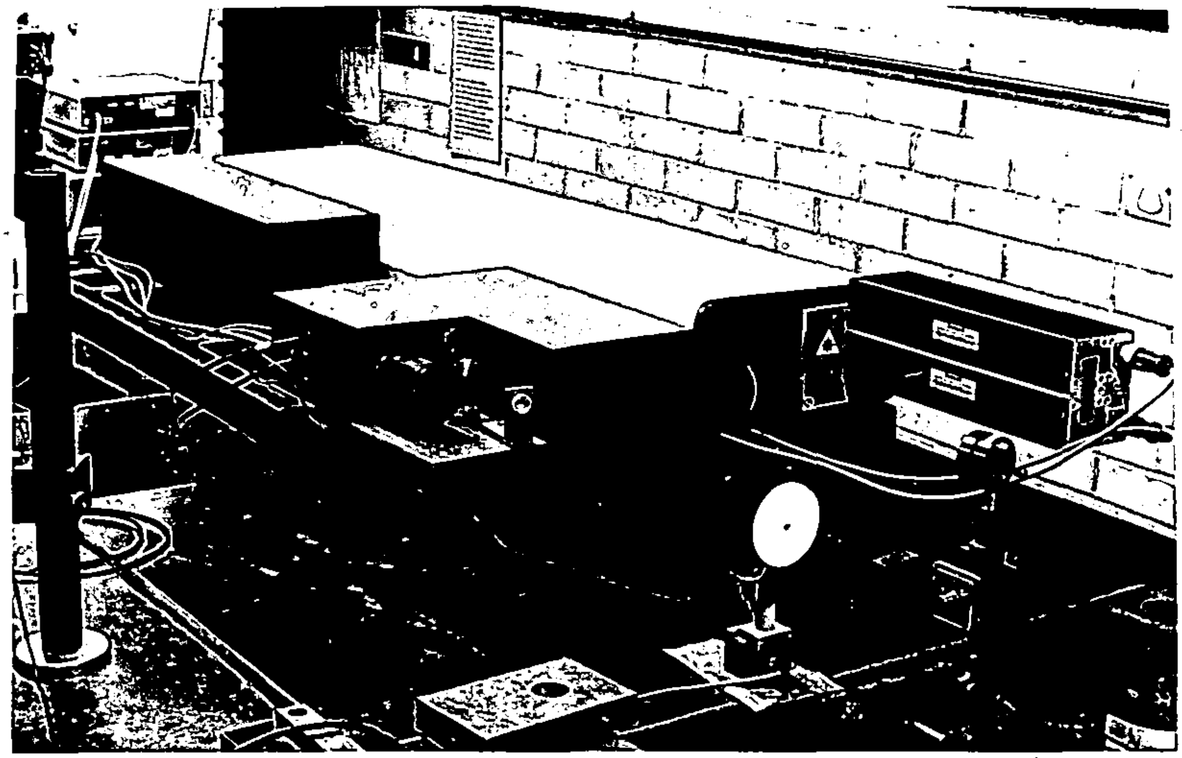

b

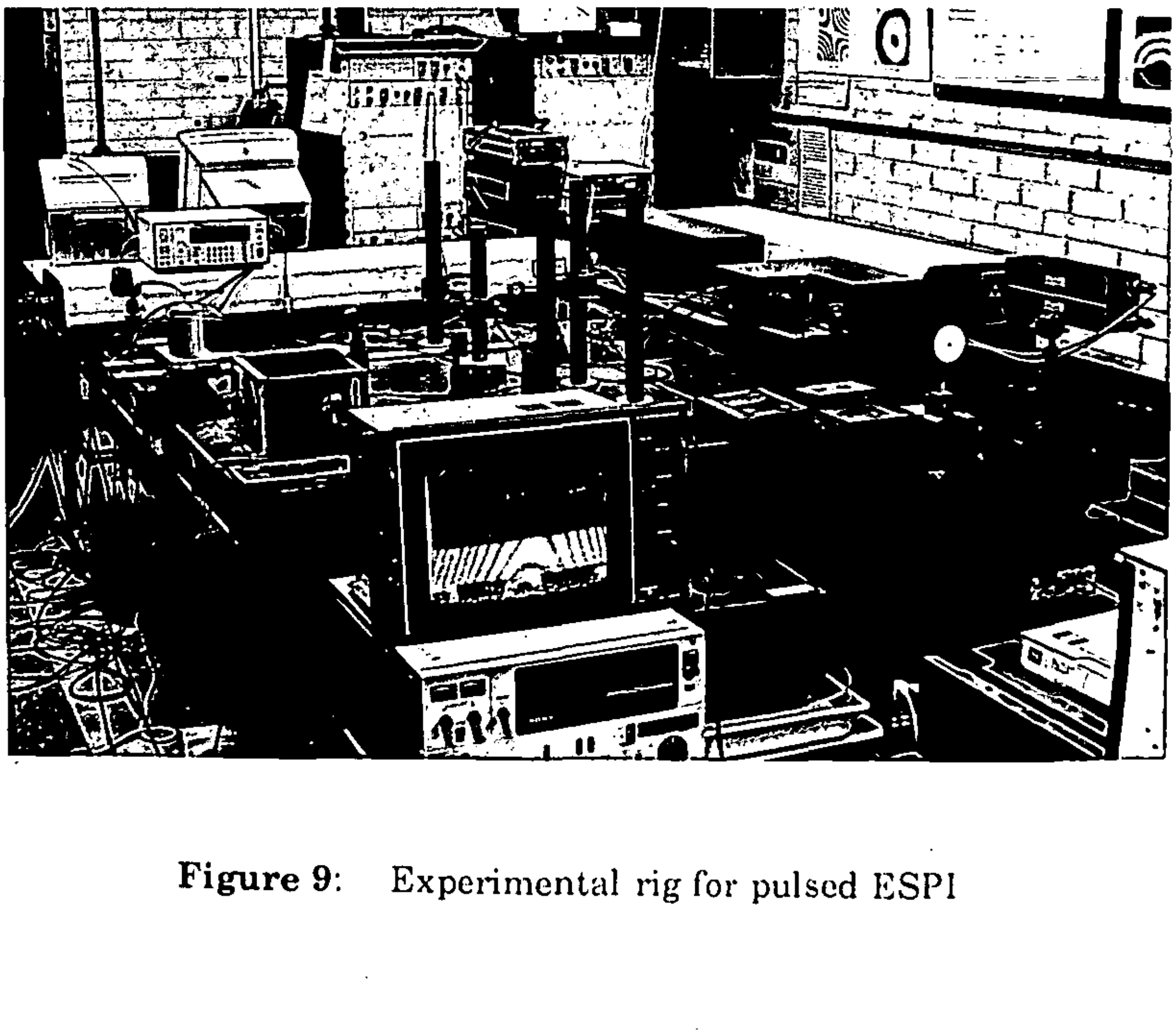

Figure 9: Experimental rig for pulsed ESPI

3.3 IMAGE PROCESSING AND FRINGE ANALYSIS

Fringe patterns such as those produced by ESPI contain quantitative information about the deformation of the observed object, but it is often desirable to present that information in a different form (for example numerical values of displacement). The process of manipulating the fringe patterns to extract or deduce such information is called fringe analysis. This is generally a computationally intensive process because of the large quantity of data (typically 512×512 data points or 'pixels' per image), and as such is much better suited to solution by a computer than by manual methods. However in engineering situations fringe patterns typically have several features which make automatic analysis very difficult, and these usually require image processing and arithmetic routines as part of the analysis. A methodology for tackling these problems and suitable computer hardware and software have been developed at Loughborough and used for this research. The computer system used for most of the results comprises a Kontron image processor hosted by a DEC Microvax II minicomputer, and has been described in detail by Kerr and Tyrer[116]. Features which are relevant to this study are outlined in the following sections.

3.3.1 Filtering

One problem inherent with ESPI is that the image as recorded at the video camera contains random noise due to the resolved speckles. This means that the fringes are identified by loci of constant contrast, having constant mean intensity (averaged over a significant number of speckles) but a large variance. Since the fringe pattern is represented in the computer by a matrix of pixels whose digital value is proportional to intensity, adjacent pixels on the same fringe may have widely differing values, so the computer cannot generally track fringes as loci of local maxima unless the variance is greatly reduced. With time-averaging the variance can be reduced by speckle averaging (section 3.2.1), but with pulsed ESPI it must be achieved by post-processing of speckled images. Several methods can be used to smooth images in an image processor. One simple method is neighbourhood averaging in the spatial domain, where the value of each pixel is replaced by a weighted average of the intensity values within a surrounding matrix of pixels. The degree of smoothing can be controlled by varying the size of the matrix and the number of passes, and the optimum combination depends on the fringe spacing. A more complex alternative method is to transform the image into the frequency domain, typically by applying a Fourier transform, and to filter out the high frequencies which contain the speckle noise whilst leaving the lower frequency fringe information. This requires much more computation, but using a fast Fourier transform (FFT) algorithm with a fast processor enables it to be performed in an acceptable time (<1 s). The relative performance of different filters has been studied by Moore[117], and Fourier filtering has been found to be the most effective for general application.

3.3.2 Phase determination

A second problem with unprocessed fringe patterns is that they contain a directional ambiguity, because it is not possible to tell directly whether a given fringe corresponds to positive or negative displacement. This information is not always necessary for qualitative observations, but it can be important for understanding the object motion and is also necessary for correct determination of three-dimensional vectors (see section 3.1.3).

The process of time-averaging removes the phase information from the fringe function (see Appendix A, equation A.14). However it is possible to map out regions of constant phase as well as amplitude by using the method of phase modulation[74,75]. If one of the interferometer beams is modulated such that its phase varies at the same frequency as the object vibration, then this has the effect of shifting the Bessel function fringes of equation (A.14), so that the zero order fringe maps the locus of points at which the phase shift due to the object vibration is equal and opposite to that due to the beam modulation. Hence by varying the phase and amplitude of the applied modulation it is possible to measure phase across the image.

With pulsed ESPI the phase information is retained in the fringe function (see for example Appendix A, equation (A.17)) but still needs to be extracted. The most common way of achieving this is to use a temporal phase-stepping method whereby a set of fringe patterns are recorded with phase shifts introduced into one of the interferometer beams. These fringe patterns can then be solved pixel by pixel as simultaneous equations to determine the optical phase, and hence deduce the mechanical phase, which can be displayed as a map of phase values in modulo 2π. This then requires unwrapping to remove the 2π discontinuities and give continuous phase values. Many different algorithms have been developed for extracting phase, which vary in the number of images required, the magnitude of the phase steps and the method of solution; these have been reviewed by Creath[86]. The method used for all the results presented here is the single phase step (SPS) technique developed by Kerr et al[109] at Loughborough, because it only requires two phase-stepped images which can be recorded in 0.08 s. This minimises the errors caused by environmental changes or instabilities during the total recording time, which is important for vibration analysis in engineering situations.

3.3.3 Computer programs

One of the aims of ESPI research in general is to create a system which is as automated as possible, requiring a minimum of user intervention. The pulsed ESPI system described above goes some way towards achieving this by linking the laser-object synchronisation, the phase stepping and the fringe analysis through a central computer. The pulse timing is currently controlled manually via external pulse generators, although it is hoped to incorporate this within the computer in the future. The phase stepping and fringe analysis are controlled by software programs written in Fortran. Most of the software used for the results presented here is based on programs and subroutines originally written by Kerr and Moore at Loughborough. Where necessary for particular applications, these have been further modified by Mendoza Santoyo and the author. The procedure for calculating quantitative data from the pulsed ESPI system is outlined below, mentioning important features of the programs used.

Pulsed subtraction or double-pulsed addition fringes can be viewed on a monitor in real time, and these are used to identify features of interest (typically a resonant vibration mode) and to optimise the fringe quality. Having obtained the required fringe pattern, the single phase step program is run. This grabs an initial fringe pattern into an image memory, sends a signal via the UART to the PZT to shift the phase by $\pi/2$, then grabs the phase-stepped image into a second memory. The voltage sent to the PZT is calibrated by program variables according to the PZT sensitivity and the optical geometry of the system. Other variables control the time delay between grabbing the two images. The images are then grey-level normalised to optimise fringe visibility, and a two-dimensional FFT is performed to obtain the Fourier power spectrum (these operations are performed using standard routines from within the image processor). The operator inspects the power spectrum and specifies a mask filter of suitable size and shape to retain the fringe information which is contained in the central peaks, whilst excluding the higher frequency components further from the centre. In most cases a symmetrically centred circular aperture is used for the mask as this is simple to generate and usually effective. A second program uses this mask to filter the images in the frequency domain, producing smooth fringe patterns. A third program then applies the single phase step algorithm to each pixel in turn, using the intensity values from the two smoothed fringe patterns to produce the modulo 2π phase map.

The final stage is unwrapping the phase map and displaying the results. Again a number of approaches are possible, details of which have been explained and discussed by Osten[87]. Various routines have been used in this work but all involve unwrapping along a vector, detecting the phase discontinuities and adding or subtracting 2π to the phase as appropriate. Choice of starting point and direction of vectors depends on the fringe pattern, but a typical routine would unwrap down the left edge first and then take horizontal vectors from this edge. If the discontinuities break down in some regions of the phase map then care must be taken in choosing the unwrapping order and choice of the discontinuity detection parameter to avoid propagating errors across the image. The result is a matrix of relative phase values, which can be converted to absolute values by referencing to a stationary point defined by the operator. These phase values can be converted to displacement vectors by substituting into equation (3.1) with the fringe sensitivity factors and sensitivity vectors as given in sections 3.1.1 and 3.1.2. For out-of-plane displacements the results can be plotted as an isometric wire-frame plot which can be rotated and viewed from different angles. For in-plane displacements the x- and y-components are added vectorially at a specified grid of points and plotted as a matrix of two-dimensional vectors. Numerical values of x-, y- and z-displacement components can also be output as a file and used to calculate three-dimensional vector displacements if required.

4. DEMONSTRATION OF EXPERIMENTAL TECHNIQUES

This chapter presents the results of experiments which were undertaken to demonstrate that the techniques and experimental apparatus described in Chapter 3 could measure vibrations in three dimensions. All of the experimental techniques described in sections 3.2 and 3.3 are demonstrated, including out-of-plane and in-plane measurements using both time-averaged and pulsed interferometry. Simple geometrical structures have been chosen for the test objects, as they enable particular types of motion to be isolated and studied separately. Three types of object have been studied: a beam, a thin plate and a thick cylinder. These represent one-, two- and three-dimensional structures respectively, and demonstrate corresponding complexities of vibration. Where possible the experimental results are compared with theoretical solutions or published results from previous studies.

4.1 CANTILEVER BEAM

In order to test the ability of the experimental system to measure out-of-plane and in-plane vibration components independently, an object was designed which could simultaneously display surfaces undergoing pure out-of-plane and pure in-plane vibrations. This is shown in Figure 10. The object is a 25mm square section hollow aluminium tube, cantilevered at its base. A piezoelectric translator is used to apply a load normal to one surface along an axis 100mm above the base. When a sinusoidally varying voltage is applied to the translator at a frequency well below the fundamental resonance of the system, the beam undergoes forced bending vibrations in a plane parallel to one pair of surfaces and perpendicular to the other pair. Observing in directions 1 and 2 as indicated in Figure 10 should therefore

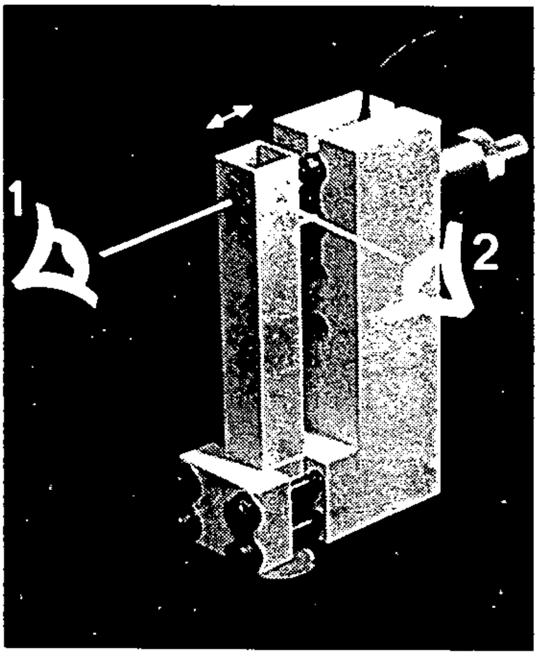

Figure 10: Cantilever beam rig

indicate pure out-of-plane and pure in-plane vibrations respectively. Although this cantilever beam is obviously a three-dimensional structure, the nature of the boundary conditions and the applied load effectively constrain it to be a single degree of freedom system undergoing (for small deflections) uniaxial motion. This therefore represents the case of one-dimensional vibrations.

4.1.1 Time-average analysis

A time-average analysis of the cantilever beam vibrations was performed using the experimental apparatus described in section 3.2.1 and shown in Figure 6. The experimental results are shown in Figure 11. (a) is a live video image of the beam viewed in direction 1 by the ESPI imaging system. Figure 11(b) and (c) are subtracted time-average ESPI fringe patterns (see Appendix A.3) of the beam vibrating at 200 Hz, at applied peak-to-peak voltages of 10 V and 20 V respectively, viewed with the z-sensitive interferometer. Figure 11(d), (e) and (f) are corresponding images viewing in direction 2 with the x-sensitive interferometer, under identical vibration conditions. Maximum displacement profiles are shown adjacent to each fringe pattern. These have been calculated by substituting the zeros of the J_0^2 function into the fringe function (see Appendix A.3, equation A.16) to obtain values of a_n, which are plotted at the centre of each dark fringe. The amplitude a along the axis of the applied load is marked on each plot, and compares well between the corresponding z- and x-measurements in each case.

Viewing in direction 1 with the x-sensitive interferometer gave a bright image with no fringes, proving that the in-plane sensitive interferometer is insensitive to vibrations parallel to the line of sight. Similarly, viewing in direction 2 with the z-sensitive interferometer produced no fringes, indicating insensitivity to vibrations normal to the line of sight. These results demonstrate that the different interferometer configurations do isolate the orthogonal components of vibration as predicted.

4.1.2 Pulsed phase-stepped analysis

The measurements described in section 4.1.1 using the z-sensitive interferometer were subsequently repeated using the pulsed Nd:YAG laser, to demonstrate the technique of phase stepping (see sections 3.3.2 and 3.3.3) on the same object. The experimental system used was the out-of-plane interferometer described in section 3.2.2, and shown in Figure 9(a). Figure 12 shows a set of experimental results from the out-of-plane interferometer. Figure 12(a) is a white light image of the cantilever as seen by the CCD camera. Figure 12(b) is a single pulse subtraction fringe pattern (see Appendix A.4) produced by firing two laser pulses at different points in the vibration cycle, and Figure 12(c) is a similar fringe pattern produced after a phase shift of +90° in the reference beam. These are cosinusoidal fringes and have fairly good visibility, but also contain a high degree of speckle noise. This needs to be filtered out, as discussed in section 3.3.1. The result of applying a fast Fourier transform (FFT) to Figure 12(b) is shown in (d), which is the power spectrum of the fringe pattern. Here the grey-level represents the power content plotted on complex frequency-phase axes with the origin at the centre. It can be seen that this consists of a bright central spot corresponding to the d.c. (zero frequency) term, with two adjacent 'lobes' of medium intensity which contain the low frequency content, surrounded by a fairly random distribution of higher frequencies in the darker region around the outside. The fringe information is contained in the low frequency lobes, whereas the high frequency content is due to the background speckle noise. Therefore removing the high frequency terms whilst retaining the central region should filter out the speckle noise leaving the fringe information intact. This can be done using a circular mask filter with a radius that just encloses the central lobes, as shown in Figure 12(e). Convolving (d) with (e) and performing an inverse FFT produces the filtered fringe pattern shown in Figure 12(f). The same procedure was followed for the phase-stepped fringe pattern (c), and the single phase step (SPS) algorithm[109] was applied to the two filtered patterns to yield the modulo 2π phase map in Figure 12(g). This contains the directional displacement of the cantilever, and unwrapping the phase values along a line to remove the 2π phase discontinuities yields the displaced profile shown in Figure 12(h). This result agrees well with those produced manually in Figure 11, but has been generated automatically.

The effect of using different filtering methods is shown in Figure 13. The circular mask filter used in Figure 12 was chosen for convenience because it is easy to generate. If it is required to be more specific about which frequency components are to be filtered out then a custom mask can be drawn manually using a 'mouse'. The power spectrum is shown again in Figure 13(a), with a custom filter in (b) which fits the central lobes more closely than the circle. The result of using this mask with FFT filtering is shown in (c), with the subsequent phase map in (d) and unwrapped vector displacement plot in (e). It can be seen that extending the filter aperture horizontally has included more horizontal frequency components, giving an appearance of vertical bands. The fringe pattern in Figure 13(f) is the result of using two passes of a 5x5 pixel neighbourhood average filter, which gives the phase map and displacement plot shown in (g) and (h).

All three filters have worked quite effectively in this simple example. For more complicated fringe patterns where the fringe spacing and orientation vary significantly across the image it was found that Fourier filtering was usually more effective than neighbourhood average filtering. The circular mask has been used for all subsequent results as it is quicker to generate than a custom mask and has been found to give acceptable results in most cases.

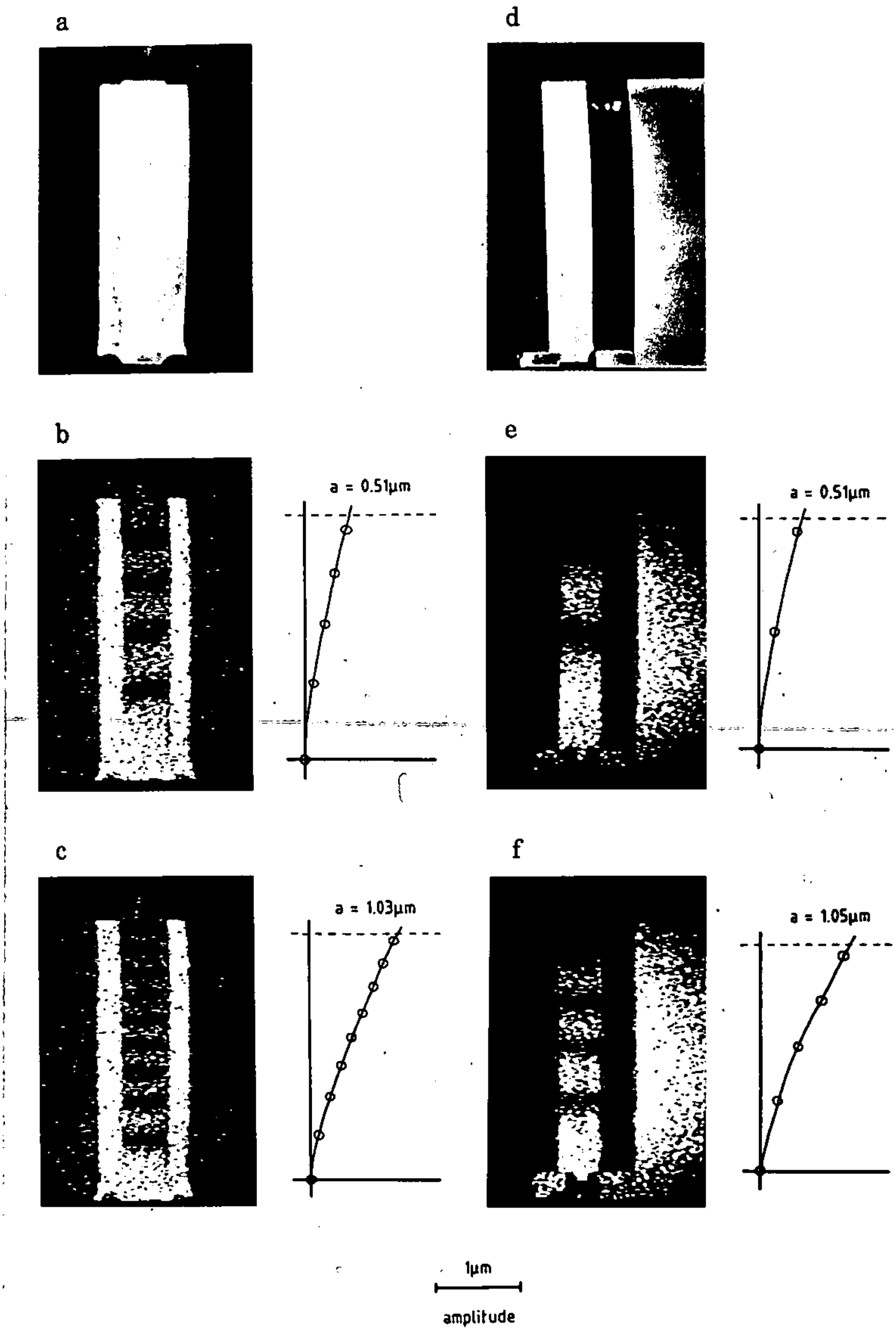

Figure 11: Cantilever beam vibrations

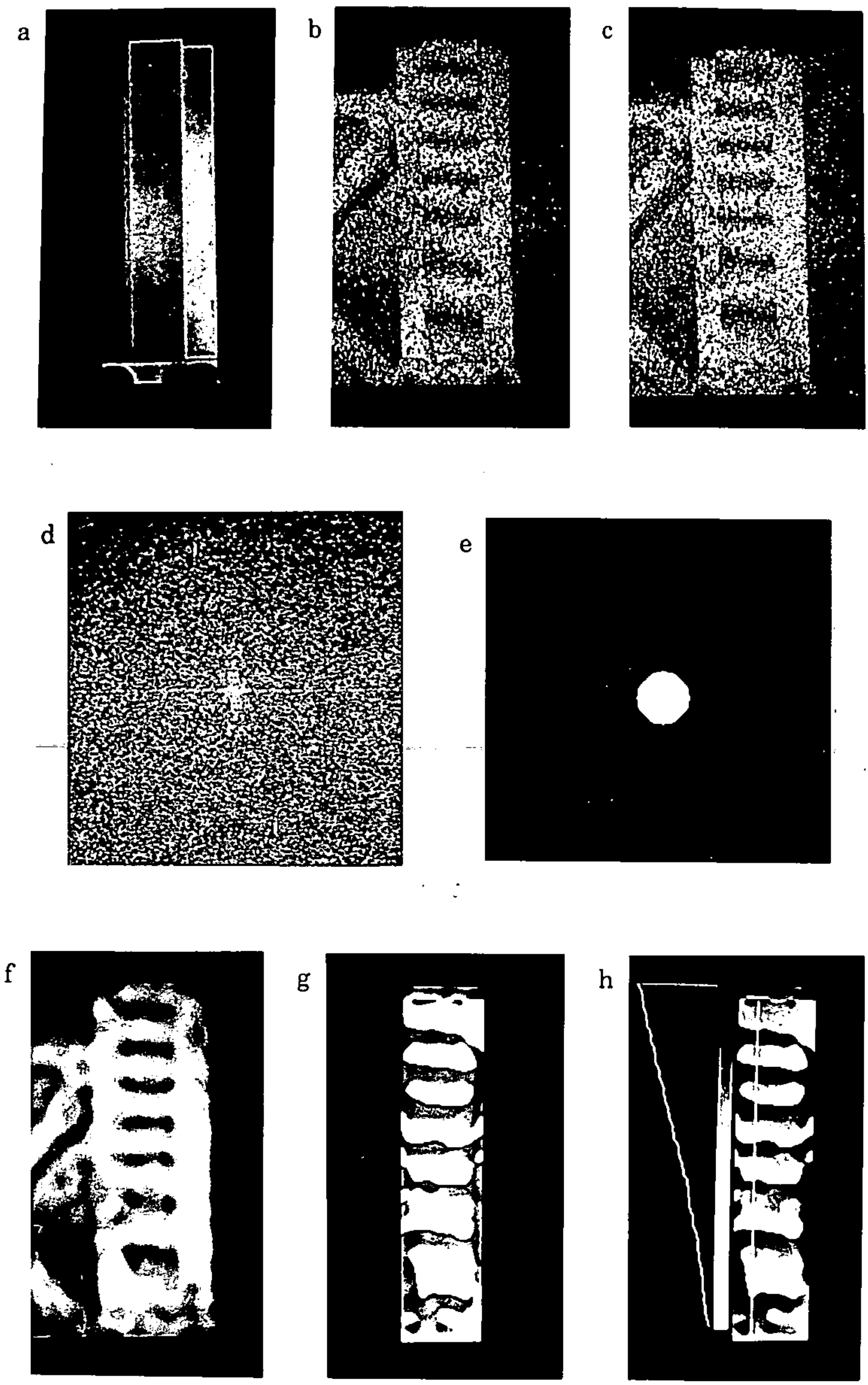

Figure 12: Phase-stepped analysis of cantilever beam vibration using circular-mask Fourier filtering

a b c d e f g h

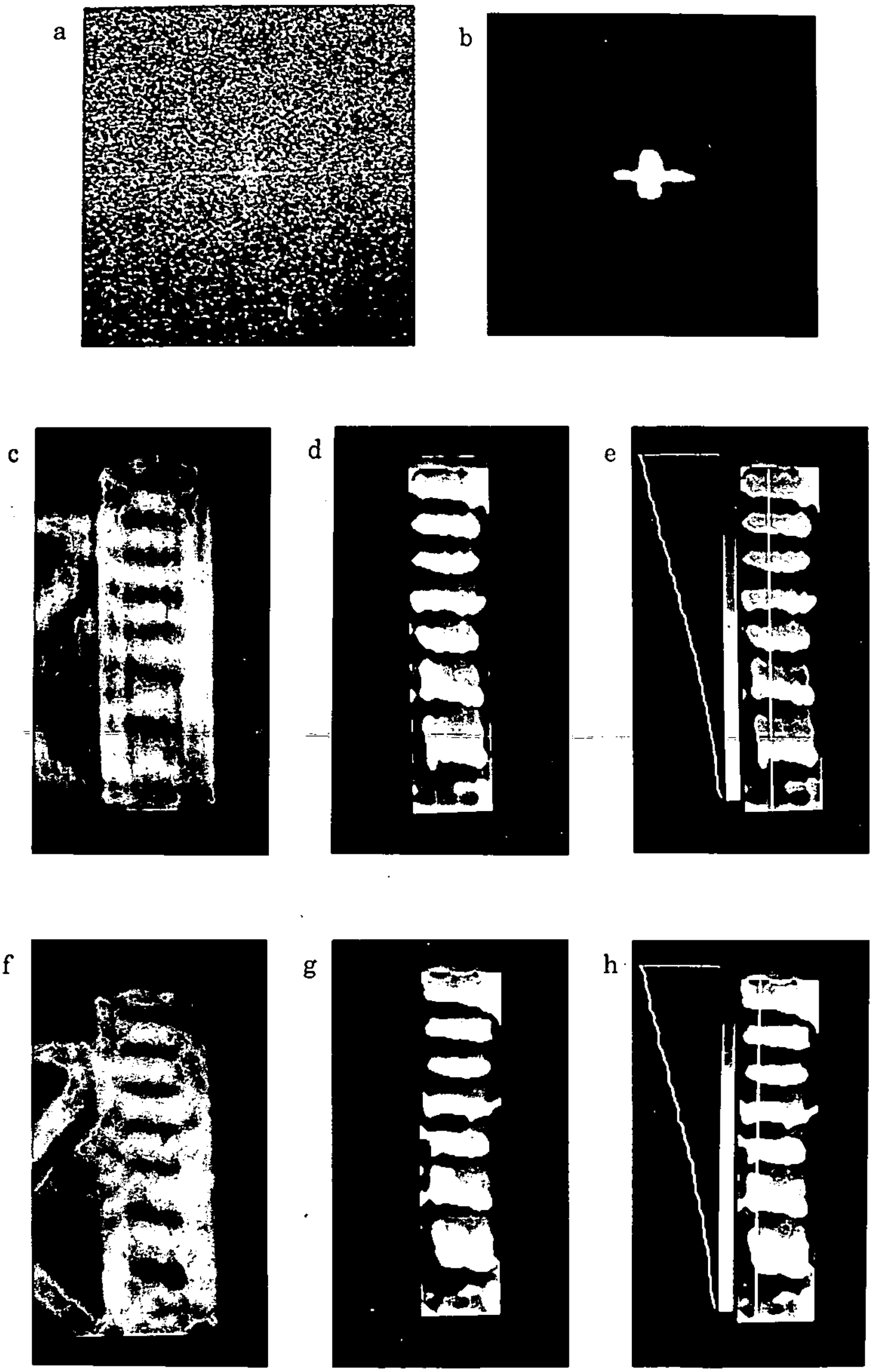

Figure 13: Phase-stepped analysis of cantilever beam vibration using alternative filters

4.2 FLAT PLATES

A plate can be defined as a structure which is symmetrical about a medial plane and in which the thickness (measured perpendicular to that plane) is very small in comparison to the other dimensions. The modes of vibration of plates can be grouped into classes, the principal classes being flexural, extensional and shear (see Appendix C). In flexural vibration the displacement is almost entirely out-of-plane. The vibration vector varies in two spatial dimensions across the plate but only requires one-dimensional (uniaxial) measurement to define it at any given point. This can be achieved using a single z-sensitive interferometer. In extensional and shear vibrations the displacement is almost entirely in-plane. The vibration vector can lie in any direction within the plane of the plate and therefore needs two-dimensional measurement at each point to define it completely. This can be achieved using two interferometers with x- and y-sensitivity. For ideal plates which are thin and flat the out-of-plane and in-plane modes are completely uncoupled, and can therefore be considered separately. Section 4.2.1 considers flexural vibrations of a circular plate, identifying effects of symmetry including degeneracy and combination modes. Sections 4.2.2 and 4.2.3 investigate a square plate, using three-dimensional measurements but concentrating on in-plane modes.

4.2.1 Circular plate

The circular plate which has been studied is made of brass, 6 inches diameter by ⅛ inch thick, constrained only by a central screw attached to a support post, and excited by a piezoelectric crystal attached near the circumference. It was observed with a z-sensitive time-average ESPI system using speckle averaging. Resonant modes were identified by slowly sweeping through a frequency range with sinusoidal excitation whilst viewing real-time subtraction ESPI, and observing amplitude fringes appear and disappear. The peak response frequency for each resonance was located by varying the frequency to obtain the maximum number of fringes for a given excitation level, and monitoring with a digital frequency counter.

For an ideal circular plate (i.e. one which is homogeneous, isotropic and perfectly axisymmetric) the normal flexural modes consist of concentric nodal circles and equi-spaced nodal diameters separating adjacent regions vibrating in antiphase. Each mode can be identified as (n,s), where n and s are the numbers of nodal diameters and circles respectively. Many such modes were observed, and a selection of the results including the first fourteen resonances are shown in Figures 14 to 17. Each is labelled with the measured frequency, and the normal mode or combination of normal modes which best describes the observed pattern. The frequencies are also tabulated in Table I and compared with experimental results obtained by Waller[12] and with theoretical predictions[118].

Some interesting points can be noted from these results about the information obtainable from time-average ESPI. All of the expected modes were observed in practice.

The fringe patterns as presented are spatially continuous, showing the time-averaged vibration amplitude across the entire surface at a single frequency. Although only discrete frequencies have been recorded, during testing it is possible to vary the excitation frequency at will and observe the changing response. In some cases this draws attention to behaviour which is not clear from the still pictures. Certain modes appeared as single resonances; those shown are (2,0), (1,1), (5,0), (8,0) and (5,1). As the frequency increased through resonance the fringe density in the vibrating regions increased to a maximum then decreased again to zero, whilst the nodal (zero order) fringe remained stationary but became narrower as the fringe density increased. The other modes appeared as twin resonances, with the normal mode degenerating into a pair of conjugate modes appearing at slightly different frequencies (the higher frequency conjugate is indicated by an asterisk in Figures 14 to 17). This indicates a degree of non-uniformity in the plate, which could be due to geometric asymmetry, inhomogeneity, anisotropy, localised force input, etc. In these cases the fringe density increased to a maximum, then the nodal pattern was observed to change shape and rotate to a second maximum similar in form to the first, before decaying again. This is shown graphically by the sequence of five fringe patterns for the (3,0) mode. The fringe density increases through the pattern shown at 1130 Hz to the first resonance at 1135 Hz. The second (conjugate) mode occurs at 1140 Hz. At the intermediate frequencies (1136 and 1138 Hz) the motion of the plate comprises significant components of each of the conjugate modes superposed in phasor addition. Because the two components have different nodal positions around the circumference the time-averaged fringe pattern is nodal only at the centre. The phenomenon of the nodal pattern changing position with varying frequency indicates that more than one vibration mode is being excited simultaneously, and has been studied by Stetson[31]. In fact all frequencies will excite components of many modes (see Appendix B.3), but these will not affect the fringe pattern unless the contribution is large enough to be detected by the interferometer. It is likely that the modes which appeared to be single were also degenerate, but with the response of one of the conjugates being negligible. Another phenomenon which was observed in some cases was the nodal pattern oscillating rotationally after sudden changes in frequency; this has been observed and discussed by Rayleigh[119], and is due to the slight difference in frequency between the conjugate modes. It is noticeable that the (4,0) and (7,0) modes appear to be highly distorted from the expected symmetrical patterns. This can be accounted for by the resonances actually being combination modes having contributions from the (1,1) and (2,1) modes respectively. Similar effects have been observed and discussed by Waller[12,13], Grinsted[14] and Molin[28].

Two higher frequency modes, (16,1) and (4,6), have been included to demonstrate the ability to observe fringe patterns at high frequencies (50 kHz) and high nodal densities.

Table I: Resonant modes of centre-pinned circular plate

Diameters n	Circles s	Frequency (Hz)		
		Observed	Waller†	Calculated‡
2	0	487	487	491
3	0	1135	1115	1143
4	0	1950	1997	-
1	1	2005	1943	1918
5	0	3010	3015	-
2	1	3290	3307	3294
6	0	4260	4285	-
3	1	4900	5016	4945
7	0	5650	5698	-
1	2	5800	5698	5594
4	1	6650	6720	-
8	0	7250	7354	-
2	2	7600	7840	7840
5	1	8600	8815	-
		⇓		
16	1	41500	-	-
4	6	50000	-	-

† Experimental frequency ratios for a free circular brass plate from reference 12 are quoted relative to the observed frequency of the (2,0) mode.

‡ Calculated from the equation for a free circular plate given in reference 118 (p.240), using typical values for brass of $E=106\times10^9$ N/m^2, $\rho=8.55\times10^3$ kg/m^3, $\nu=0.324$.

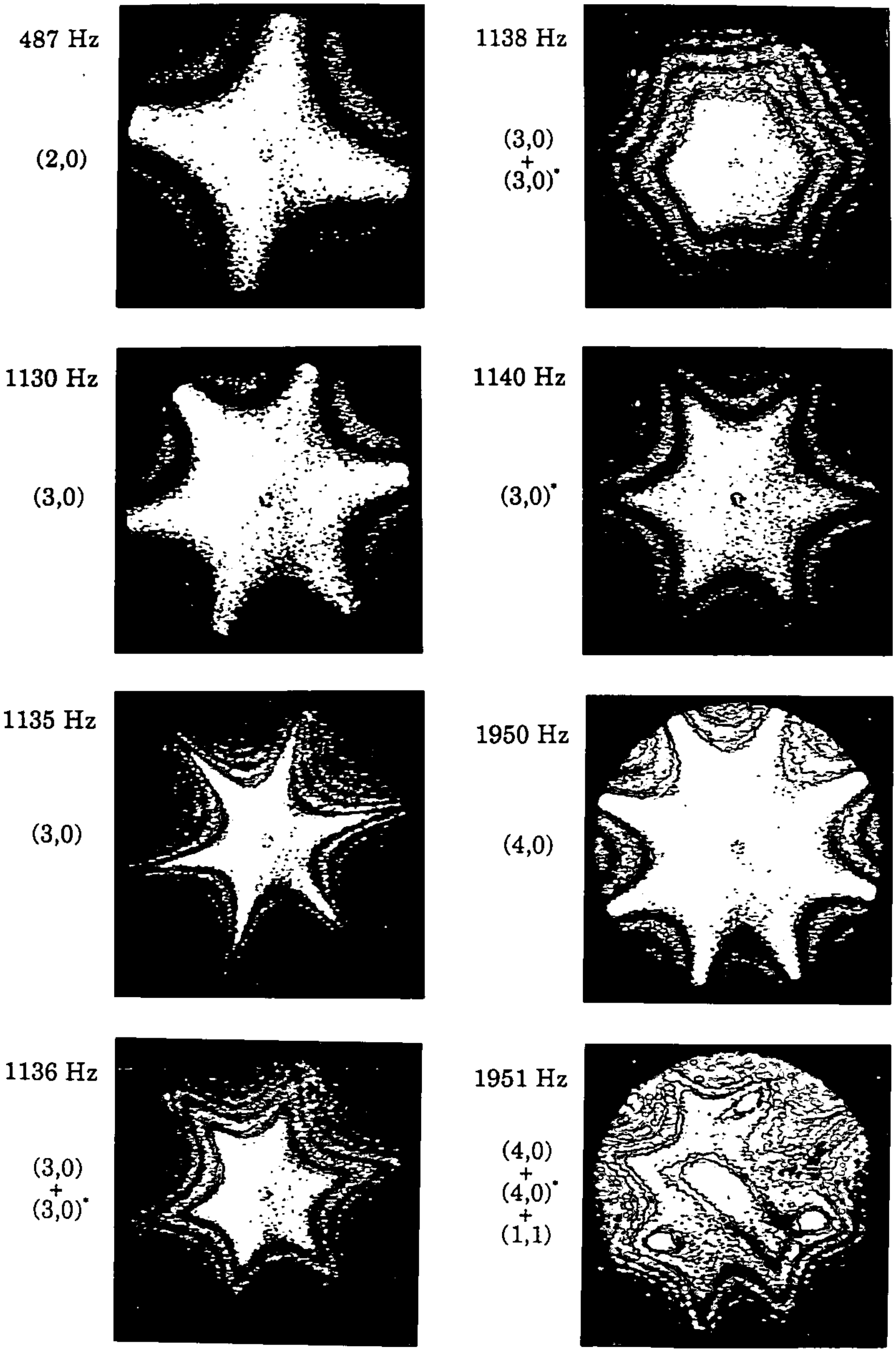

Figure 14: Circular plate flexural modes

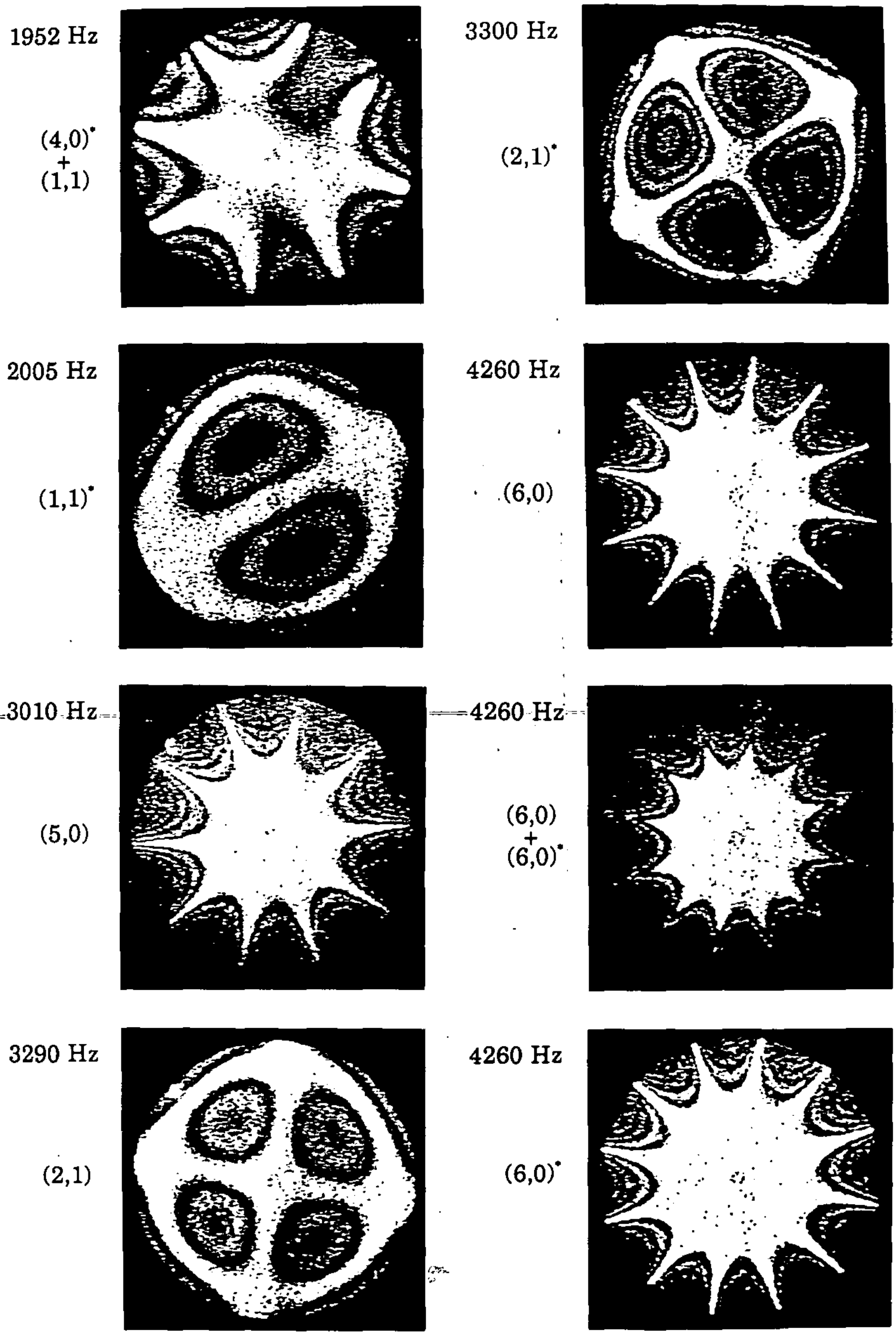

Figure 15: Circular plate flexural modes (continued)

4900 Hz

(3,1)

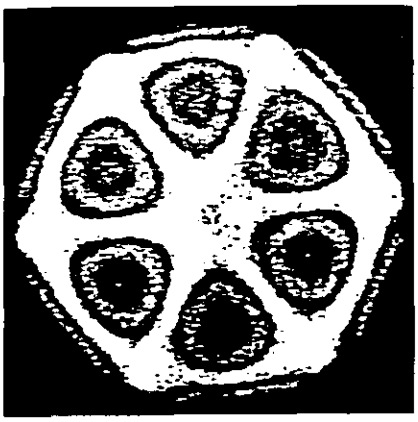

4900 Hz

(3,1) + (3,1)*

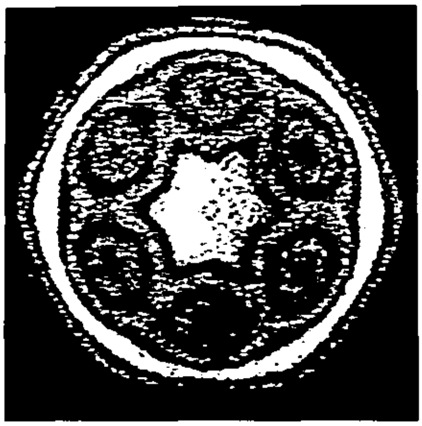

4900 Hz

(3,1)*

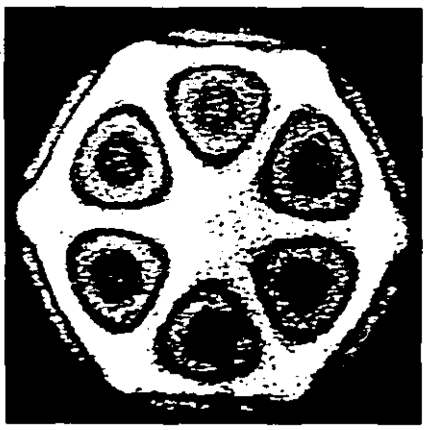

5650 Hz

(7,0) + (1,2)

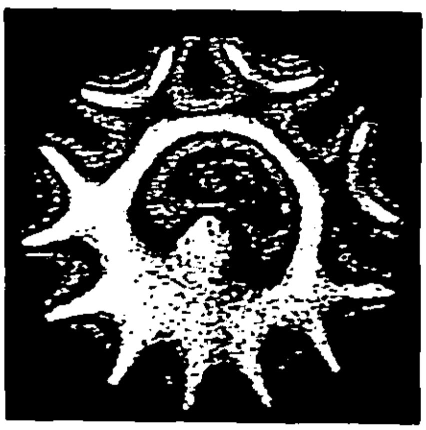

5650 Hz

(7,0) + (7,0)* + (1,2)

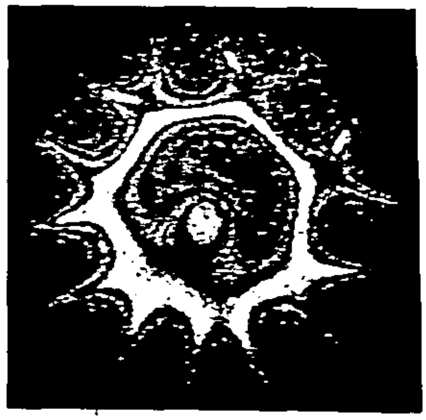

5650 Hz

(7,0)* + (1,2)

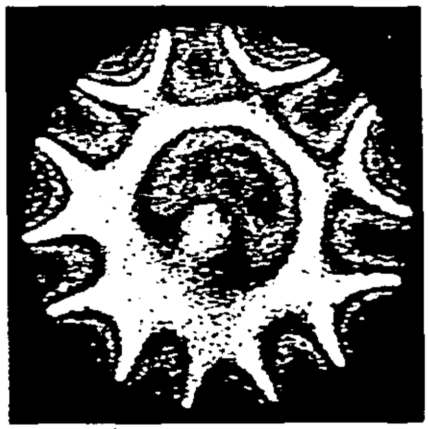

5800 Hz

(1,2)

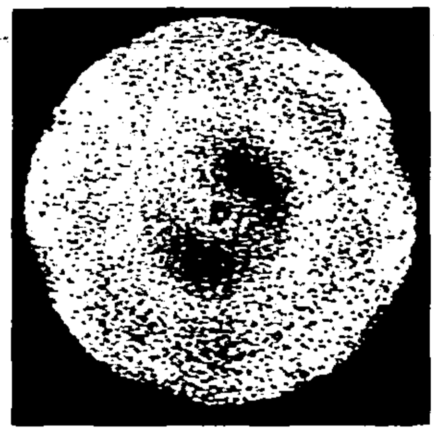

5800 Hz

(1,2)*

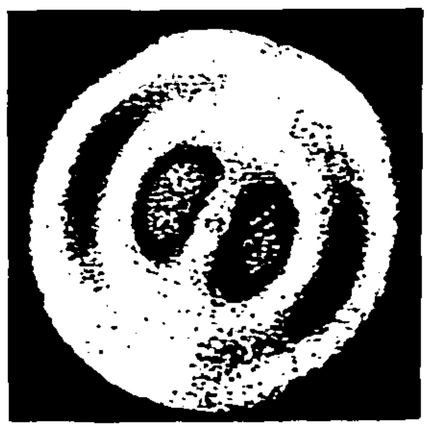

Figure 16: Circular plate flexural modes (continued)

6650 Hz

(4,1)

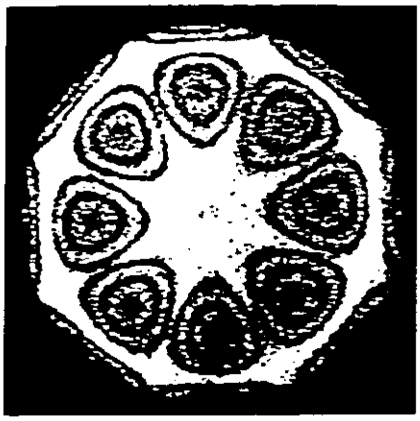

7600 Hz

$(2,2)^*$

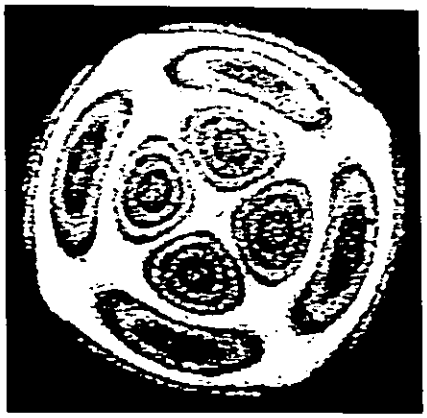

7250 Hz

(8,0)

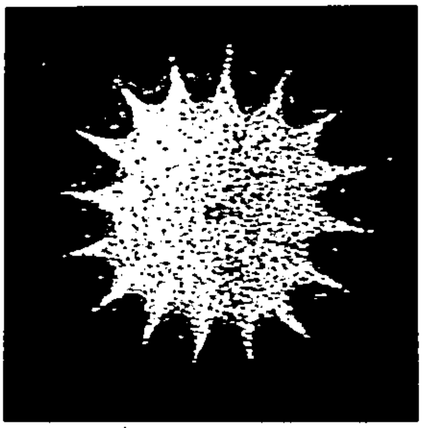

8600 Hz

(5,1)

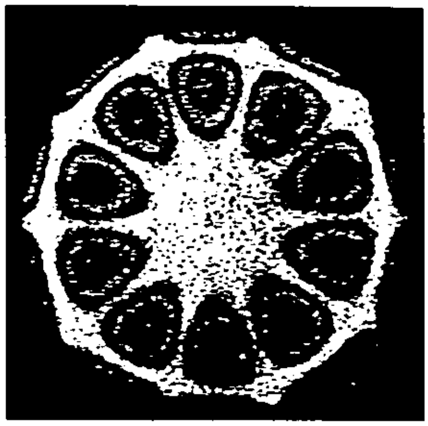

7600 Hz

(2,2)

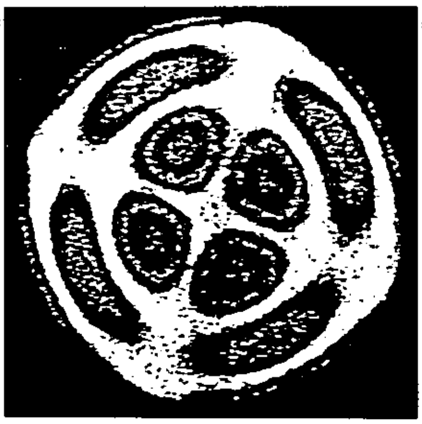

41.5 kHz

(16,1)

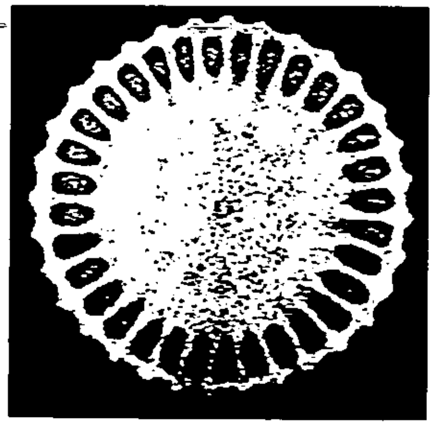

7600 Hz

(2,2)
+
$(2,2)^*$

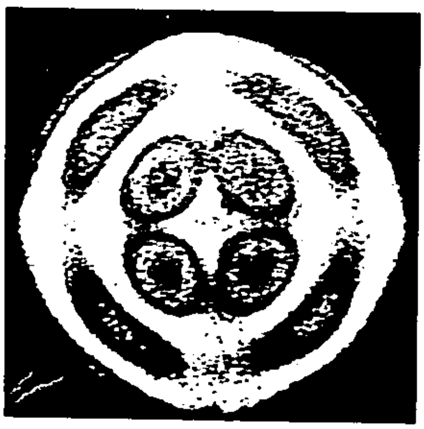

50.0 kHz

(4,6)

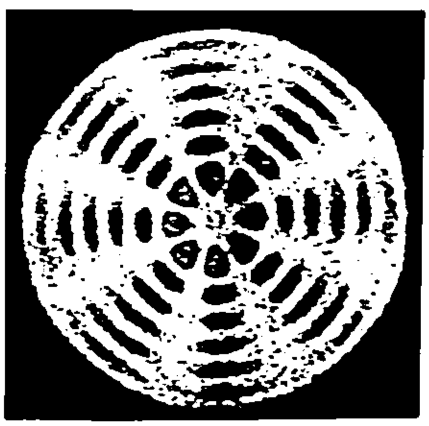

Figure 17: Circular plate flexural modes (continued)

4.2.2 Square plate, time-averaged analysis

The square plate used for this study was brass, 80x80x1.5 mm, centrally pinned and excited by a piezocrystal near the edge of the plate. Initially it was studied using the three-dimensional time-average system (described in section 3.2.1), with the plate lying in the xy plane and the central support in the z-axis. In this way the entire plate could be rotated about the z-axis without disturbing the vibration, enabling different in-plane components to be measured. The orientation of the plate was defined as the clockwise rotation of the piezocrystal location from the positive y-axis. Resonant modes were identified as for the circular plate, but using the in-plane sensitive interferometer to observe in-plane modes (which can be defined as those in which the in-plane displacement components are greater than the out-of-plane components). Each of the modes was observed using the z-sensitive interferometer with the plate at 0° orientation, and using the x-sensitive interferometer at 0°, +90° and +45° orientations. This is equivalent to measuring with $\hat{x}$, $\hat{y}$ and $\hat{x}$-$\hat{y}$ sensitivity vectors respectively, the latter being necessary to determine the phase relationship between the two former amplitude measurements. In-plane vector plots have been obtained by plotting scaled x- and y-component vectors at the intersections of the fringe centres for corresponding x- and y-sensitive fringe patterns, and adding or subtracting the two vectors as required to satisfy the 45°-sensitive fringe pattern. Some examples of the results which were obtained are shown in Figures 18 to 21.

Figure 18 shows the results with the plate vibrating at 4.98 kHz. (a) is the fringe pattern from the z-sensitive interferometer, indicating the out-of-plane components. It has a symmetrical nodal pattern which is typical of the many resonances that were observed. This particular mode corresponds to the 10th flexural mode (in order of increasing eigenvalue) predicted for a completely free square plate by Gorman[120], and the 13th such mode as predicted by Downs[121]. Gorman's result was obtained using the method of superposition with analytical solutions, and is presented in Figure 18(e) as the nodal lines on the lower-right quadrant of the plate (the mode is doubly symmetric). Downs used dynamically corrected finite elements, and his result is shown as a wire-mesh plot in Figure 18(f). Viewing the plate under identical conditions with the in-plane interferometer produced a uniformly bright image with no fringes, indicating no detectable in-plane motion. However when the amplitude of vibration was increased to a level at which the out-of-plane fringes were too densely spaced to be resolved, fringes could be seen indicating in-plane motion. The x-, y- and 45°-sensitive fringe patterns are shown in Figure 18(b), (c) and (d), as indicated. Inspection of these fringe patterns reveals that the regions vibrating in each of the in-plane directions correspond to regions where the slope in the sensitivity direction ($\partial z/\partial x$ for (b) and $\partial z/\partial y$ for (c)) is non-zero as indicated by Figure 18(a). These results suggest that the flexural motion is not entirely out-of-plane, and also demonstrate that in-plane fringe patterns can be obtained even in the presence of much larger out-of-plane motion.

Figure 19 shows the results obtained at 21.8 kHz. The out-of-plane fringe pattern (d) indicates a high order flexural mode in which the symmetry is breaking down. By contrast the in-plane fringe patterns in Figure 19(a)-(c) show a simple nodal pattern with symmetrical x- and y-components. The total in-plane motion is shown by the vector plot (e) which has been constructed from (a) and (b), using (c) to deduce the phase relationship. It is obvious that the out-of-plane mode is not related to the in-plane mode, and real-time observation confirmed that the pattern in Figure 19(d) was due to an out-of-plane mode having a resonant frequency close to that of the in-plane mode. The vectors indicate that this a low order mode involving in-plane rotation about nodal points. The motion of the outer boundary is very similar to the second longitudinal mode (so called because the x_x and y_y normal strain components are large in comparison to the x_y shear strain) predicted by Ekstein[122], which is shown in Figure 19(f). Ekstein states that "none of... [the longitudinal modes] ...has nodal lines, but only nodal points", which is in agreement with this result. However the experimental results indicate a reversal of the motion in the centre portion of the plate which does not occur in the predicted mode shape.

The fringe patterns in Figure 20 correspond to those in Figure 19 but at 25.3 kHz. The out-of-plane fringe pattern is actually a weak off-resonance response of the flexural mode having eight vertical and three horizontal nodal lines. The in-plane motion is almost uniform radial expansion and contraction, and this definitely corresponds to Ekstein's third longitudinal mode which is shown in (f).

Finally, Figure 21 shows another in-plane mode at 30.5 kHz, which is a higher order mode again involving in-plane rotation.

4.2.3 Square plate, phase-stepped analysis

The in-plane vector plots in section 4.2.2 were produced manually by tracing fringe patterns and graphically constructing the vectors. This process is tedious and time-consuming, and clearly unacceptable for a commercial system. Subsequently these measurements were repeated using the pulsed laser ESPI system with phase-stepping to automate the data extraction.

Figure 22 shows the results for the same mode as Figure 20, at 25.3 kHz. [N.B. higher frequency readings were obtained in this later experiment due to using a less accurate meter, but to avoid confusion the values from section 4.2.2 are used throughout]. Figure 22(a) is a single pulse subtraction fringe pattern produced as in section 4.1.2. Figure 22(b) is a similar fringe pattern produced after a phase shift of +90° in one of the illuminating wavefronts. Both these images were recorded with x-sensitivity, and have been grey-level normalised to maximise fringe visibility. Figure 22(c) shows the modulo 2π phase map calculated by the image-processing computer from (a) and (b). Figure 22(d) is the same image overlaid with horizontal amplitude vectors at a grid of points. These vectors have been calculated by unwrapping and normalising the phase values across the image, taking the pinned centre point as reference. Figure 22(e) shows the result of following the same procedure with y-sensitivity, under identical conditions. Finally, Figure 22(f) shows the resultant vectors at each grid point after vector addition of the horizontal and vertical components. These are overlaid on a white light image of the object, to show the total in-plane vibration pattern across the object surface. This result is in good agreement with Figure 20(e).

Figure 23 and Figure 24 show the phase-stepped results for the 21.8 and 30.5 kHz modes respectively. In each figure (a) is the x-sensitive phase map with component vectors, (b) is the y-sensitive phase map with component vectors, and (c) is the total in-plane displacement vector plot. Again the results agree well with Figure 19(e) and Figure 21(e).

These results demonstrate that by using phase stepping and computer processing it is possible to automatically produce two-dimensional displacement data. They also indicate some of the problems and limitations associated with this method. One obvious feature is that the centre screw, which is seen clearly in the white light images, appears as a grey oval in each of the phase maps. This is because the screw stands proud of the plate surface and casts shadows from the oblique illumination, creating dark areas of zero correlation in the original interferograms, which then become indeterminate during calculation of the phase values. This causes two problems. The first is that the indeterminate zone does not take its correct grey-level intensity (corresponding to modulo 2π phase value). Since in this case the stationary reference point lies within this zone it has been necessary to interpolate the required reference phase value from the adjacent grey levels, and this has necessitated a certain amount of operator intervention in the otherwise automated procedure. The second problem is that for some fringe patterns the indeterminate zone interrupts a phase discontinuity, which can cause errors in the phase unwrapping. This has happened in Figure 22(d), where the phase values have been incorrectly unwrapped along the central horizontal line, and this has led to errors at the corresponding points in Figure 22(f). Similar errors can occur elsewhere if the phase discontinuities break down due to poor original data or filtering effects; examples can be seen in the corners of Figure 24(a). Such problems can be overcome by allowing operator intervention in an interactive computer program, as has been used here, or by using more complex phase unwrapping procedures[88,123].

Most of the data acquisition and processing is performed automatically by the computer in this system, but operator intervention is still necessary for some tasks. One of these is that, depending on the fringe quality, it is sometimes necessary to alter the threshold value for detecting phase discontinuities in the unwrapping process. The other is choosing a reference pixel for normalising the vectors. The unwrapping process yields vector amplitudes which are relative to the starting point, and this is unlikely to correspond to a suitable reference. Where there is a known fixed point, such as the centre pin in this case, the choice is obvious, but in other cases it may be necessary to try different references to indicate the required information clearly.

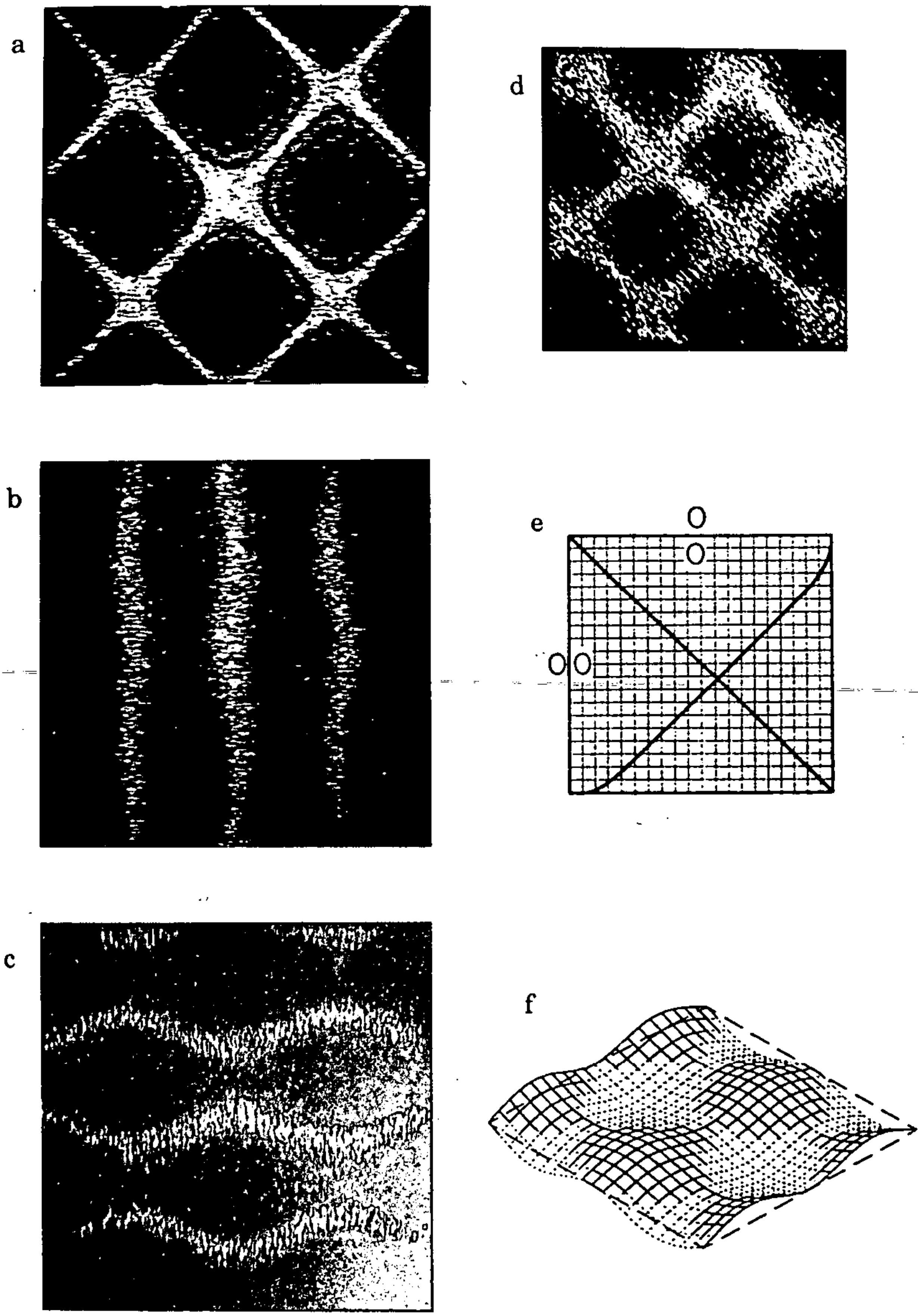

Figure 18: Square plate vibrating at 4.98 kHz, time-average ESPI

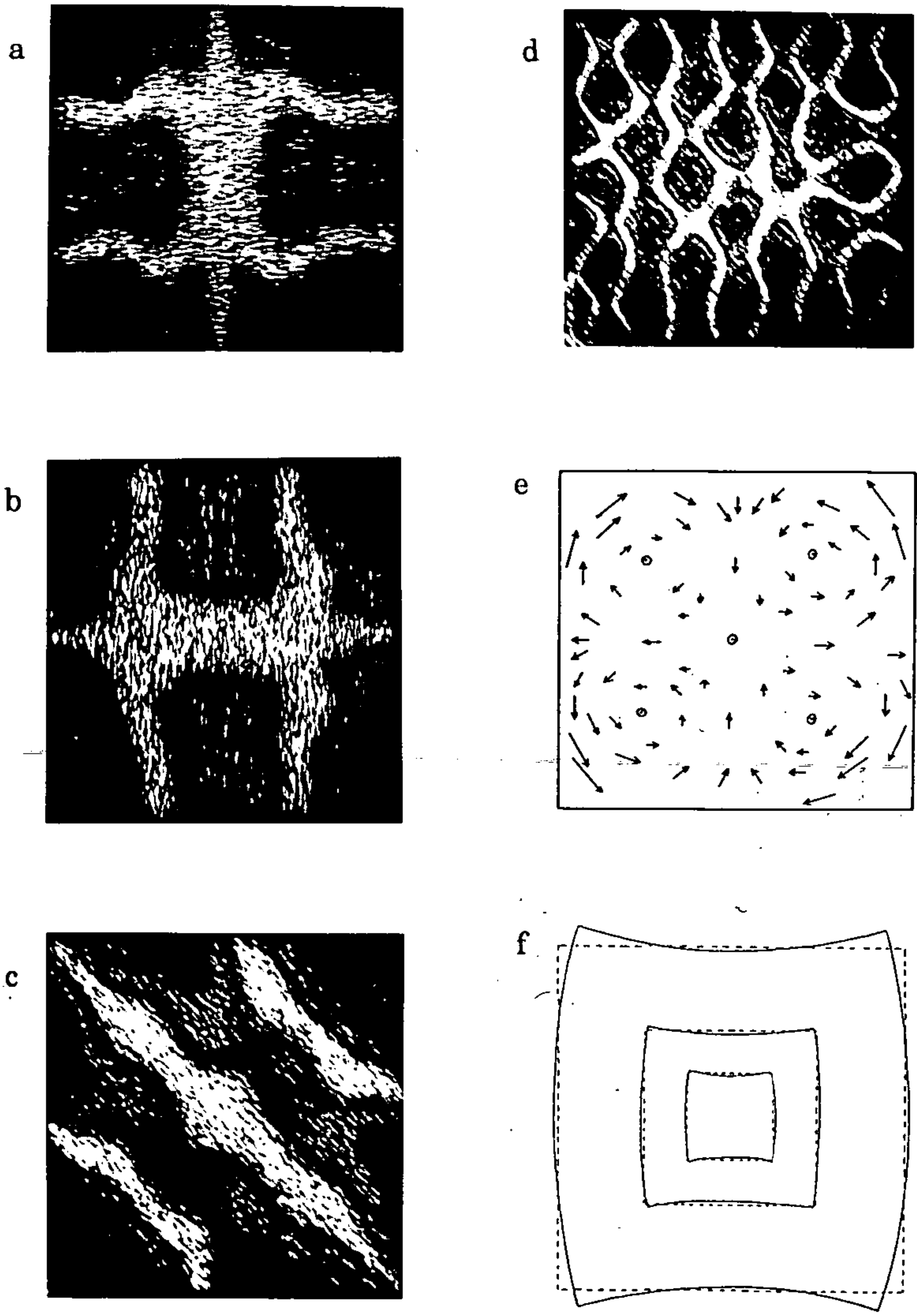

Figure 19: Square plate vibrating at 21.8 kHz, time average ESPI

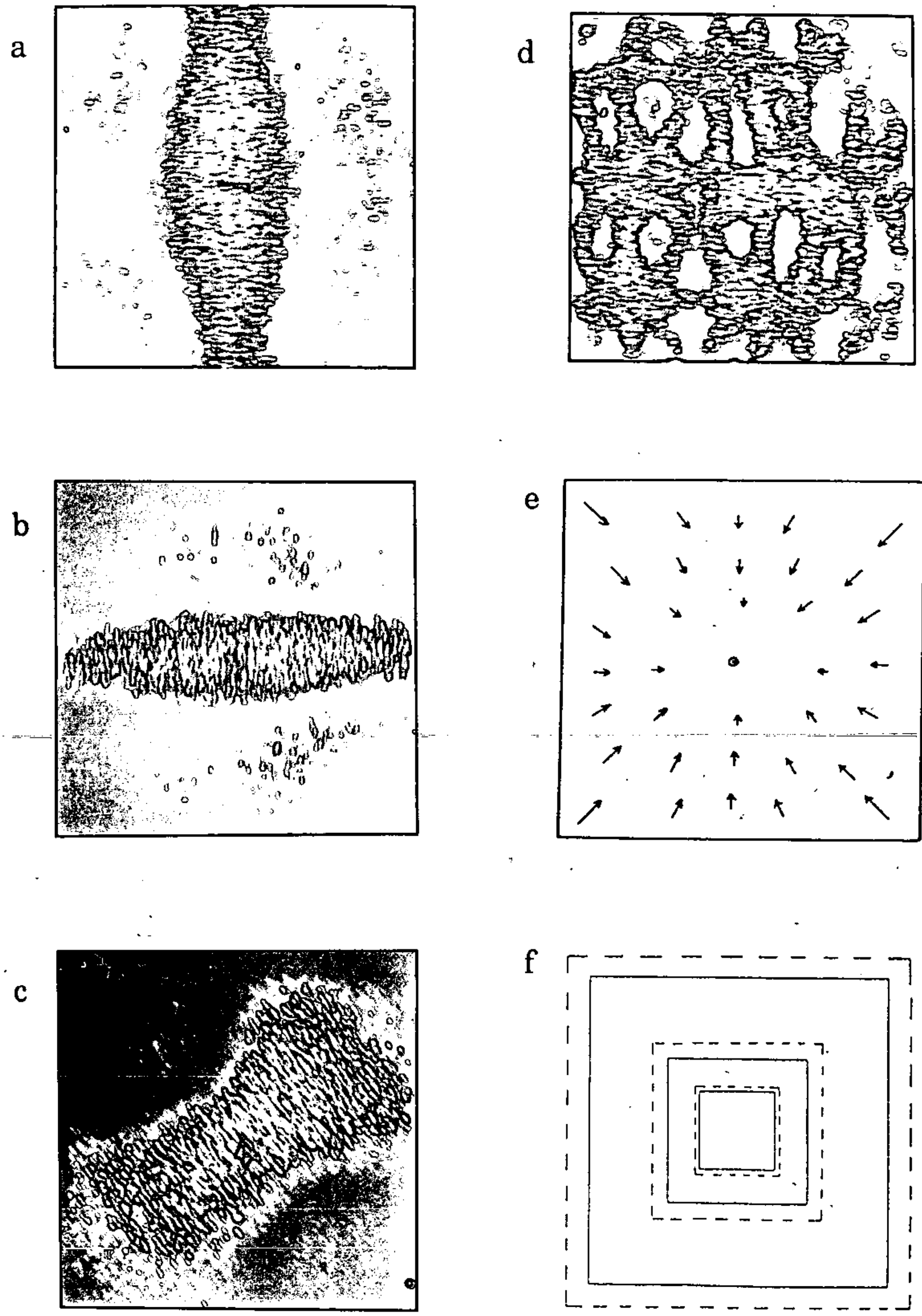

Figure 20: Square plate vibrating at 25.3 kHz, time average ESPI

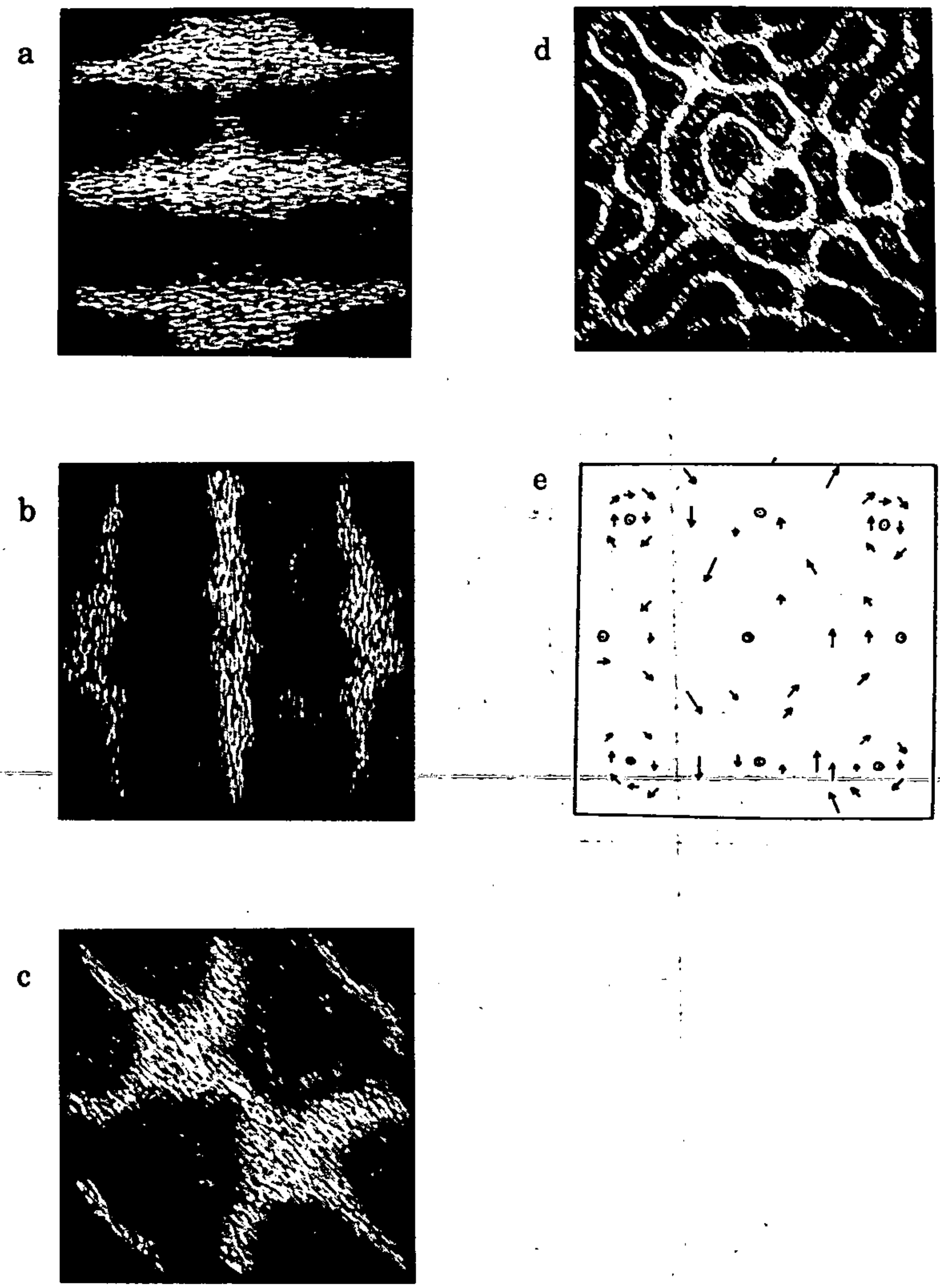

Figure 21: Square plate vibrating at 30.5 kHz, time average ESPI

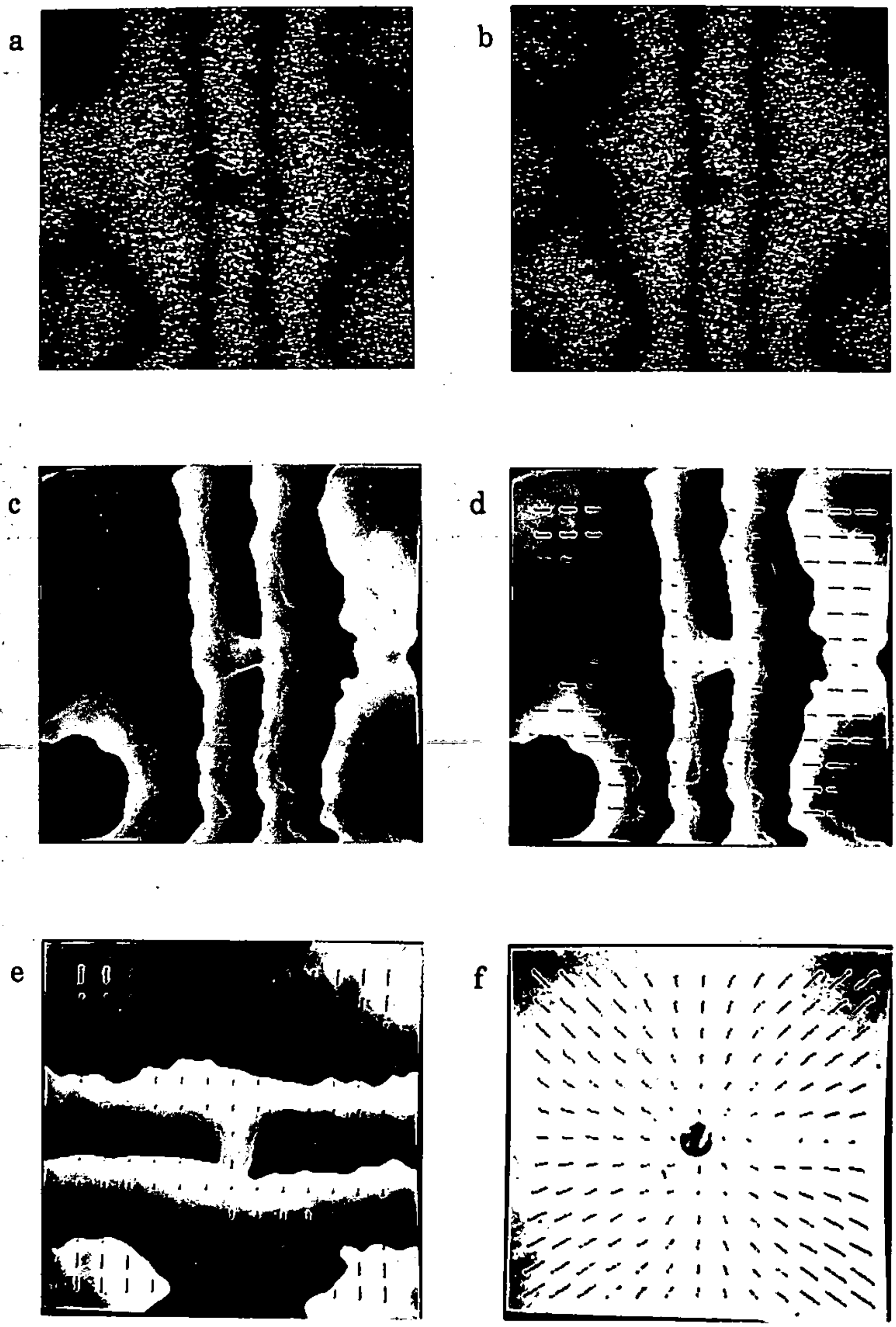

Figure 22: Square plate vibrating at 25.3 kHz, phase-stepped analysis

(a) (b) (c)

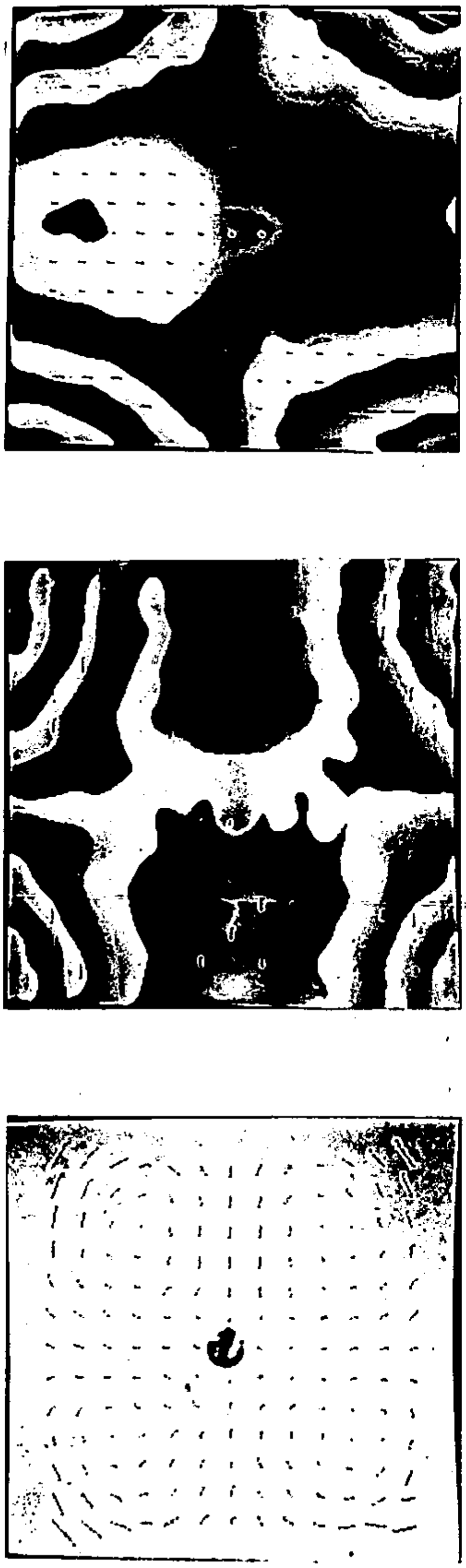

Figure 23: Square plate vibrating at 21.8 kHz, phase-stepped analysis.

(a) (b) (c)

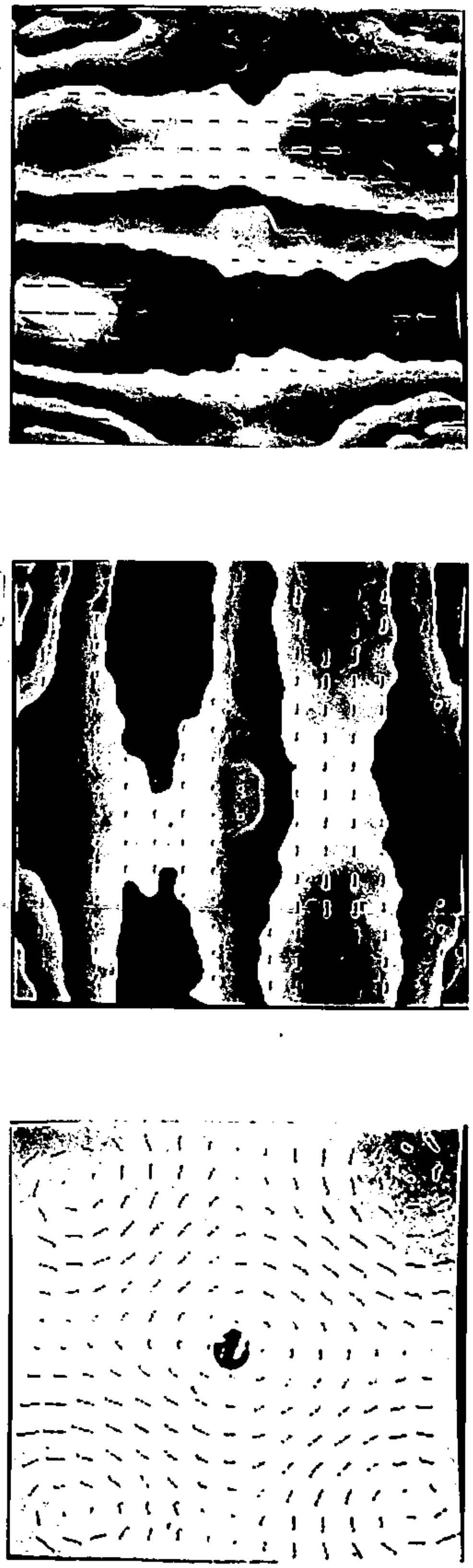

Figure 24: Square plate vibrating at 30.5 kHz, phase-stepped analysis

4.3 THICK CYLINDER VOLUME VIBRATIONS

For the general case of a structure with arbitrary geometry, the resonant modes are truly three-dimensional and require three measurement axes for complete characterisation. This is also the case for plates as the thickness becomes large or the medial section becomes curved, as these effects cause the out-of-plane and in-plane modes to become coupled.

The object chosen to demonstrate three-dimensional vibration is shown in Figure 25, and schematically in Figure 26. This is an ultrasonically-assisted forming die (see section 5.1), which is in the form of a thick cylinder excited by a magnetostrictive transducer attached at the top. The normal modes for such a structure are described in Appendix C.2, and have been calculated by Cheers[124] using finite element (FE) analysis. These include some which have predominantly radial motion (r in Figure 26), some predominantly axial (z) and some predominantly tangential (θ). The results have been plotted as contour maps of x-, y- and z-components of displacement, so as to correspond to the measurements made by x-, y- and z-sensitive ESPI interferometers. The FE plots have four contour levels normalised to the largest value for each plot, so the FE 'fringes' should have the same form but not necessarily the same spacing as the corresponding ESPI fringe patterns.

A full modal analysis of this object was performed and is discussed in section 5.1, but selected results are presented here to demonstrate the ability to identify the different types of motion. The ESPI fringe patterns were obtained using the three-dimensional time-average system described in section 3.2.1, viewing the cylinder axially as shown in Figure 26.

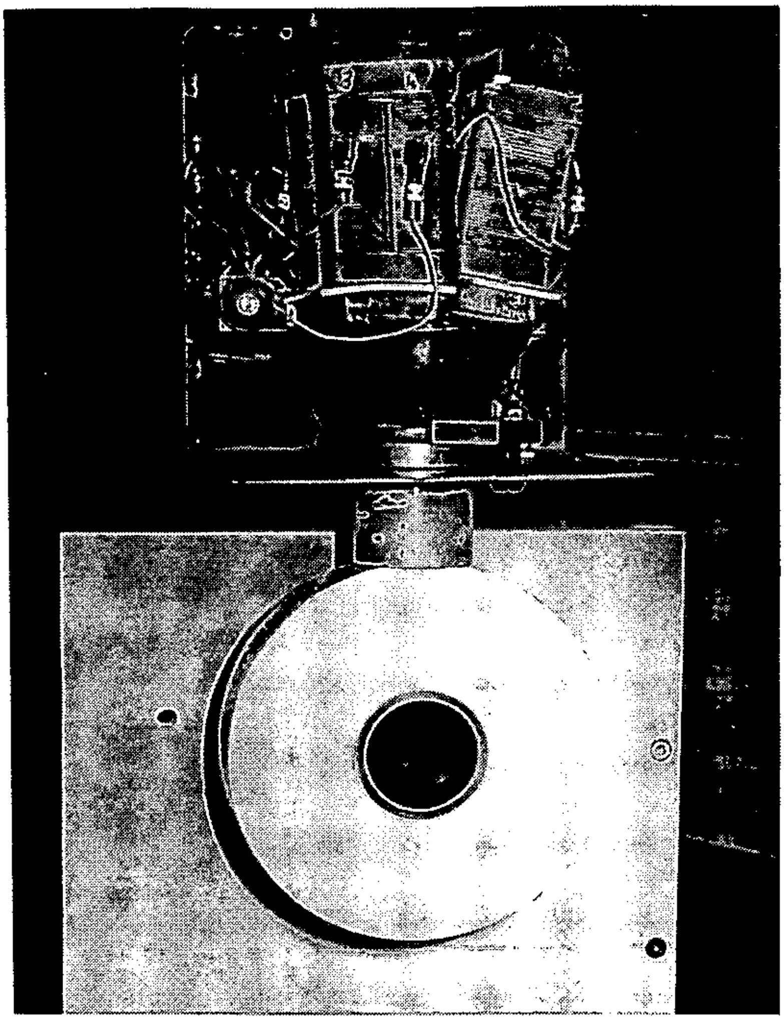

Figure 25: Ultrasonically-assisted forming die

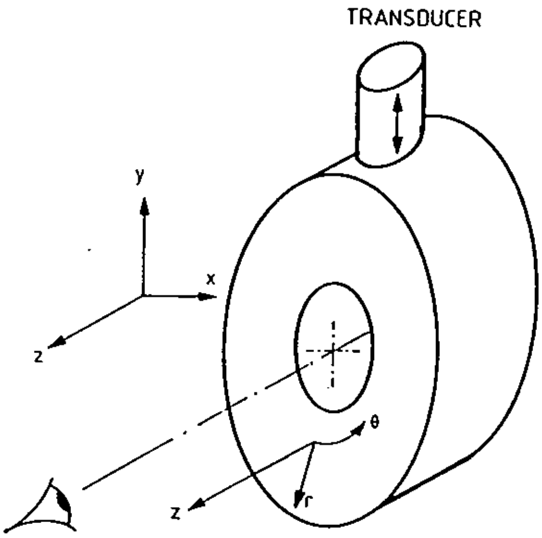

Figure 26: Schematic of ultrasonic die

Figure 27 shows experimental results (a-c) from a steel die similar to the aluminium one shown in Figure 25 vibrating at 14.40 kHz, with the FE predictions (d-f) for the zero order torsional (T0) mode. (a) and (d) show the z-component, (b) and (e) the x-component, and (c) and (f) the y-component. The agreement between the ESPI and FE results is very close, which enables the experimentally observed mode to be identified to a high degree of confidence and shows that there is very little deviation from the expected mode shape. The main difference between actual and predicted behaviour is that (c) is slightly asymmetrical about a horizontal axis; this is probably due to the added mass of the transducer at the top, which was not included in the FE model. The poor quality of the x and y fringe patterns is largely due to the fact that the motion for torsional modes is predominantly in the z direction.

Figure 28 shows the results for the aluminium die of Figure 25 at 16.76 kHz, with FE predictions for the first order radial (R1) mode. The correspondence is excellent for the x- and y-components, but significantly different for z. This is due to the influence of a high response torsional (T1) mode at a slightly lower frequency (see section 5.1). The T1 mode is predominantly out-of-plane whereas the R1 is predominantly radial in-plane, so only the z fringe pattern is significantly affected. Because this is an in-plane mode the motion is best understood by constructing the in-plane vector plot, which is shown in Figure 28(g). This shows that the radial component of motion passes through one complete cycle around the circumference, being radially outwards at the top at the same time that it is radially inwards at the bottom and zero along the horizontal radii.

Figure 29 shows the aluminium die at 24.00 kHz and the predicted second order diametral rotation (D2) mode. Again the agreement is good enough to identify the mode with confidence, and it appears to be very pure apart from the same distortion in the y-component due to the transducer. The motion is predominantly tangential in-plane, as shown by the vector plot in Figure 29(g). This mode is the equivalent of the second longitudinal mode for the square plate in section 4.2.2, and comparison with Figure 19(e) shows that the motion of the two modes is very similar.

Not all of the resonances which were detected correspond to the predicted normal modes, but some of them appear to share features from two different modes. Where these resonances occurred at frequencies close to the predicted modes, combination modes were modelled in the FE analysis by phasor addition of the two adjacent normal modes in varying proportions to try and match the observed fringe patterns. This approach was reasonably successful in most cases. As an example, the ESPI fringe patterns shown in Figure 30 are from a resonance at 20.75 kHz, between the predicted R0 mode at 20.00 kHz and the R3 mode at 21.42 kHz. The FE plots are for a combination of R3-0.2(R0). The match is not perfect, but is close enough to suggest that the mode is a result of this type of combination. A further example is shown in Figure 31. A sharp resonance was detected by the z interferometer at 17.66 kHz, as shown in (a), but no fringes were observed with the x or y interferometers. The z fringe pattern was particularly puzzling as it appeared to have an odd number of antinodes around the circumference, which should not occur for normal modes (for comparison see Figure 14). The adjacent predicted modes are T1 at 17.11 kHz and T4 at 19.53 kHz, and a combination of T1+0.7(T4) gives a similar pattern as shown in Figure 31(b). Because the combining modes are both torsional the motion is predominantly out-of-plane, and inspection of the x- and y-components shown in Figure 31(c) and (d) reveals that the in-plane components are concentrated in a few small areas, so this accounts for the lack of x and y fringe patterns.

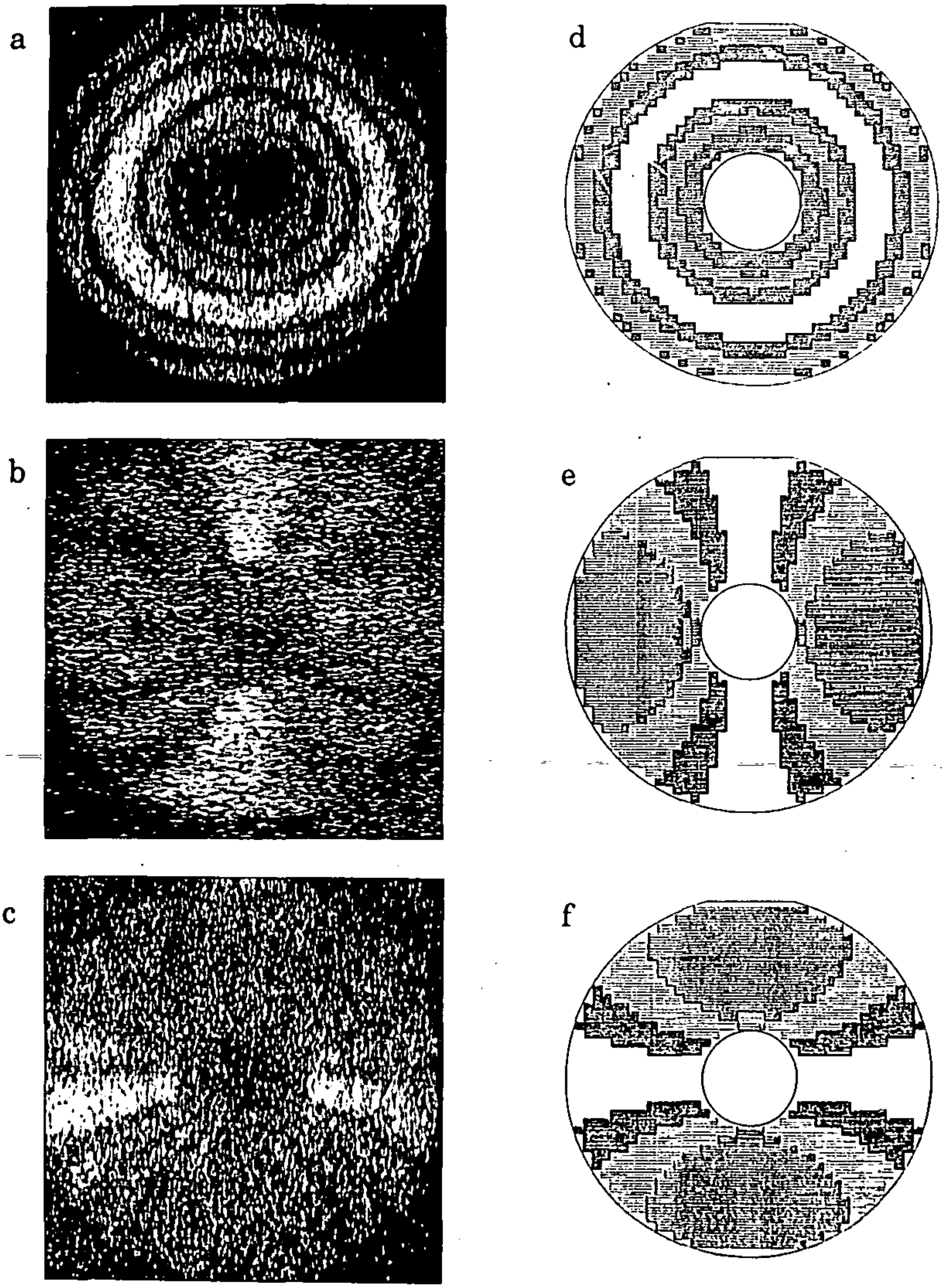

Figure 27: Steel die vibrating at 14.40 kHz, and FE plots of T0 mode

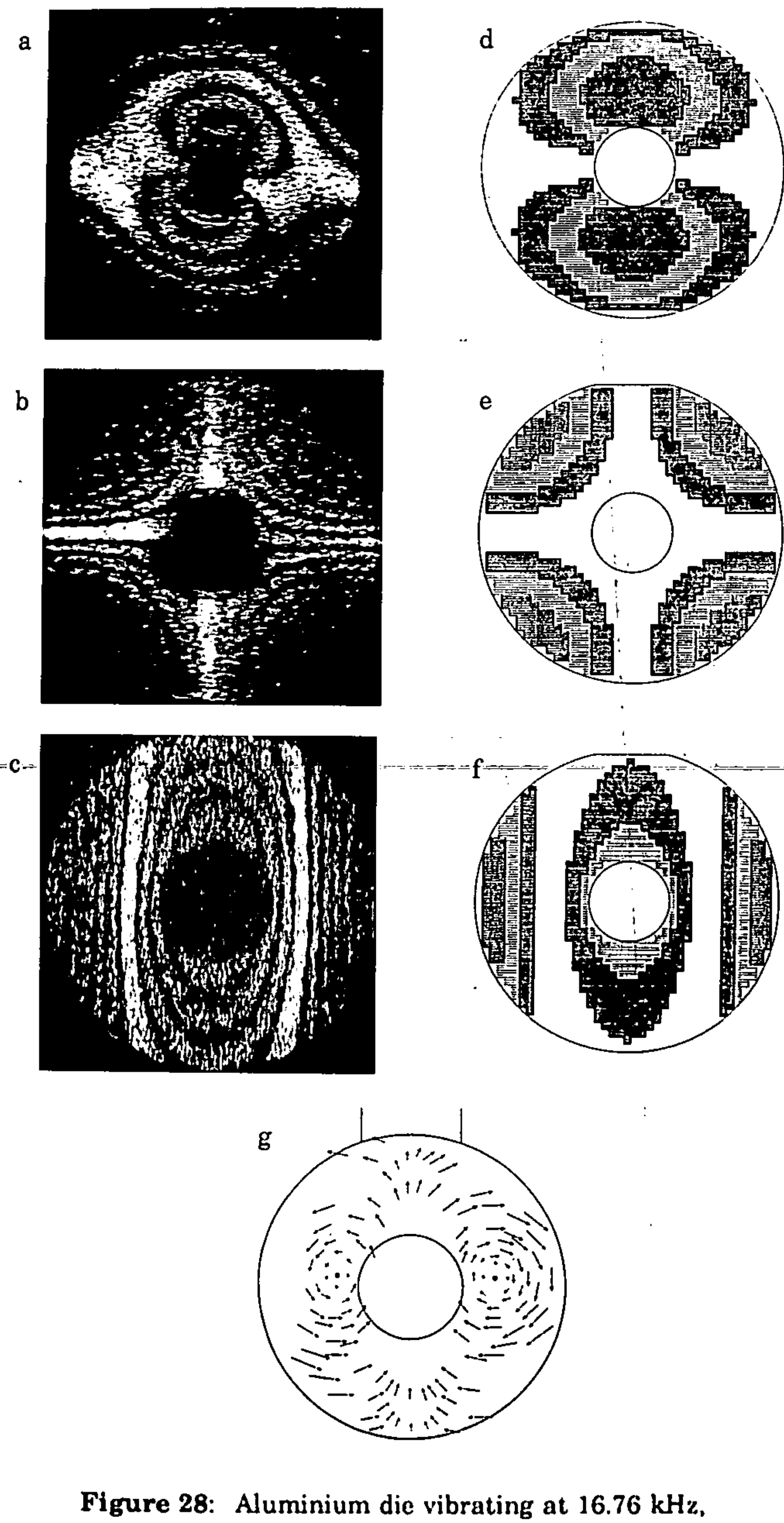

Figure 28: Aluminium die vibrating at 16.76 kHz, and FE plots of R1 mode

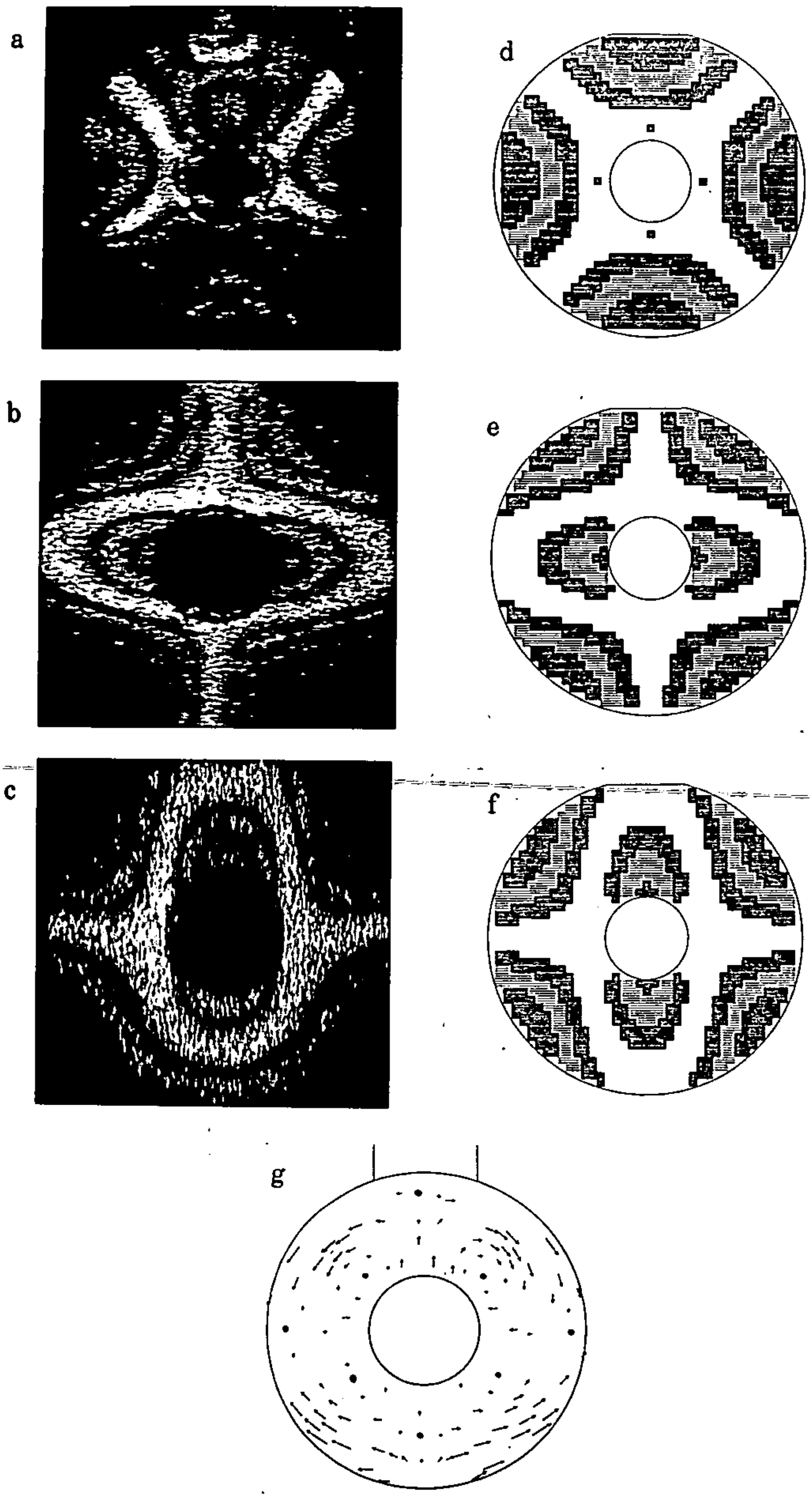

Figure 29: Aluminium die vibrating at 24.00 kHz, and FE plots of D2 mode

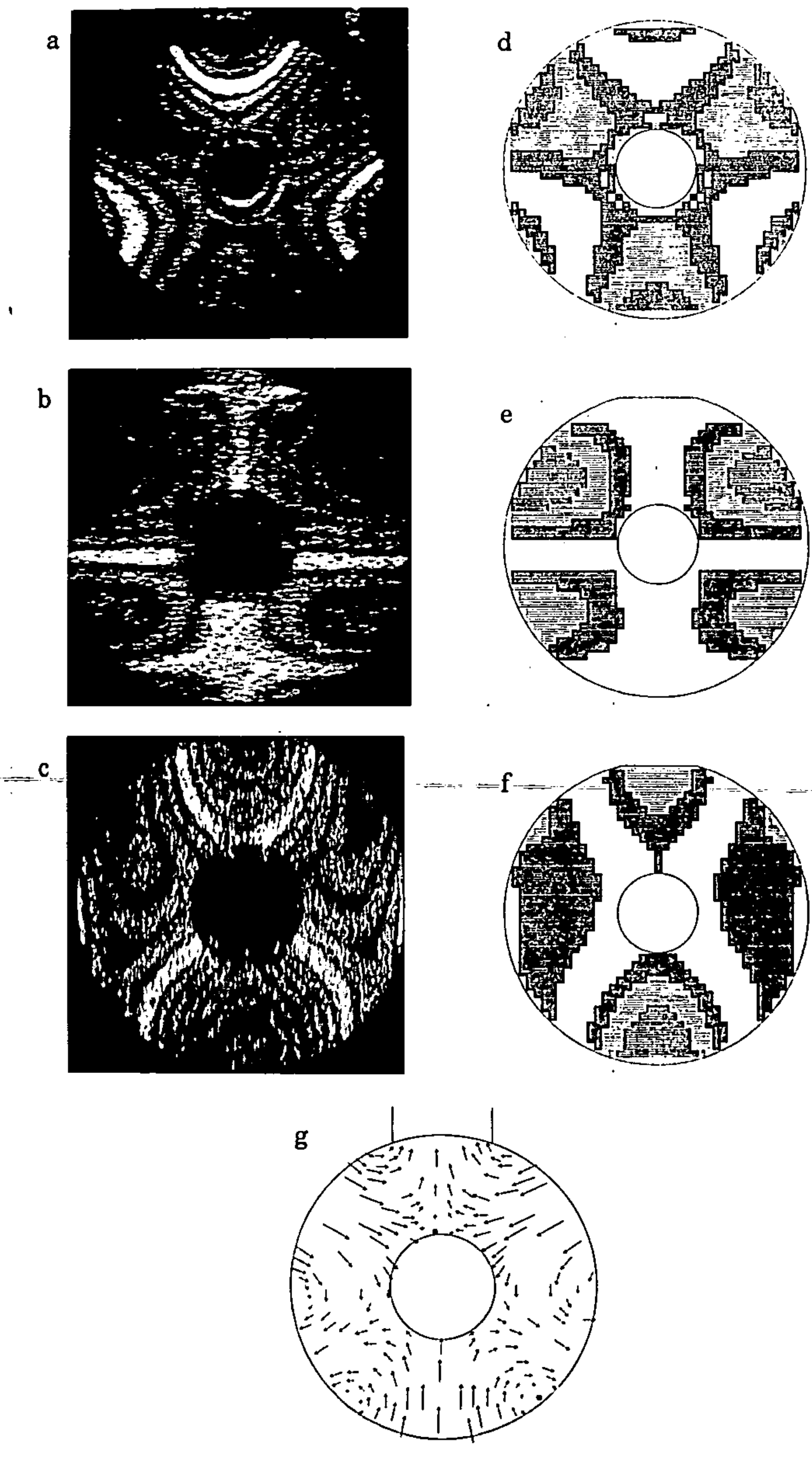

Figure 30: Aluminium die vibrating at 20.75 kHz,

and FE plots of R3-0.2(R0) mode

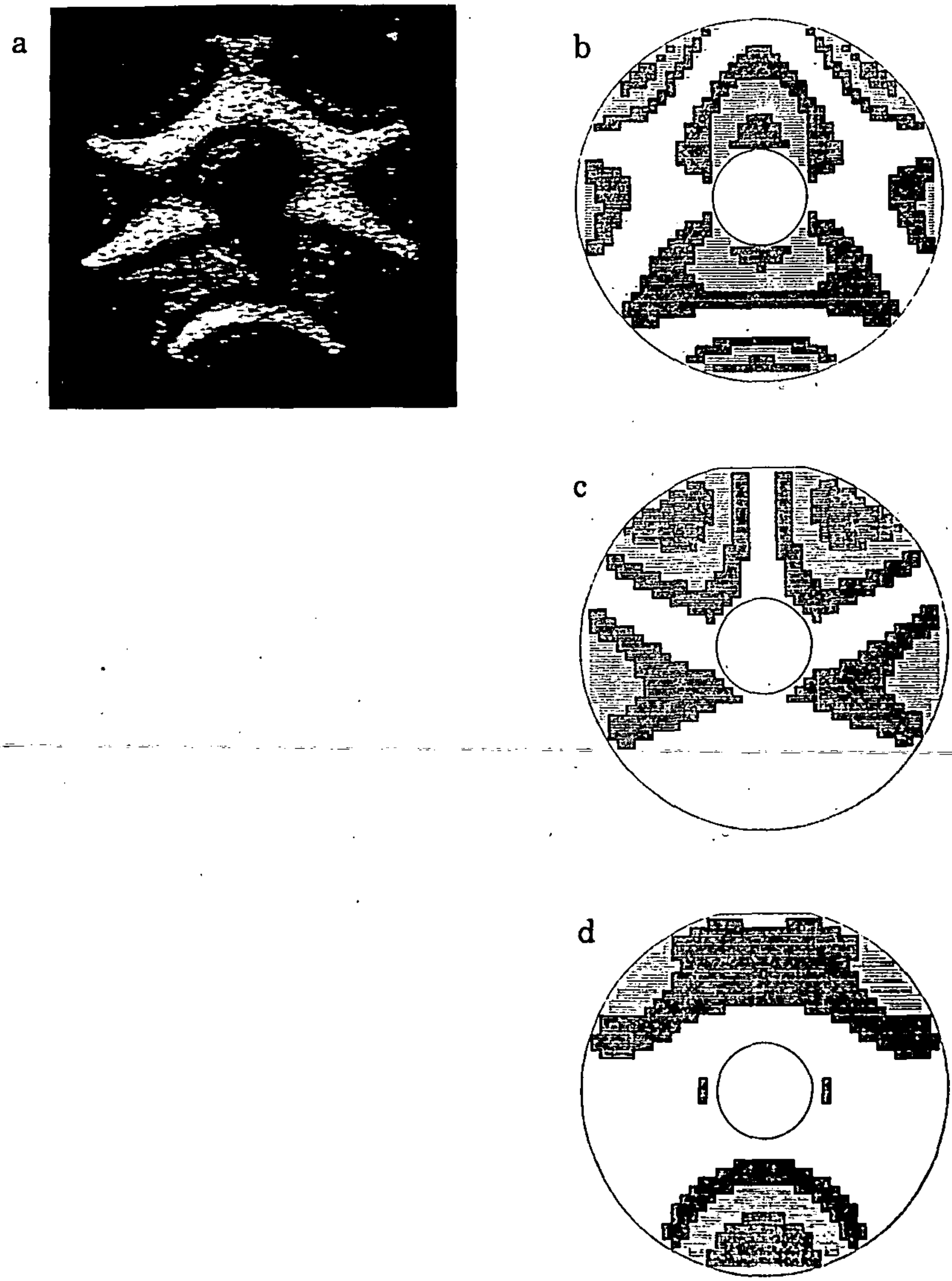

Figure 31: Aluminium die vibrating at 17.66 kHz, and FE plots of T1+0.7(T4) mode

5. VIBRATION ANALYSIS OF ENGINEERING STRUCTURES

It has been demonstrated in Chapter 4 that the ESPI system is capable of measuring arbitrary three-dimensional vibrations of simple structures. In order for the system to be of practical use in engineering it must be able to be applied to real engineering components, and that ability has been demonstrated with three case studies: an ultrasonic forming die, an ultrasonic cutting system, and a turbocharger blade. All of these are examples of situations in which a one-dimensional measurement system is insufficient to provide all the required information, so they provide a test for the three-dimensional system. The results of these studies are given in the following three sections, and their implications will be discussed in section 7.1. All the tests were performed in a laboratory using the time-average ESPI system described in section 3.2.1.

5.1 FORMING DIE

The object described in section 4.3 is a prototype forming die, utilising mechanical vibration at ultrasonic frequencies to improve production performance and efficiency. It had been designed by Metal Box plc[125,126] to perform die necking of thin-walled cylindrical tubes for aerosol cans, and was required to vibrate resonantly in an axisymmetric radial (R0) mode at 20 kHz (see Appendix C.2 for a description of mode shapes). Resonators of this type have previously been applied to wire and tube drawing[127,128], but not to tube necking. Designing a system to operate effectively requires careful matching of the required resonant mode with the driving system frequency, and avoidance of other resonances at close frequencies which might affect the performance. Hence a full modal analysis was required around the operating frequency, and three-dimensional measurement was required to correctly identify the modes. This was undertaken as a collaborative project combining the techniques of finite element (FE) analysis, accelerometer-based experimental modal analysis (EMA) and ESPI.

5.1.1 ESPI modal analysis

Examples of ESPI fringe patterns and FE predictions have been given in section 4.3 to show how the modes were identified. A full set of ESPI results is sketched in Figure 32 and Figure 33 for one particular prototype, an aluminium die with a tubular mount. The same method of modal analysis was used as for the circular plate in section 4.2.1, slowly sine-sweeping to detect resonances, but in this case most of the resonances were broad (i.e. low Q-value) so that the fringe patterns often varied continuously between peaks without vanishing. The results shown therefore represent points sampled from a continuous frequency response function, rather than isolated modes. Results have been recorded at 33 frequencies in the range 13.5-25.8 kHz. All these results have been recorded with the z interferometer, which is the most sensitive, whereas x- and y-components are only presented at maxima of in-plane response. The input excitation level was adjusted in each case to give an optimum fringe pattern for identification (ideally 3-4 fringe orders). Identical settings were used for x and y measurements at the same frequency, but otherwise the individual results cannot be directly compared.

Because of the continuously varying nature of the response, it is desirable to present the ESPI results as a frequency response function (FRF) which can be compared with the FE and accelerometer results. This requires quantitative determination of the vibration amplitude at each frequency (f). Because all the normal modes have motion which is either predominantly out-of-plane (T modes) or predominantly in-plane (R, D and F modes) it is reasonable to plot the out-of-plane and in-plane response functions separately. The out-of-plane (axial) response R_o has been calculated by dividing the highest bright fringe order N_o for each z fringe pattern in Figure 32 by the power level E_o indicated by the ultrasonic generator for that recording:

$$R_o = \frac{N_o}{E_o}$$

For the in-plane response, the corresponding amplitude has been calculated as:

$$N_i = 2\left(\sqrt{N_x^2 + N_y^2}\right)\max \qquad \text{(assuming the x and y components are in phase)}$$

where N_x and N_y are the fringe orders at corresponding points in the x and y fringe patterns, and the factor of 2 is to correct for the relative sensitivity of the in-plane interferometer with illumination angle θ=30° (see section 3.1). The in-plane response is then given by:

$$R_i = \frac{N_i}{E_i}$$

where E_i is the corresponding power input. The calculated values are presented in Table II. It should be emphasised that these values are only approximate, due to the following points: (i) the reading accuracy for N is ±½ fringe, which for values of N = 1 to 6 gives a high relative error bound; (ii) amplitude values have not been corrected for the non-periodic Bessel function, which introduces an error of approximately ½ fringe; (iii) the method assumes linearity between the generator output and the die displacement amplitude, which has not been proven. However they are useful as an indication of relative response, and more accurate response values can be obtained from the accelerometer measurements (see section 5.1.3). The values from Table II have been used to create the FRFs plotted in Figure 34, where the functions have been estimated between the plotted points taking account of the behaviour observed during sine-sweep testing. The transparent overlay shows for comparison the FRF for radial motion at one point on the circumference as measured by an accelerometer (see section 5.1.3).

Table II: Modal response from ESPI fringe patterns

f (kHz)	N_o	E_o	R_o	N_i	E_i	R_i	R_o/R_i
13.50	2	150	0.013	6.1	75	0.163	0.08
13.98	4	260	0.015	-	-	-	-
14.06	3	260	0.012	-	-	-	-
14.24	4	30	0.133	3.2	120	0.053	2.51
15.07	3	740	0.004	-	-	-	-
15.40	2	640	0.003	-	-	-	-
16.42	3	200	0.015	-	-	-	-
16.47	3	200	0.015	3.2	160	0.040	0.38
16.50	3	200	0.015	-	-	-	-
16.66	2	90	0.022	-	-	-	-
16.76	5	60	0.082	6.7	30	0.442	0.19
17.66	3	340	0.009	-	-	-	-
17.83	1	620	0.002	-	-	-	-
19.70	2	100	0.020	-	-	-	-
19.82	2	20	0.100	-	-	-	-
19.92	3	50	0.060	-	-	-	-
20.05	7	100	0.070	4	40	0.200	0.35
19.48	2	180	0.011	-	-	-	-
19.80	4	210	0.019	-	-	-	-
19.95	2	30	0.067	-	-	-	-
20.20	2	110	0.018	-	-	-	-
20.75	3	100	0.030	3.6	30	0.240	0.13
21.00	2	575	0.004	-	-	-	-
21.20	1	600	0.002	-	-	-	-
21.35	1	600	0.002	-	-	-	-
21.55	2	550	0.004	2.2	400	0.011	0.36
23.50	1	550	0.002	3	290	0.021	0.10
23.80	3	370	0.009	4.1	190	0.044	0.20
24.00	2	610	0.003	3.6	290	0.025	0.12
24.22	3	470	0.007	4.2	270	0.031	0.23
25.20	1	500	0.002	-	-	-	-
25.60	1.5	530	0.003	-	-	-	-
25.77	2	570	0.004	-	-	-	-

Table III: Natural frequencies of ultrasonic die predicted by FE analysis

MODE	PREDICTED FREQUENCY (kHz)		$\hat{a}_o/\hat{a}_i$
	2D MODEL†	3D MODEL‡	
T2	6.115	5.842	2.04
T0	9.634	9.552	1.72
R2	11.910	11.598	0.15
T3	12.846	12.228	1.63
R1	16.703	16.431	0.09
T1	17.106	16.875	1.58
T4	19.532	18.923	-
R0	19.995	20.142	0.16
R3	21.423	21.458	0.23
D2	24.237	24.120	-
FD2	26.856	26.325	-
R4	28.204	28.466	-

† Results from Cheers[124] using 2D axiharmonic analysis with ANSYS software.

‡ Results from Lucas[129] using 3D analysis with PAFEC software.

Table II because hysteresis was sometimes observed in this range. The T4 mode was observed as the frequency was increased up to 20.05 kHz, but then switched to the R0 mode, which persisted if the frequency was decreased again.

It is evident from Figure 36 that the combination of ESPI and FE has enabled the fairly complex vibration behaviour of this component to be well understood. The ESPI results successfully provided the three-dimensional amplitude distribution at each frequency, but were not sufficient on their own to understand the response in terms of the normal modes. This understanding is necessary in order to determine how to modify the design to alter a particular feature of its dynamic behaviour, and it was made very much easier by having the FE predictions for comparison. The FE analysis proved to be reasonably accurate in predicting the modal frequencies, but would not have been sufficient on its own for a complete understanding. It was not possible to predict the modal damping, nor the presence of the T1+0.7(T4) and R3-0.2(R0) combination modes (see section 4.3). The principal limitation of the combined results is that because ESPI and FE both produce results at discrete frequencies, and because of the limitations discussed earlier, the calculated response levels are only approximations. However this information was provided by the accelerometer results.

5.1.3 Accelerometer analysis and redesign

The accelerometer results were obtained by Lucas[129] at a grid of points over the surface of the die. The acceleration was measured at each point whilst sine-sweeping through a frequency range and monitoring the excitation input level. The FRF at each point was generated by calculating the response (i.e. acceleration per unit excitation) for a set of frequencies and performing a Fourier transform. A typical result is shown on the overlay of Figure 34, which is for an accelerometer attached to the circumference of the die and measuring radial acceleration. It can be seen that the resonant frequencies are in good agreement, but the accelerometer response appears larger at higher frequencies. This is because* the acceleration is proportional to the square of the frequency.

In contrast to ESPI, the accelerometer results are spatially discrete but continuous in the frequency domain. Therefore to understand the mode shape it is necessary to obtain a large enough set of points to give sufficient spatial resolution for the given mode. This is demonstrated in Figure 37, which is a waterfall plot of the measurements taken at 32 points around the circumference. The dominant in-plane modes are clearly identifiable: R1 at 16.7 kHz having one wavelength around the circumference; R0 at 20.1 kHz and uniphase; R3 at 20.8 kHz with three wavelengths; and a pair of D2 modes at 23.7 and 24.3 kHz having four wavelengths each.

* for a given displacement amplitude

5.1.2 Identification of modes

The FRF contains a number of obvious peaks which indicate resonant modes. These have been identified with the help of the FE plots from Cheers[124] which are sketched in Figure 35, and the predicted natural frequencies which are tabulated in Table III for two different FE analyses. Identification of the modes was sometimes difficult, because in several cases the out-of-plane and in-plane components of different modes look similar (see Figure 35, for example R0 and T0, R3 and T3, T2 and D2 out-of-plane). Also the modes did not occur in increasing mode order, as might have been expected intuitively; for example the frequencies of the radial modes occur in the order R2, R1, R0, R3, as predicted by the FE analyses. It was usually possible to identify whether each mode was predominantly out-of-plane or in-plane from the relative response measured by each interferometer, as indicated by the R_o/R_i values in Table II. The out-of-plane fringe patterns and in-plane vector plots (see section 4.3) then gave a good visualisation of the vibrating shape, and the three fringe patterns for each mode could be compared with the FE plots for confirmation.

The modes which have been identified to a high degree of certainty are labelled on the frequency response function in Figure 36; the mode shapes are shown as z fringe patterns for the out-of-plane (T) modes and as vector plots for the in-plane (R and D) modes. Table III also gives the ratio $\hat{a}_o/\hat{a}_i$ for each mode (where available), where $\hat{a}_o$ and $\hat{a}_i$ are the maximum out-of-plane and in-plane amplitude components calculated from the 2D axiharmonic FE analysis. These can be compared with the R_o/R_i values in Table II. The corresponding values differ significantly but nevertheless are of the same order of magnitude in almost every case, providing further evidence for identifying whether the mode is out-of-plane (ratio >1) or in-plane (ratio <1). The exception is the mode observed at 16.47 kHz, which has a much lower value than that predicted for the T1 mode. This can be explained by reference to the FRF, which shows that the in-plane component is greatly exaggerated due to the influence of the R1 mode at a slightly higher frequency. Values between 19.48 and 20.05 kHz appear twice in Figure 34 and

The resonant frequencies can be obtained from the response maxima, and modal damping values can be calculated provided that the modes are sufficiently separated to measure the half-power points (see Appendix B). Curve-fitting of the responses from different positions gives the mode shape at a given frequency. Hence it is possible to obtain all the dynamic characteristics (see section 1.2.2) and perform a full experimental modal analysis (EMA).

Test operation revealed a problem that the R3 mode (or R3/R0 combination mode) was being excited preferentially to the R0 mode when the die was under load. This is likely to happen if the R3 frequency is close to the driving frequency, because the R3 mode is more dynamically balanced than the R0 mode. To avoid the problem it is necessary to increase the separation between the required (R0) and undesirable (R3) modes. One advantage of EMA is that the results can be interfaced with computer software to predict the effect of structural modification on modal response. This enables one to determine how much mass or stiffness needs to be added or removed at specified locations to shift the frequency of any mode by a given amount. This method was used to modify the design of the die so that the R3 frequency would be increased without affecting the R0 frequency. The modified die design has material removed at three regions around the circumference, and the FRFs from retesting with ESPI and EMA are shown in Figure 38. This shows how the R3 frequency has now increased to 21.59 kHz while the R0 is at 20.03 kHz. The improvement was confirmed by further operational testing during which the R0 mode was retained under load.

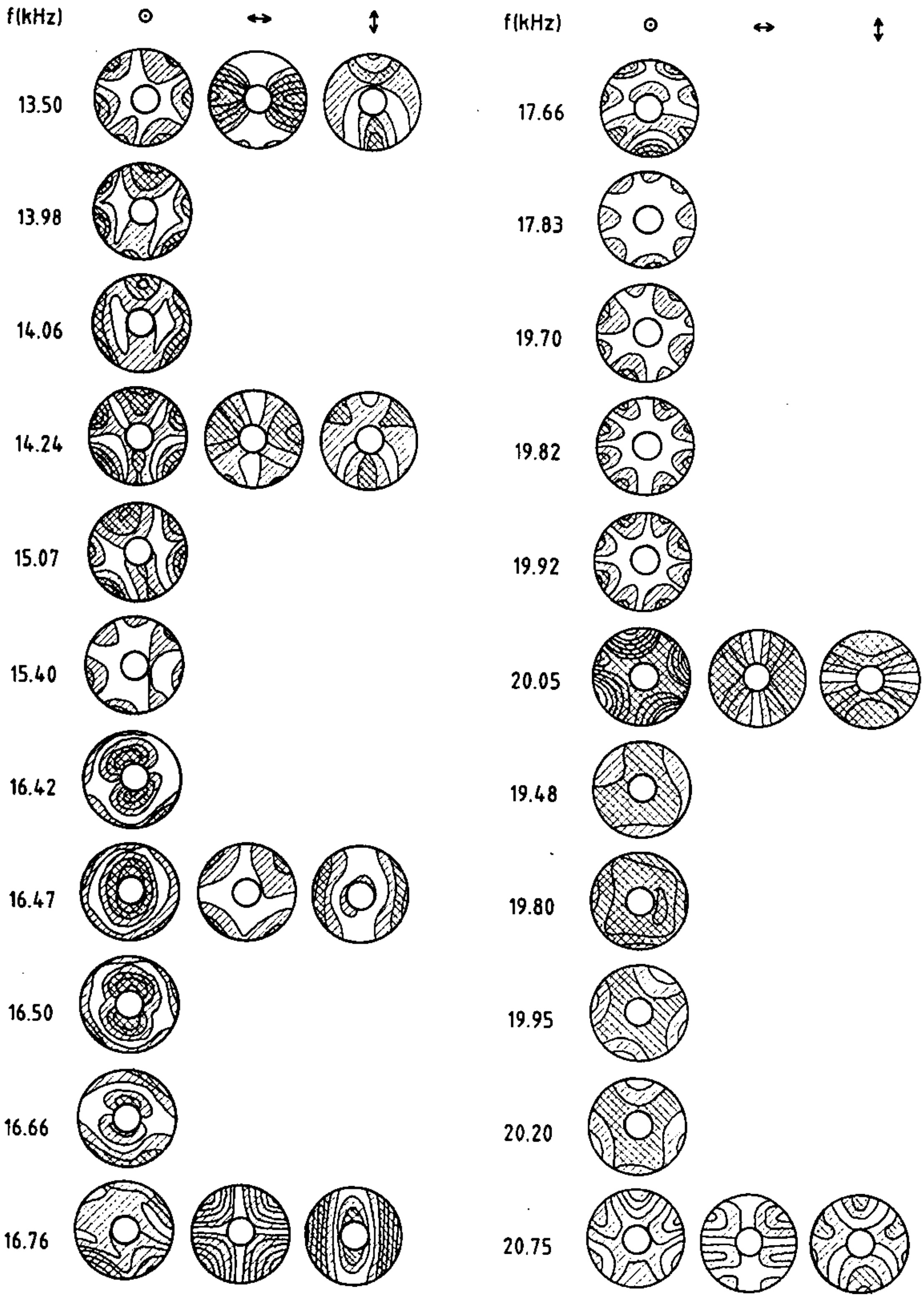

Figure 32: ESPI analysis of ultrasonic die

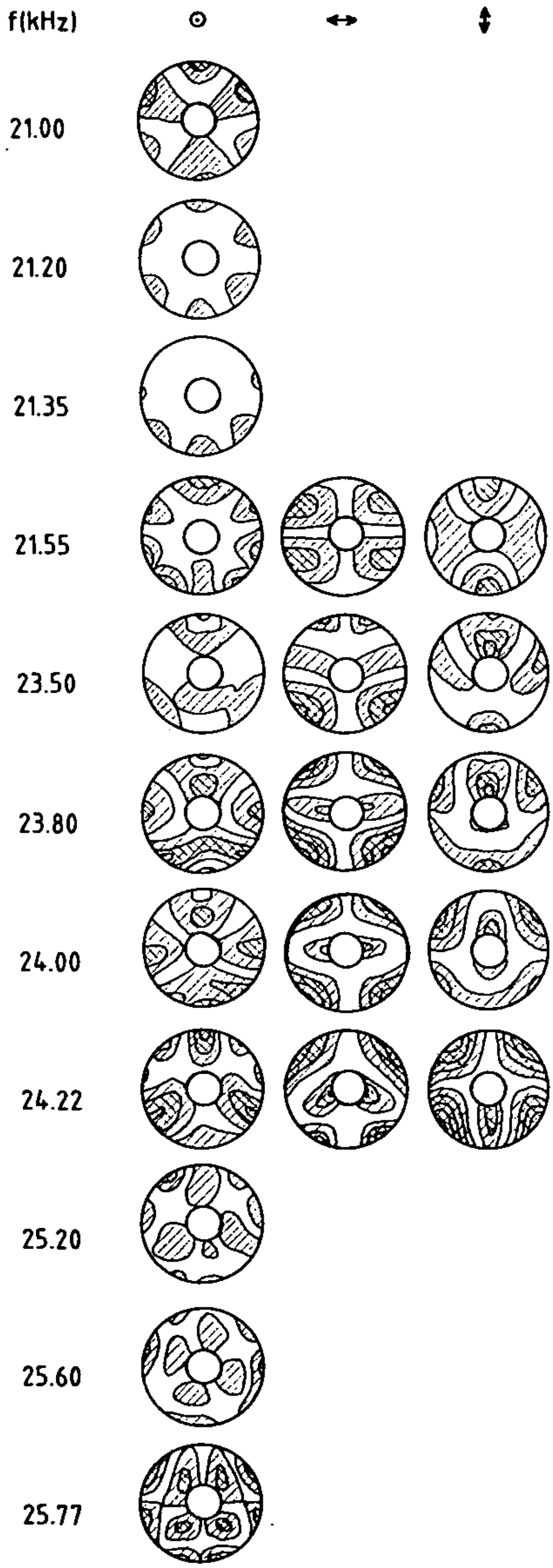

Figure 33: ESPI analysis of ultrasonic die (continued)

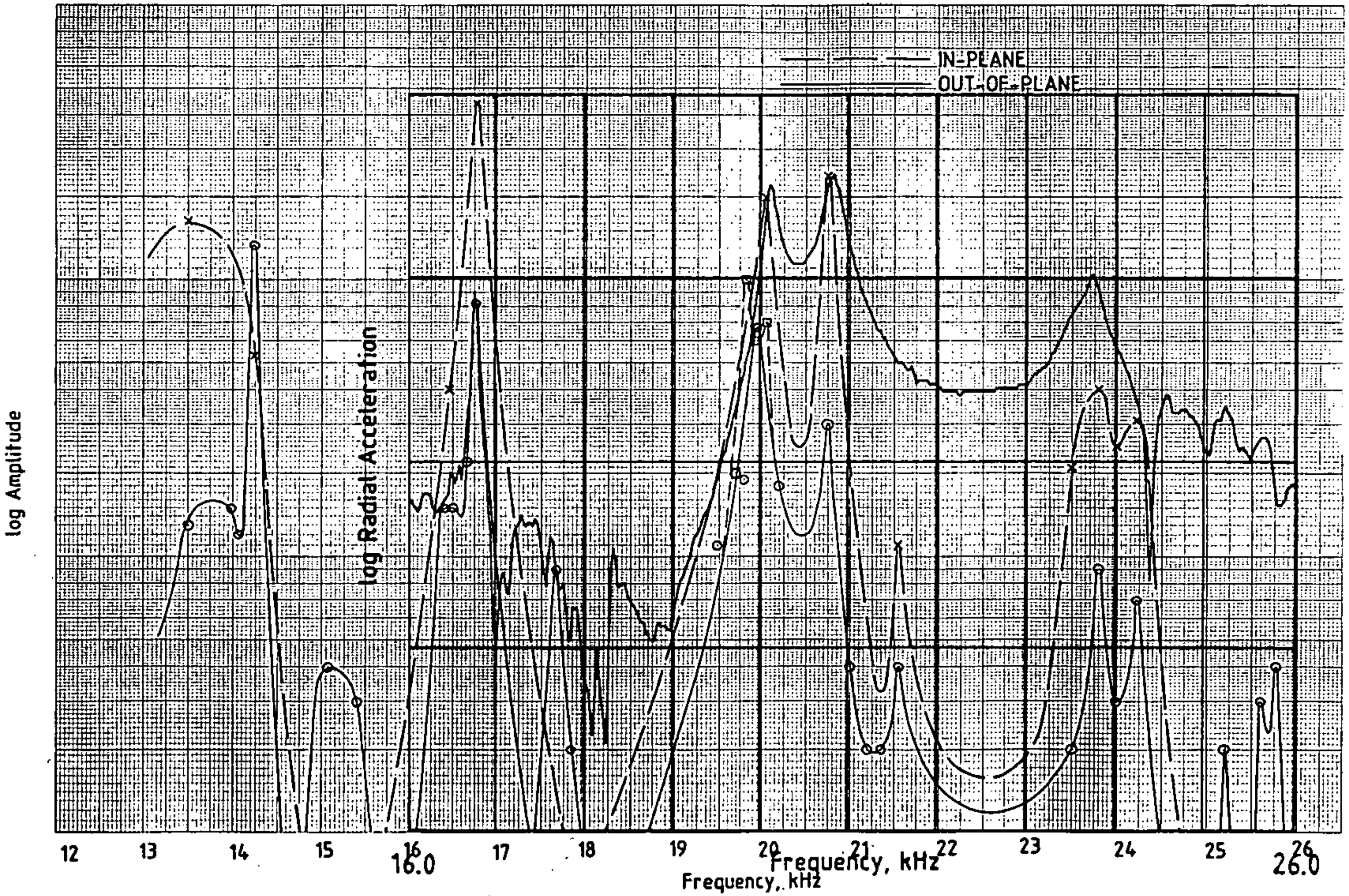

Figure 34: ESPI FRF for aluminium die, overlaid with accelerometer FRF

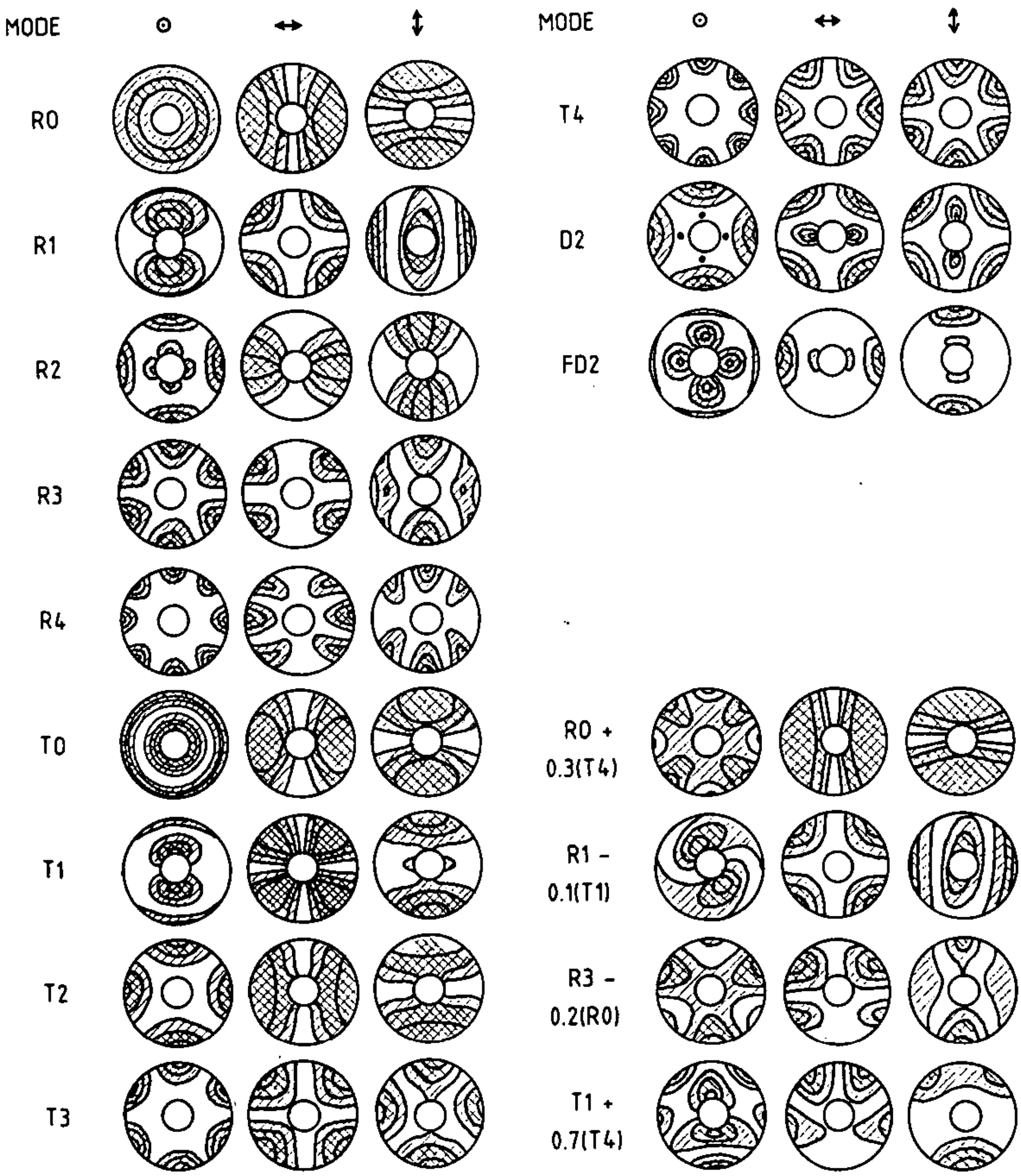

Figure 35: Finite element plots for ultrasonic die modes

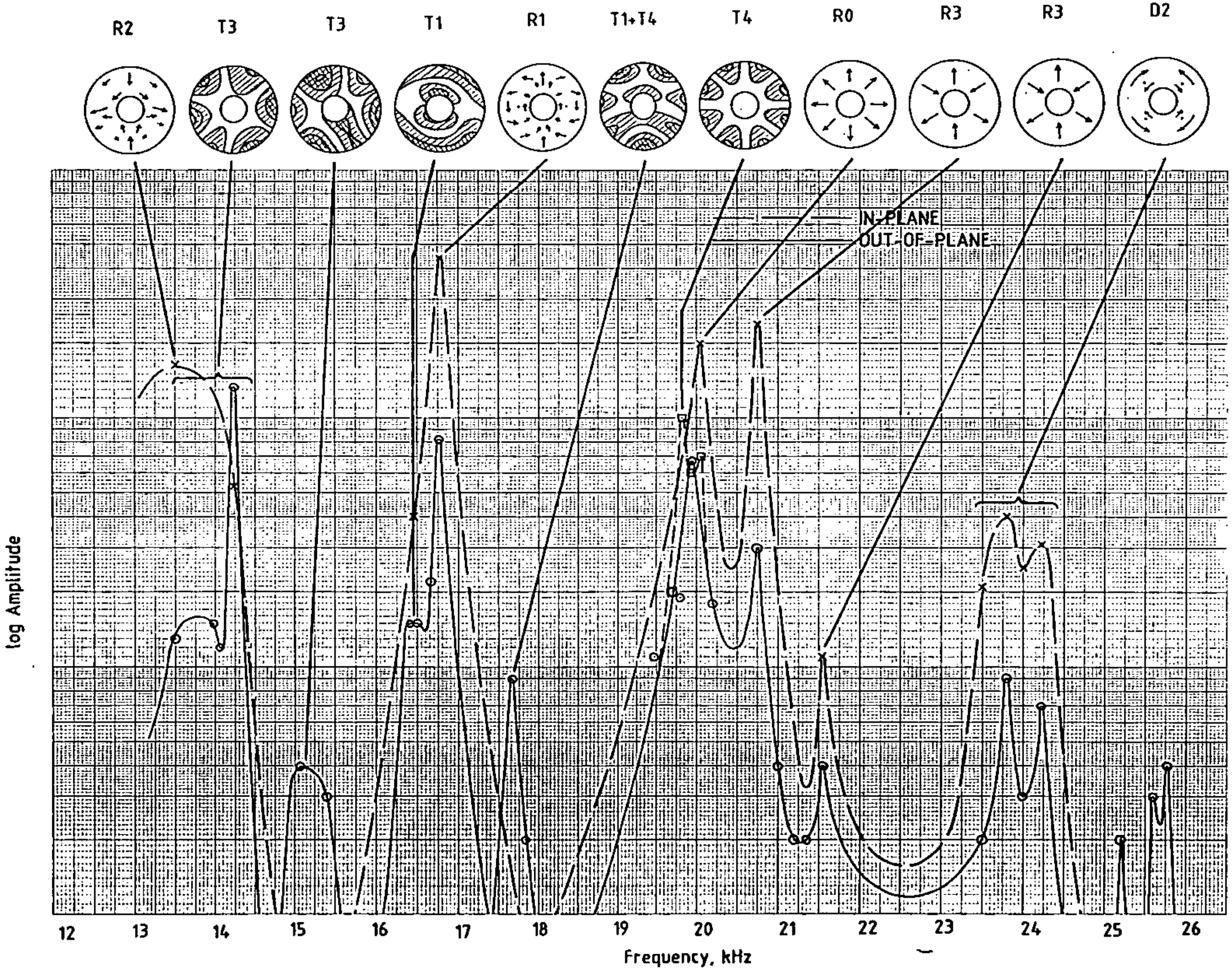

Figure 36: Resonant modes identified from ESPI frequency response function

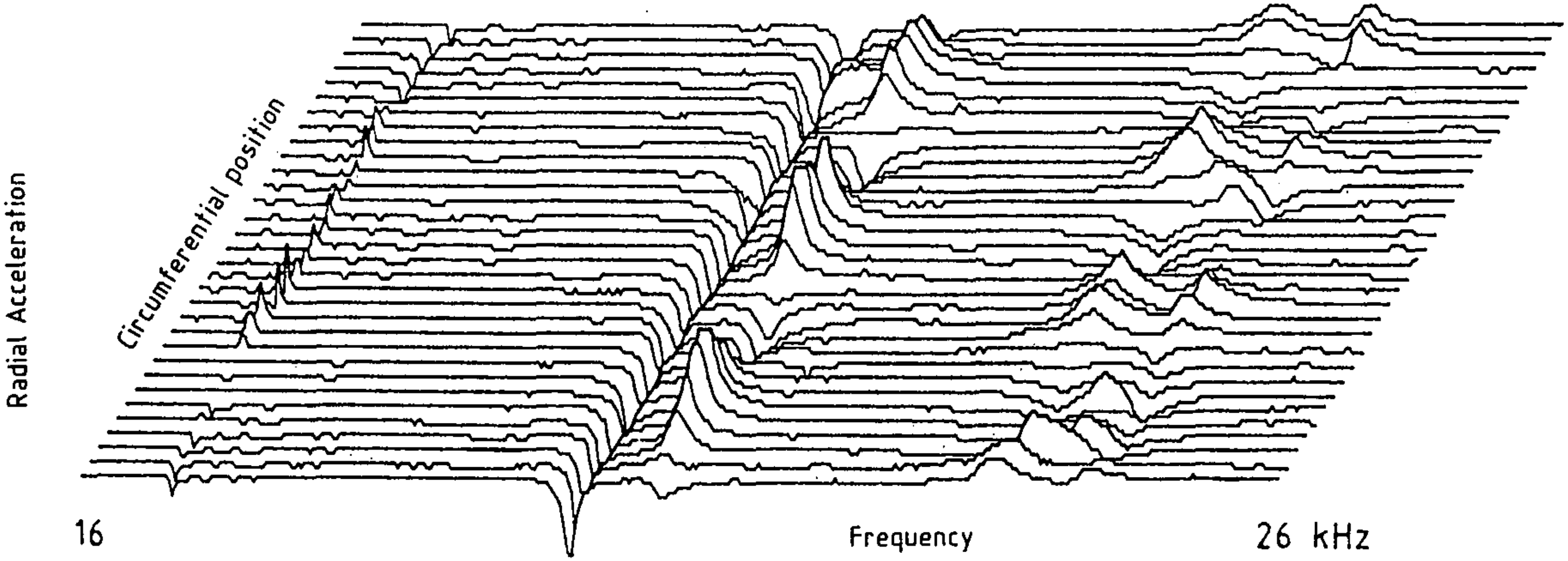

Figure 37: Waterfall plot of accelerometer results around circumference of aluminium die

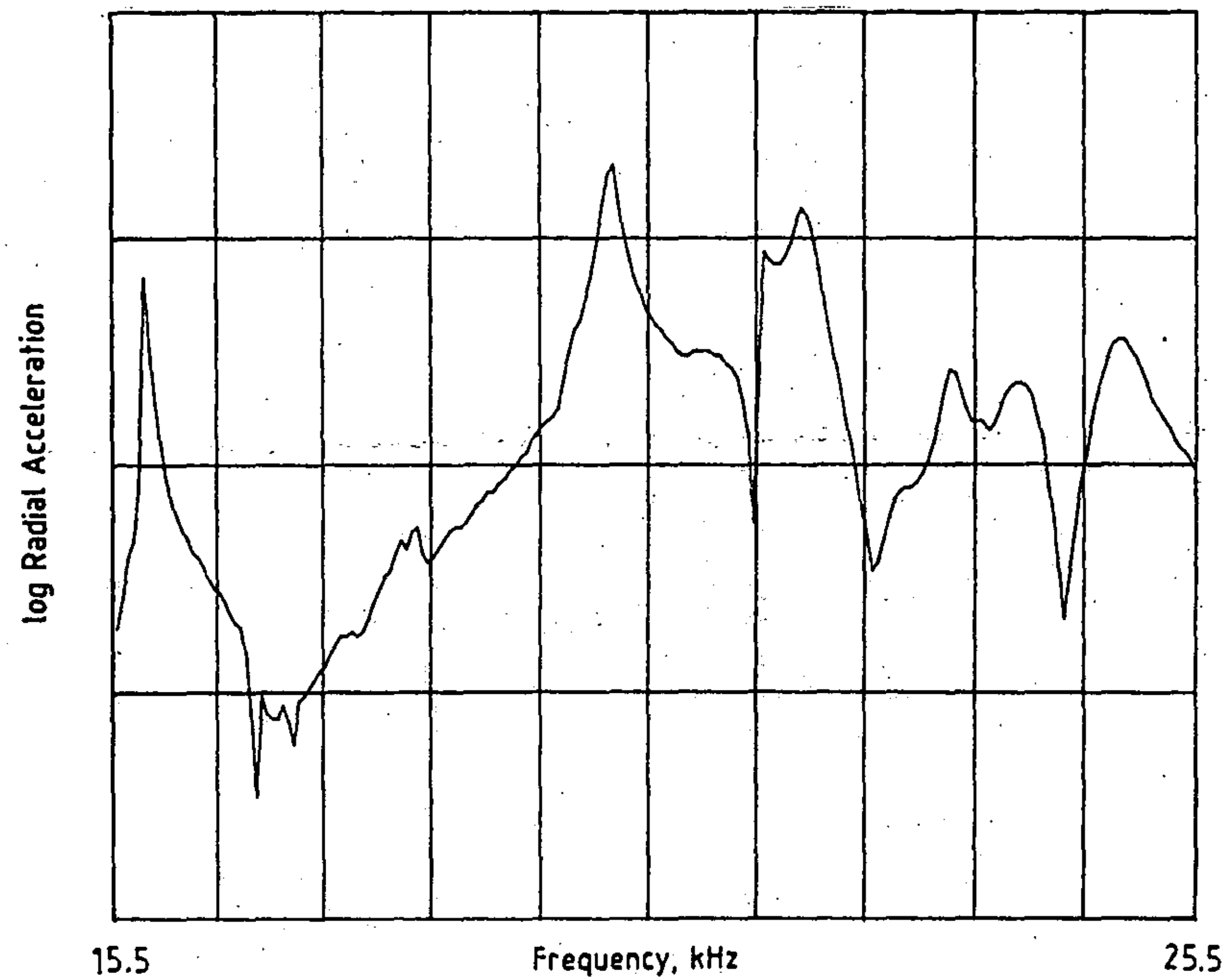
log Radial Acceleration
15.5
Frequency, kHz
25.5

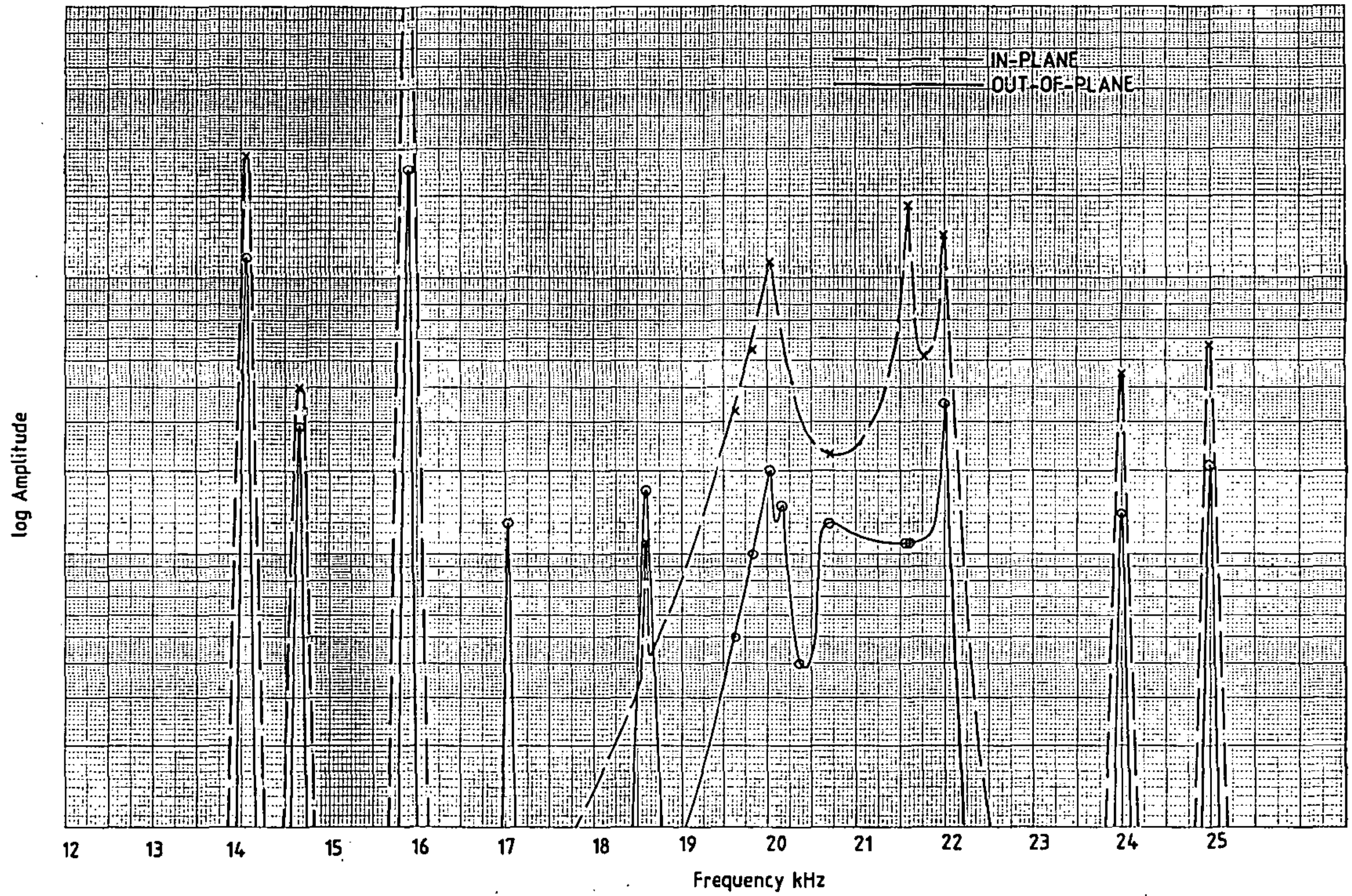

Figure 38: ESPI FRF for modified (3-flat) die, overlaid with accelerometer FRF

5.2 ULTRASONIC CUTTING SYSTEM

Ultrasonic vibration can be applied beneficially in a variety of engineering processes in addition to drawing and necking. A common feature which makes ultrasonics particularly useful is the ability to transmit the vibrational energy to the point where it is required, i.e. where the work is being done. For maximum efficiency this generally requires a resonant tuned system which produces the required mode shape at the workpiece from a suitable input source. In the case of the forming die (section 5.1) the driving transducer was attached directly to the die, but in some cases it is necessary to design a tuned transmission system to deliver the energy. This can be custom designed, or constructed from standard components such as half-wavelength spacers, velocity amplifiers, splitters etc. An example of the latter is a prototype device[130] for making multiple cuts in paper, card and friable or brittle products which has been studied using three-dimensional ESPI.

The system can be put together in many different permutations according to the application, one example of which is shown in Figure 39. The element furthest left is a piezoelectric transducer tuned to resonate in the fundamental longitudinal mode at 20 kHz, which drives the system. This is studded to a velocity amplifier horn which is mounted at a nodal plane to the support bracket. This transmits the ultrasonic energy to a rectangular mother horn, which in turn couples the energy into a pair of cylindrical spacer horns. Successive pairs of horns can be added which support the cutting blades, examples of which are shown in Figure 40. For the system to function effectively it is necessary that the blades and different horn sections be connected together at antinodal points, and hence the lengths of the horns are designed to be one half-wavelength of the ultrasonic wave energy. The horns are designed to vibrate in a longitudinal mode and the blades in a flexural mode, so this is an ideal application for the three-dimensional interferometer. Prior to testing with ESPI,the system was suffering a problem due to the blades fracturing along a straight line across the width, and the aim was to investigate possible causes of failure and recommend improvements in design.

Figure 41 and Figure 42 show the results of in-plane and out-of-plane analysis of the transducer and the various elements of the transmission system at the fundamental resonance of the transducer. Each image is labelled with the frequency and driving voltage as indicated by the ultrasonic generator; resonant frequencies were found to vary significantly with changes in power level. The fringe pattern in Figure 41(b) shows that the in-plane (longitudinal) motion of the transducer is nodal at the centre and vibrating symmetrically at each end. There is very little out-of-plane (radial) motion, Figure 41(c), just a slight bulging around the piezoelectric element stack. This confirms that the transducer is operating as intended. Figure 41(d)-(f) show a single cylindrical horn connecting the velocity amplifier to the rectangular horn. Here the longitudinal motion is again as intended, but the out-of-plane fringe pattern reveals significant radial motion (in the centre) and tangential motion (at the right). This suggests that some of the energy is being converted to flexural and torsional vibration which will not transmit the required longitudinal motion efficiently. Similar effects were observed on the rectangular horn, Figure 42(a)-(c), and the pair of output horns, Figure 42(d)-(f). The second order torsional mode is particularly obvious in (f). In each case the degree of out-of-plane motion observed varied considerably as the stud connections were loosened and re-tightened, and this led to a recommendation that a more consistent clamping arrangement should be a high priority.

The original blade design had straight parallel edges as shown in Figure 43(a), and this was studied using the out-of-plane interferometer. A large number of resonant modes were observed, some of which could easily be identified as normal modes of a clamped-free-clamped-free rectangular plate. Figure 43(b), (c) and (d) show three examples recorded at 10.973, 20.122 and 24.912 kHz respectively, and (e) is an example of a non-symmetric mode at 20.906 kHz. These experimental results showed excellent agreement with predictions made by Lucas[131] using FE analysis. The predicted normal modes were mostly of the form (i,j), where i is the number of lateral nodal lines across the width of the blade (including the clamped ends) and j is the number of longitudinal nodal lines. The resonances shown in Figure 43(b), (c) and (d) correspond to the predicted (5,0) at 10.572 kHz, the (7,0) at 22.171 kHz and the (2,4) at 24.531 kHz respectively. These are shown in Figure 43(f), (g) and (h). The (7,0) mode was excited at the fundamental resonance of the driving transducer, and this explains the problem of the fractured blades. Stress plots produced from the FE analysis showed that this mode has high bending stress values with maxima along the lateral antinodes. Under high frequency vibration this is likely to lead to very rapid fatigue failure. From this analysis it was recommended that a new blade should be designed which would resonate in the (2,2) mode at 20 kHz. This mode has no nodes along the cutting edge (except for the clamped ends), has maximum amplitude at the centre of that edge, and has much lower maximum stress.

Figure 44 shows two blades of modified design being driven simultaneously by the system shown in Figure 39. They are viewed slightly obliquely with the out-of-plane interferometer so that both can be seen together, as shown in Figure 44(a). Figure 44(b) demonstrates that both blades can be excited simultaneously into the desired (2,2) mode at a frequency close to 20 kHz, although again this was sensitive to variations in clamping torque. With a slight reduction in frequency the modes distort due to the influence of a different mode having a close resonant frequency, as shown in Figure 44(c). Figure 44(d) shows another resonant mode at a close frequency, and Figure 44(e) shows a speckle averaged close-up of the same mode demonstrating better fringe visibility. Inspection of Figure 44(d) revealed a set of fringes along the cylindrical horn, and radial out-of-plane observation, Figure 44(f), showed clearly that there is a strong flexural resonance of the horn at this frequency. This is undesirable as it is likely to reduce the operating efficiency and increase the cyclic stresses. These results indicate that with some fine tuning of the blade and horn design the resonant response can be optimised, and indeed operational tests of this blade design have shown improved performance and blade life.

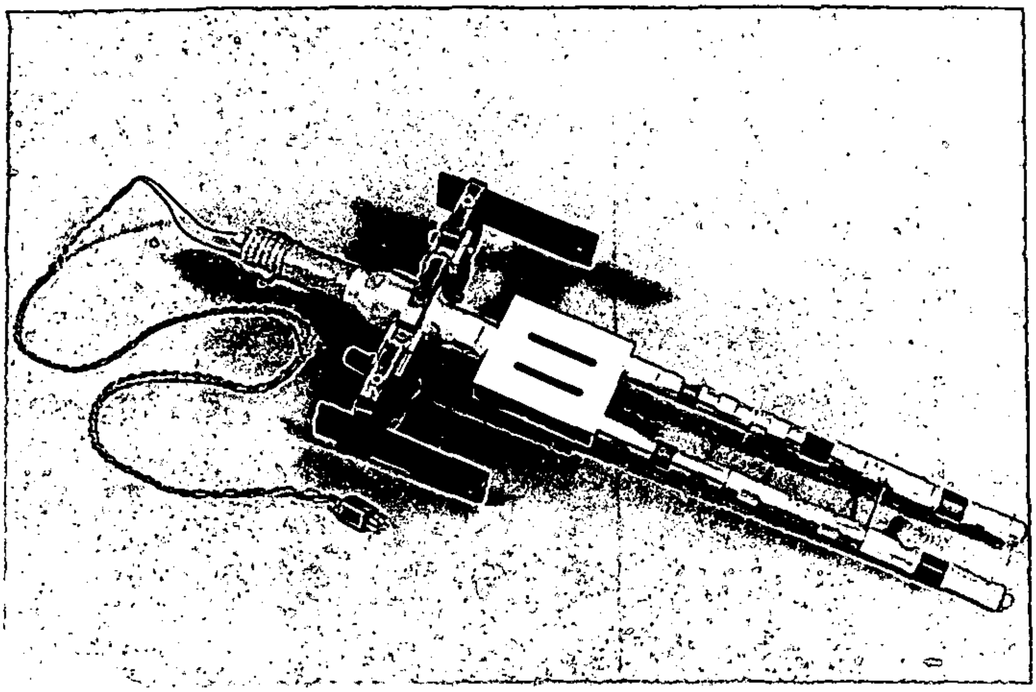

Figure 39: Ultrasonic cutting system

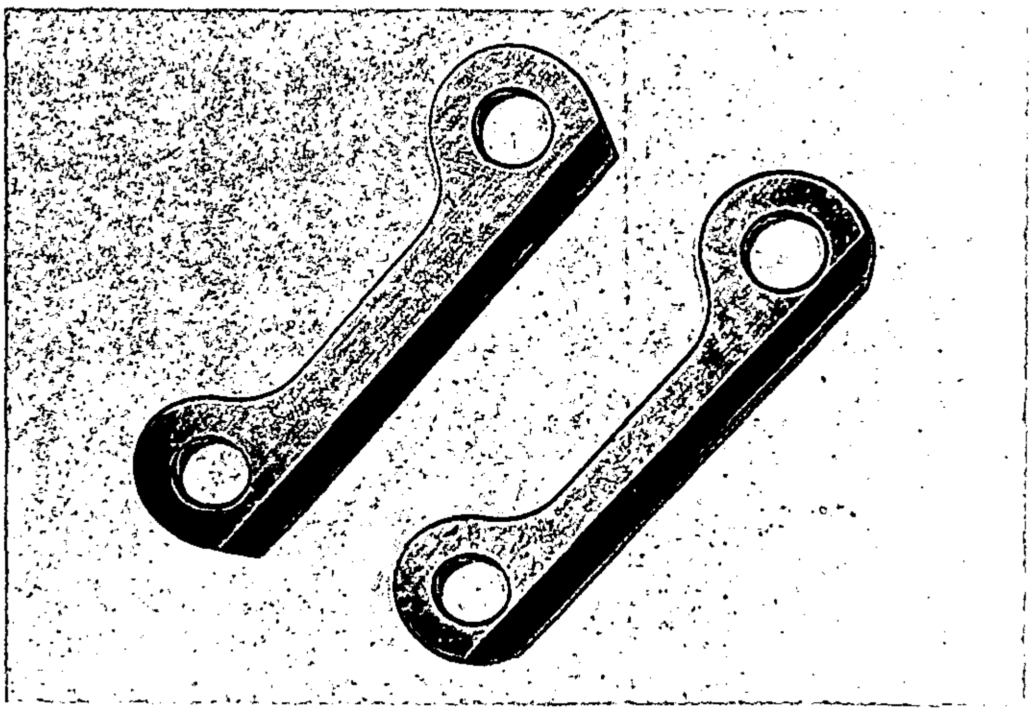

Figure 40: Ultrasonic cutting blades

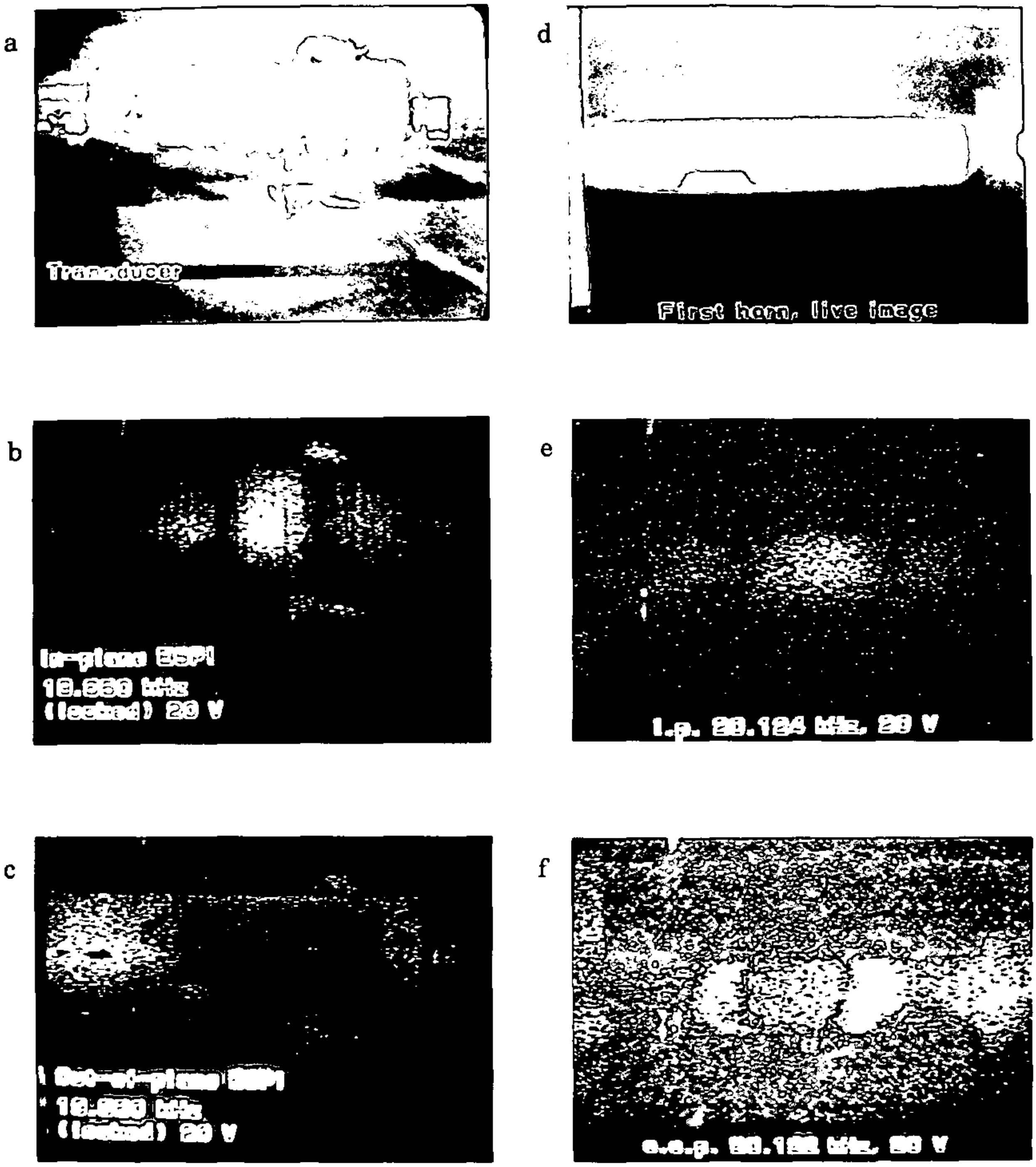

Figure 41: Ultrasonic cutting system: transducer and horn vibrations

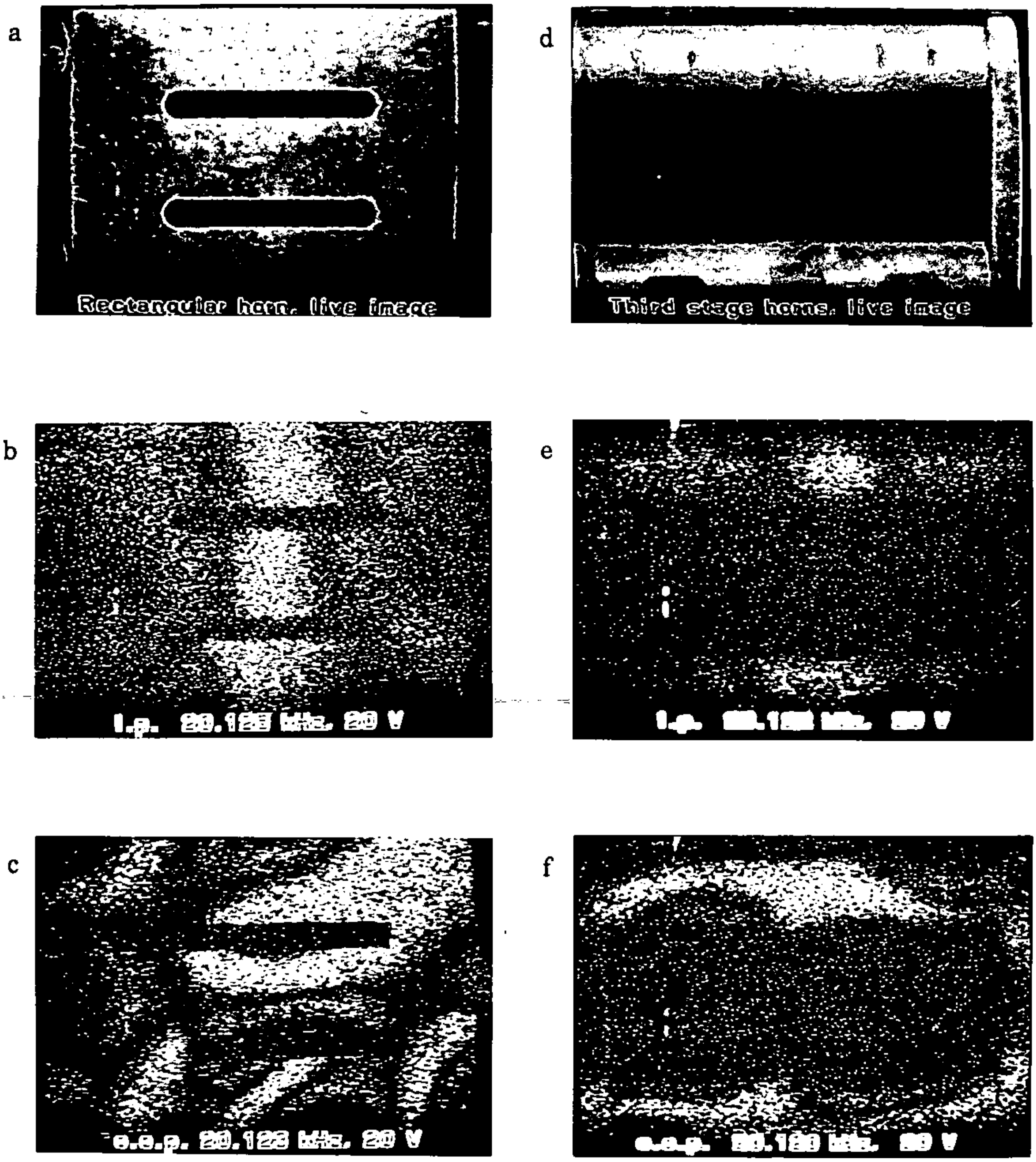

Figure 42: Ultrasonic cutting system: horn vibrations (continued)

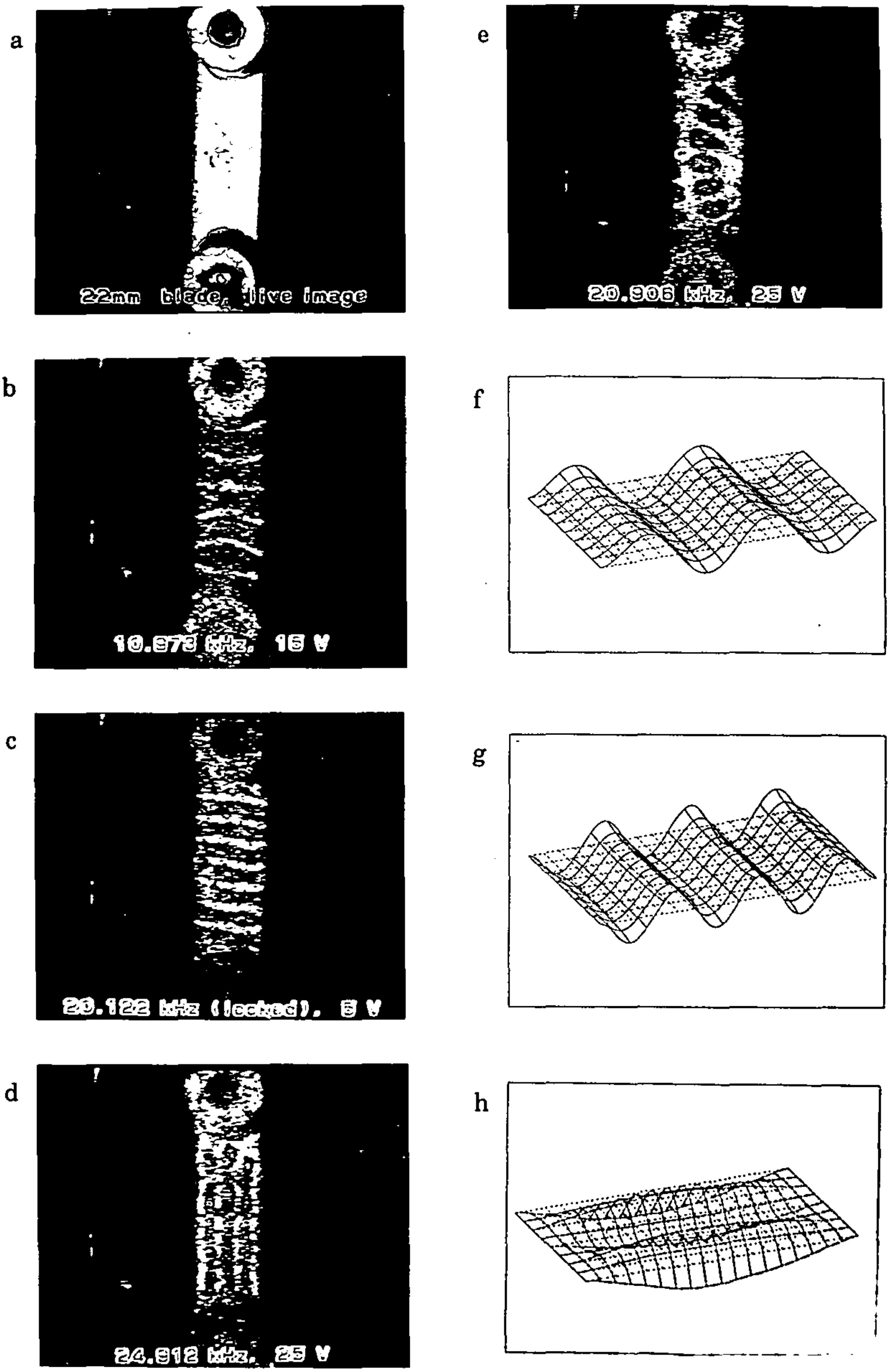

Figure 43: Ultrasonic cutting system: blade flexural vibrations

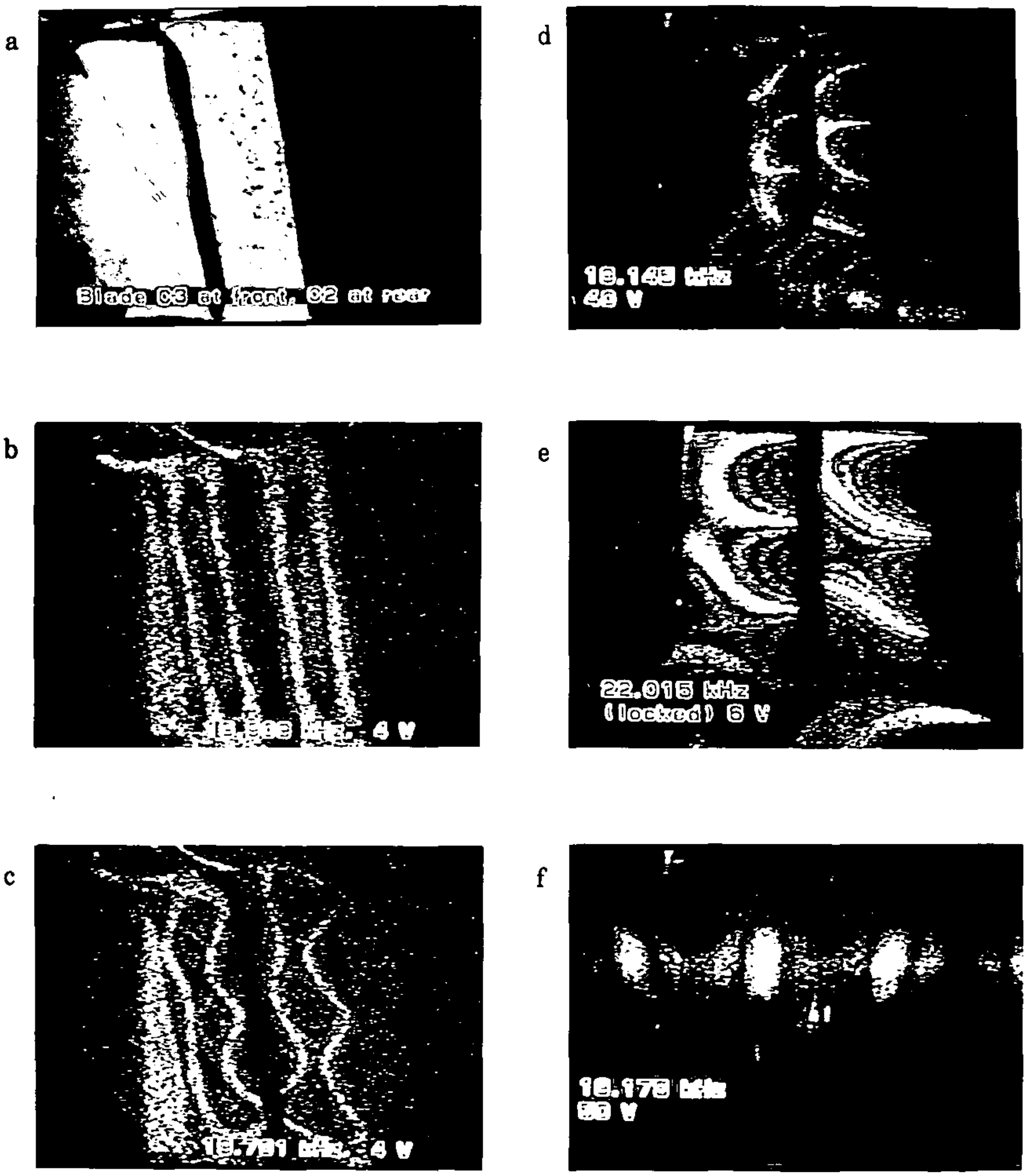

Figure 44: Ultrasonic cutting system: coupled horn/blade vibrations

5.3 TURBOCHARGER BLADE

Turbomachinery blades, including turbine and compressor blades, have been the subject of great interest in engineering vibration studies. As components of high speed rotating machinery they are often subjected to complex cyclic force inputs, and if the induced blade vibrations cause excessive stresses or fatigue cracking then the results can be catastrophic. Hence it is essential to try and prevent resonances which could cause such conditions from occurring during operation. A previous project at Loughborough[114] had studied the modal response of a single turbocharger blade using conventional out-of-plane ESPI in conjunction with FE and accelerometer EMA, and had concluded that "ESPI is an extremely powerful and fast method for obtaining results but is limited by its inability to view three-dimensionally". The principle problem was that the nodal lines indicated by the fringe patterns sometimes suggested a different type of mode to that which was actually occurring. The same problem occurred whilst trying to interpret FE results presented as isometric wire mesh plots. In both cases the problem was due to viewing in one direction only, because the displacement which is shown to be zero is in fact only the component resolved in the viewing direction. This will clearly make it difficult to identify different types of mode by viewing them in the same direction. To try and overcome this limitation the three-dimensional ESPI system was subsequently applied to studying the same blade.

The blade is shown in Figure 45 with the vibrator used to excite it and the global coordinate axes of the interferometer. The blade resembles a cantilevered beam but has fairly complex geometry, with varying curvature and thickness and a high degree of twist from root to tip. This causes the normal beam-type flexural, torsional and extensional modes to couple together and become three-dimensional in character (see Appendix C). For this blade the 'span' modes which involve stretching in the y direction (equivalent to extensional modes) occur at high frequencies and are difficult to excite in a stationary blade, and the $\partial^2 z/\partial y^2$

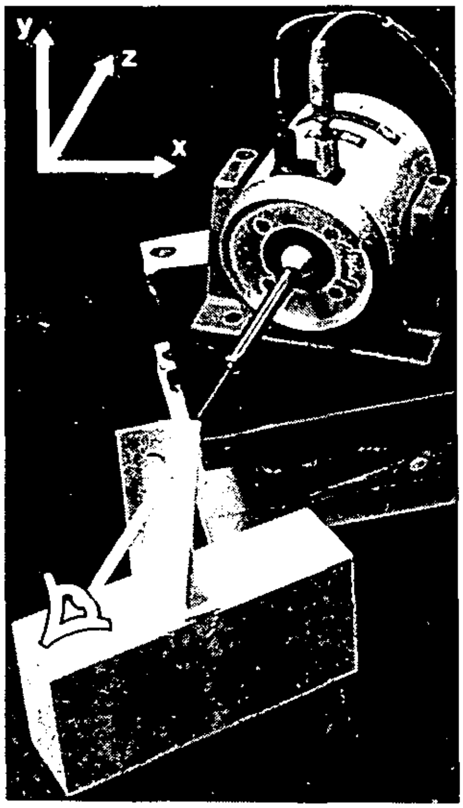

Figure 45: Turbocharger blade with viewing axes

curvature is everywhere small so that the other modes do not produce significant y components of motion. Hence it was sufficient for the purposes of the study to view with z- and x-sensitive interferometers.

Figure 46 and Figure 47 show the first six resonant modes as seen by the z and x interferometers, with unidirectional views of the deformed FE model as computed by Wang[132]. The mode at 1400 Hz is readily identifiable as the first order flap (1F) mode, having very large z components but very little motion in the x direction. The mode at 2360 Hz proved to be the most difficult mode to interpret in the original study as the z fringe pattern is very similar to that observed at 4900 Hz, both of which suggest a second order flap (2F) mode. However the x interferometer reveals that the lower mode is vibrating in a beam-like manner in the x direction, and hence identifies it as the first order edge (1E) mode. The higher mode has much smaller x components and is the 'true' 2F mode. The other modes can similarly be identified as the first order torsional (1T) at 4510 Hz, 3F at 7450 Hz and 2T at 9900 Hz.

The existence of significant z motion in the 1E mode and x motion in the F and T modes is due to the curved shape of the blade. The direction of the surface normal varies from approximately -45° to +45° (with respect to the z-axis) across the image, so that although the 1E mode is predominantly in-plane motion, this includes significant z-motion in the areas which are viewed obliquely. This is a good example of the need for surface contouring to relate global coordinate measurements to local out-of-plane and in-plane components, as discussed in section 3.1.3. The oblique angle of the z nodal lines in the 2F and 3F modes is principally due to the taper from the leading to trailing edge of the blade. It should also be pointed out that the individual modes were isolated by careful choice of excitation force input position, and in general many of the resonances were combination modes.

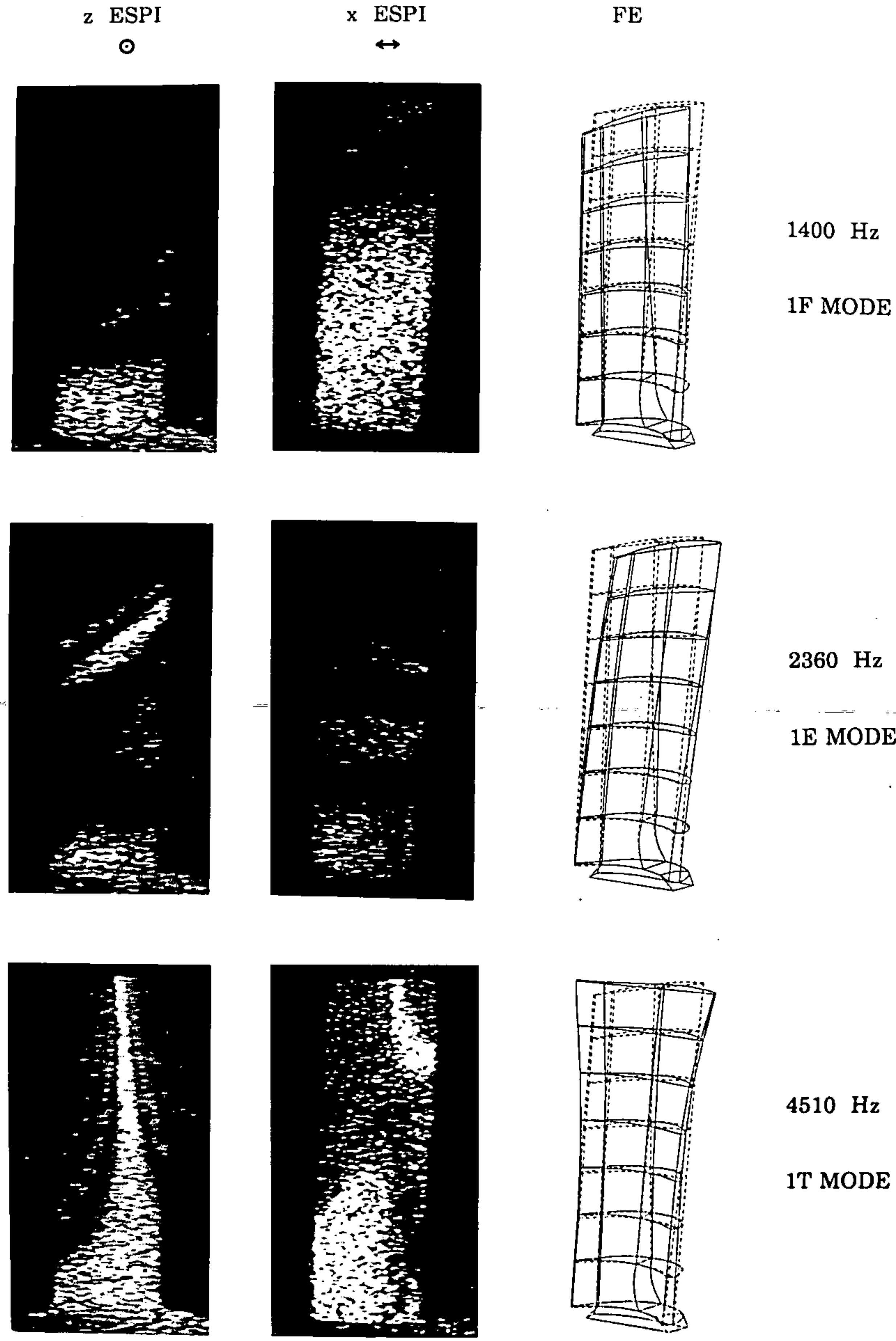

Figure 46: Turbocharger blade vibrations

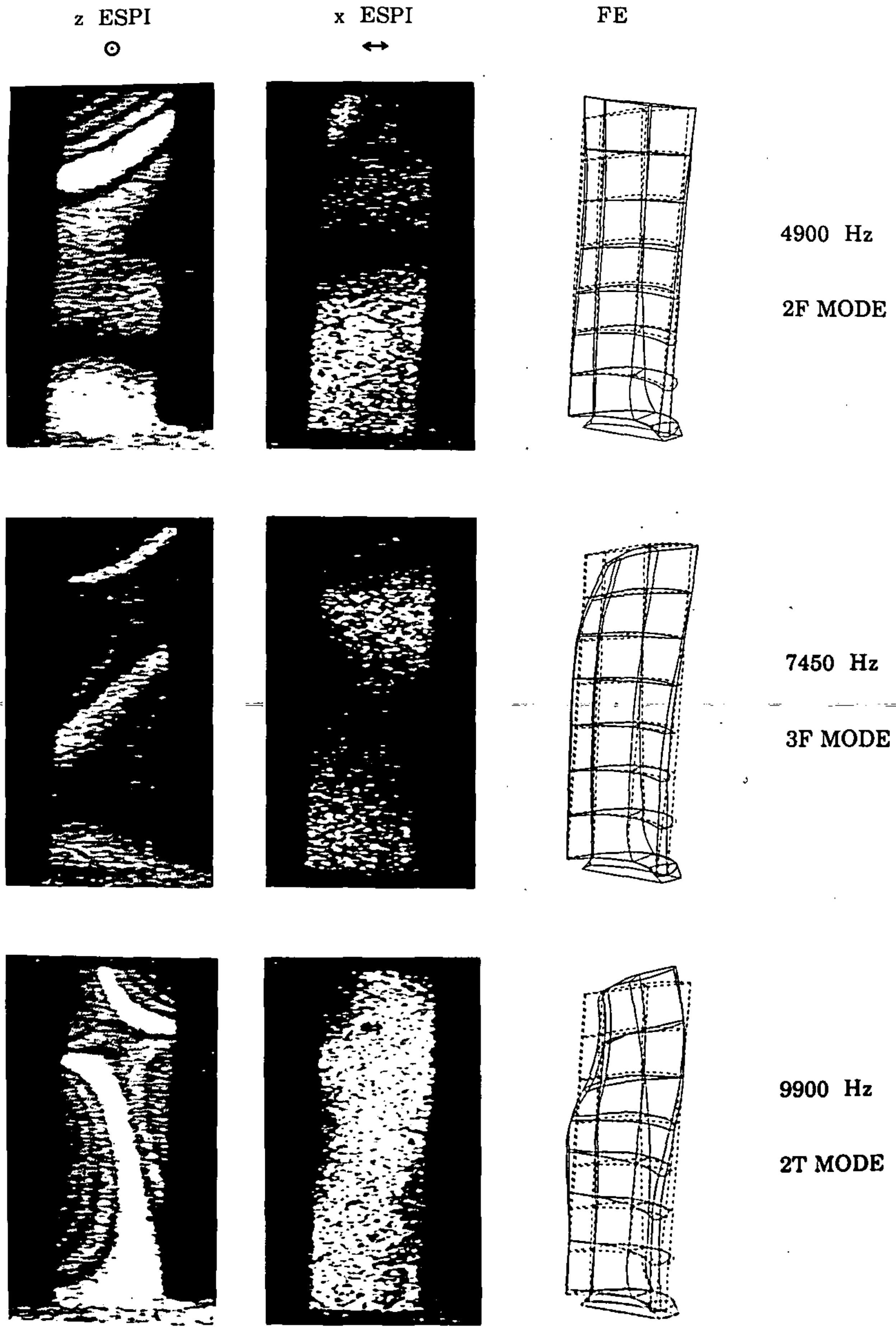

Figure 47: Turbocharger blade vibrations (continued)

6. NON-STEADY STATE VIBRATION ANALYSIS

All the results presented in the previous two chapters have been for steady-state resonant vibrations of stable objects within laboratory conditions. Many engineering vibration problems occur under less ideal conditions, where the vibration may be time-variant or the object may be subject to more than one type of excitation simultaneously. For example, in an industrial environment a machine will typically experience low frequency vibration and shock transmitted through the ground in addition to any self-induced resonance. These situations have always proved problematic for time-average study, and this chapter demonstrates how pulsed ESPI can be used to overcome some of the problems and produce results which have not previously been possible with continuous wave illumination. Three studies are described: (i) simultaneous standing wave and travelling wave vibration in a beam; (ii) simultaneous translation and vibration of a plate; and (iii) measurements of machine vibration in a factory environment.

6.1 TRAVELLING WAVES

Appendix B describes how vibrational energy is propagated through a structure by travelling waves, which at resonance interfere to produce a standing wave pattern. In the examples considered so far almost all the vibrational energy has been reflected back by the boundaries and interfaces of the system so that the travelling waves almost completely cancel out at resonance leaving very low net power flow through the system. Under non-resonant conditions or in situations where some of the interfaces disperse a significant proportion of the incident energy as well as reflecting some, power is transmitted through the system by travelling waves which may co-exist with standing waves caused by partial reflection. It is desirable to be able to measure the travelling wave component for calculating the structural power flow[133]. The time-average of a pure travelling wave gives a constant amplitude across the surface, hence this cannot be measured using continuous wave illumination. Pulsed ESPI measures the net displacement between two instants or phase epochs, hence the travelling wave component can be isolated by synchronising the laser pulses to the zero displacement phase in the standing wave cycle. Similarly, by varying the pulse timing the total motion due to both components can be analysed.

The object chosen to demonstrate vibrational power flow was a steel beam of rectangular section 5x50mm, as sketched in Figure 48. The beam has a free length of 750mm, with one end tapered and packed in sand to give a dispersive interface and the other end excited by an electromechanical shaker. End effects are likely to occur in the vicinity of the shaker and the sand box, but provided that the wavelength of the vibration is small compared to the beam length it should be possible to observe approximately harmonic standing and travelling wave components in the central region. Assuming that the vibration is induced as a

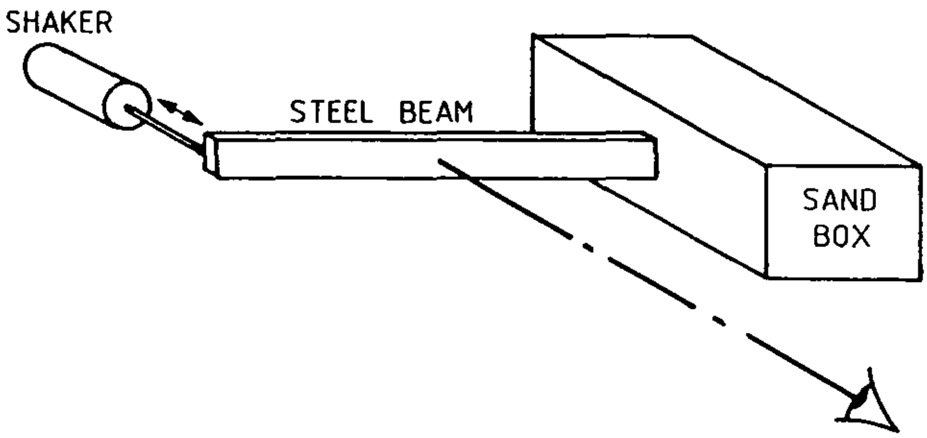

Figure 48: Experimental rig for observing travelling waves

bending wave, the phase velocity c in a homogeneous beam is given by[134]:

$$c = \omega^{1/2}\left(\frac{EI}{m}\right)^{1/4}$$

where ω is the angular frequency, E is Young's modulus, I is second moment of area, and m is mass per unit length of beam. The wavelength λ is then given by:

$$\lambda = \frac{c}{f}$$

where $f=\omega/2\pi$ is the driving frequency.

The central section of the beam was observed normally using the z-sensitive pulsed interferometer (section 3.2.2) to measure the out-of-plane bending motion. Initially the laser pulse triggering was synchronised with the driving signal. The driving amplitude was reduced to zero and a reference interferogram was stored with the beam stationary, then the amplitude was increased and single pulse subtraction used to observe the vibration fringe patterns. Because the travelling and standing wave components were induced at the same frequency the synchronised fringe patterns were stationary. Varying the time delay of the triggering enabled the observed phase epoch to be altered. In the case of a pure standing wave this causes the fringe density to vary whilst the nodal and antinodal positions remain stationary, but in this case the fringe pattern could be seen to be translating whilst the fringe density cycled without passing through zero. This confirmed the presence of a significant travelling wave component.

The laser pulse generator was then connected to a separate frequency generator. With fine adjustment it was possible to match the triggering and driving frequencies and freeze the motion as before. Then, by applying a slight offset to the triggering frequency, the captured phase epoch could be slowly varied so that the motion of the beam was observed in animated slow motion. This is shown in Figure 49 with the beam being excited at 2059 Hz. At this frequency the wavelength predicted by theory is 0.149m and the value measured in practice was 0.147m, or approximately one fifth of the free length of the beam. The fringe patterns shown in Figure 49(a)-(h) are every fourth frame from a recorded video sequence. Figure 49(a) is very similar to that expected for pure flexural vibration of a beam. There are no fixed points in the image to use as a zero reference, but the bending maxima and minima can be clearly identified by the hyperbolic form of the fringes caused by anticlastic behaviour[42,48], and these correspond to the positive and negative maxima of deflection. Points of zero deflection show up as straight fringes midway between adjacent hyperbolas, indicating lines of bending inflexion. This information has been used to plot the deflected form of the beam from the fringe pattern in Figure 49(a), as shown on the transparent overlay. Scaled displacements are plotted along the centre line of the beam, with the point of inflection nearest the left arbitrarily chosen as zero (with pulsed subtraction ESPI points of zero deflection appear as a dark fringe). Similar plots are shown for (b) to (h), maintaining the same dark fringe as zero, and the sequence clearly identifies a travelling wave motion along the beam. The complete sequence shows one cycle of the combined vibration, the reference inflexion point in (h) having moved on approximately one wavelength from (a). The displacement plots indicate some rigid-body rotation of the beam about a vertical axis and also some asymmetry of the hyperbolic fringes (particularly in Figure 49(c)-(e)) which might be caused by rotation about a horizontal axis. It was difficult to prevent such rotation, as the necessary constraints would also have the effect of diminishing the travelling wave component.

The displacement plots overlaid on Figure 49(a)-(h) also show how the travelling wave component can be separated from the standing wave component. The same plots are shown in Figure 50(a)-(h) with the amplitude of the combined wave motion indicated at each phase epoch. This is calculated from the mean distance between lines joining the positive and negative displacement maxima. It can be seen that this amplitude varies in a cyclic manner, being maximum between (d) and (e) and between (h) and (a), and minimum between (b) and (c) and between (f) and (g). The phase and magnitude values of the maxima and minima could be obtained to greater accuracy by including measurements at intermediate phase values. The cyclic waveform indicated by the set of displacement plots is the result of phasor addition of the travelling and standing components. In general the magnitude and phase terms of each will be unknown, but in this case both are excited by the same local force input so that the displacement maxima of each of the two components must coincide spatially and temporally. Hence the maximum total amplitude corresponds to the algebraic sum of the component amplitudes, and the minimum total amplitude corresponds to the travelling wave component only (i.e. as the standing wave passes through zero):

$$a_{max} = a_s + a_t$$

$$a_{min} = a_t$$

where s and t denote the standing and travelling components respectively. In this example $a_{max} \approx 1.20\mu m$ and $a_{min} \approx 0.532\mu m$, giving the ratio $a_s:a_t \approx 5:4$.

Figure 51 shows every fourth frame from another video sequence recorded under similar conditions except that the beam has undergone a small rigid-body rotation about a horizontal axis in its own plane. It can be seen that every vertical section cuts two fringes, indicating a relative displacement between the top and bottom edges of approximately 0.53μm. This is equivalent to rotating the illumination vector, and has the effect of introducing carrier fringes[135] which remove the ambiguity in the turning points. This validates the interpretation given in the displacement plots of Figure 49. These fringe patterns can be analysed in the same way, but show more clearly the travelling nature and variation in amplitude of the combined waveform.

As with the studies presented in chapter 4, it is desirable to automate the fringe analysis and remove the phase ambiguity by applying the phase stepping technique. Figure 52 shows the results of using the single phase step algorithm on the same beam with the laser pulses synchronised to the driving signal. (a) and (b) show the fringe patterns at 0° and 90° phase, and (c) shows the modulo 2π phase map with the unwrapped displacement plot from a horizontal line vector.

It can be seen that this compares favourably with the form of the displacement plots in Figure 49. With the laser and shaker synchronised the maximum and minimum amplitude conditions can be found by varying the triggering delay, and the amplitude values determined automatically by phase-stepping in each case to calculate the magnitude of the travelling wave component.

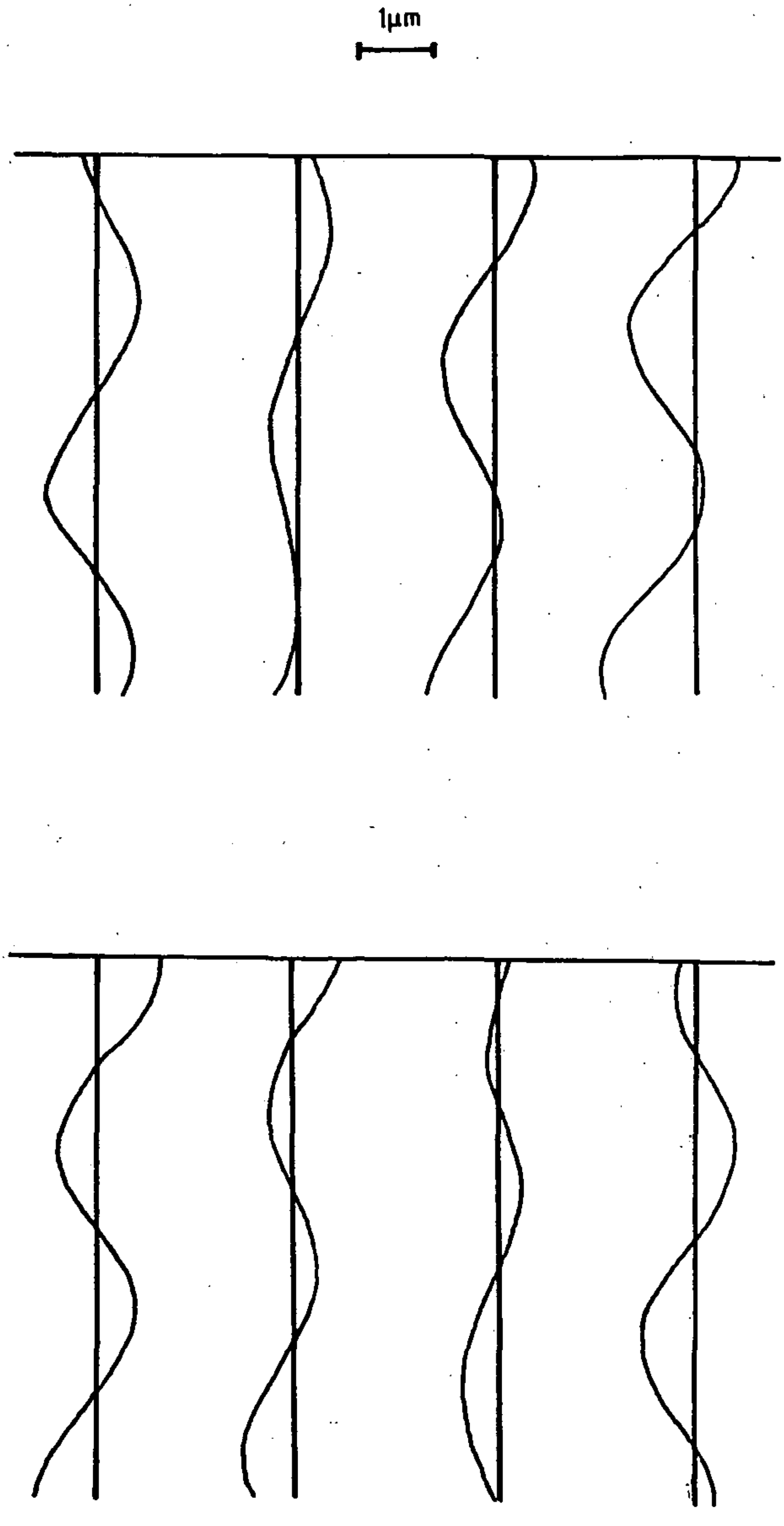
1μm

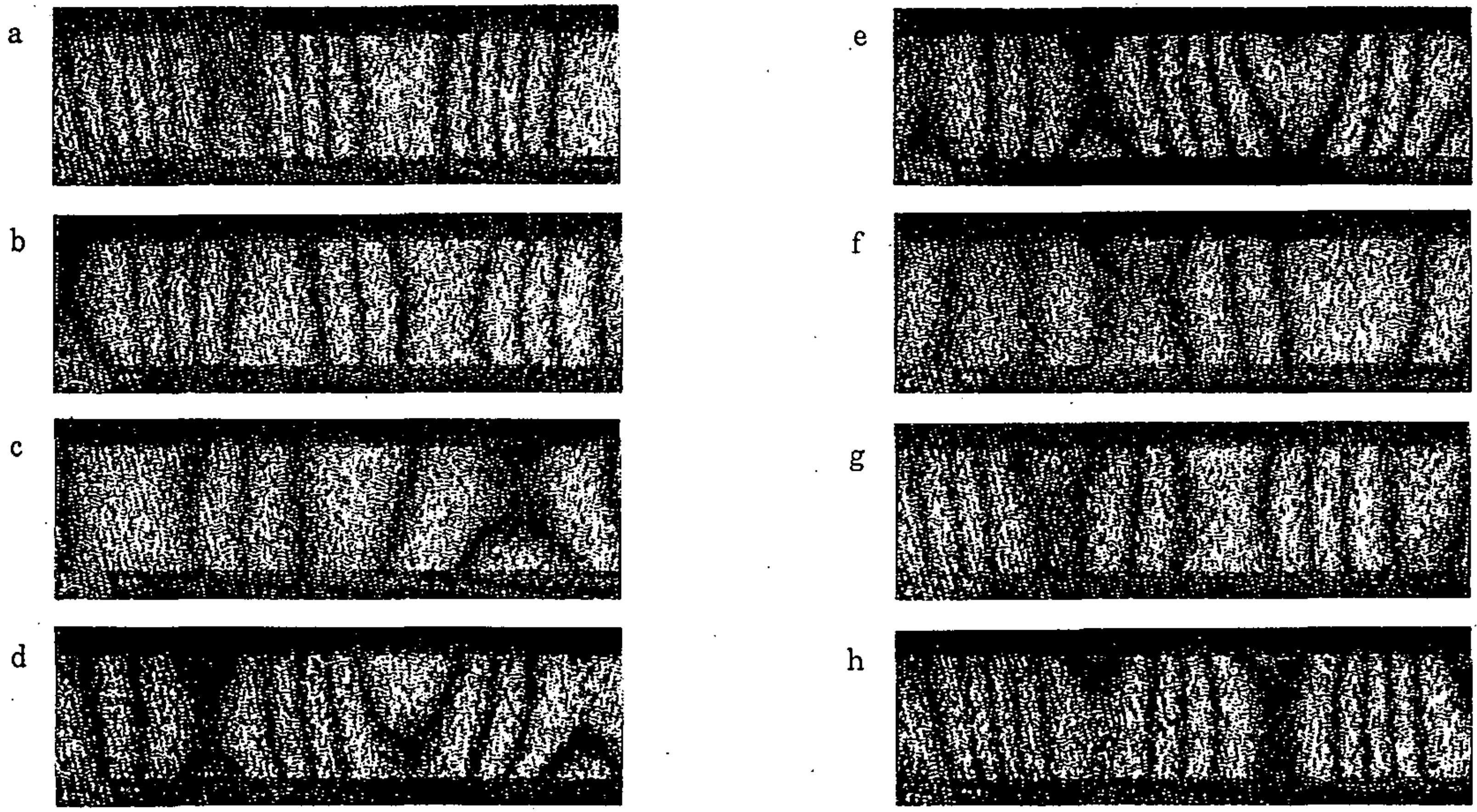

Figure 49: Flexural travelling wave in steel beam vibrating at 2059 Hz

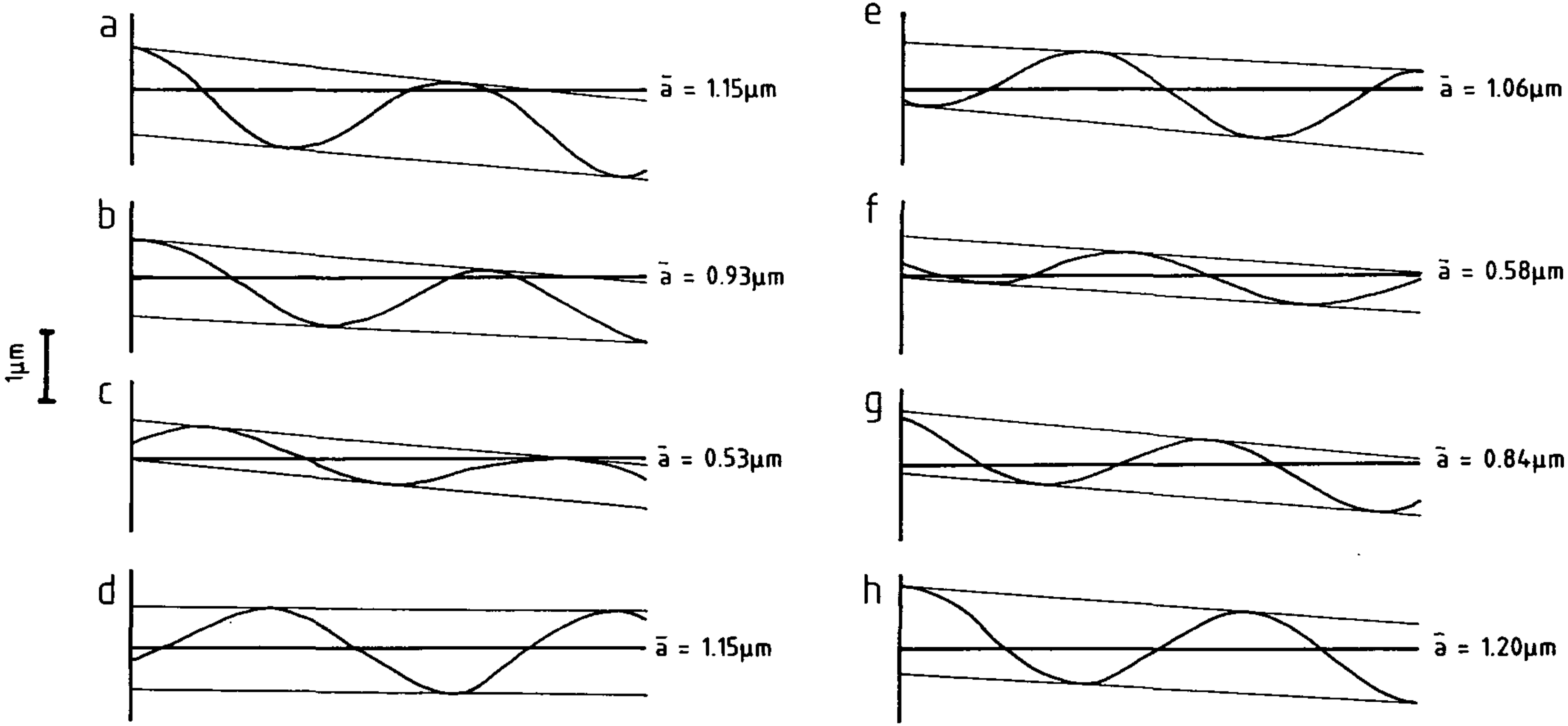

Figure 50: Time-varying amplitude of combined standing and travelling waves

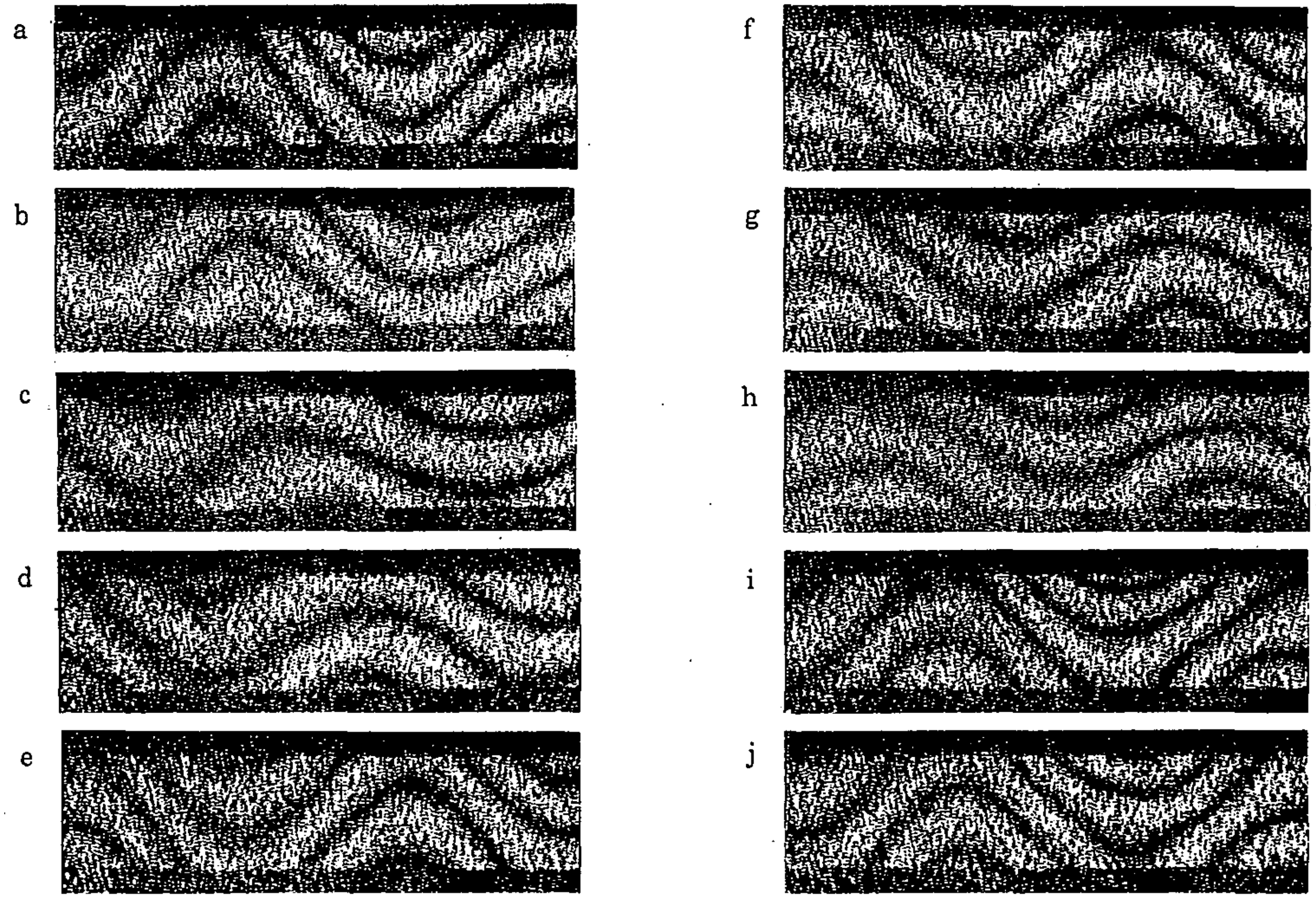

Figure 51: Flexural travelling wave in steel beam vibrating at 2072 Hz

a

b

c

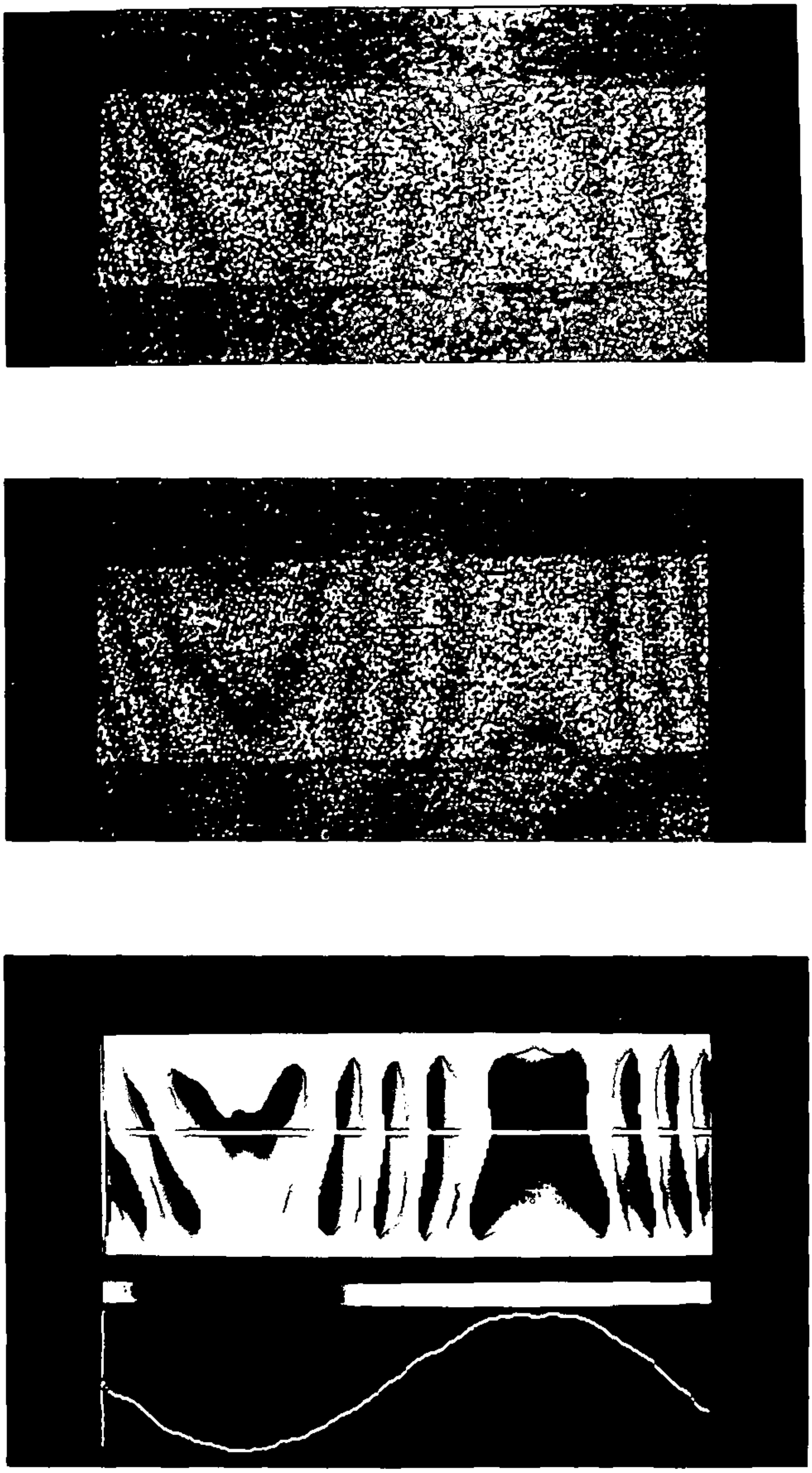

Figure 52: Phase-stepped analysis of combined standing and travelling waves

6.2 SIMULTANEOUS TRANSLATION AND VIBRATION

All the pulsed ESPI results presented so far have used single pulse subtraction to form the fringe patterns. It has been shown in section 6.1 that this can give good results in the presence of some rigid-body motion, and in section 4.2.3 that it can freeze motion at frequencies in excess of 30 kHz. However if the motion of the target between consecutive video frames is sufficient to move the image by more than the speckle size then the speckle patterns will not correlate and fringes will not form. This problem can be overcome by using twin-pulse addition, firing two laser pulses during one camera exposure as described in section 3.2.2 and Appendix A.4. Because the pulse separation is now much shorter, the target movement and hence also the decorrelation are greatly reduced. Correlation by addition does not remove any of the existing noise, so addition fringes have much higher noise levels than subtraction fringes and therefore much poorer visibility. With interferometer configurations which use a reference beam (for example the out-of-plane sensitive interferometer) this can be partially offset by subtracting the reference beam optical noise prior to addition, but this is not always possible. Another technique which can be used is to subsequently subtract two fringe patterns which have been formed by addition[106]. This can sometimes produce fringes of much improved visibility, but requires very careful interpretation as the fringes now indicate correlation of two vibration patterns, rather than a direct measure of surface displacement.

To test the performance of pulsed addition ESPI for studying unstable objects, a laboratory experiment was designed in which a target could be simultaneously vibrated and translated. This used a variable speed translation stage to carry either the pinned square plate (as studied in sections 4.2.2 and 4.2.3) or a similar clamped square plate, which could be studied using the pulsed laser in either an out-of-plane or in-plane interferometer configuration.

The results are shown in Figure 53. (a) shows twin-pulse addition fringes obtained from an out-of-plane interferometer, observing the clamped plate vibrating in a flexural mode whilst stationary. The fringe visibility is poorer than pulsed subtraction fringes (see for example Figure 12), and several rings of optical noise can be seen which have not been subtracted out. The advantage of using addition is indicated by Figure 53(b), in which the pinned plate is simultaneously vibrating out-of-plane at 5 kHz and translating towards the camera at 15 mm/s (i.e. 600 μm between video frames). Fringe quality has deteriorated but the fringes are still visible, and the visibility was significantly better when viewed live than it appears in the still photograph. These fringe patterns are still not of sufficient quality for reliable post-processing using the same methods as for subtraction fringes, but high visibility fringes can be obtained by subtracting two addition fringe patterns. This is demonstrated in Figure 53(c), which is the result of subtracting two images from a previously recorded sequence of twin-pulse addition interferograms of the stationary clamped plate. The time invariant optical noise has been removed to yield high visibility fringes, and the mode shape is clearly visible. Because this image is a correlation of two fringe patterns, the extraction of quantitative data (e.g. using a phase step algorithm) would be more complex and would require the timing of the laser pulses for the original interferograms to be accurately known. Figure 53(d) shows what happens when this method is applied in the presence of rigid body translation at 1 mm/s; here the vibration fringes are superimposed with tilt fringes caused by low frequency shaking of the target due to the translation. Figure 53(e) was produced by the same method as Figure 53(c), but using an in-plane interferometer with the stationary pinned plate vibrating in an in-plane mode. Fringe quality is again considerably improved, and similar effects are again observed with the target translating at 15 mm/s, as shown in Figure 53(f).

a b c d e f

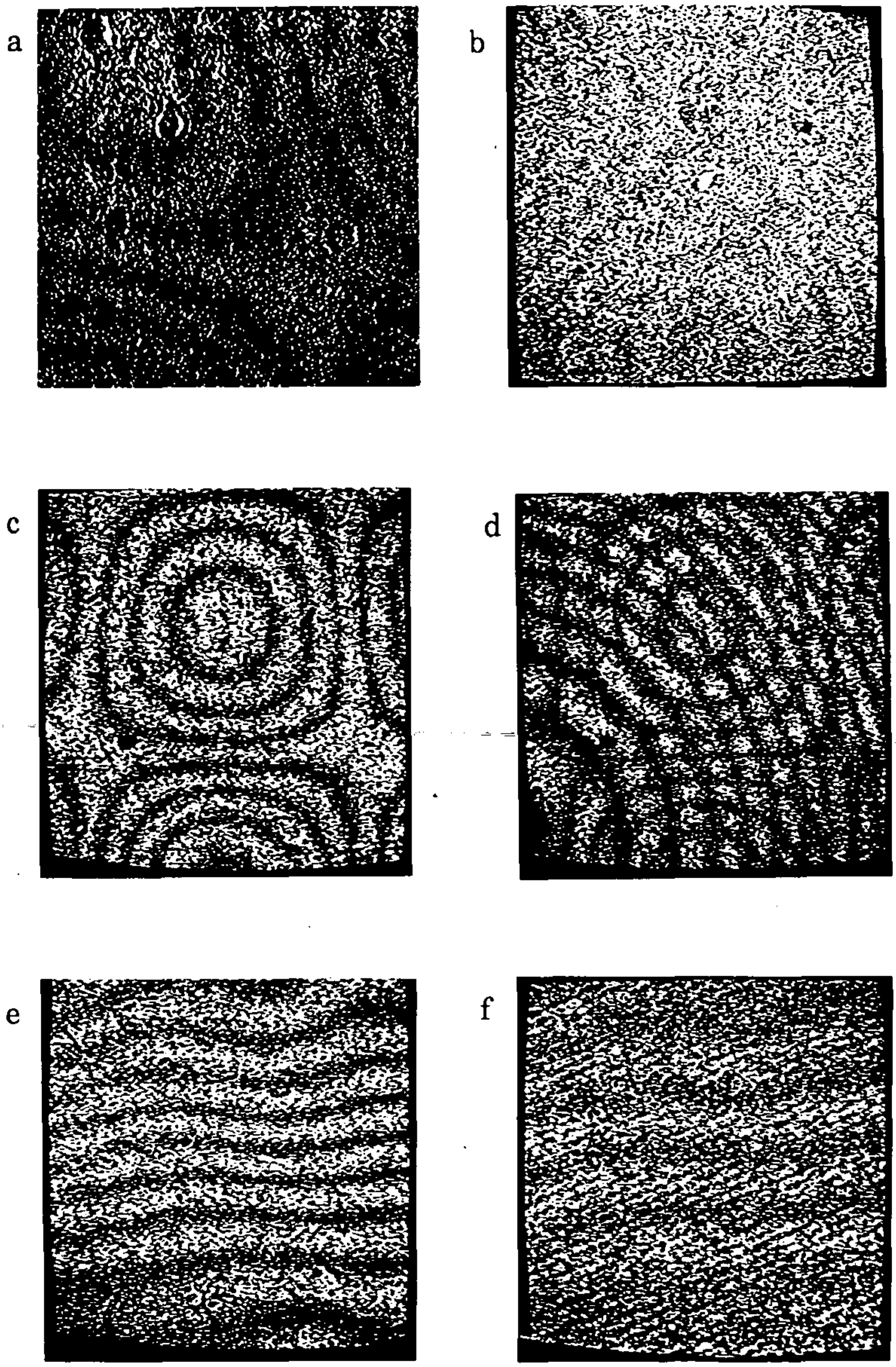

Figure 53: Pulsed addition ESPI of a translating plate

6.3 MEASUREMENTS IN A FACTORY ENVIRONMENT

The best way of proving the pulsed ESPI system's ability to operate in an industrial environment is to demonstrate it working in such an environment. This was done as a part of the Metal Box research project, studying a prototype machine incorporating the ultrasonically assisted forming die. Figure 54 shows the pulsed laser ESPI system installed adjacent to the machine, and clearly demonstrates the industrial environment with other high-speed machinery operating in the vicinity and very little mechanical isolation or acoustic shielding. The machine itself is supported by a raised steel-plate floor, which proved to be fairly compliant and resulted in considerable rigid-body motion of the machine during operation. The laser is positioned on the ground under this false floor, with the power supply unit against the rear wall and ancillary equipment (pulse generators, video cassette recorder, monitor and personal computer) on an adjacent table. The laser beam was reflected up through a metal pipe for safety, then manipulated into the required interferometer configuration using a beam-splitter, mirrors, lenses and diffuser plates mounted magnetically to the machine frame. Optical access was considerably restricted because the object of interest (the forming die) was enclosed within the machine frame, as shown in Figure 55. This shows the illumination for a horizontal in-plane sensitive interferometer, which was used to study the radial R0 vibration mode of the die.

A selection of the results which were obtained is shown in Figure 56. (a) is a live image with a metal cylinder in position ready to be necked by the die. This illustrates some of the difficulties experienced when using optical interferometry: part of the die cannot be seen as it is obscured by the cylinder, which also casts shadows from the oblique in-plane illumination and prevents interferometry in the shadowed region. The die also has to be viewed obliquely due to the position of the support frame. Figure 56(b) shows the result of using single pulse subtraction, with in-plane sensitivity and the cylinder removed. The radial fringe pattern is similar to the finite element prediction and laboratory result for this mode (see section 5.1), and confirms that the vibration is as required. Figure 56(c) shows a similar result on an enlarged view of the lower portion of the die, this time with a cylinder in position. Figure 56(d) was recorded under similar conditions but with the laser pulses fired at different points on the vibration cycle, and gives an indication of the maximum fringe resolution obtainable. Finally Figure 56(e) shows the result of subtracting two twin-pulse addition interferograms from a recorded sequence. This is the same method as was used to produce Figure 53(e), and again shows the vibration fringe pattern superimposed with parallel fringes, caused by a rigid-body tilt between the two recordings.

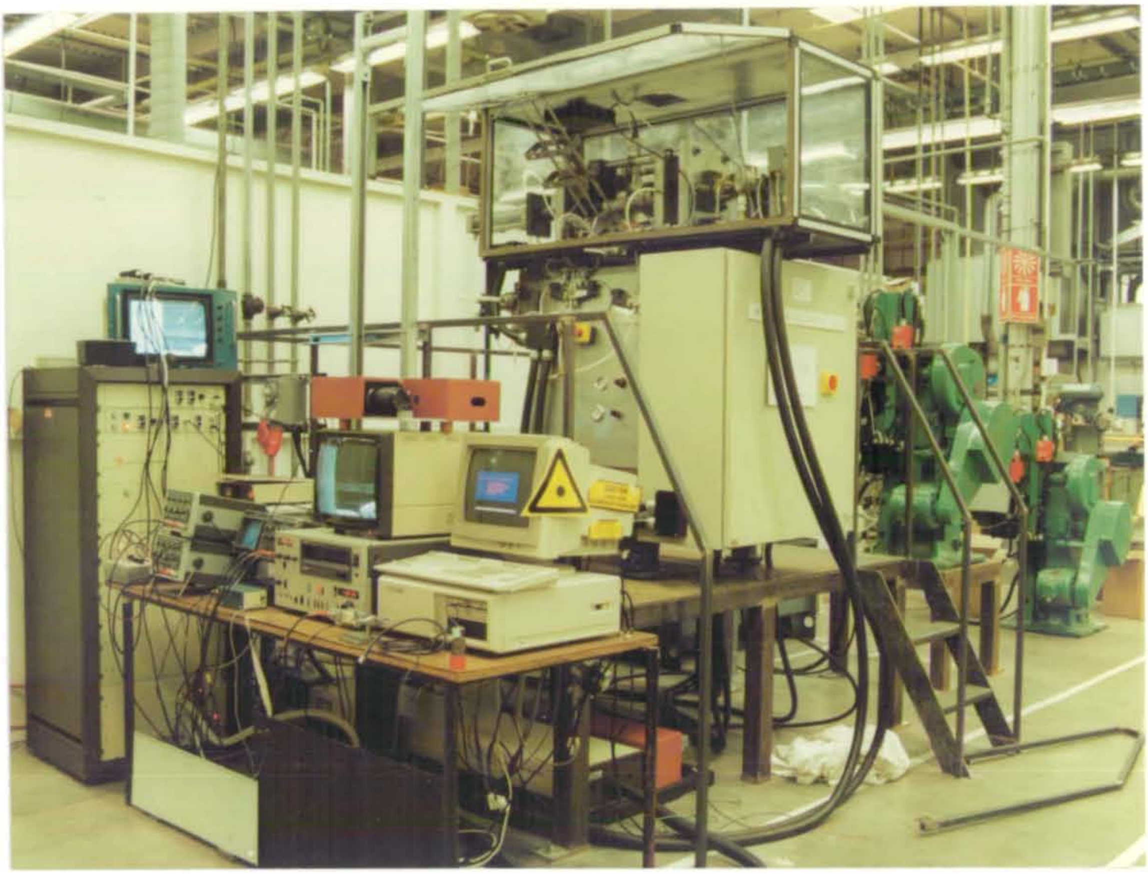

Figure 54: Pulsed laser system installed in a factory environment

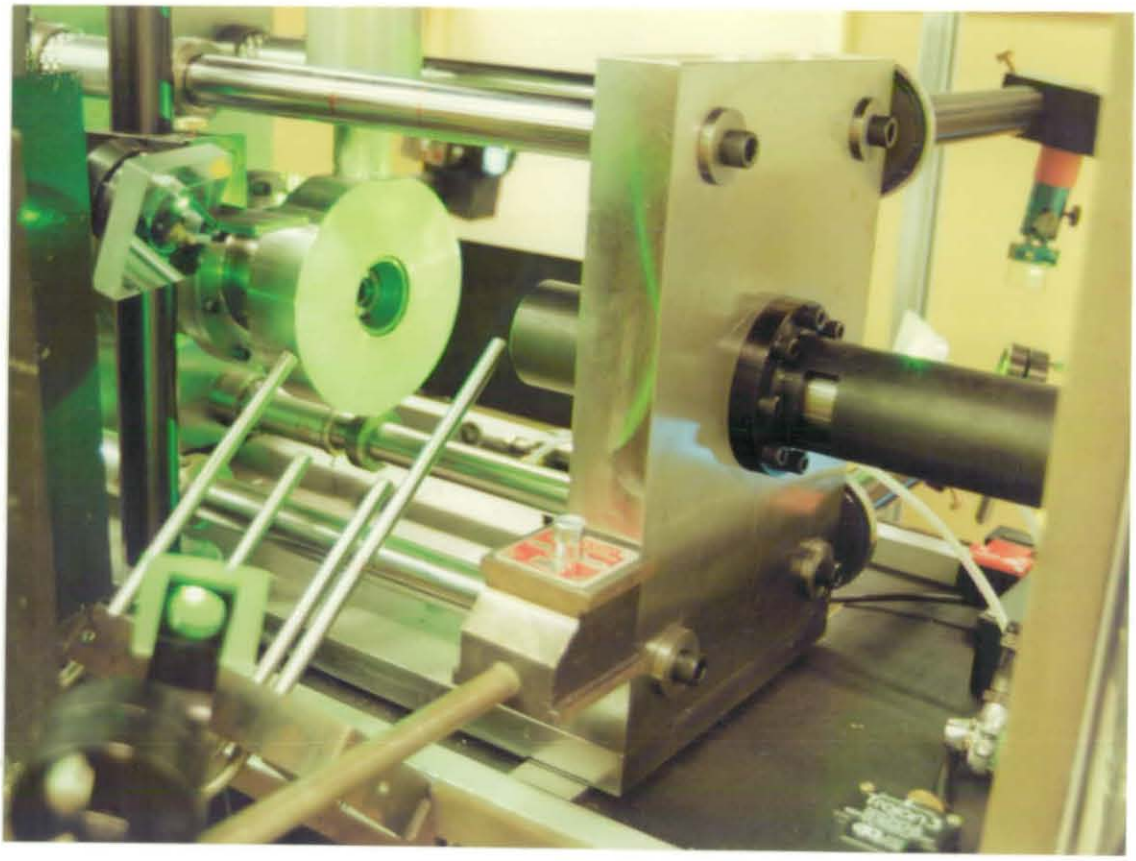

Figure 55: Illumination of the forming die for pulsed in-plane ESPI

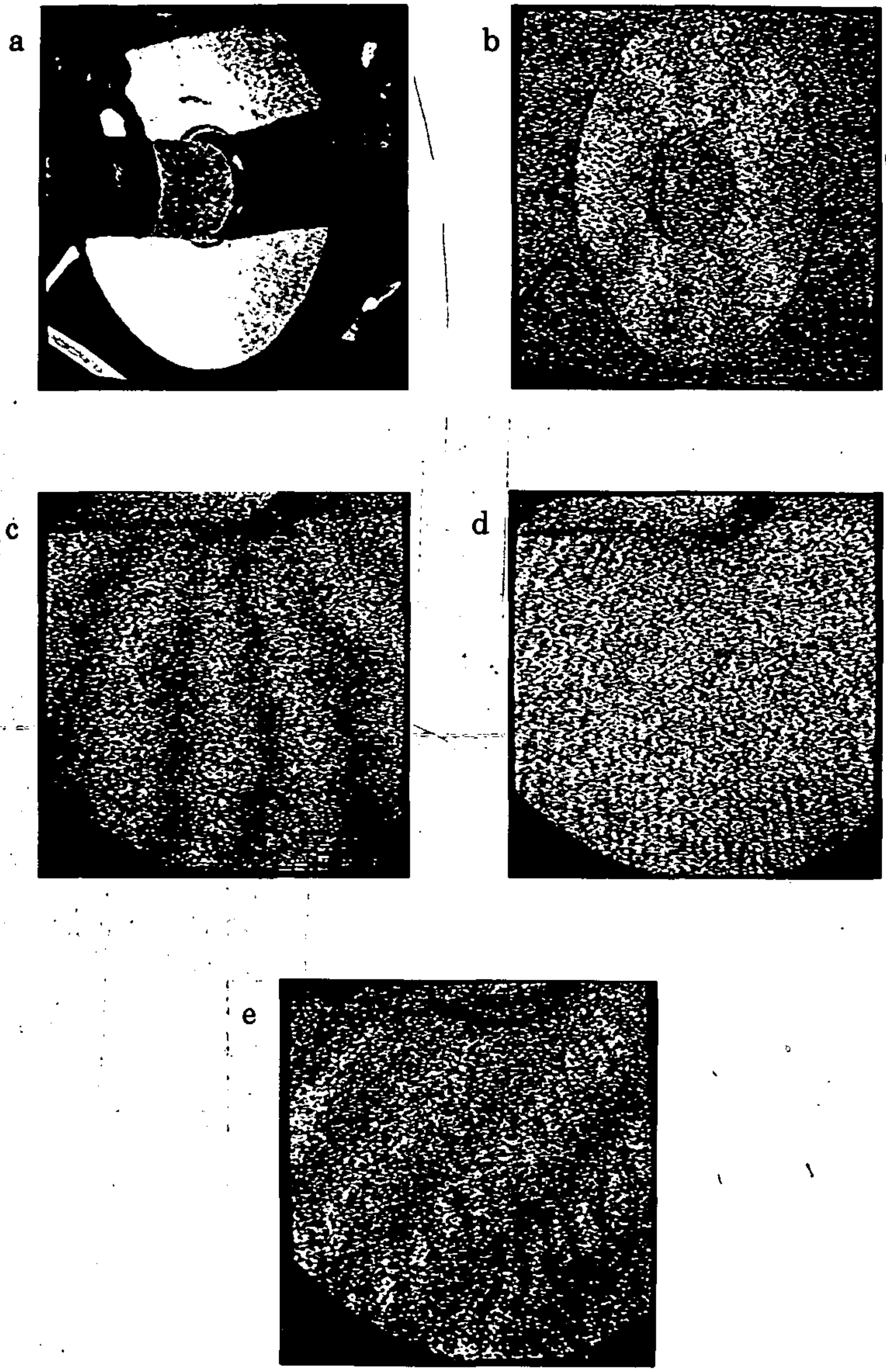

Figure 56: Pulsed ESPI analysis of forming die

7. DISCUSSION

It is the purpose of this chapter to discuss the work that has been done, and the extent to which it has achieved the aims as set out in section 1.1. This will be done in three parts. Section 7.1 considers the experimental studies which have been undertaken and discusses the implications of the results obtained. Section 7.2 considers the hardware and software which have been used, and assesses the performance and relative advantages of different components, including possible future developments. Section 7.3 gives a critical assessment of three-dimensional ESPI in general, by judging the performance against the requirements outlined in chapter 1 and by comparison with other available techniques.

7.1 EXPERIMENTAL RESULTS

The studies presented in chapters 4, 5 and 6 included discussions of individual results and their interpretation. Here it is intended to consider the results of those studies in more general terms: the scope of information which has been obtained; the practical limitations and problems which have been encountered; and the relevance to engineering vibration analysis in general. Each of the chapters dealt with a different type of problem, and they will be considered in turn in the following three sections.

7.1.1 Chapter 4 results

The aims of chapter 4 were twofold: (i) to demonstrate results from the different interferometer configurations (out-of-plane and in-plane) and illumination methods (continuous wave and pulsed); and (ii) to show how ESPI can measure vibrations on appropriate objects in one, two and three dimensions. The only method not demonstrated here was twin-pulse addition ESPI, which was subsequently dealt with in chapter 6.

The cantilever beam in section 4.1 is an exception in this chapter, as the vibrations are non-resonant. However this design does provide a motion which is known *a priori* and can therefore be used to test the experimental method, and in this respect the experiment has been successful. The time-average results demonstrate that both out-of-plane and in-plane interferometer configurations can measure vibrations, and the results from each correspond with good agreement. The graphical method used to produce the displacement plots is relatively straightforward but tedious and time-consuming, and the results from the pulsed phase-stepped analysis demonstrate how the procedure can be automated effectively. The comparison between different filtering methods shows little difference in overall effectiveness in this case, but nevertheless demonstrates the image processing procedure for extracting unambiguous displacement data from cosinusoidal fringe patterns. Phase-stepped analysis was not extended to the in-plane interferometer in this study, but was later demonstrated in section 4.2.3.

The circular plate study (section 4.2.1) provides a good demonstration of how a simple time-averaging out-of-plane system can perform a useful modal analysis. The results are similar to some earlier studies (for example references 12 and 31) and do not involve any technological advances in ESPI, however they do demonstrate a number of interesting vibration phenomena. These can help to give a better understanding of more complex vibrations (part of the reason for this study was to aid the interpretation of results from the forming die in section 5.1). Three phenomena in particular are worth mentioning. First, the frequency separation of the conjugate mode pairs which occur in symmetric objects, which was observed at several different frequencies. Second, the effect of two separate modes being excited simultaneously at the same frequency. This was often observed at frequencies between the resonant peaks of conjugate mode pairs, for example at 1138 Hz and 4900 Hz, and gives a fringe pattern corresponding to the time-average of the phasor sum of the two modes. Third, one mode being influenced by another mode, where the two have significantly different resonant frequencies. This is best demonstrated by the (7,0) mode at 5650 Hz, which clearly includes a significant contribution from the (1,2) mode which occurs on its own at 5800 Hz. Previous studies (for example Waller[12]) have sought to eliminate such modal combinations, by varying the excitation and constraints in order to isolate the normal modes. However it is instructive to appreciate that these effects are likely to occur if, as here, the excitation is fixed. This is often the case in practical systems (for example the forming die and ultrasonic cutting system in chapter 5).

The square plate study (section 4.2.2) extends the same method to three-dimensional analysis by adding an in-plane interferometer to the experimental system. The importance of doing this for obtaining a complete understanding of the object motion is demonstrated by the results in Figure 19. At this frequency the out-of-plane interferometer shows that the plate is resonating in a high order flexural mode, but gives no indication of any in-plane motion. Observing with the in-plane interferometer reveals that the plate is simultaneously resonating in an extensional mode, so that the total surface motion is predominantly in-plane. It is possible that an in-plane mode like this could create critical stresses in a vibrating component, but it is unlikely that it would be detected using conventional uniaxial testing techniques. Figure 18 demonstrates that in-plane fringe patterns can also be obtained for flexural modes, where the out-of-plane motion is dominant. The in-plane vector plots for these modes provide an excellent description of the in-plane motion, but are even more tedious to construct graphically than the cantilever deflection graphs in section 4.1. Once again the pulsed phase-stepped analysis (section 4.2.3) shows how this can be automated, and only requires two in-plane views. These results also show good agreement. Some problems were experienced with the phase unwrapping, but methods are now available[88,123] which should be able to overcome these problems in future.

The thick cylinder in section 4.3 proved to give an excellent demonstration of three-dimensional vibration, and the results presented for five different resonant modes show that any combination of in-plane and out-of-plane motion can be measured. In this case an out-of-plane sensitive interferometer on its own would be inadequate for understanding the object motion. Figure 30 shows that the R3 mode at 20.75 kHz is significantly influenced by the R0 mode at a lower frequency, in the same way that the (7,0) mode was for the circular plate. Figure 31 demonstrates a different phenomenon, as this appeared to be a discrete resonant mode comprising components of two normal modes which were each observed at different frequencies.

7.1.2 Chapter 5 results

The principal aim of the research project was to show that ESPI could be a useful tool for three-dimensional vibration analysis and to apply it to engineering structures. This has been achieved, as demonstrated by the results in Chapter 5. The three case studies which are presented were all 'real' problems: the first was an industrial research and development idea which formed the basis of a collaborative research project; the second required solving a problem of component failure; and the third was to overcome difficulties which had been experienced in another project.

The ultrasonic forming die study (section 5.1) was a major project which extended to several different die designs, but the portion of that work reported here is sufficient to demonstrate all the techniques which were applied. Although the object geometry is relatively simple, having rotational symmetry and a flat surface, the complex three-dimensional nature of the resonant modes (as identified in section 4.3) made it a difficult problem. The results show that a good understanding of the vibration behaviour was obtained, but the main conclusion of the study in experimental terms was that the combination of all three techniques (ESPI, accelerometers and FE) was required to achieve this. ESPI and accelerometers both detected the resonant peaks without difficulty, but understanding the response in terms of normal modes was sometimes difficult, as discussed in section 5.1. The ability of the FE analysis to predict both natural frequencies and mode shapes was of considerable help in interpreting the observed results. In cases where the motion is not so clearly separable into in-plane and out-of-plane components, for example non-symmetric geometries, this could be even more useful. However in these situations it is less likely that a specific mode shape would be required.

Plotting the frequency response function from the ESPI results was a useful exercise, and showed how much more information can be extracted from the results than just mode shapes. However the method of calculating the magnitude of response from fringe patterns involved several stages, and the relative error bounds were often high due to the low number of fringe orders visible for some modes. Modal damping values have not been calculated from the ESPI results, but would also be subject to high errors for the same reasons. It is clear that accelerometers are much better suited to measuring response in the frequency domain, whereas ESPI is better for measuring response in the spatial domain (i.e. mode shapes). This again demonstrates the advantages of using them together as complimentary techniques.

This study started with a component suffering from a problem (i.e. the tendency to resonate in the R3 mode preferentially to R0 during operation), and ended with a redesigned die in which the problem was solved. The fact that it was possible from the experimental measurements to redesign the die, and to achieve the required improvement in performance, is the best possible demonstration of the validity of this work. Although the experimental modal analysis (EMA) and structural modification analysis were performed from accelerometer results, ESPI was very important in gaining an understanding of the modal behaviour, and the results show the usefulness of three-dimensional ESPI in a design process.

The ultrasonic cutting system study (section 5.2) started in a similar way, with a need to investigate why the blades were fracturing and to recommend design improvements. Unlike the previous study, this component is not well suited to conventional EMA using accelerometers: the thin blades would be likely to suffer significant mass loading effects due to attached accelerometers, and the nodal spacing of only a few millimetres in the modes of interest demands a high spatial resolution. However it was well suited to ESPI analysis, and the cause of the problem was identified literally within minutes: the operating frequency coincided with the high-stress (7,0) mode shown in Figure 43(c). Further analysis revealed other modes such as the (2,2) which seemed likely to give improved performance. FE analysis confirmed this and enabled redesign to produce the required modes at the operating frequency, and subsequent retesting with ESPI confirmed the feasibility of the design. The improvement in performance which was achieved again demonstrates the usefulness of the technique. In addition to the blade analysis, it was shown that the three-dimensional system is ideal for studying ultrasonic transducers and horns which vibrate in longitudinal modes.

Turbomachinery blades have been studied using holographic interferometry (HI) and ESPI for many years, and such components usually have a curved and twisted form, which causes coupling between modes and three-dimensional vibration behaviour. Hariharan[41] has shown the necessity for two- or three-dimensional measurements and used HI with two illumination directions to achieve it. The results in section 5.3 demonstrate an alternative method of achieving the same result, using the 3D ESPI system. These results are purely qualitative, but the method of phase-stepping which was demonstrated in chapter 4 for both in-plane and out-of-plane ESPI could be applied to the same results to give quantitative three-dimensional vectors. The computation involved would be much simpler than with the Hariharan method. Even as a qualitative technique the advantages are obvious, as demonstrated by the comparison of the 1E and 2F mode fringe patterns. With different blade geometries it may be that some in-plane modes are difficult to detect using a uniaxial measurement system, as was the case for the plate in section 4.2.2., and in such cases the 3D system would have distinct advantages.

The forming die and ultrasonic cutting system were both excited by a fixed transducer, so that the position of the excitation force could not be varied, and in both cases vibrations were observed which were combinations of the normal modes. With the turbocharger blade the force was input from an external shaker, whose position could be varied. In general the response was again found to include many mode combinations, and it was only possible to isolate the normal modes (to correspond with the FE predictions) by careful choice of excitation position. Therefore it must be expected that in studies of self-excited objects, some of the normal modes will appear as combinations.

7.1.3 Chapter 6 results

The pulsed laser became available for use about two and a half years into the research project, and was subsequently used to overcome some of the limitations which had been experienced with the continuous wave laser. One of the applications is phase stepping for automatic fringe analysis, which has been covered in chapter 4. Another application is to time-variant vibration problems, such as transient response and travelling waves; this has been investigated through the travelling wave study in section 6.1. A third application is in situations where it is not possible to achieve temporal stability between the object and the interferometer, and this has been studied in the laboratory with a translating target and demonstrated practically in a factory environment.

The study of travelling waves in section 6.1 serves two purposes: it is the first stage of a project to develop a new method of measuring structural power flow, and it illustrates the way in which pulsed ESPI can be applied to non-resonant vibration analysis in general. With regard to the former, it can be considered a successful feasibility study. It has been shown that by manipulating the laser pulse timing it is possible to isolate only the travelling wave component, which transmits the power flow. This gives a whole-field view of the power transmission path through the structure, and quantitative displacement values which can be used to calculate the net power flow. A method of calculating the power flow using laser vibrometer techniques has been described by Baker et al[135], which requires measurements of spatial velocity gradient. For single frequency harmonic vibrations the velocity can be obtained by multiplying the ESPI displacement values by the angular frequency ω, and for more complex waveforms the displacement could be sampled at different phase epochs and differentiated with respect to time (i.e. temporal phase). Spatial gradients can be obtained either by differentiation of the fringe spacing, or by using an image-shearing interferometer[136] to measure slope directly. For obtaining both velocity and slope it is desirable to avoid numerical differentiation, which inevitably introduces computational errors. Although only the first stage has been demonstrated so far, this indicates that there is potential for a successful measurement system to be developed. A further benefit of three-dimensional ESPI is that both flexural and longitudinal wave power flow can be observed, by using the out-of-plane and in-plane sensitive interferometers respectively.

Section 6.2 introduces twin-pulse addition ESPI, and demonstrates that it can be used to observe in-plane and out-of-plane vibration modes even on targets that are highly unstable and undergoing significant rigid-body motion. This enables measurements to be made which would be impossible with time-averaging, stroboscopic and even single pulse subtraction techniques. However, the visibility of addition fringe patterns is much poorer than for the other techniques, and this creates difficulties for automatic fringe analysis. A method of post-processing has been demonstrated whereby addition interferograms are subsequently subtracted. This yields high visibility fringes which can indicate both vibration mode shapes and bulk body motion, although it also makes quantitative analysis of vibration amplitudes more difficult.

Section 6.3 puts into practice the techniques of section 6.2, and shows that useful results can be obtained on an engineering machine under fairly harsh conditions. This study also demonstrates an inherent limitation of ESPI, that being the requirement to be able to illuminate and view the surface being studied. It was not possible to study the entire die face at once because the position of the metal cylinder obscured part of the view and also cast shadows from the in-plane interferometer illumination, as shown in Figure 56(a). Another problem that was experienced during this study was that the optical components (mirrors etc.) used for illumination had to be clamped to the machine frame, and suffered from transmitted shock and vibrations which caused instability in the fringe patterns. This problem should be significantly reduced by using fibre optic illumination, where only one clamping point is required at the fibre output. Containing most of the beam paths within fibres would also be highly desirable from a safety viewpoint in a factory environment.

7.2 ESPI TECHNOLOGY

A variety of methods and technologies has been used throughout this research. Some have been chosen due to suitability for a particular application, and others have been introduced as a result of technological advances. The purpose of this section is to review the different types of component that have been tested or are available, and to assess their relative advantages and limitations. Three general categories are covered: lasers, fibre optics, and imaging systems.

7.2.1 Lasers

All the time-averaged results in this thesis were obtained using an argon-ion gas laser, and all the pulsed results were from a Nd:YAG solid state laser. Gas lasers are the conventional source for continuous wave and stroboscopic illumination, normally using helium-neon for low power (<50 mW) and argon for high power (up to ~2 W) applications. The reason for using an argon laser in this work was to enable the beam to be split several times into out-of-plane and in-plane configurations, still giving sufficient illumination power after coupling losses from optical fibres (see section 7.2.2). Argon lasers also have the advantage of considerably longer coherence length than helium-neon lasers, but are very much more expensive to purchase and to run. An alternative which has become viable in recent years is solid state diode lasers, which are cheap, compact, have long coherence lengths, and are capable of being modulated for stroboscopic output. Their suitability for ESPI has been studied by Wykes[137], and the Newport HC4000 speckle camera uses a diode laser source. Until recently they have suffered from being limited to low power output (a few milliwatts) at invisible infra-red wavelengths, but the technology is advancing rapidly, and visible diode lasers are likely to become the dominant source for low power applications.

It has been shown that pulsed ESPI offers considerable advantages in terms of being able to study unstable objects and non-steady state vibrations, and producing cosinusoidal fringes suitable for automatic analysis. However pulsed lasers in general, and especially the laser used for this work, are very expensive. For low frequency vibration applications it may often be adequate to use stroboscopic illumination from chopping or modulating a continuous wave source. But for freezing high frequency vibrations, or temporal sampling of a waveform, it is still necessary to use a Q-switched pulsed laser. Ruby lasers have conventionally been used for pulsed holography, but suffer problems with ESPI due to the low pulse repetition rate and intensity variations between double-pulses[79]. The development of frequency-doubled Nd:YAG lasers which can pulse at video camera frame rate (50 Hz) has solved the first problem, although pulse-to-pulse stability can still be a problem when extracting double pulses from a single resonator[97]. The twin-cavity diode-seeded laser used for this work[106] gives excellent twin-pulse performance, and represents the current state of the art in twin-pulse lasers.

7.2.2 Fibre optics

Optical fibres offer several advantages over mirrors for guiding laser beams. The number of optical components required is minimised, as it is only necessary to use one lens to couple the laser into the fibre, and optionally one other lens at the fibre output if it is required to alter the beam divergence. Single mode fibres produce a high quality smooth output which does not require further spatial filtering. Changing the optical configuration or illumination direction can be done quickly and easily, as it only requires moving the fibre output end. It is also possible to illuminate otherwise inaccessible areas, such as the inside of enclosed components, by inserting fibres through small holes[138], and with fibre optic imaging systems this opens up the possibility of endoscopic ESPI. Fibre-guided beams are also inherently safer than exposed beams because they are enclosed. The main disadvantage of fibre optics is that a high proportion of the incident light is wasted, typically ~50% with single mode fibres. This is largely due to the difficulty of coupling the laser beam into the small core, which also requires precision manipulators for optimising the position and angle of the fibre input end. Dissipation losses within the fibre are negligible over lengths up to a few metres. The maximum illumination power is limited by the power density which can be accepted by the fibre. This is not generally a problem with continuous wave illumination, and outputs of the order of 100 mW have been obtained from single mode fibre with 4 µm diameter core during this research. With the pulsed laser this is a limitation, due to the high energy density, but it has been demonstrated that pulsed ESPI can be performed using large diameter (1000 µm) multi-mode fibres (this work occurred too late for results to be included in this thesis). Phase shifting or modulation can be performed before the beam is coupled into the fibre, as shown in Figure 7, or by stretching the fibre using a piezoelectric element[93]. It should also be possible to phase-shift simply by axially translating the fibre output end.

The fibre optic ESPI head described in section 3.2.1 was found to operate well, and could be moved around without requiring any realignment. The coherence length of the argon laser was sufficient for objects to be studied in the range 0.5-3m without moving the position of the illuminating fibre, and the fibre input couplers also required virtually no adjustment over a period of several weeks (except for varying the reference beam intensity).

7.2.3 Imaging systems

The imaging system in ESPI comprises three parts: a lens, a camera, and a means of introducing the reference beam. 35mm format single lens reflex camera lenses have been used throughout, as they are readily available in a range of focal lengths (including zoom), are easy to change, and have a focal plane sufficiently far behind the lens to permit a beam-combining element to be inserted for the reference beam. Amplitude-division type beam-splitters have been used to introduce the reference beam. The Ealing Vidispec (as shown in Figure 6) uses a wedge, which causes astigmatism in the image. This problem was eliminated by using a cube (see Figure 7), which required partial shielding to prevent internal reflections. Most of the time-averaged results were observed using the Insight video camera supplied with the Vidispec, which gave good results. As part of the pulsed ESPI development, a charge-coupled device (CCD) type camera was introduced which has increased sensitivity and an effective exposure of 19 ms per 20 ms frame, the image being downloaded in the final 1 ms. This feature is important for twin-pulse addition, where two images must be summed within the same exposure period. This camera also performed well, and was more compact than the Insight, so it was subsequently incorporated in the fibre-optic ESPI head as well (Figure 7). One problem with the CCD camera is that the imaging area of 6×4.5mm is much smaller than the 35mm format for which the lenses are designed, with the result that the field of view is much reduced. Various methods can be used to overcome this problem, the simplest being to use a wide angle lens. A 28-70mm focal length zoom lens was used for all the results that have been presented, but a 18mm lens has also been used to view larger objects of up to 1m width at a distance of 3m.

7.3 CRITICAL APPRAISAL OF TECHNIQUE

The usefulness of the three-dimensional ESPI technique as a tool for practical engineering vibration analysis can be assessed in two ways: first, by objective assessment of the attributes required by measuring systems in general; and second, by comparison with alternative techniques which could be applied to the same types of problem. These two approaches are considered in the following two sections.

7.3.1 Performance parameters

The performance of the various different techniques used, and ESPI in general, can be assessed by considering the parameters for measurement systems which were listed in section 1.3:

(i) Ease of use.

The ease of use with ESPI is largely determined by the type of object being studied. In the case of objects which are mobile and small enough to be placed on an optics table, they can be analysed with a laboratory-based system (as used for all the studies in chapters 4 and 5). The interferometer usually requires a skilled operator to set up initially, but subsequently only requires simple adjustments to the lens (zoom, focus and aperture) and beam intensities. It is necessary to clamp the object rigidly to the table (to prevent rigid-body motion relative to the interferometer), and to arrange a suitable method of excitation. If the excitation source is internal then some form of transducer may be required for triggering in the case of pulsed ESPI. Operation becomes more difficult for objects which cannot be mounted rigidly to the same surface as the interferometer. Continuous wave illumination can sometimes be used in these circumstances, but usually requires a common path arrangement with the reference beam (for an out-of-plane sensitive interferometer) being derived from a point on or adjacent to the object. Pulsed subtraction ESPI may require similar action, but twin-pulse addition alleviates the problem in all but the most severe cases (as demonstrated in sections 6.2 and 6.3). The other situation which can create difficulties is where optical access is restricted, and it may be necessary to construct an arrangement of mirrors or a fibre-optic system to illuminate and view the area of interest. Having set up the measurement system, a lot of information can usually be gathered in a short time. This is due to the whole-field measurement capability, and the ability to observe results in real-time whilst changing variables such as excitation frequency. As an example, the full modal analysis of the circular plate in section 4.2.1 was completed within one day.

(ii) Ease of interpretation of results.

Time-averaged fringe patterns are normally reasonably straightforward to interpret in the case of simple structures undergoing resonant vibration, for example the plates in section 4.2 and the ultrasonic cutting system in section 5.2, because the Bessel function fringes give a clear indication of nodal areas and relative amplitudes. However even in these circumstances the presence of combination modes or simultaneous excitation of normal modes (as discussed in section 7.1.1) can make interpretation difficult. In general, motion at any point may differ from sinusoidal, and relative phase can vary across a vibrating surface. Pulsed ESPI can yield time-resolved displacement data to analyse such motions, but the cosinusoidal fringes are usually very difficult to interpret as they do not uniquely identify stationary points. This has been the reason behind the development of post-processing to present the displacement data as wire-frame or vector plots, and in these formats the results are very much easier to interpret.

(iii) Accuracy and resolution of measurement.

The range of measurement with basic time-average ESPI is limited at the lower end by the requirement of at least one fringe, and at the upper end by the minimum fringe spacing at which individual fringes can be resolved. In practice this is usually no more than 20 fringe orders across the image (see for example Figure 28). For an out-of-plane configuration with illuminating wavelength ~0.5μm, this gives a range of approximately 0.25μm to 5μm peak-to-peak amplitude. Amplitude values between fringes can be interpolated with a resolution of approximately ±¼ fringe. With pulsed ESPI the fringe density can be reduced by sampling a portion of the vibration cycle, so that displacements can be measured up to the limit at which the two speckle patterns no longer correlate. This extends the range considerably beyond that of time-average ESPI. The lower limit is determined by the accuracy of fringe interpolation, and this is greatly increased by using phase stepping to convert the cosinusoidal fringe function to a saw-tooth function which can be linearly interpolated; the errors involved in the phase stepping process have been analysed by Kerr et al[109]. In this case it is likely that the measurement error will be determined by experimental and environmental factors rather than the resolution of fringe interpolation (see for example Figures 12(h) and 52(c).

(iv) Spatial and temporal continuity.

ESPI measurements can be considered spatially continuous within the field of vision, subject to the fundamental limitation that measurements can only be made on surfaces which can be illuminated and viewed in the appropriate manner. The spatial resolution is determined by the image sensor. In vibration studies it is necessary to have a density of measurement points sufficient to resolve the wavelength of vibration, and it can be seen from the results (for example Figure 17, 50 kHz) that the lower limit of displacement resolution will normally be reached well before spatial resolution becomes a problem. It is also a simple matter to increase the spatial resolution by zooming in with the lens to view a smaller surface area. The temporal sampling rate for time-average ESPI is determined by the video frame rate of 25 frames per second (although there is no reason why high-speed video technology could not be used if necessary), and for pulsed ESPI by the maximum repetition rate of the laser. With periodic vibrations, or accurately repeatable transient vibrations, the temporal resolution can be increased by using twin-pulsed ESPI. In this case the resolution is only limited by the pulse duration (~15ns) and the control electronics.

(v) Speed of data acquisition.

Raw data in the form of fringe patterns can be acquired from two consecutive video frames (i.e. 0.08s), or one frame in the case of twin-pulse addition. If this is the final form of the results, as is often the case with time-averaging, then the technique is effectively real-time. If however it is necessary to post-process the results then the total time can increase considerably. The time required for image processing and computing (as described in section 3.3) depends on three factors: the processing speed of the computer, the efficiency and complexity of the program code, and the degree of operator intervention required. The total time taken to produce the two-dimensional vector plots in section 4.2.3 from the raw data was in some cases several hours, but the majority of that was due to operator intervention. It should be possible to reduce this to a few minutes or less by developing a more sophisticated computer program. Hardware developments such as parallel processing are also likely to increase the speed in future.

(vi) Format and compatibility of results.

ESPI results are in the form of displacement plots over an area, either time-averaged or (for pulsed ESPI) at discrete instants in time. It has been demonstrated that FE results can be obtained in a similar form for comparison with ESPI fringe patterns, see for example Figure 27 to Figure 31, and Figure 43. Qualitative comparisons with results from point measurement techniques can be made by constructing a frequency response function from the ESPI measurements or a waterfall plot from the point measurements (see section 5.1). For quantitative comparison with acceleration values (from accelerometers) or velocity values (from velocimeters) it may be necessary to obtain time-resolved displacements using pulsed ESPI and to differentiate once or twice with respect to time. The combination of measurement and computational errors are likely to make this relatively inaccurate. However for harmonic vibrations, amplitude values from time-average ESPI can be converted to peak velocity or peak acceleration simply by multiplying once or twice by the angular frequency ω. In-plane strain values (e.g. for comparison with strain gauge results) can be obtained by differentiating in-plane displacement values with respect to distance. The results that have been presented have not been interfaced with any other systems, but are at the stage where they are available as data files within the image-processing computer. This gives the potential for a computer program to be written which could generate three-dimensional plots, similar to the FE results in Figure 46 and Figure 47.

(vii) Tolerance to environmental conditions.

Time-average ESPI is inherently susceptible to external influences (i.e. other than the surface motion being studied) which can change the optical path length of the interferometer beams. The most common causes are external forces which move the interferometer relative to the object, and thermal currents which alter the refractive index of the surrounding medium. Both effects can be reduced with the out-of-plane interferometer by using a common path arrangement or by subtracting consecutive video frames (see section A.3), but sometimes they cannot be eliminated. Twin-pulse ESPI overcomes these problems in all but the most extreme conditions. High levels of incoherent illumination or radiation will reduce fringe visibility, but can be removed by using a narrow bandpass optical filter matched to the laser wavelength.

7.3.2 Comparison with other techniques

Many different techniques have been developed for vibration analysis, as reviewed in section 2.1. In this section these techniques will be compared with the 3D ESPI system, following the order of section 2.1 except that the numerical and point measurement techniques will be considered last.

Despite having been of seminal importance in experimental vibration analysis, the Chladni method has now been largely superseded by modern techniques, in particular the optical methods. These enable the same nodal patterns to be observed but give additional information on the amplitude of vibration. They can also be applied to more highly curved surfaces, and do not suffer any mass loading effects. ESPI is particularly well suited to this type of measurement due to the ease and speed of data gathering, although moiré is also a good alternative, particularly for amplitudes larger than a few microns. The Chladni method still retains the advantages of being extremely cheap and requiring virtually no equipment, and for these reasons it is still used where these considerations are important. Classical interferometry has similarly been superseded in most vibration applications by HI and ESPI, because it offers few advantages over the coherent techniques. Moiré is mainly used for quasi-static studies, but in the time-average mode is a complimentary technique to ESPI. It can perform much the same function, being able to measure both out-of-plane and in-plane vibrations, but is most suitable for amplitudes in the range of tens to hundreds of microns. Many moiré techniques also require some form of surface preparation.

Holographic interferometry (HI) is directly comparable to ESPI, as the two produce results in a very similar way. ESPI is generally faster and more convenient to use, as it does not require any photographic processing and produces real-time results directly on video. It also has less stringent stability requirements for time-average measurements and can work in daylight, and for these reasons is more suitable as a 'shop floor' technique. HI has become more 'user-friendly' through the use of thermoplastic recording, but is still generally restricted to the laboratory for time-average measurements. The advantages of HI are that it gives higher spatial resolution and better fringe quality, and it records a three-dimensional image of the object (which can be of benefit in some circumstances). For measurements of in-plane or three-dimensional vibrations ESPI definitely has an advantage, as it is able to measure the orthogonal components directly (see section 3.1), whereas with HI it is necessary to calculate these numerically from other measurements. The only advantage of the Løkberg method[72] for observing in-plane vibrations is that it does not require a video frame store, and since most ESPI systems now include such a device the 3D system as described here is more suitable for both in-plane and three-dimensional measurements. Of all the speckle techniques which have been developed, ESPI is by far the most commonly used for vibration measurement. This is due to its whole-field ability for observing mode shapes, and the real-time operation which enables rapid identification of resonant frequencies.

The accelerometer is the most widely used instrument for engineering vibration measurement, and particularly for experimental modal analysis (EMA), so it is possibly the most important technique to compare with ESPI. The use of both techniques together has already been discussed in section 7.1.2 with regard to the forming die study. While ESPI measures amplitude across an entire surface at one frequency, accelerometers measure the response over a range of frequencies at one point. This makes them excellent complimentary techniques, the combination yielding considerably more information than either in isolation. ESPI has better spatial resolution, whereas accelerometers have better frequency resolution. Accelerometers can be mounted with the sensitivity axis in different directions, or as triaxial accelerometers, so both techniques can make three-dimensional measurements. ESPI has the advantage of being non-contact, so is more suitable for lightweight structures, but accelerometers do not require interferometric stability. Laser Doppler velocimetry (LDV) combines a similar frequency response to accelerometers with the non-contact performance of ESPI.

Finite element (FE) modelling is also widely used as an analytical technique. This has the advantage of being predictive, and can therefore give information on an object before it even exists. A wide range of information can be obtained, including natural frequencies, mode shapes and stresses, but the obvious disadvantage is that the information is at best an approximation, inherently reliant on the accuracy of the model. Therefore it is imperative that the predicted results are validated by experimental measurements. This has been demonstrated in the forming die study (section 5.1), which shows that FE is capable of quite accurate predictions of normal mode shapes and frequencies, but is incapable of predicting how those modes might couple and combine with each other under conditions of forced damped vibration. It can be concluded that FE and ESPI are suitable as complimentary techniques, the former for prediction and interpretation, and the latter for confirmation and correction.

Other studies have been undertaken specifically to compare the performance of different techniques for vibration analysis, including ESPI. Hancox et al[10] compared time-averaged HI, time-averaged ESPI and scanning LDV for mapping mode shapes of a vibrating compressor blade. Kyösti et al[139] similarly compared time-averaged HI and ESPI with FE modelling and impact EMA for measuring mode shapes of a rectangular plate with a cut-out. In both cases the conclusions were, broadly speaking, similar to those discussed above.

8. SUGGESTIONS FOR FURTHER WORK

Although the main aims of the research have been achieved, there is obviously considerable scope for further development and improvements. In section 8.1 suggestions are made for aspects of the hardware and software which might benefit from further work to improve the performance or versatility of the technique. Section 8.2 then suggests some areas of study to which three-dimensional ESPI could usefully be applied.

8.1 TECHNOLOGICAL IMPROVEMENTS

Fibre optics offer several practical advantages in ESPI, and the fibre optic system shown in Figure 7 has proved to be very versatile for out-of-plane studies. This could be extended to include an in-plane capability, to make a flexible three-dimensional system. Equipment is available, for example the York Launchmaster, which can rapidly and efficiently switch the laser output into different fibre inputs for the three interferometer configurations; however this would make a very expensive system. A simpler approach would be to split the laser output into two fibre input connectors via a half-wave plate and polarisation beam-splitter, so that the intensity splitting ratio can be varied to 50:50 for the in-plane sensitive configuration or as required (usually ~95:5) for the out-of-plane sensitive configuration. For in-plane measurements, two fibres of equal length are inserted into the connectors, and the outputs positioned in either the xz or yz plane as required (see section 3.1.3). For out-of-plane measurements, one fibre is replaced by a longer one (for path length matching, see section 3.2.1) which guides the reference beam, and the output of the other is repositioned adjacent to the viewing lens. The input ends of the York LDS fibres which have been demonstrated incorporate coupling optics, and can be easily inserted into the connectors and aligned using fine-adjustment screws in a few seconds. Such a system would enable the viewing direction, sensitivity vector and in-plane sensitivity factor (determined by illumination angle) to be altered with little effort.

It has been stated in section 3.1.3 that knowledge of the object shape is required to convert the measured vibration vectors to local out-of-plane and in-plane components, and that this can be measured by ESPI contouring. Fibre optic illumination is ideal for this, as it enables the illumination wavefronts to be translated (to generate the contour fringes) simply by moving the fibre output ends. By mounting the fibre outputs on triaxial piezoelectric translators controlled from the computer, it could be possible to automate the contouring process as well as the three-dimensional vibration analysis, all using the same apparatus. The same method could also be used for phase stepping, by axially translating the output end of one fibre.

The advantages for modal analysis of using both whole-field and point measurement techniques has been demonstrated in this work. There is potential for combining both in one measurement system, and ESPI and laser Doppler velocimetry (LDV) would seem to be ideal for this as they are both laser-based non-contact techniques. They have already been demonstrated for independent measurements on the same object[95] and as an integrated system for mutual phase locking[94], and if the benefits of both could be combined to give point mobility measurements and automatic phase modulation then this would produce a highly versatile time-average system.

With the equipment which has been used so far it has only been possible to measure the orthogonal components of vibration sequentially, and this has limited the application to steady state vibrations, or transients which are repeatable in a controlled manner. Pulsed ESPI is already capable of producing interferograms at the rate of 50 per second, and future advances in the design of the Nd:YAG laser may increase this to some hundreds per second, opening up the possibility of ESPI with high speed video. This gives the potential for studying transient events such as impacts and explosive shock waves through solids in real-time. In order to extend this to three-dimensional measurement it must be possible to detect the three components simultaneously, and this requires being able to discriminate between the different interferometer illuminations. One method of achieving this could be to use the polarisation discrimination technique which has been developed by Moore[113] for two-dimensional in-plane measurement. Other methods could also be considered, for example wavelength discrimination.

Phase extraction has been shown to be of great benefit for fringe analysis, but the temporal phase stepping technique that has been demonstrated cannot be applied to real-time transient analysis. Spatial phase measurement could be performed from a single fringe pattern using the Fourier transform technique[86] if parallel carrier fringes are generated in each interferogram, and this can be achieved by translating or rotating the illumination as for ESPI contouring.

The method of phase unwrapping along vectors has been shown to be unsuitable for phase maps which contain errors or breaks in the 2π discontinuities. This is likely to be the case with complex mode shapes, or on surfaces which cast shadows or contain holes, for phase maps produced by either temporal or spatial phase measurement techniques. It would be desirable to use a more sophisticated unwrapping technique which can accommodate these features, such as the cellular automata method which has been demonstrated on complex phase maps[93].

The electronics for controlling the pulsed laser and the computing for phase-stepped fringe analysis in this work have both used a 'breadboard' approach, linking together separate components or programs to perform the required task. Recent work by West at Loughborough has incorporated the fringe analysis software and the laser pulse timing control within the personal computer. This will eliminate the need for using external delay circuits and interfacing with a separate image processing computer, as has been done so far, and should enable experiments to be controlled better and completed more rapidly.

8.2 POTENTIAL APPLICATIONS

The main areas of application for the 3D ESPI system are those types of component which have already been shown to be suitable for optical methods, but which involve significant in-plane or three-dimensional motion.

The study of plate vibrations has received considerable attention over many years, both theoretical and experimental, but there has been remarkably little experimental study of in-plane vibration modes. Flexural vibrations are often the most important from an engineering viewpoint because they generally occur in a lower frequency range than in-plane modes and are the main source of radiated noise, but in-plane resonances can nevertheless be important. 3D ESPI is ideal for studying the whole range of plate vibration modes (see Appendix C), as has been demonstrated in section 4.2. A thorough study of these modes on different types of plate, for example isotropic metal plates and quartz crystal devices, could add considerable knowledge to this subject area. In order to identify the different mode types it would be best to use pulsed phase-stepped analysis, with the phase referenced to the object excitation, so that both sides of the plate could be viewed in turn and the vibration phase compared. It would also be useful to extend the study to thick and curved plates, in which the out-of-plane and in-plane modes are coupled.

Another application which has been demonstrated is to ultrasonic machining equipment. Ultrasonic excitation is being applied to many processes including cutting, drilling, plastic welding, wire drawing, die forming, etc., and many of these would benefit from further research. Transducers, horns and other vibrating components often vibrate in a three-dimensional manner, as demonstrated in sections 5.1 and 5.2, so this is again ideal for 3D ESPI analysis. A research project[140] in this subject area is due to commence shortly at Loughborough.

The turbocharger blade analysis showed that three-dimensional measurements can also be useful in situations where uniaxial measurements have previously been applied, and there are likely to be many similar applications with other engineering components, particularly those which have curved or thick sections.

9. CONCLUSIONS

1. It has been demonstrated that mechanical vibrations can be observed with both in-plane and out-of-plane sensitive electronic speckle pattern interferometer configurations. Each case has been demonstrated using both continuous wave illumination, to measure time-averaged amplitude, and pulsed illumination to measure net displacement between pulses. This is believed to be the first time that the in-plane interferometer has been applied to vibration measurement, having previously been restricted to quasi-static displacements and strains, and it has resolved the confusion that previously existed over whether the in-plane interferometer could be used for time-average measurements. Time-averaged in-plane sensitive fringe patterns have been observed visually, but it has been confirmed that a subtraction process is required to produce fringes of reasonable visibility.

2. Theory has been derived for a method of measuring three orthogonal components of vibration by using three different interferometer configurations: one with sensitivity parallel to the line of sight (out-of-plane) and two with perpendicular sensitivities normal to the line of sight (in-plane). Using only measurements of component amplitudes it is possible to calculate the total amplitude at any point as the square root of the sum of the squares of the three components.* If both amplitude and phase are measured then the three-dimensional vibration vector can be calculated at any point by phasor addition of the components. This method has advantages over methods previously used in holographic interferometry and ESPI where three non-orthogonal components are measured, because the calculation is simpler and less prone to computational errors.

* (assuming the x and y components are in phase)

3. Examples of one-, two- and three-dimensional mechanical vibrations have been presented, confirming the abilities of the different interferometer configurations to measure orthogonal components as predicted. The method for combining the measurements has been demonstrated for two dimensions to yield the total in-plane vibration. With time-averaged observation it is only possible to measure amplitudes of vibration, but the relative phases of the two independent in-plane components have been deduced by obtaining a third measurement in the same plane. In-plane vector plots have been produced manually from these measurements. The method of phase-stepping has been applied to pulsed ESPI, enabling both displacement and phase to be measured. A computer has been used to perform the phase-stepping and to automatically calculate both out-of-plane and in-plane vector displacement plots. The same procedures could be used to calculate three-dimensional displacement plots, but for the objects which have been studied the information can be most clearly understood when presented as in-plane and out-of-plane components.

4. It has been shown that ESPI is capable of performing a full modal analysis of an engineering structure undergoing vibrations of a three-dimensional nature. The information which can be obtained includes resonant frequencies, three-dimensional mode shapes and amplitude response levels. Q-values and hence modal damping could be obtained by measuring the frequencies at the half-power points for each mode. The accuracy with which response and damping values can be obtained depends on the fringe analysis method used for amplitude measurement and also on how the excitation level is monitored. It was found that the use of accelerometers for rapid and accurate frequency response measurement at discrete points complimented the use of ESPI for providing good visualisation of mode shapes. The ability of computer finite element modelling to predict three-dimensional normal mode shapes and frequencies was also very useful in helping to interpret the experimental results.

5. Time-average measurement is restricted to small amplitude (i.e. the order of one micron), steady-state vibrations of relatively stable objects, and quantitative amplitude measurements are straightforward only for sinusoidal vibrations. Pulsed subtraction ESPI can be used to observe larger amplitude vibrations by sampling a portion of the vibration cycle, and to analyse non-harmonic waveforms by varying the pulse timing to observe the deformed shape at different phase epochs. This ability to perform temporal analysis of waveforms has been demonstrated on a beam vibrating with both standing and travelling wave components. Twin-pulse addition ESPI enables observations to be made on highly unstable vibrating objects by measuring displacements over a very short time duration. This has been demonstrated on an object translating at 15 mm/s whilst vibrating at 5 kHz, and also on a machine in a factory environment. Fringe patterns formed by addition correlation have much poorer visibility than by subtraction, but useful information can still be obtained. A method has been demonstrated for subsequently subtracting addition interferograms to reveal both mode shapes and bulk body motion.

   The 3D ESPI system as reported here measures the different components of vibration sequentially, and is therefore restricted to vibrations which are either steady-state or accurately repeatable. As an optical technique it is also inherently restricted to surfaces which can be illuminated and viewed in the required manner.

6. Applications of the technique in engineering vibration analysis have been investigated, and it has been shown to be useful for studying beams, plates, an ultrasonic forming die, an ultrasonic cutting system and a turbocharger blade. The three-dimensional capability has potential applications wherever vibrations are not limited to a single direction, and suggestions have been made for future areas of study.

7. ESPI is an established technique for vibration analysis, offering the advantages of whole-field, non-contact measurement. The work reported here has extended the range of application of the technique to include the study of in-plane and three-dimensional vibrations. The importance of being able to measure these types of vibration has been demonstrated for several engineering components and systems, along with the ability of the 3D ESPI system to achieve this. The new method offers distinct advantages over other currently available techniques for certain types of measurement, and is therefore a useful addition for the vibration engineer. The principal stated objective of this research has therefore been achieved.

APPENDICES

A. THEORY FOR ESPI FRINGE INTERPRETATION

ESPI produces results in the form of video images, where the useful information is contained in the spatial intensity distribution of the images (or in the temporal voltage variation of the electronic video signal). In order to extract that information it is necessary to know the relationship between the spatial intensity distribution and the quantity which is being measured (i.e. surface displacement). This is called the fringe function. The purpose of this appendix is to present the basic equations which are necessary for the interpretation of ESPI fringe patterns.

The elements of theory presented herein have all been derived individually by previous researchers, but they have not previously been consolidated into a form which is applicable to all the techniques used in the present study. Here the fringe function is derived in a general form, and then particular types of illumination are considered in turn. In each case the function is given in terms of an optical phase change, and can be applied to any of the interferometer configurations described in chapter 3.

A.1 SPECKLE PATTERN CORRELATION

The principle behind ESPI is that when an optically rough surface is illuminated by a coherent light source (e.g. a laser), the light scattered from the surface gives the appearance of a random distribution of tiny 'speckles' of varying brightness. This is because the light arriving at any point in the image plane comprises a number of components scattered diffusely from an area of the object, the area being determined by the optical resolution of the imaging system. These components have similar amplitude but varying phase, so that the resultant intensity varies randomly across the image plane giving a speckled appearance. The speckle pattern produced is unique to the particular combination of object surface and imaging system, and contains phase information about the surface. The properties of laser speckle patterns have been discussed in detail by Goodman[141].

If the surface is displaced or deformed, the phase of an individual component of light scattered from the resolution area to a given point in the image plane changes. Provided, however, that the displacement and/or the displacement gradient are not too large, the phase change of all the components scattered from the resolution area to the image plane point are approximately equal. This means that the position of each speckle remains substantially the same, but its intensity varies according to the displacement of the resolution area. If a second illumination is added which is mutually coherent with the existing source, it acts as a phase reference for the speckle pattern. The image is now a function of the phase relationship between the two illuminating wavefronts, which will be altered by displacements at the object surface. If two such speckle patterns are recorded from the same surface before and after it is deformed, the difference between the two patterns is a function of the surface deformation: where the surface has not moved the speckles keep the same intensity and the pattern is unchanged, but where the surface has moved the speckle intensity changes accordingly. By comparing (or 'correlating') the two patterns, these differences show up as variations in speckle contrast in the resulting interferogram, which are seen as alternating bright and dark fringes corresponding to loci of equal phase difference between the two wavefronts. The phase difference is determined by the changes in optical path lengths, which in turn are determined by the relative motion of the object surface and the interferometer beams.

In ESPI the images are recorded by a video camera, which produces an analogue voltage signal proportional to the image intensity. The correlation process is normally performed either by addition of intensities on the camera faceplate or by electronic subtraction using a video store.

A.2 GENERALISED FRINGE FUNCTION

Consider a general two-beam interferometer, where the two interfering beams are mutually coherent. We can define a global co-ordinate system with cartesian x, y and z axes such that the imaging system views the object along the z-axis. A focused-image viewing system is used, with sufficient depth of field to view the whole object. Any point in the object space can then be defined by co-ordinates (x, y, z), and we can define corresponding co-ordinates (x′, y′) for the point in the two-dimensional image plane where it is focused. The instantaneous complex amplitudes U of the wavefronts arriving at a point P(x′,y′) in the image plane from each beam (whether they be smooth or speckled) can be described in complex notation as:*

$$U_A = u_A \, e^{i(\omega_A t + \psi_A)} \tag{A.1}$$

and

$$U_B = u_B \, e^{i(\omega_B t + \psi_B)} \tag{A.2}$$

where the subscripts $_A$ and $_B$ denote the two beams, u is real amplitude, ω is angular frequency, ψ is phase and t is time. U, u and ψ are functions of x′, y′ and t (the z′ coordinate is constant due to the image being planar). We will only consider the case where $\omega_A = \omega_B = \omega$, i.e. both interferometer beams have the same constant wavelength.

The total complex amplitude of the two combined wavefronts is:

$$\begin{aligned} U_T &= U_A + U_B \\ &= u_A \, e^{i(\omega t + \psi_A)} + u_B \, e^{i(\omega t + \psi_B)} \\ &= e^{i\omega t} \, \{ \, u_A \, e^{i\psi_A} + u_B \, e^{i\psi_B} \, \} \end{aligned} \tag{A.3}$$

* N.B. Neglecting polarization effects

The total intensity at P(x′,y′) is given by:

$$I = U_T . U_T^* \tag{A.4}$$

where U^* is the complex conjugate of U. Hence we can write:

$$\begin{aligned} I &= (u_A e^{i\psi_A} + u_B e^{i\psi_B})(u_A e^{-i\psi_A} + u_B e^{-i\psi_B}) \\ &= u_A^2 + u_B^2 + u_A u_B \{e^{i(\psi_A - \psi_B)} + e^{-i(\psi_A - \psi_B)}\} \\ &= u_A^2 + u_B^2 + 2u_A u_B \cos(\psi_A - \psi_B) \end{aligned} \tag{A.5}$$

where the third term is due to mutual interference of the two beams. This can be written in terms of intensities:

$$I = I_A + I_B + 2\sqrt{I_A I_B} \cos(\psi_A - \psi_B) \tag{A.6}$$

Any relative phase shift $\Delta\psi$ between the two wavefronts at P will cause the intensity to change to:

$$I = I_A + I_B + 2\sqrt{I_A I_B} \cos(\psi_A - \psi_B + \Delta\psi) \tag{A.7}$$

The phase shift $\Delta\psi$ can be caused by deformation of the object surface, which will alter the phase of any wavefronts reflected from it, or by phase-shifting of either of the interferometer beams:

$$\Delta\psi = \Delta\psi_O + \Delta\psi_A + \Delta\psi_B \tag{A.8}$$

$\Delta\psi_O$ is the phase shift at the image plane due to phase changes in the scattered wavefronts caused by the surface deformation, and is a function of (x′,y′,t). $\Delta\psi_A$ and $\Delta\psi_B$ are phase shifts in the incident illuminating beams which cause a uniform phase change across the image and hence do not affect the fringe positions.

Any single interferometer is only sensitive to one spatial component of displacement at any point in the object space. The direction of sensitivity can be defined by a unit vector **n** called the ‘sensitivity vector’. If the three-dimensional vector displacement of each object point is **d**, then the interferometer will be sensitive to the component of **d** resolved along the sensitivity vector:

$$d_n = \boldsymbol{n}.\boldsymbol{d} \tag{A.9}$$

where d_n and **d** are functions of (x,y,z,t). The optical phase change per unit displacement is determined by the wave number $k = 2\pi/\lambda$ (where λ is the wavelength of the illuminating light), and the phase change at the image plane due to a unit phase change in the object space can be defined as a 'fringe sensitivity factor' Γ (which determines how many fringes correspond to a given surface displacement). The $\Delta\psi_O$ term in equation (A.8) is then given by:

$$\Delta\psi_O = k\Gamma d_n \tag{A.10}$$

Γ and **n** are determined by the optical geometry of the interferometer, and are functions of (x,y,z).

The instantaneous image intensity I given in equation (A.7) is detected by a video camera (or similar sensor) which measures the total energy (proportional to intensity) incident at each detector point during a finite exposure period. Hence the measured quantity is a time integral over the exposure period τ, given by:

$$I_\tau = \frac{1}{\tau}\int_t^{t+\tau}\{\, I_A + I_B + 2\sqrt{I_A I_B}\;\cos(\psi_A - \psi_B + \Delta\psi)\,\}\, dt \tag{A.11}$$

This is the generalised fringe function as seen by the camera.

If the object motion does not vary with time (when it is stationary or undergoes a static displacement) the integral vanishes and the fringe function takes the form of equation (A.7).

For three-dimensional vibration analysis it is required to determine values of the object displacement function **d**(x,y,z,t). The information measured by ESPI is in the form $I_\tau(x',y')$ for various values of t. Hence it is necessary to process that information using equation (A.11) to extract values of $\Delta\psi(x',y',t)$, and then to substitute into equations (A.8) and (A.10) using known values of $\Delta\psi_A$, $\Delta\psi_B$, k and Γ to obtain d_n. However each measurement of d_n only gives one resolved component of **d**. Therefore to completely define the vector **d** in three dimensions it is necessary to obtain at least three different measurements of d_n, and this requires different sensitivity vectors **n** for each measurement. Ideally three mutually perpendicular sensitivity vectors should be used, as this obviates the need to solve simultaneous equations. Interferometer configurations which can satisfy this condition are described in section 3.1.

The form of the time integral in equation (A.11) depends on the type of illumination used as well as the surface motion; the effects of different illumination methods are considered in sections A.3 and A.4.

A.3 CONTINUOUS WAVE ILLUMINATION

Evaluation of the time integral in the generalised fringe function given in equation (A.11) can be quite complicated, as $\Delta\psi$ varies with both the object motion and any variations in the illumination during the exposure period. In practice ESPI systems invariably use illumination which is either constant with time (continuous wave) or varies as a simple function of time (stroboscopic or pulsed), and in many cases the object motion is also periodic. Both of these factors greatly simplify the evaluation of the integral. Continuous wave illumination is suitable for periodic motion, but the analysis of non-periodic motions requires stroboscopic or pulsed illumination (see section A.4).

In the simplest case of continuous illumination, the intensities and phases of both illuminating beams are time independent. Equation (A.11) then becomes:

$$I_\tau = I_A + I_B + \frac{2}{\tau}\sqrt{I_A I_B}\int_t^{t+\tau}\cos(\psi_A - \psi_B + \Delta\psi_O)\,dt \tag{A.12}$$

For an object which is undergoing steady-state harmonic vibration:

$$d = a \sin(2\pi f t) \tag{A.13}$$

where a and f are the amplitude and frequency of vibration. Provided that $1/f \ll \tau$ the time integral can be evaluated for a whole number of vibration cycles (reference 69 p.170), giving:

$$I_\tau = I_A + I_B + 2\sqrt{I_A I_B}\,\cos(\psi_A - \psi_B)\, J_0(k\Gamma a_n) \tag{A.14}$$

where J_0 is a zero order Bessel function and a_n is the component of amplitude resolved along the sensitivity vector. Examination of equation (A.14) shows that the time-averaged image intensity contains random components from the speckle patterns due to wavefronts A and/or B, modulated by a Bessel function of the vibration amplitude term a_n. The Bessel function J_0 cycles between positive maxima and negative minima with the magnitude of the turning points tending asymptotically to zero, as shown in Figure 57. The resulting image is therefore a fringe pattern where the bright and dark fringes are regions of maximum and minimum speckle contrast determined by $J_0(k\Gamma a_n)$. Maxima of $J_0(x)$ occur at x=0, 3.8, 7.0, 10.2, 13.3, 16.4 . . . , and minima at x=2.4, 5.5, 8.6, 11.8, 14.9, 18.1 . . .

All the useful information in equation (A.14) is contained in the $J_0(k\Gamma a_n)$ term, so the effect of the added I_A and I_B terms is to reduce the signal to noise ratio giving poor fringe visibility. This problem can be overcome by subtracting the stationary noise terms. In practice this can be achieved by storing the image I_τ from one video frame and subtracting subsequent images whilst introducing a phase shift between ψ_A and ψ_B. It can be seen from equation (A.14) that the first two terms will disappear leaving a fringe function of the form:

$$I_{subt} \propto J_0(k\Gamma a_n) \tag{A.15}$$

A phase shift of π gives the maximum fringe visibility. Equation (A.15) contains both positive and negative values of intensity, which will give proportional voltages in the video signal. Television monitors cannot display negative voltages, so in order to avoid losing half of the information it is necessary to rectify the signal or to square it, giving a fringe function of the form:

$$I_{subt} \propto J_0^2(k\Gamma a_n) \tag{A.16}$$

In this case the bright and dark fringes correspond to the maxima and minima of the J_0^2 function, as shown in Figure 58.

Quantitative measurements of the resolved vector amplitude a_n can be obtained by substituting abscissa values of maxima and minima from the appropriate fringe function (e.g. J_0 or J_0^2) for the corresponding bright and dark fringes on the monitor image. Stationary or nodal regions (where a_n=0) are easily identified by the zero order fringe being brighter than higher order fringes, and this gives a reference for numbering the fringe orders.

The solution for harmonic vibration as given above is very useful as it covers many engineering problems. However if the surface motion is periodic but non-harmonic then it becomes difficult to interpret quantitative information other than nodal regions. Wall[142] has demonstrated for holographic interferometry that a square wave-form is equivalent to a single step displacement and produces a cosinusoidal fringe pattern (see section A.4), whereas a triangular or saw-tooth wave-form is equivalent to a linear motion and satisfies the condition for minimum fringe visibility. In cases where it is required to analyse surface motions which are either non-harmonic or non-periodic it is generally necessary to sample points on the waveform using stroboscopic or pulsed illumination. This is explained in the following section.

A.4 STROBOSCOPIC AND PULSED ILLUMINATION

The effect of incoherent light (such as daylight or ambient room lighting) in ESPI is to add a constant noise term to the image intensity, which does not contribute to the form of the fringe pattern. Therefore the fringe function can be determined by evaluating the time integral only over the periods of laser illumination within the exposure duration. Stroboscopic illumination is the case where the object is illuminated at regular intervals for periods which are shorter than the vibration period of the object. The measured intensity I_t is then given by the sum of the time-averaged intensities for each illumination period within the exposure. Even for the relatively simple case of harmonic vibrations with the illumination synchronised to the same frequency this generally gives a complicated integral, which is a function of the periods of the illumination and vibration cycles and the phase relationship between them[143]. However, as the duration of illumination becomes very small compared to the period of vibration, the variation of $\Delta\psi$ within each illumination becomes negligible and I_t effectively becomes a sum of instantaneous intensities. This happens in practice when the object is illuminated by a Q-switched laser producing pulses of very short duration. The image plane intensities created by two consecutive pulses are given by equations (A.6) and (A.7), where $\Delta\psi$ is now the phase shift between the two pulses. Comparing equations (A.6) and (A.7) it can be seen that they can be correlated by addition or subtraction, yielding a fringe pattern which is a function of $\Delta\psi$.

If the two pulses occur within the same exposure (i.e. in one video frame) then they will correlate by addition as for time-averaging. This is known as double-pulse (or twin-pulse) addition ESPI, and produces a fringe function:

$$I_{add} = 2I_A + 2I_B + 4\sqrt{I_A I_B}\ \cos(\psi_A - \psi_B + \frac{1}{2}\Delta\psi)\ \cos\frac{1}{2}\Delta\psi \tag{A.17}$$

Hence the fringe pattern contains stationary noise terms and is modulated by a cos function of the phase change $\Delta\psi$. If the signal is squared this becomes a $\cos^2$ function. In either case the intensity I is maximum (i.e. bright fringes) for $\Delta\psi$ = 0, 2π, 4π . . . and minimum (i.e. dark fringes) for $\Delta\psi = \pi, 3\pi, 5\pi$ . . .

If two single pulses are fired in separate video frames, they can be correlated by electronic subtraction. In this case the stationary noise is removed as described above. This gives fringes of the same form as equation (A.17) but sinusoidal rather than cosinusoidal (i.e the fringe maxima of subtraction fringes correspond to fringe minima of addition fringes, and vice versa) and with no addition noise terms.

The fringe patterns produced by pulsed ESPI map loci of constant displacement d_n (see equation A.9) between the points in time at which the two correlated speckle patterns were produced. If the laser pulses are synchronised to coincide with the positive and negative maxima of a periodic object vibration cycle then this corresponds to the peak-to-peak vibration amplitude, i.e. $d_n = 2a_n$, so in this case the amplitude can be calculated directly. However if the pulses occur at any other points on the vibration cycle then the fringes indicate a fraction of the total amplitude which is dependent on the relative phase. In this case it is necessary to know the timing of the pulses in order to obtain the total amplitude. Transient and non-harmonic wave-forms can be analysed by varying the timing of the laser pulses to measure the surface displacement at different instants in time.

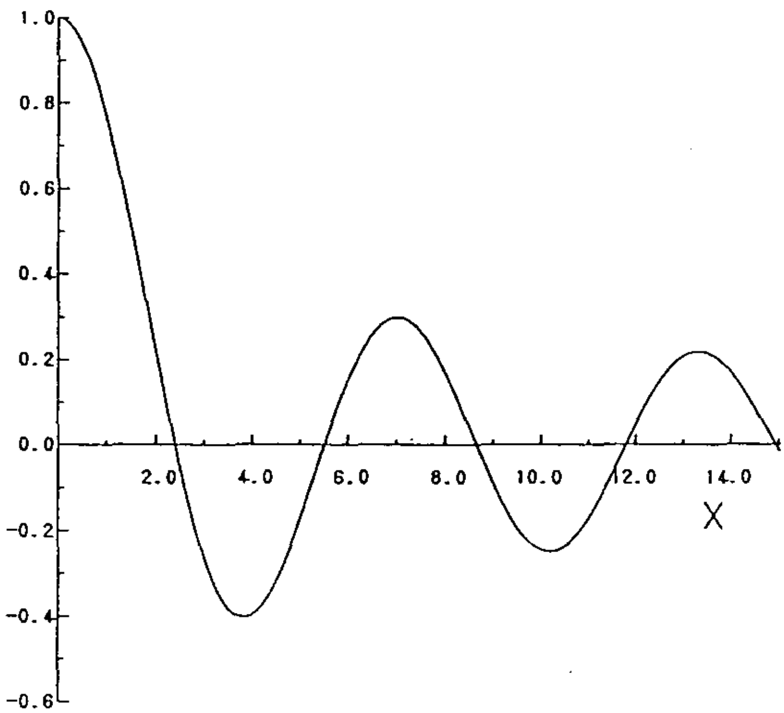

Figure 57: Plot of $J_0(x)$

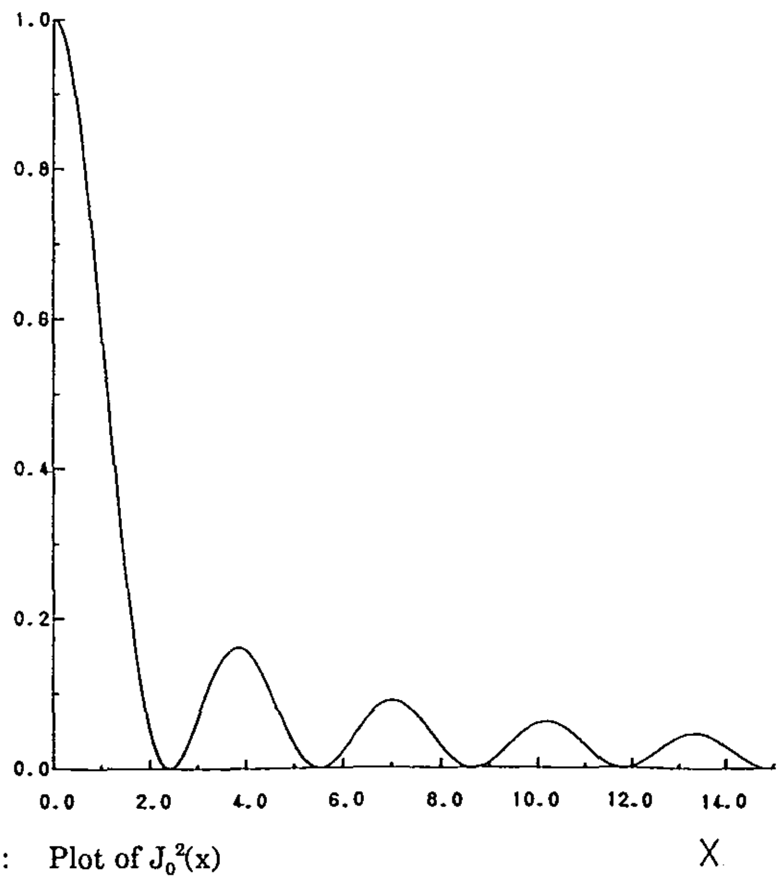

Figure 58: Plot of $J_0^2(x)$

B. THEORY FOR MECHANICAL VIBRATIONS

The purpose of this appendix is to present in a concise form all the concepts of vibration theory which are necessary for a good understanding of the results which have been presented. Most text books start by dealing with simple idealised systems and gradually expand the theory to cover more general cases. The philosophy chosen here is instead to start with the most general concepts which are applicable to all mechanical systems, and then describe how those concepts can be applied to understand the behaviour that is observed in the experimental results. In this way it is hoped that the specific structures which have been studied can be seen as special cases which are accommodated within and fully explained by the overall theory.

B.1 MECHANICAL WAVES AND DEFORMATION

Mechanical vibrations can be defined as time-dependent deformations of an elastic medium. The energy which causes the deformation propagates through the medium as a mechanical wave. A mechanical wave is an action whereby energy is transmitted through the medium by particles being displaced in the presence of elastic restraining forces, so that the particles oscillate about their undisplaced position[144]. Two types of mechanical wave can occur: (i) transverse, where the particles are displaced perpendicular to the direction of energy propagation, and (ii) longitudinal, where the particles are displaced parallel to the direction of energy propagation. The two types of wave cause the medium to deform in different ways. Transverse waves create an equivoluminal deformation, where each elemental volume within the medium changes shape but maintains its same volume. Longitudinal waves create a dilatational deformation, where each element expands and contracts. The type of wave will be determined initially by the way the force is applied, but in general both types will occur simultaneously[145].

The action of a wave propagating through a medium is altered by any change in the material properties, geometry or applied constraints. In particular, when a travelling wave is incident upon a discontinuity or an interface between two regions having different dynamic properties, some degree of reflection must occur in order to maintain dynamic equilibrium[134]. The amplitude and phase of the reflected and transmitted waves are determined by the 'mechanical impedance' of the interface. Two special cases are of particular importance: waves incident on an unconstrained (free) solid boundary are reflected with the same phase, and waves incident on a totally constrained (clamped) solid boundary are reflected with 180° phase reversal. Interference will occur between the incident and reflected waves, creating a complex vibration field throughout the medium. In the special case where two harmonic waves having equal frequency and amplitude are propagating in opposite directions, a standing wave will be created. These conditions are known as 'phase coincidence'.

B.2 NATURAL FREQUENCIES AND MODES

For any bounded structure, certain combinations of material properties, geometry, boundary conditions and wave frequency will create conditions under which phase coincidence occurs. Hence for a particular structure under specified conditions, certain frequencies of free vibration will cause standing wave fields to form. These are known as the characteristic or natural frequencies of that structure. The spatial form of the standing wave fields corresponding to these frequencies is known as the characteristic function, or the natural mode shape. These mode shapes often include stationary points having zero vibration amplitude, which are called 'nodal points', and local maxima of amplitude called 'antinodes'. Some types of mode are characterised by nodal lines or surfaces which divide regions vibrating in antiphase to each other.

The number of natural frequencies that can occur in a particular system is dependent on the number of degrees of freedom associated with that system. This in turn is determined by the distribution of mass and stiffness within the system, and the applied constraints. The simplest conceivable system capable of vibration has only one degree of freedom. This could be, for example, an infinitely stiff mass attached to a spring of negligible mass and constrained so that the mass can only translate along one axis. Such a system would possess one unique natural frequency, at which its motion would be described by the unique characteristic function. Two degrees of freedom could be obtained by attaching a second similar mass-spring system to the first, constrained on the same axis; the system would then have two natural frequencies, each with a unique characteristic function. Alternatively the second degree of freedom could be obtained by removing a constraint so that the mass can rotate about one axis as well as translating; the system would then have one translational and one torsional natural mode. Such idealised systems cannot strictly exist in practice, but can be used to approximate certain real systems. Modelling a system with discrete mass and stiffness elements is sometimes called the 'lumped parameter' method[146]. Real structures generally have distributed mass and stiffness, and are called 'continuous' or 'distributed parameter' systems. A continuous structure effectively has an infinite number of degrees of freedom, and should therefore possess an infinite number of natural frequencies. In practice the phenomenon of cut-off[147] places an upper limit on the frequency which can be transmitted through a dispersive medium by each type of wave, and hence also limits the number of modes for a given structure.

It can be shown[148] that the normal modes (or characteristic functions) corresponding to each natural frequency are 'orthogonal' with respect to the mass and stiffness of the system. The practical consequence of this is that changes in the response of any one mode do not necessarily affect any of the other modes.

Mathematically it means that the equations describing the response of each mode are mutually independent, and therefore the total response can be described in terms of a set of independent simultaneous equations. It should be noted that for the special case of two modes having exactly the same natural frequency, the modes are not necessarily orthogonal. Under conditions of linear vibration, that is when the magnitude of response is directly proportional to the magnitude of excitation, the total response due to a number of normal modes being excited simultaneously is a simple superposition of the responses of each individual mode in isolation.

All real systems contain some degree of damping, and this has the effect of dissipating the energy of waves propagating through the system. Damping forces can arise due to several effects: (i) structural damping, caused by internal friction due to strain in an elastic medium; (ii) viscous damping, caused by resistance to motion through a fluid; (iii) Coulomb damping, caused by sliding friction between two solid surfaces. For mathematical analysis it is usual to model all the damping with a single equivalent viscous damping term. The effect of damping is to cause free vibrations to decay with time, and forced vibrations to reach a steady-state where the energy being input to the system by the applied force is balanced by the energy being dissipated by the damping.

B.3 FORCED VIBRATION AND RESONANCE

When energy is introduced into a system as a mechanical wave, it will only induce significant vibrations if it occurs at one of the natural frequencies of the system. Energy input at a natural frequency will rapidly build up a standing wave pattern corresponding to the normal mode for that frequency, which will then decay due to damping. Waves of any other frequency will decay rapidly as they propagate through the system without creating a standing wave; this is called the 'transient response'. In most situations a range of frequencies are generated. For example a shock impulse will generate waves over a broad spectrum of frequencies, and will cause the system to vibrate in a number of normal modes simultaneously. Vibration in the absence of externally applied forces is called 'free vibration'.

When energy is input into a system as a continuous periodic function, known as 'forced vibration', then after the initial transient response has decayed there will remain a steady state response which contains all the frequency components of the driving force but no others (the frequency components can be determined by Fourier analysis of the forcing function). If the driving force function is a pure sinusoid then the response will be a single frequency vibration. If the function contains any frequency components which correspond to any of the natural frequencies of the system, then phase coincidence will occur and a normal mode standing wave will form. This coincidence of excitation frequency with natural frequency is called 'resonance'. The presence of damping in the system means that the standing wave occurs not only at the discrete undamped natural frequency, but also to a lesser extent at frequencies above and below the natural frequency. This is shown in Figure 59(a), which plots amplitude of response against forcing frequency for a single degree of freedom system at various levels of damping (assuming linear-elastic behaviour and proportional damping). The response amplitude is normalised to the magnitude of the driving force, and the damping is expressed as the damping coefficient ζ, which is the ratio of modal damping to the critical damping[146]. It can be seen that as the damping increases, the damped natural frequency (i.e. the resonant frequency) and the peak response (at the resonant frequency) both decrease, but the off-resonance response increases relative to the response at resonance. In all cases the normalised response tends to unity as the forcing frequency decreases below resonance, and tends to zero as the frequency increases above resonance. The frequency range over which a significant response occurs is commonly expressed in terms of the 'half-power bandwidth', at the limits of which the root-mean-square response is $1/\sqrt{2}$ times the peak resonant response. The sharpness of resonance can then be defined by a quantity Q given by the resonant frequency divided by the half-power bandwidth. This is related to the modal damping by $Q = 1/2\zeta$. The phase angle by which the response lags the excitation is also a function of the damping coefficient, as shown in Figure 59(b). In all cases the phase angle increases with forcing frequency from zero to 90° at the undamped natural frequency, and tends to 180° as the frequency increases above resonance.

All of the normal modes of vibration of a linear-elastic system will have a response characteristic of the form shown in Figure 59. For a continuous system there will be a very large number of normal modes and, because of the finite damping, the response curves of these modes overlap. Each mode has a different spatial form, so the response is now a function of both the spatial position within the system and the spatial distribution of the forcing function, as well as the frequency. The degree to which each mode participates in the response to a given force distribution is called the 'mode participation factor'[148]. The most obvious demonstration of this is that an excitation applied at a resonant frequency but at a point which is nodal in the corresponding normal mode shape will not produce an amplified response; similarly no response will be measured at any nodal points of a mode which is being excited. The resultant response of the system to a specified excitation is a weighted summation of all the contributing modal responses, and is called the frequency response function. The contribution of each mode is determined by its resonant frequency and modal damping, weighted by the participation factor. Figure 60 shows the frequency response function as observed at one point in a typical continuous system over a particular window in the frequency range[8]. Figure 61 shows how this consists principally of contributions from three resonant modes which occur within that frequency range.

B.4 MODE COUPLING AND COMBINATION

Modal coupling occurs when the action of one vibration mode creates displacements which are associated with a different mode. For example, the longitudinal strain due to an extensional motion in one direction can create a significant transverse strain in a perpendicular direction due to the Poisson's ratio of the medium. Similarly, bending of thick or curved sections in one plane can cause significant bending in a different plane due to anticlastic behaviour. This interaction can have considerable influence on the vibration modes of a structure, and has been studied in isotropic and orthotropic rectangular plates by Caldersmith and Rossing[17]. Mode combination can occur when two different normal modes have similar natural frequencies. In these circumstances it is possible for the two normal modes to be replaced by two different modes which share some of the characteristics of the normal modes. This phenomenon is often observed in nominally symmetric objects which suffer some asymmetry in geometry, material properties, boundary constraints and/or excitation force. Detailed investigations and discussions have been published by Grinsted[14] and Waller[13].

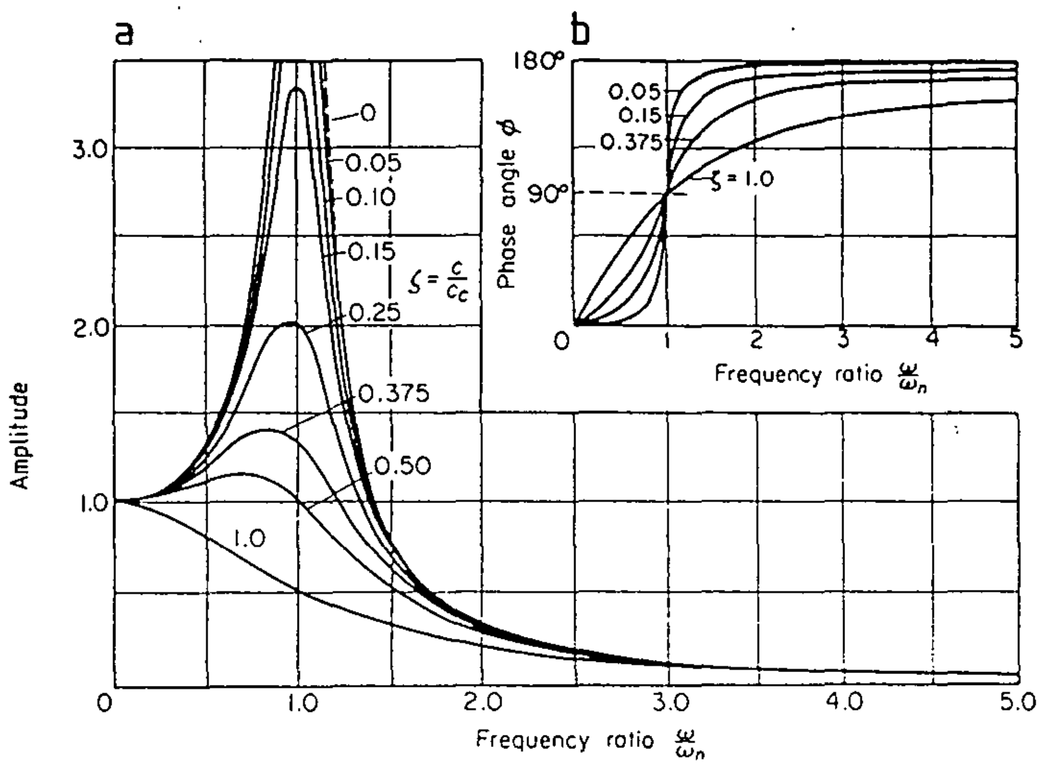

Figure 59: Vibration response of single degree of freedom system

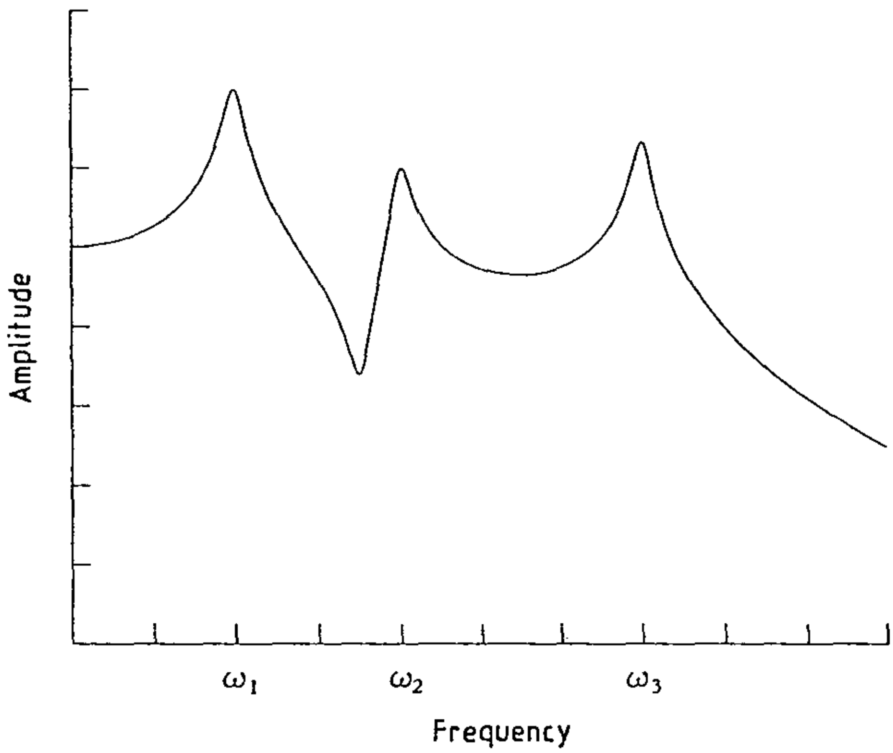

Figure 60: Frequency response function for multiple degree of freedom system

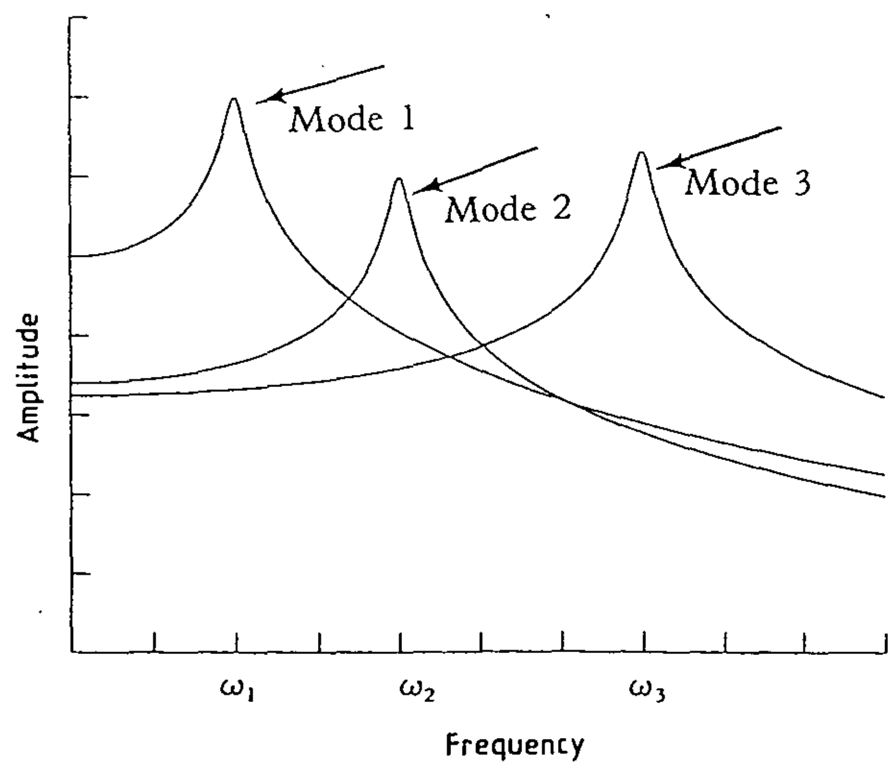

Figure 61: Single degree of freedom modal contributions

C. VIBRATION MODE CLASSIFICATION

The types of natural vibration mode which occur in a structure are determined by the type of wave motion (i.e. transverse or longitudinal), the direction of wave propagation and the geometry of the boundaries and/or interfaces. It is only possible to classify these modes in a simple manner for structures which have symmetry. The following sections describe the principal classes of mode for some of the types of object which have been studied: plates, thick cylinders and turbocharger blades.

C.1 PLATES

The principal classes of wave motion in plates are shown diagrammatically in Figure 62. Flexural motion is due to the action of a transverse wave propagating in the plane of the plate and causing particle displacements normal to that plane. Extensional motion is caused by longitudinal waves, which create displacements in the direction of the wave propagation vector. The example shown in Figure 62 is for a wave propagating in the plane of the plate. Displacements are predominantly in-plane in this case, but the longitudinal strains cause corresponding changes in the thickness due to the Poisson effect. Hence there is some out-of-plane motion, which is shown exaggerated in Figure 62. Extensional motion can also occur in the thickness direction due to a longitudinal wave propagating normal to the plane of the plate, i.e. through the thickness. Thickness shear is due to a flexural wave propagating through the thickness, and face shear is due to a flexural wave propagating in the plane of the plate and causing particle displacements in the same plane. Thickness twist is a term used for higher orders of face shear, where the displacement varies through the thickness. These types of motion are described in more detail by Salt[149].

Natural modes of vibration which arise principally from these types of wave motion can be classified as flexural, extensional and shear modes. In general the different motions will couple together and create more complicated mode shapes. Plate modes and the effects of coupling are described by Sykes[150], with particular application to quartz crystals. The mathematical theory of waves and vibrations in isotropic, elastic plates is considered in detail by Mindlin[145].

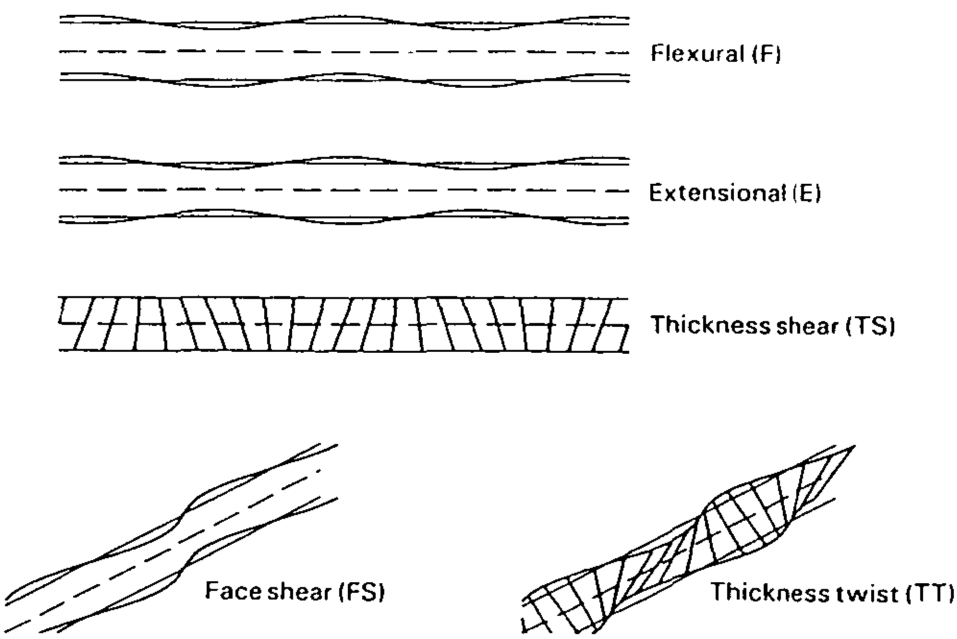

Figure 62: Classes of wave motion in plates

6.5 THICK CYLINDER

The normal modes for the thick annular cylinder described in section 4.3 can be classified[124] into different types, as explained below and illustrated in Figure 63.

i)	Radial (R)	-	Cross-section (through a plane containing the cylinder axis) translates radially in its own plane.
ii)	Axial (A)	-	Cross-section translates axially in its own plane.
iii)	Torsional (T)	-	Cross-section rotates in its own plane.
iv)	Face (F)	-	Front and rear faces rotate in opposite sense about the axis.
v)	Diameter (D)	-	Inside and outside diameters rotate in opposite sense about the axis.

Some modes are likely to couple and produce motions which are combinations of the above types, e.g. FD, where adjacent corners of the cross-section rotate in opposite sense about the axis.

Each classification defines a set of modes which can be identified by their harmonic number. This indicates the number of wavelengths around the circumference of the cylinder. For example: R1 has radial amplitude varying as $\cos\theta$ around the circumference, T3 has axial amplitude varying as $\cos 3\theta$ around the circumference, etc.

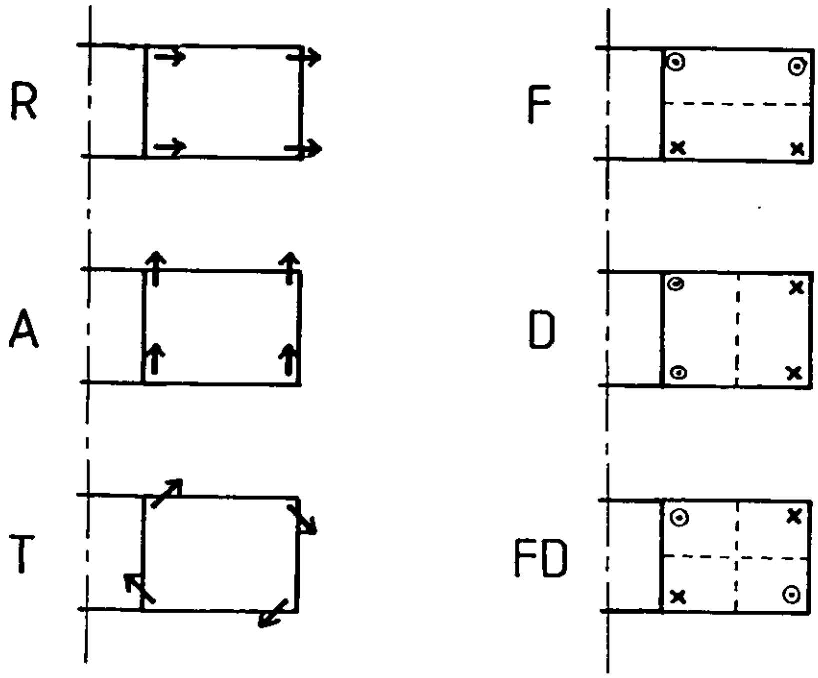

Figure 63: Classes of vibration mode for a thick annular cylinder

C.3 TURBOCHARGER BLADE

The turbocharger blade studied in section 5.3, and turbomachinery blades in general, have non-symmetric geometry and therefore non-symmetric normal modes. However, the blade can be approximated by a cantilevered rectangular plate[14] (i.e clamped-free-free-free, the clamped edge representing the blade root) and the modes identified using the notation for such a plate. The classes of mode which can give rise to significant amplitudes and are therefore of principal interest are:

i) Flap (F) - Out-of-plane flexural motion, bending along the length.

ii) Torsion (T) - Out-of-plane flexural motion, twisting about the medial axis.

iii) Edge (E) - Equivalent to face shear, the predominant motion being in the plane of the plate and parallel to the clamped edge.

iv) Span (S) - Extensional motion in the plane of the plate and perpendicular to the clamped edge.

In general, some of these modes are likely to be coupled.

D. LIST OF SYMBOLS

a	spatial component of phasor amplitude of mechanical vibration
a	phasor amplitude of mechanical vibration
A	indicates first beam or wavefront in interferometer
B	indicates second beam or wavefront in interferometer
c	phase velocity of mechanical wave
d	spatial component of object displacement vector
d	object displacement vector
E	modulus of elasticity
E	ultrasonic power level (arbitrary units)
f	frequency of mechanical vibration
I	intensity at image plane
I	second moment of area
J_0	zero order Bessel function
k	wave number ($=2\pi/\lambda$)
m	mass per unit length of beam
n	sensitivity vector
N	maximum fringe order (for calculating R)
P	arbitrary point in image plane
Q	arbitrary point in object space
Q	sharpness of resonance for mechanical vibration
Q′	displaced point in object space
R	dynamic amplitude response
t	time
u	amplitude of electromagnetic wave
U	instantaneous complex amplitude of electromagnetic wave
x	Cartesian coordinate in object space
x′	Cartesian coordinate in image plane

$\hat{x}$	unit vector on positive x-axis
y	Cartesian coordinate in object space
y′	Cartesian coordinate in image plane
$\hat{y}$	unit vector on positive y-axis
z	Cartesian coordinate in object space
$\hat{z}$	unit vector on positive z-axis
Γ	fringe sensitivity factor
Δl	change in optical path length
$\Delta\psi$	phase shift of electromagnetic wave
ζ	damping ratio for mechanical vibrations
θ	angle between illuminating beam and z-axis
λ	wavelength of electromagnetic or mechanical wave
ν	Poisson's ratio
ρ	material density
σ	standard deviation
τ	exposure period
ψ	phase of electromagnetic wave
ω	angular frequency of electromagnetic or mechanical wave

E. PUBLICATIONS

The following conference papers and publications have been generated from the research presented in this thesis:

1. Shellabear, M.C. and Tyrer, J.R., "Three-dimensional vibration analysis using electronic speckle pattern interferometry (ESPI)", in *Laser Technologies in Industry*, Soares, O.D.D. (ed.), Proc. SPIE, **952**, 251-259, 1988.

2. Shellabear, M.C. and Tyrer, J.R., "Three-dimensional analysis of volume vibrations by electronic speckle interferometry", in *Stress and Vibration: Recent Developments in Industrial Measurement and Analysis*, Stanley, P. (ed.), Proc. SPIE, **1084**, 252-261, 1989.

3. Shellabear, M.C. and Tyrer, J.R., "Application of ESPI to three-dimensional vibration measurements", Opt. Lasers Eng., in print (accepted for publication 12/3/90).

4. Mendoza Santoyo, F., Shellabear, M.C. and Tyrer, J.R., "Whole field in-plane vibration analysis using pulsed phase-stepped ESPI", Appl. Opt., in print (accepted for publication 11/10/90).

5. Shellabear, M.C., Mendoza Santoyo, F. and Tyrer, J.R., "Processing of addition and subtraction fringes from pulsed ESPI for the study of vibrations", in *Hologram Interferometry and Speckle Metrology*, Stetson, K.A. and Pryputniewicz, R.J. (eds.), SEM, 238-244, 1990.

Results from this research have also been presented in the following papers by other authors:

6. Lucas, M. and Chapman, G.M., "Vibration analysis at ultrasonic frequencies", 12th Biennial ASME Conf. on Mechanical Vibration and Noise, Montreal, Sept. 1989.

7. Chapman, G.M. and Lucas, M., "Frequency analysis of an ultrasonically excited thick cylinder", Int. J. Mech. Sci., **32**(3), 205-214, 1990.

REFERENCES

1. Science and Engineering Research Council project GR/E 09474, "Investigation and design of a container production process using ultrasonics to reduce friction", completed 1990.

2. A.E.H. Love, *A Treatise on the Mathematical Theory of Elasticity* (4th edition), Cambridge University Press, 1927.

3. Young, D., "Vibration of rectangular plates by the Ritz method", J. Appl. Mech., **17**, 448-453, 1950.

4. Timoshenko, S.P., Young, D.H. and Weaver, W.,*Vibration Problems in Engineering* (4th edition), Wiley, 1974.

5. Zienkiewicz, O.C. and Taylor, R.L., *The Finite Element Method* (4th edition vols. 1 & 2), McGraw-Hill, 1989.

6. Han, S. and McConnell, K.G., "Measuring true acceleration vectors with triaxial accelerometers", Exp. Tech., **14**(3), 36-40, 1990.

7. Broch, J.T., *Mechanical Vibration and Shock Measurements*, Brüel & Kjær, 1980.

8. *The Fundamentals of Modal Testing*, Application note 243-3, Hewlett-Packard Co. (USA), 1986.

9. Bream, R.G., Gasper, B.C., Lloyd, B.E. and Everett, G.M., "Application of vibration pattern imaging to modal analysis: a comparison with full-field and point measurement techniques", in *Stress and Vibration: Recent Developments in Industrial Measurement and Analysis*, Stanley, P. (ed.), Proc. SPIE, **1084**, 279-292, 1989.

10. Hancox, J.E., Brownell, J.B., Parker, R.J. and McKee, V.B., "Evaluation of several optical techniques for vibration mode shape mapping", in *Stress and Vibration: Recent Developments in Industrial Measurement and Analysis*, Stanley, P. (ed.), Proc. SPIE, **1084**, 240-251, 1989.

11. Waller, M.D., *Chladni Figures: a Study in Symmetry*, G. Bell & Sons (London), 1961.

12. Waller, M.D., "Vibrations of free circular plates. Parts 1-3", Proc. Phys. Soc., **50**, 70-86, 1938.

13. Waller, M.D., "Concerning combined and degenerate vibrations of plates", Acustica, **3**, 370-374, 1953.

14. Grinsted, B., "Nodal pattern analysis", Proc. I. Mech. E., **166**(3), 309-326, 1952.

15. McMahon, G.W., "Experimental study of the vibrations of solid, isotropic, elastic cylinders", J. Acoust. Soc. Am., **36**(1), 85-92, 1964.

16. Ravenhall, F.W. and Som, A.K., "Some recent observations on Chladni's figures", Acustica, **29**, 14-21, 1973.

17. Caldersmith, G. and Rossing, T.D., "Determination of modal coupling in vibrating rectangular plates", Appl. Acoust., **17**, 33-44, 1984.

18. Theocaris, P.S., "Optical nodal-pattern analysis", Exp. Mech., **8**, 237-240, 1968.

19. Bergmann, L., "Experiments with vibrating soap membranes", J. Acoust. Soc. Am., **28**(6), 1043-1047, 1956.

20. Osterberg, H., "An interferometer method of studying the vibrations of an oscillating quartz plate", J. Opt. Soc. Am., **22**, 19-35, 1932.

21. Shaw, E.A.G., "On the resonant vibrations of thick barium titanate disks", J. Acoust. Soc. Am., **28**(1), 38-50, 1956.

22. Sciammarella, C.A., "The moiré method - a review", Exp. Mech., **22**, 418-433, 1982.

23. Hazell, C.R. and Niven, R.D., "Visualization of nodes and antinodes in vibrating plates", Exp. Mech., **8**, 225-231, 1968.

24. Kao, T.Y. and Chiang, F.P., "Family of grating techniques of slope and curvature measurements for static and dynamic flexure of plates", Opt. Eng., **21**(4), 721-742, 1982.

25. Vest, C.M. and Sweeney, D.W., "Measurement of vibrational amplitude by modulation of projected fringes", Appl. Opt., **11**(2), 449-454, 1972.

26. Vest, C.M., *Holographic Interferometry*, Wiley, 1979.

27. Powell, R.L. and Stetson, K.A., "Interferometric vibration analysis by wavefront reconstruction", J. Opt. Soc. Am., **55**(12), 1593-1598, 1965.

28. Molin, N-E. and Stetson, K.A., "Measuring combination mode vibration patterns by hologram interferometry", J. Phys. E: Sci. Instrum., **2**, 609-612, 1969.

29. Wilson, A.D. and Strope, D.H., "Time-average holographic interferometry of a circular plate vibrating simultaneously in two rationally related modes", J. Opt. Soc. Am., **60**(9), 1162-1165, 1970.

30. Wilson, A.D., "Computed time-average holographic interferometric fringes of a circular plate vibrating simultaneously in two rationally or irrationally related modes", J.Opt. Soc. Am., **61**(7), 924-929, 1971.

31. Stetson, K.A. and Taylor, P.A., "The use of normal mode theory in holographic vibration analysis with application to an asymmetrical circular disk", J. Phys. E: Sci. Instrum., **4**, 1009-1015, 1971.

32. Stetson, K.A., "Perturbation method of structural design relevant to holographic vibration analysis", AIAA Jnl., **13**(4), 457-459, 1975.

33. Tonin, R. and Bies, D.A., "Analysis of 3-D vibrations from time-averaged holograms", Appl. Opt., **17**(23), 3713-3721, 1978.

34. Tonin, R. and Bies, D.A., "General theory of time-averaged holography for the study of three-dimensional vibrations at a single frequency", J. Opt. Soc. Am., **68**(7), 924-931, 1978.

35. Katzir, Y. and Glaser, I., "Separation of in-plane and out-of-plane motions in holographic interferometry", Appl. Opt., **21**(4), 678-683, 1982.

36. Pirodda, L. and Griffiths, L.J., "Developments and applications of conjugate-wave holographic interferometry", Opt. Lasers Eng., **14**, 39-53, 1991.

37. Neumann, D.B., Jacobson, C.F. and Brown, G.M., "Holographic technique for determining the phase of vibrating objects", Appl. Opt., **9**(6), 1357-1362, 1970.

38. Rowley, D.M., "A speckle reference beam holocamera capable of determining the relative phase of mechanical vibrations from an unisolated platform", J. Phys. E: Sci. Instrum., **21**, 280-286, 1988.

39. Levitt, J.A. and Stetson, K.A., "Mechanical vibrations: mapping their phase with hologram interferometry", Appl. Opt., **15**(1), 195-199, 1976.

40. Stetson, K.A. and Brohinsky, W.R., "Fringe-shifting technique for numerical analysis of time-average holograms of vibrating objects", J. Opt. Soc. Am., **5**(9), 1472-1476, 1988.

41. Hariharan, P., Oreb, B.F. and Freund, C.H., "Stroboscopic holographic interferometry: measurements of vector components of a vibration", Appl. Opt., **26**(18), 3899-3903, 1987.

42. R. Aprahamian, D.A. Evensen, J.S. Mixson and J.E. Wright, "Application of pulsed holographic interferometry to the measurement of propagating transverse waves in beams", Exp. Mech., **11**(7), 309-314, 1971.

43. Fällström, K.-E., Gustavsson, H., Molin, N.-E. and Wåhlin, A., "Transient bending waves in plates studied by hologram interferometry", Exp. Mech., **29**(4), 378-387, 1989.

44. Felske, A. and Happe, A., "Double pulsed laser holography as a diagnostic method in the automotive industry", in *The Engineering uses of Coherent Optics*, Robertson, E.R. (ed.), Cambridge University Press, 595-614, 1976.

45. Hyodo, Y. and Konomi, T., "Application of superposition technique to vibration mode analyses using laser holography", JSAE Rev., **7**(3), 44-51, 1986.

46. Tozer, B.A., "The use of pulsed lasers for vibration analysis in the nuclear power industry", in *Vibration Control in Optics and Metrology*, Proc. SPIE, **732**, 100-109, 1987.

47. Crawforth, L., Lee, C.-K. and Munce, A.C., "Application of pulsed laser holographic interferometry to the study of magnetic disk drive component motions", in *Hologram Interferometry and Speckle Metrology*, Stetson, K.A. and Pryputniewicz, R.J. (eds.), SEM, 404-412, 1990.

48. Aprahamian, R. and Evensen, D.A., "Applications of holography to dynamics: high-frequency vibrations of beams", J. Appl. Mech. (Trans. ASME), **37**, 287-291, 1970.

49. Aprahamian, R. and Evensen, D.A., "Applications of holography to dynamics: high-frequency vibrations of plates", J. Appl. Mech. (Trans. ASME), **37**, 1083-1090, 1970.

50. Pryputniewicz, R.J., "Holographic and finite element studies of vibrating beams", in *Optics in Engineering Measurement*, Proc. SPIE, **599**, 54-62, 1985.

51. Engelstad, M.J., Chambless, D.A., Swinson, W.F. and Turner, J.L., "Hybrid stress analysis of vibrating plates using holographic interferometry and finite elements", Exp. Mech., **27**, 23-30, 1987.

52. Hazell, C.R. and Mitchell, A.K., "Experimental eigenvalues and mode shapes for flat clamped plates", Exp. Mech., **26**(4), 337-344, 1986.

53. Gottenberg, W.G., "Some applications of holographic interferometry", Exp. Mech., **8**, 405-410, 1968.

54. Tuschak, P.A. and Allaire, R.A., "Axisymmetric vibrations of a cylindrical resonator measured by holographic interferometry", Exp. Mech., **15**, 81-88, 1975.

55. Manderscheid, T., "Adjustment of sonotrodes by holographic interferometry", in *Optics in Engineering Measurement*, Proc. SPIE, **599**, 40-45, 1985.

56. Erf, R.K., "Turbine blade inspection", chapter 8.10 in *Holographic Nondestructive Testing*, Erf, R.K. (ed.), Academic Press, 1974.

57. MacBain, J.C., "Vibratory behaviour of twisted cantilevered plates", J. Aircraft, **12**(4), 343-349, 1975.

58. Anderson, D.A., "Modeling of gas turbine engine compressor blades for vibration analysis", J. Aircraft, **12**(4), 357-359, 1975.

59. Groh, G., "Engineering uses of laser-produced speckle patterns", in *The Engineeering Uses of Holography*, Robertson, E.R. and Harvey, J.M. (eds.), Cambridge University Press, 483-494, 1970.

60. Ek, L. and Molin, N-E., "Detection of the nodal lines and the amplitude of vibration by speckle interferometry", Opt. Comm., **2**(9), 419-424, 1971.

61. Leendertz, J.A., "Interferometric displacement measurement on scattering surfaces utilizing speckle effect", J. Phys. E: Sci. Instrum., **3**, 214-218, 1970.

62. Hung, Y.Y. and Hovanesian, J.D., "Full-field surface-strain and displacement analysis of three-dimensional objects by speckle interferometry", Exp. Mech., **12**, 454-460, 1972.

63. Tiziani, H.J., "Application of speckling for in-plane vibration analysis", Optica Acta, **18**(12), 891-902, 1971.

64. Archbold, E. and Ennos, A.E., "Two-dimensional vibrations analysed by speckle photography", Opt. Laser Tech., 17-21, Feb. 1975.

65. Chiang, F.P. and Juang, R.M., "Vibration analysis of plate and shell by laser speckle interferometry", Optica Acta, **23**(12), 997-1009, 1976.

66. Forno, C., "White-light speckle photography for measuring deformation, strain, and shape", Opt. Laser Tech., **7**, 217-221, 1975.

67. Asundi, A. and Chiang, F.P., "White light speckle method for vibration of plates", in *Photomechanics and Speckle Metrology*, Proc. SPIE, **814**, 149-152, 1987.

68. Erf, R.K., *Speckle Metrology*, Academic Press (New York), 1978.

69. Jones, R. and Wykes, C., *Holographic and Speckle Interferometry*, Cambridge University Press, 1983.

70. Cookson, T.J., Butters, J.N. and Pollard, H.C., "Pulsed lasers in electronic speckle pattern interferometry", Opt. Laser Tech., **10**, 119-124, 1978.

71. Wykes, C., "Use of electronic speckle pattern interferometry (ESPI) in the measurement of static and dynamic surface displacements", Opt. Eng., **21**, 400-406, 1982.

72. Løkberg, O.J., "Mapping of in-plane vibration modes by electronic speckle pattern interferometry", Opt. Eng., **24**(2), 356-359, 1985.

73. Tyrer, J.R., "Critical review of recent developments in electronic speckle pattern interferometry", in *Holographic Nondestructive Testing*, Proc. SPIE, **604**, 95-111, 1986.

74. Løkberg, O.J. and Høgmoen, K., "Use of modulated reference wave in electronic speckle pattern interferometry", J. Phys. E: Sci. Instrum., **9**, 847-851, 1976.

75. Løkberg, O.J. and Høgmoen, K., "Vibration phase mapping using electronic speckle pattern interferometry", Appl. Opt., **15**(11), 2701-2704, 1976.

76. Davies, J.C., Montgomery, P.C. and Tyrer, J.R., "The application of electronic speckle pattern interferometry to modal analysis", Proc. Int. Symposium on Automotive Technology and Automation (Graz, Austria, Sept. 1985), vol. 1, 73-91, 1985.

77. Moran, S.E., Law, R.L., Craig, P.N. and Goldberg, W.M., "Optically phase-locked electronic speckle pattern interferometer", Appl. Opt., **26**(3), 475-491, 1987.

78. Nakadate, S., "Vibration measurement using phase-shifting speckle-pattern interferometry", Appl. Opt., 25(22), 4162-4167, 1986.

79. Tyrer, J.R., "Application of pulsed holography and double pulsed electronic speckle pattern interferometry to large vibrating engineering structures", in *Optics in Engineering Measurement*, Proc. SPIE, **599**, 181-188, 1985.

80. Reid, G.T., "Automatic fringe pattern analysis: a review", Opt. Lasers Eng., **7**, 37-68, 1986.

81. Winther, S., "3D strain measurements using ESPI", Opt. Lasers Eng., **8**, 45-57, 1988.

82. Button, B.L., Dobbins, B.N., He, S.P., Kapasi, S. and Wang, L.S., "3D deformation measurement using DSPI", in *Applied Optics Digest*, Dainty, J.C. (ed.), Institute of Physics, 283-284, 1990.

83. Gülker, G., Hinsch, K., Hölscher, C., Kramer, A. and Neunaber, H., "In-situ investigations of deformations of natural stones by electronic speckle pattern interferometry (ESPI)", in *Laser Technologies in Industry*, Soares, O.D.D. (ed.), Proc. SPIE, **952**, 1988.

84. Gülker, G., Haack, O., Hinsch, K., Hölscher, C., Kuls, J. and Platen, W., "ESPI system for three dimensional deformation measurement in the investigation of stone decay", in *Hologram Interferometry and Speckle*

Metrology, Stetson, K.A. and Pryputniewicz, R.J. (eds.), SEM, 284-287, 1990.

85. Joenathan, C., Pfister, B. and Tiziani, H.J., "Contouring by electronic speckle pattern interferometry employing dual beam illumination", Appl. Opt., **29**(13), 1905-1911, 1990.

86. Creath, K., "Phase-measurement techniques for nondestructive testing", in *Hologram Interferometry and Speckle Metrology*, Stetson, K.A. and Pryputniewicz, R.J. (eds.), SEM, 473-479, 1990.

87. Osten, W. and Höfling, R., "The inverse modulo process in automatic fringe analysis - problems and approaches", in *Hologram Interferometry and Speckle Metrology*, Stetson, K.A. and Pryputniewicz, R.J. (eds.), SEM, 301-309, 1990.

88. Spik, A. and Robinson, D.W., "Investigation of the cellular automata method for phase unwrapping and its implementation on an array processor", Opt. Lasers Eng., **14**, 25-37, 1991.

89. Breuckmann, B., Janke, P. and Hermann, T., "On-line fringe analysis by real-time phase-shift-processing", in *Image Processing II*, Proc. SPIE, **1027**, 91-95, 1988.

90. Ellingsrud, S. and Rosvold, G.O., "Recording and analysis of sinusoidal vibrations using TV-holography and PC-based image processing", in *Applied Optics Digest* (Proc. Applied Optics and Opto-Electronics Conf., Nottingham, 17-20 Sept. 1990), Dainty, J.C. (ed.), Institute of Physics, 1990.

91. Stetson, K.A., "Theory and applications of electronic holography", in *Hologram Interferometry and Speckle Metrology*, Stetson, K.A. and Pryputniewicz, R.J. (eds.), SEM, 294-300, 1990.

92. Oh, K. and Pryputniewicz, R.J., "Application of electro-optic holography in the study of cantilever plate vibrations with concentrated masses", in *Hologram Interferometry and Speckle Metrology*, Stetson, K.A. and Pryputniewicz, R.J. (eds.), SEM, 245-253, 1990.

93. Buckberry, C. and Davies, J., "The application of TV holography to engineering problems in the automotive industry", in *Hologram Interferometry and Speckle Metrology*, Stetson, K.A. and Pryputniewicz, R.J. (eds.), SEM, 268-278, 1990.

94. Valera, J.D., Harvey, D. and Jones, J.D.C., "Mutual phase locking of television holography and laser velocimetry", in *Applied Optics Digest* (Proc. Applied Optics and Opto-electronics Conf., Nottingham, 17-20 Sept. 1990), Dainty, J.C. (ed.), Institute of Physics, 117-118, 1990.

95. Pechersky, M.J. and Bergen, T.F., "ESPI measurements of submerged composite plate vibrations", in *Hologram Interferometry and Speckle Metrology*, Stetson, K.A. and Pryputniewicz, R.J. (eds.), SEM, 254-259, 1990.

96. Preater, R.W.T. and Swain, R.C., "In-plane strain measurement on high speed rotating components using pulsed laser ESPI", in *Hologram Interferometry and Speckle Metrology*, Stetson, K.A. and Pryputniewicz, R.J. (eds.), SEM, 288-293, 1990.

97. Spooren, R., "TV-holography using a double pulsed single oscillator Nd:YAG laser; restrictions and possibilities", in *Hologram Interferometry and Speckle Metrology*, Stetson, K.A. and Pryputniewicz, R.J. (eds.), SEM, 260-267, 1990.

98. Ealing Electro-Optics plc, Greycaine Road, Watford WD2 4PW, UK, technical sales literature.

99. Newport Ltd., Pembroke House, Thompson Close, Harpenden, Herts. AL5 4ES, UK, technical sales literature.

100. Conspectum AS, Jarleveien 4, N-7041 Trondheim, Norway, technical sales literature.

101. Eos GmbH (Electro Optical Systems), Pasinger Straße 2, 8033 Planegg bei München, Germany, technical sales literature.

102. Recognition Technology Inc., Westborough MA, USA, technical sales literature.

103. Spectradata GmbH, Uferstrasse 74, D-2900 Oldenburg, Germany, technical sales literature.

104. Montgomery, P.C., *Forward Looking Innovations in Electronic Speckle Pattern Interferometry*, Ph.D. thesis, Loughborough University of Technology, 1987.

105. Mendoza Santoyo, F., *On the Underlying Optical Mechanisms of the Electronic Speckle Pattern Interferometer (ESPI)*, Ph.D. thesis, Loughborough University of Technology, 1988.

106. Tyrer, J.R., *Toward Commercial Realisation of Whole Field Interferometric Analysis*, Ph.D. thesis, Loughborough University of Technology, 1989.

107. Kerr, D. and Tyrer, J., "Use of high resolution real-time image processing techniques in generation and analysis of ESPI fringe patterns", Opt. Lasers Eng., **8**, 109-121, 1988.

108. Kerr, D., Mendoza Santoyo, F. and Tyrer, J.R., "Manipulation of the Fourier components of speckle fringe patterns as part of an interferometric analysis process", J. Mod. Opt., **36**(2), 195-203, 1989.

109. Kerr, D., Mendoza Santoyo, F. and Tyrer, J.R., "Extraction of phase data from electronic speckle pattern interferometric fringes using a single-phase-step method: a novel approach", J. Opt. Soc. Am., **7**(5), 820-826, 1990.

110. Mendoza Santoyo, F., Tyrer, J.R., West, T.C. and Kerr, D., "Vibration analysis using phase stepped pulsed electronic speckle pattern interferometry",in *Stress and Vibration: Recent Developments in Industrial Measurement and Analysis*, Stanley, P. (ed.), Proc. SPIE, **1084**, 262-278, 1989.

111. Science and Engineering Research Council (Specially Promoted Programme) project GR/E/21711, "Development of a frequency doubled Nd:YAG laser powered electronic speckle pattern interferometer", completed 1990.

112. Tyrer, J.R., "Optical Inspection", UK Patent 8712933, 1987.

113. Moore, A.J. and Tyrer, J.R., "An electronic speckle pattern interferometer for complete in-plane displacement measurement", Meas. Sci. Tech., **1**(10), 1024-1030, 1990.

114. Chapman, G.M. and Wang, X., "Interpretation of experimental and theoretical data for prediction of mode shapes of vibrating turbocharger blades", J. Vib. Acoust. Stress Rel. Des. (Trans. ASME), **110**, 53-58, 1988.

115. Turnbull, J.B. and Chapman, G.M., "Strategies for the vibration analysis of a large turbocharger", Proc. I. Mech. E., **C272/88**, 193-199, 1988.

116. Kerr, D. and Tyrer, J.R., "The application of phase stepping to the analysis of ESPI fringe patterns", in *Photomechanics and Speckle Metrology*, Proc. SPIE, **814**, 379-389, 1987.

117. Moore, A.J.and Tyrer, J.R., "Phase-shifting speckle interferometry for complete in-plane displacement measurement", in *Applied Optics Digest* (Proc. Applied Optics and Opto-electronics Conf., Nottingham, 17-20 Sept. 1990), Dainty, J.C. (ed.), Institute of Physics, 1990.

118. Blevins, R.D., *Formulas for natural frequency and mode shape*, Robert E. Kreiger Publishing Co. (Florida), 1984.

119. Rayleigh, Lord, *The Theory of Sound*, vol. 1 [§221, p.364], Dover Publications (New York), 1945.

120. Gorman, D.J., "Free vibration analysis of the completely free rectangular plate by the method of superposition", J. Sound Vib., **57**(3), 437-447, 1978.

121. Downs, B., "The generation of dynamically corrected flat plate finite elements and their application to the transverse vibration of flat plates", J. Sound Vib., **122**(1), 43-68, 1988.

122. Ekstein, H., "Free vibrations of anisotropic bodies", Phys. Rev., **66** 108-118, 1944.

123. Vrooman, H.A. and Maas, A.A.M., "Image processing in digital speckle interferometry", Proceedings of Fringe Analysis '89 Conference (FASIG), 1989.

124. Cheers, C.F., CMB Packaging Technology, Wantage, UK, private communication.

125. Metal Box plc, "Reducing the diameter of tubular bodies", UK Patent Application GB 2206304A, published 5th January 1989.

126. CMB Packaging Technology plc, "Maintaining a preferred vibration mode in an annular article", UK Patent Application GB 2230724A, published 31st October 1990.

127. Young, M.J.R., Winsper, C.E. and Sansome, D.H., "Radial mode vibrators for oscillatory metal forming", Appl. Acoust., **3**, 299-308, 1970.

128. Young, M.J.R., Winsper, C.E. and Sansome, D.H., "The design of high intensity radial vibrators for metal working applications", J. Phys. D: Appl. Phys., **4**, 212-216, 1971.

129. Lucas, M., Loughborough University of Technology, UK, private communication.

130. Rawson, F.F.H. and Morris, P.S., "Improvements relating to cutting", UK Patent Application GB 2219245 A, 1989.

131. Lucas, M., "Finite element analysis of FFR ultrasonic cutting blades", Loughborough University consultancy report, 1990.

132. Wang, X., formerly Loughborough University, private communication.

133. Baker, J.R., Halliwell, N.A., Horner, J.L. and White, R.G., "Laser technology for measuring vibrational power transmission in beam-like structures", in *Stress and Vibration: Recent Developments in Industrial Measurement and Analysis*, Stanley, P. (ed.), Proc. SPIE, **1084**, 160-170, 1989.

134. F. Fahy, *Sound and Structural Vibration*, chapter 1, Academic Press, 1985.

135. Plotowski, P.D., Hung, Y.Y., Hovanesian, J.D. and Gerhart, G., "Improved fringe carrier technique for unambiguous determination of holographically recorded displacements", Opt. Eng., **24**(5), 754-756, 1985.

136. Leendertz, J.A. and Butters, J.N., "An image-shearing speckle-pattern interferometer for measuring bending moments", J.Phys. E., **6**, 1107-1110, 1973.

137. Wykes, C. and Flanagan, M., "The use of a diode laser in an ESPI system", Opt. Laser Tech., **19**(1), 37-39, 1987.

138. Preater, R.W.T and Swain, R.C., "In-plane strain measurement on high speed rotating components using pulsed laser ESPI", in *Hologram Interferometry and Speckle Metrology*, Stetson, K.A. and Pryputniewicz, R.J. (eds.), SEM, 288-293, 1990.

139. Kyösti, A., Ek, L. and Molin, N-E., "Four ways to determine modes of vibration in a plate", Proc. 3rd Int. Modal Analysis Conf. (Orlando, Florida), 627-633, 1985.

140. Science and Engineering Research Council project GR/G/60765, "Closed loop design and monitoring of ultrasonic cutting equipment".

141. Goodman, J.W., "Statistical properties of laser speckle patterns", chapter 2 in *Laser Speckle and Related Phenomena*, Dainty, J.C. (ed.), Springer-Verlag, 1975.

142. Wall, M.R., "The form of holographic vibration fringes", in *The Engineering Uses of Holography*, Robertson, E.R. and Harvey, J.M. (eds.), Cambridge University Press, 1970.

143. Løkberg, O.J., "Use of chopped laser light in electronic speckle pattern interferometry", Appl. Opt., 18(14), 2377-2384, 1979.

144. D. Halliday and R. Resnick, *Fundamentals of Physics* (2nd edition), chapter 17, Wiley, 1981.

145. Mindlin, R.D., "Waves and vibrations in isotropic, elastic plates", in *Structural Mechanics* by Goodier, J.N. and Hoff, N.J. (eds.), Pergamon Press, 1960.

146. W.T. Thompson, *Theory of Vibration with Applications* (2nd edition), Prentice-Hall, 1981.

147. A.P.French, *Vibrations and Waves*, Van Nostrand Reinhold, 1982.

148. W.C. Hurty and M.F. Rubinstein, *Dynamics of structures*, Prentice-Hall, 1964.

149. Salt, D., *Quartz Crystal Devices*, Van Nostrand Reinhold (UK), 1987.

150. Sykes, R.A., "Modes of motion in quartz crystals, the effects of coupling and methods of design", Bell Sys. Tech. J., **23**, 52-96, 1944.